SLAC-214
UC-34d
(E)

A MEASUREMENT OF THE PROTON STRUCTURE FUNCTIONS USING INELASTIC ELECTRON SCATTERING*

MAC DONALD MESTAYER
STANFORD LINEAR ACCELERATOR CENTER
STANFORD UNIVERSITY
Stanford, California 94305

PREPARED FOR THE
DEPARTMENT OF ENERGY UNDER CONTRACT NO. EY-76-C-03-0515

May 1978

Printed in the United States of America. Available from National Technical Information Service, U.S. Department of Commerce, 5285 Port Royal Road, Springfield, Virginia 22161. Price: Printed Copy $9.00; Microfiche $3.00.

*Ph.D. Dissertation

ABSTRACT

Measurements of inclusive electron scattering cross sections from hydrogen are reported for beam energies between 6.5 GeV and 19.5 GeV and for electron scattering angles of 6^{o}, 10^{o}, 15^{o}, 18^{o}, and 20.6^{o}. These measurements were taken using the Stanford Linear Accelerator and the 20 GeV spectrometer. Details of the experiment and the analysis are presented along with an estimate of the systematic errors on the cross section.

The data were taken simultaneously (but not in coincidence) with similar measurements at 50^{o} and 60^{o} using the SLAC 1.6 GeV spectrometer, sharing beam and target. By combining large angle data taken on the 1.6 GeV spectrometer with the data taken on the 20 GeV spectrometer, we are able to separately determine the proton structure functions σ_L and σ_T (or equivalently, νW_2 and $2MW_1$). We determine that our data is consistent within systematic errors with earlier MIT-SLAC cross section measurements. We construct a combined data set for the experiments.

From the combined data set we determined an average value of $\sigma_L/\sigma_T = .21 \pm .1$ over the kinematic range covered, $3\ \text{GeV}^2 < Q^2 < 18\ \text{GeV}^2$ and $4\ \text{GeV}^2 < W^2 < 16\ \text{GeV}^2$. We study the dependence of σ_L/σ_T on different kinematic variables. We compare the Q^2 dependence with theoretical predictions of Quantum Chromo Dynamics.

We investigate the scaling behavior of the structure functions νW_2 and $2MW_1$. The values of νW_2 and $2MW_1$ are evaluated along contours for which the scaling variables are constants. The Q^2 dependence along such contours is determined and agrees qualitatively with the predictions of asymptotically free gauge theories.

ACKNOWLEDGEMENTS

I would like to thank Richard E. Taylor, my thesis advisor, for his efforts at instilling in me the proper spirit of experimental work and in particular for his invaluable guidance in teaching me how to communicate experimental results in a clear manner. I would like to thank all the members of SLAC Group A for their hard work and for providing an excellent example of how to do good, careful experiments. I would like to thank Bill Atwood for innumerable conversations about all aspects of physics; his inquisitive mind made sharing an office and an experiment together an enjoyable experience. I would like to thank Ed Taylor for the considerable work he did in developing optical models of the spectrometer, and Karl Brown for helping me understand the basics of magnetic transport systems. The experiment could never have been completed without the substantial work of the SLAC SFG group and of the surveyors; and the thesis could not have been done without the extensive work of the illustrations department and of the principal typist of the thesis, Elise Appleby. I wish to thank Hobey DeStaebler for a careful reading of the manuscript. Finally, I would like to thank my best friend, Pat Gonzales, for her steady encouragement through the years; and my parents for their confidence, guidance, and help.

TABLE OF CONTENTS

TABLES

TABLES (continued)

LIST OF FIGURES

LIST OF FIGURES (continued)

HISTORY OF THE STUDY OF MATTER

The structure of matter has been the subject of curiosity, conjecture, and experimental study throughout history. Democritus believed that matter was constructed of "hard, impervious atoms", the fundamental building blocks of matter. These beliefs were founded on philosophical reasoning, and it was almost 2000 years later that experimental science had an impact on ideas of the nature of matter. In the 17th and 18th centuries, chemists postulated that all materials were compounded of one or more of the several elements. Boyle (1661) and others believed that these elements were "primitive and simple" bodies from which all materials "are immediately compounded, and into which they are ultimately resolved." The idea of a chemical atom, that is, a smallest piece of any element, was still a philosophical concept because atoms were not needed to explain observed chemical behavior.

A slightly different concept of elementary units arose in the kinetic model of gases, as exemplified by a conjecture of Bernoulli (1738) who saw gases composed of "corpuscles" which are "practically infinite in number" and who thought that heat "may be considered as an increasing internal motion of the particles..." The kinetic model provided a picture of heat as a manifestation of the dynamics of atoms in motion, in contrast to the caloric theory of heat which gave heat a structure as a fluid. The interplay between physical models of structures and those of dynamics persists throughout physics.

Dalton (1800) combined the ideas of chemical elements with the ancient atom hypothesis and arrived at the concept of the chemical atom, *the chemically indivisible smallest piece of an element, in order to* explain the discrete combination ratios observed in chemical reactions. Dalton viewed the atoms of a gas as stationary, with spaces between them filled by caloric, which he thought to be the fluid of heat. The observations by Count Rumford of heat generated during the working of metal (1807) demonstrated the conversion of mechanical work into heat, implying that heat is a form of energy associated with the motion of

the "elementary" particles, verifying the early ideas of Bernoulli, superseding the view of heat as an indivisible fluid, and strengthening the atomic hypothesis.

Rapid progress was being made at this time toward the modern concept of chemical atoms. In 1808, Gay-Lussac measured the ratio of volumes of hydrogen and oxygen gas which combine to form water as 2:1 to an accuracy of .1%. Along with the kinetic theory of heat, this prompted Avogadro to modify Dalton's model of gases. He postulated that gas particles are small compared to the volume occupied by them, and that equal volumes of gas (at the same temperature and pressure) contain equal numbers of molecules which may consist of one or more chemical atoms. These arguments cleared up many discrepancies in Dalton's picture of atoms, though it was not yet clear why atoms grouped together in two's and three's yet did not coalesce completely. From these considerations arose the concept of valence in the 1850's and the construction of Mendeleev's periodic table which demonstrated the systematic connection between valence and atomic weight. Valence was thought of as "hooks" by which atoms held fast to one another. Each kind of atom had a definite number of these "hooks", i.e., a definite valence. Then, in 1897, J. J. Thomson discovered the electron, demonstrating that electric charge was quantized and carried by particles much ligher than the atom itself. This was the first evidence that the chemical atoms were not elementary, but composed of smaller bodies. It was then realized that the atom itself was neutral and consisted of equal amounts of positive and negative charge. But still, valence was not realized to be the manifestation of lightly bound electrons. Thomson's picture of the atom was that of a positively charged sphere with the much smaller electrons embedded within it; hence the name "plum pudding" model.

This picture had to be revised fundamentally in 1911 following an experiment done by Geiger and Marsden on alpha particle scattering and Rutherford's interpretation of their results. Alpha particles of seven MeV were scattered from thin gold foils (approximately 1000 atoms thick). Most went through the foils with very little deflection, but a few of the alphas scattered through large angles. No backscattering can occur from electrons; the electron is so much lighter than the alpha that it can

absorb only .01% of the alpha's momentum even in a head-on collision. No backscatters could occur if the scattering were from an evenly distributed positively charged matter distribution. Rutherford realized that the alphas were undergoing a single hard scatter off a small, positively charged core of the atom containing most of its mass. His calculations based on Coulomb scattering from a massive point charge agreed with the angular distribution of scatters. This implies that the alpha does not enter the nucleus and, therefore, that the radius of the nuclear core is smaller than the distance of closest approach of the alphas (3×10^{-12} cm). The nucleus is more than a factor of 1000 smaller than the atom's radius yet contains almost all the mass.

A view of the atom developed which was analagous to the solar system with electrical attractions replacing gravity. Since the work of Maxwell, the forces between moving charged objects were understood and orbits could be calculated for the atom. Contradictions arose concerning the behavior of the electrons in such a model. The electrons were charged and were continually accelerated by the positive attraction of the nucleus; therefore, they should radiate, lose energy, and spiral into the nucleus. Niels Bohr provided an answer to the paradox. In 1913, he modified Rutherford's nuclear atom model with some postulates which had their roots in the newly developing field of quantum mechanics, spawned by the increasing observation of quantization in physical phenomena. The quantization of electric charge in the form of the electron, the observation of discrete lines in the optical spectra of gases, and the work of Planck and Einstein demonstrating the quantum nature of light and the existence of the photon all called for a quantum description of the atom. Bohr's main postulates were that there are certain stable orbits of the electron in which it does not radiate energy, that a photon is emitted when an electron goes from one stable orbit to another and that the frequency of the emitted photon equals the energy level change divided by Planck's constant, h.

By applying the correspondence principle, assuming that in the limit of a large radius the radiated photon's frequency equals the orbit frequency, Bohr was able to show that angular momentum of atomic states was quantized and was able to calculate Rydberg's constant and the spectra

of hydrogen gas. So in Bohr's model the atom was a small, massive nucleus with electrons in orbit about it, with quantized radii and energy levels. An experiment carried out by Franck and Hertz in 1914 using the inelastic scattering of electrons in mercury vapor verified the existence of quantized atomic energy levels.

The success of the Bohr model stimulated the growth of quantum mechanics. The idea of de Broglie (1924) that matter could be considered as waves with frequency and energy related by Planck's constant ($\nu = E/h$) led to the development of quantum mechanical equations of motion by Schrodinger and Heisenberg (1925) and their extension to the relativistic case by Dirac (1928). The Uncertainty Principle of Heisenberg (1927) superseded classical ideas of measurement and observability in the domain of the very small.

A very precise and exact theory of the electron was formulated by Dirac, combining relativistic quantum mechanics and electromagnetism. The theory of at least the simpler atoms was becoming well understood. The nucleus itself was still a mystery, however. The nucleus was thought to be composed of protons and electrons; protons having been identified as the nucleus of a hydrogen atom.

As in the case of the atom and Maxwell's equations, there were conflicts between the new quantum mechanics and this picture of the nucleus. The wave nature of the electron implies that if it is confined within the nucleus, its kinetic energy must be on the order of 100 MeV, but the electrons emitted during beta decay have energies of 2 or 3 MeV. The magnetic moments of electrons are about a thousand times greater than those of the nucleus itself. It therefore seemed unlikely that electrons exist within the nucleus. In addition, the spin and statistics of nuclei are not compatible with the idea that they consist of electrons and protons. The discrepancies were resolved in 1932 when James Chadwick put forth the hypothesis that a recently discovered new form of neutral radiation was not a high energy photon but a heavy, neutral constituent of the nucleus, the neutron.

With the development of accelerators, the range of nuclear phenomena that could be studied was expanded greatly. It became possible to create new particles not seen in ordinary matter and to study their

properties. Hadron beams were particularly useful in this respect because they interact strongly with nuclear matter, copiously producing particles and providing much information on their classification and spectroscopy. Another common use of accelerators involves the scattering of high energy particles, extending the kinds of study begun by Geiger, Marsden and Rutherford. In the rest of this account, we will consider scattering experiments using beams of high energy electrons and show how the electron's simple structure has been utilized to obtain information about nuclear and nucleon structure.

The present theory of electrons and their interactions (Quantum Electrodynamics) has been very precisely tested and verified in experiments such as e^-e^- scattering and e^+e^- annihilation and precisely predicts the anomalous magnetic moments of the muon and electron and a variety of phenomena in the spectroscopy of positronium. The electron-photon coupling constant, α, is small (1/137), so the dominant process by which an electron scatters from a charged object is through the exchange of a single virtual photon. Because the electron has a well-understood structure and the scattering process is simple, its value as a scattering probe is enhanced. Deviation from behavior expected for scattering from a point charge reflects properties of the object studied and not properties of the electron itself. Electron scattering is useful in measuring nucleon structure because the form of the cross section formulas are determined.

By 1950, the electron was recognized as a useful probe of the charge distributions in the nuclei. Hofstadter and co-workers used electron scattering to measure the size and structure of various nuclei. If the charge of a nucleus extends over a finite region of space, then when the electron approaches near enough to enter the nucleus, deviations from Coulomb scattering will be observed; small distances imply large momentum transfers for the scattered electrons. The Hofstadter group analysed their data in terms of an extended charge distribution model, and their results indicated that the nuclear charge density was not confined to a point but occupied a finite volume approximately proportional to the atomic number.

The experimenters then turned their attention and beam to a hydrogen target, in order to investigate electron scattering from a nucleus consisting of a single proton. The rate of decrease of the elastic cross section with increasing momentum transfer was much faster than expected for scattering from a point charge. An analysis of the results in terms of a spatial charge distribution (also called structure function or form factor) yielded the result that the proton was not a point charge but an extended object with a charge radius of approximately 10^{-13} cm (1 fermi).

When the high energy (approximately 20 GeV) beams became available at SLAC, one of the first experiments done was electron scattering from hydrogen. With higher energy beams, a wider range of inelastic scattering processes could be studied; that is, where the proton is excited to higher mass states. The cross section for scattering of the proton into mass states above 2 GeV fell much more slowly with momentum transfer than had the elastic scattering results. This slow fall-off of large angle scattering suggests structures which have characteristic sizes smaller than that of the proton.

For inelastic scattering, the extra degree of freedom afforded by the variable mass of the final state means that the inelastic structure function is, in general, a function of not only the square of the invariant momentum transfer, Q^2, but also of the invariant hadronic mass, W. For elastic scattering there is a kinematic relation $Q^2=2P\cdot Q$ where P,Q are the 4 momenta of the proton and photon. This follows from the elastic scattering condition, $W^2=M^2$, because $W^2=2P\cdot Q-Q^2+M^2$. If we now consider quasi-elastic scattering from "point" particles within a proton having fraction X of its momentum, then we have a similar constraint; $Q^2=2Q\cdot XP$ or $X=Q^2/2Q\cdot P$. If the electron scatters incoherently from these point particles with no internal structure, then the structure functions of the proton will depend only on $X=Q^2/2Q\cdot P$ and not on Q^2 or $2Q\cdot P$ independently. This phenomenon was observed in the early SLAC deep inelastic electron-scattering experiments and is known as "scaling". It was predicted by Bjorken who derived it using dispersion relations. Feynman was instrumental in interpreting scaling as a consequence of scattering from elementary sub-particles comprising the nucleon.

Knowledge about the dynamical behavior of the constituents in such a theory can be deduced from the study of electron scattering from hadrons. The scattering results (both elastic and inelastic) can be roughly explained by using a model of the proton in which it is composed of several, approximately structureless, charged objects (these are the quarks), each sharing part of the proton's momentum. These are often called "parton" models. Electron scattering is viewed as quasielastic scattering from these objects, and the structure functions of the proton are simply related to the charge and the momentum distribution of the objects within the proton. By examining the kinematic dependence of the structure functions of the nucleon, we may be able to deduce not only the wave function of these constituents, but also some characteristics like charge or spin. Here lies the motivation of the present experiment; to study further the nucleon, which is not yet the fundamental building block of nature.(1)

LEPTON-NUCLEON SCATTERING

The scattering of electrons from nucleons proceeds primarily through the electromagnetic force, since electrons do not participate in the strong interaction directly. (In the simplest models of the weak interaction, the weak and electromagnetic forces are unified in a gauge theory, but at this experiment's range of four-momentum transfer (Q^2), the effects of the electron's weak interactions are negligibly small).

The scattering proceeds via an interaction of the electromagnetic current of the nucleon with the field generated by the electron's current. Since the electron is a spin ½ Dirac particle, this field can be expressed as:

$$A_\mu = \frac{4\pi e^2}{Q^2}\,\bar{\psi}\gamma_\mu\psi$$

where $\bar{\psi}\gamma_\mu\psi$ is the electron's current and $1/Q^2$ is the photon propagator.

The hadronic current is $\bar{\psi}_f J_\mu \psi_i$ where ψ_i and ψ_f represent the initial and final hadronic wave function and J_μ is a general Lorentz 4 vector.

The first order scattering amplitude for one-photon exchange is:

$$M_{if} = \bar{\psi}\gamma_\mu\psi \frac{4\pi e^2}{Q^2} \bar{\psi}_f J_\mu \psi_i \equiv A_\mu * (J_\mu)_{\text{nucleon}}$$

A diagram depicting this process is:

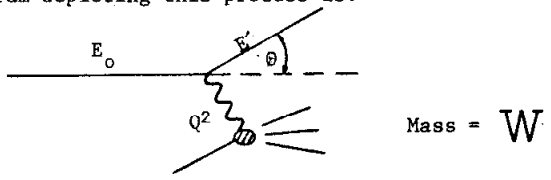

where E_o and E' are the energies of beam and scattered electron and θ is the scattering angle. Q^2 is the 4-momentum squared of the virtual photon; $Q^2 = 4E_o E' \sin^2\theta/2$. W is the mass of the hadronic final state; $W^2 = (P+Q)^2 = 2M\nu + M^2 - Q^2$, where $\nu = E_o - E'$.

The scattering cross section is proportional to the square of the matrix element:

$$M_{if}{}^2 \equiv \langle\bar{\psi}\gamma_\mu\psi\rangle\langle\bar{\psi}\gamma_\nu\psi\rangle \frac{(4\pi e^2)^2}{Q^4} \underbrace{\sum_i \langle\bar{\psi}_f|J_\mu|i\rangle\langle i|J_\nu|\psi_i\rangle}_{W_{\mu\nu}}$$

which can be written as the product of two tensors:

$$M_{if}{}^2 = L_{\mu\nu} W_{\mu\nu} \frac{(4\pi e^2)^2}{Q^4}$$

where $L_{\mu\nu}$ is the leptonic part and $W_{\mu\nu}$ the hadronic part of the interaction.

Averaging over incoming electron spins and summing over outgoing electron spins (since the beam electrons are unpolarized), we obtain for $L_{\mu\nu}$:

$$L_{\mu\nu} = 2(P_\mu P'_\nu + P_\nu P'_\mu - \delta_{\mu\nu} P\cdot P')$$

where P and P' are the 4-momenta of the incoming and outgoing electron. $L_{\mu\nu}$ is symmetric in μ and ν.

In general, the hadronic tensor $W_{\mu\nu}$ can have both symmetric and antisymmetric parts, but since the contraction of a symmetric and antisymmetric matrix is zero, only the symmetric part of $W_{\mu\nu}$ contributes to our cross section.

A further restriction on $W_{\mu\nu}$ is that it must satisfy current conservation. The current conservation condition is:

$$\partial_\mu J_\mu(x) = 0 \rightarrow Q_\mu J_\mu = 0 \rightarrow Q_\mu W_{\mu\nu} = 0$$

Under these restrictions, the most general form for $W_{\mu\nu}$ is:

$$W_{\mu\nu} = \frac{W_2(Q^2,W^2)}{M^2}\left(P_\mu - Q_\mu \frac{P\cdot Q}{Q^2}\right)\left(P_\nu - Q_\nu \frac{P\cdot Q}{Q^2}\right) - W_1(Q^2,W^2)\left(\delta_{\mu\nu} - \frac{Q_\mu Q_\nu}{Q^2}\right)$$

where W_2 and W_1 are functions of Q^2 and W^2. We can see explicitly that $Q_\mu W_{\mu\nu}$ is zero for each of these terms. When we contract $L_{\mu\nu}$ and $W_{\mu\nu}$ the differential cross section we obtain is:

$$\frac{d^2\sigma}{d\Omega dE'} = \sigma_{MOTT}(W_2(Q^2,W^2) + 2\tan^2\theta/_2 W_1(Q^2,W^2)); \quad \sigma_{MOTT} = \frac{\alpha^2 E'^2 \cos^2\theta/_2}{Q^4} \qquad (1)$$

Thus, we can express the e-p cross section as that for a structureless Dirac proton, σ_{MOTT}, multiplied times an expression containing two independent form factors which describe the structure of the proton. What is the form of the hadronic charge current which couples to the photon? In the parton models, the proton is thought to be comprised of several constituents sharing the proton's energy and momentum. The electron is assumed to scatter elastically from a single constituent. By assuming that the constituents are structureless charged particles, the cross section can be written in such a form that the proton structure functions can be identified with the momentum distribution of the constituents. If $f_i(x)dx$ is the number of partons (quarks) of type i having momentum between x and x+dx, then:

$$\nu W_2(x) = \sum_i q_i^2 \, x \, f_i(x)$$

$$2mW_1(x) = \sum_i q_i^2 \, f_i(x)$$

where q_i is the charge of a parton of type i.

In an alternate way of writing Equation 1, we can describe the scattering process in terms of a flux of virtual photons of mass Q^2 produced by the electron current which are incident upon the proton and absorbed by it; i.e., as a virtual photoabsorption cross section.

The following discussion is clearly outlined in Feynman's "Photon-Hadron Interactions." [2] If ϵ_μ is the polarization 4-vector and Q_μ the momentum 4-vector of the initial photon, then the photoabsorption cross section for a photon incident upon a nucleon is:

$$\sigma = \frac{4\pi e^2}{2k2M} \sum_i |\langle i|\epsilon_\mu J_\mu|P\rangle|^2 2\pi\delta(W^2-(P+Q)^2) = \frac{4\pi e^2}{2k2M} \epsilon_\mu \epsilon_\mu W_{\mu\nu}$$

where $k = (W^2-M^2)/2M$ is the energy of the photon in the limit $Q^2 \to 0$.

There are two polarization cases:

Transverse: $\epsilon_{\mu\perp}$ to Q_μ and P_μ, (i.e. $\epsilon_\mu Q_\mu = \epsilon_\mu P_\mu = 0$)

Contracting $\epsilon_\mu \epsilon_\nu$ with $W_{\mu\nu}$ given from Equation 1 gives:

$$\epsilon_\mu \epsilon_\nu W_{\mu\nu} = 4MW_1$$

or,

$$\sigma_{\text{transverse}} = \frac{4\pi^2 e^2}{k} \; W_1$$

The other polarization case is:

Longitudinal: ϵ_x, $\epsilon_y = 0$

Since $\epsilon_\mu q_\mu = 0$ (this is the definition of polarization), we have:

$$\epsilon_T = \frac{Q_z}{\sqrt{Q^2}} \; ; \; \epsilon_z = \frac{Q_T}{\sqrt{Q^2}}$$

Contracting $\epsilon_\mu \epsilon_\nu$ with $W_{\mu\nu}$, we get:

$$\sigma_{\text{longitudinal}} = \frac{4\pi^2 e^2}{k} (1+\nu^2/Q^2)(W_2+W_1)$$

The cross section for electron scattering can be expressed in terms of these photo absorption cross sections:

$$\frac{d^2\sigma}{d\Omega dE'} = \Gamma(\sigma_T+\epsilon\sigma_L)$$

where Γ is the flux of virtual photons and ϵ is the polarization parameter reflecting the relative amount of longitudinal polarization of the photon.

Using the expressions above for σ_T and σ_L together with the equations for the differential cross section, we find that:

$$\Gamma = \frac{e^2}{2\pi^2} \frac{kE'}{Q^2 E_o (1-\epsilon)}$$

and

$$\epsilon = \frac{1}{1+2\tan^2\Theta/2(1+\nu^2/Q^2)}$$

This alternative method of describing the interaction is useful because we can investigate the dependence of the cross section upon the polarization of the virtual photon. When investigating parton models, the relative size of transverse and longitudinal polarization cross sections can distinguish between spin 0 and spin ½ constituents.

This difference is most easily seen by considering the photon-parton interaction in the parton Breit frame.

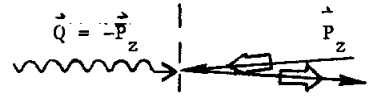

Photon | Parton absorbs photon and backscatters

Consider first the case where the constituents have spin ½. The parton absorbs the photon's momentum and is backscattered. In the limit that the parton's mass can be neglected, the helicity of the parton is conserved. Therefore, when it backscatters, its spin is flipped, and it must absorb 1 unit of angular momentum (along the Z direction) from the photon. Since a longitudinally polarized photon has helicity 0

it has no angular momentum component in the Z direction and cannot flip the parton's spin. Hence, $\sigma_L = 0$ for massless spin ½ partons.

The case of a spin 0 parton proceed similarly except that here the parton, having no spin, cannot absorb angular momentum along its direction of motion and so must couple to a photon having no angular momentum along that direction; i.e., one with longitudinal polarization. Thus, $\sigma_T = 0$ for spin 0 partons.

The argument that $\sigma_L = 0$ for spin ½ partons must be modified somewhat if they possess perpendicular momentum in the Breit frame.

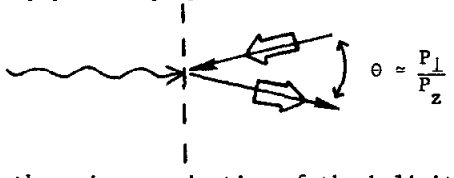

In this case, there is a projection of the helicity conserving wave function onto one which does not flip spin whose amplitude is given by:

$$A = \sin\theta/2 \cos\theta/2 = 2 \sin\theta \simeq 2 P_\perp/P_z$$

and the ratio of σ_L/σ_T is given for this simple model by:

$$R \equiv \sigma_L/\sigma_T = 4 \frac{P_\perp^2}{Q^2}$$

So measuring σ_L/σ_T can yield information about the spin of the quarks and may also probe dynamical properties such as the average $P_\perp$ of the struck quark.

The parton models are too simple and do not include effects stemming from parton-parton interactions. Presently, a theory based on a detailed model of quark dynamics is being developed, Quantum Chromo-Dynamics. It makes detailed predictions of the patterns of violation of scaling in general agreement with observations in experiments at SLAC (electron) and at Fermilab (muon). The quantity σ_L/σ_T can be calculated in the model and can be compared with experimental results. While the main emphasis of our results will be the size and kinematic dependence of $R \equiv \sigma_L/\sigma_T$, we will also present results on the scaling of the proton structure functions, νW_2 and $2MW_1$ and the pattern of scaling deviations which our data show.

CHAPTER I - REFERENCES

1. "The Really Basic, Truly Elementary, Genuinely Fundamental Building Blocks of Matter"

It was a warm summer day in the year 525 B.C. and one of the eminent Philosophers of the Pythagorian school was lecturing to a small group of graduate students on "The Structure of The Universe." He had already explained that the Earth was at the center, of course, and that it was surrounded by seven crystalline spheres of different sizes. At that point, one of the students looked puzzled, then raised his hand.

"Sir," he said, "can you tell us how the Earth is supported? I mean, what holds it up?"

"Certainly," said the smiling Philosopher. "It is well-known that the Earth is supported on the shoulders of a Giant."

The lecture continued, but after a time the same student (there's one in every crowd) again raised his hand and received the Philosopher's gracious nod.

"Sir," said the student, "where does the Giant stand while he's holding up the Earth?"

A bit impatiently, the Philosopher said, "It is well-known that the Giant is standing on the back of a huge Sea Turtle."

"Oh," said the student.

As the Philosopher continued, he could see that the student was again becoming puzzled and working up to another question. This time he was ready, however, and when the student's hand went up for the third time, the Philosopher waved it away with a masterful gesture.

"Don't ask," he said. "It's Turtles all the way down."

SLAC Beam Line, February 1977

2. R. P. Feynman, Photon Hadron Interactions, W. A. Benjamin, Inc., 1972.

DESCRIPTION OF THE EXPERIMENT

The experiment is an absolute measurement of the inclusive cross section for high energy electron scattering from hydrogen and deuterium targets. The measurements were made using the 20 GeV spectrometer facility in End Station A (ESA) at SLAC. Most of the running was done at angles of 15° and 18° with beam energies ranging from 6.5 GeV to 19.5 GeV; the range of energies and angles overlaps with data taken previously on the 8 GeV spectrometer.[1] See Figure II-1 for an illustration of the range of data. Two experiments were performed simultaneously, sharing the beam and the target. The 20 GeV spectrometer collected data at angles between 6° and 20.6° and, at the same time, data on the scattering cross sections at 50° and 60° was taken using the 1.6 GeV spectrometer. No coincidence measurements were involved, but in this way the data gathering for a certain amount of beam was doubled. The larger angle data has been analyzed to yield information on the structure function W_1.[2] Both experiments shared the designation "E89" at SLAC.

The 20 GeV spectrometer cross section measurements can be combined with the 1.6 GeV cross sections to determine the values of both nucleon structure functions, $2MW_1$ and νW_2, over a wide kinematic range, testing the hypothesis of "scaling" of the structure functions and investigating the behavior of the quantity σ_L/σ_T. The scaling behavior and the size and kinematic dependence of σ_L/σ_T are calculated in models of nucleon structure, and it is important to confront the theories with data. Early evidence that σ_L/σ_T is small provided support for simple parton models with spin ½ partons; now the models are becoming more sophisticated as they treat the problems of quark dynamics. In models such as Quantum Chromo-Dynamics, our data can be used to study the spin, momentum distribution, and dynamics of the postulated constituents of the nucleon.

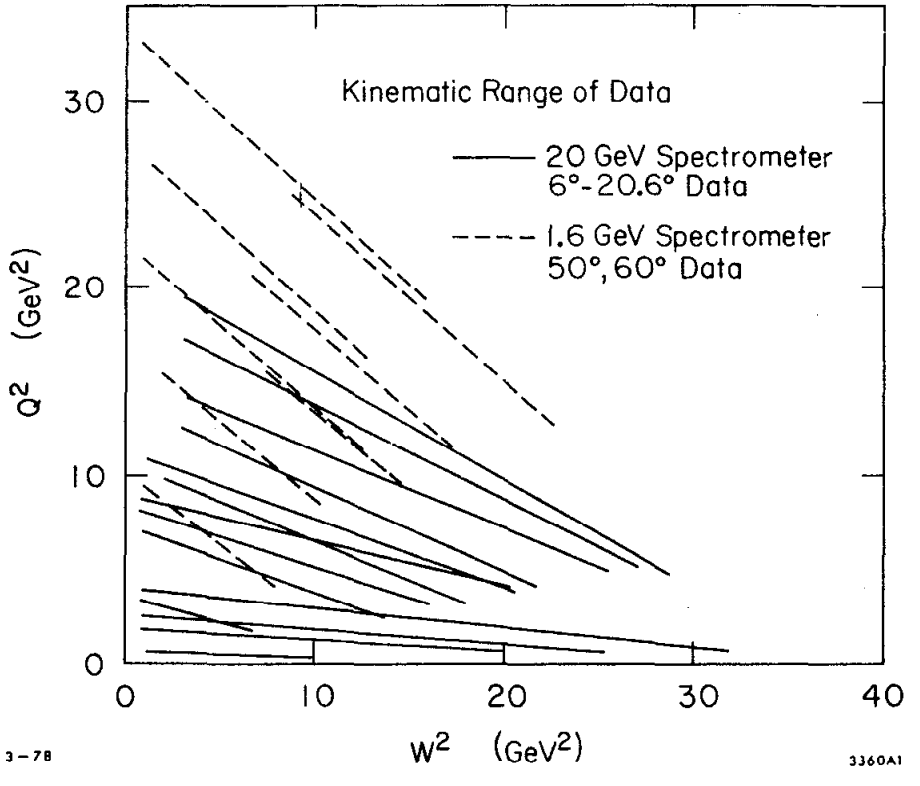

Fig. II-1

An illustration of the range of data covered by this experiment (E89). The data were taken along the "lines" at constant beam energy, E_o, and constant scattering angle, θ. The 20 GeV spectrometer data consists of 14 "lines" at angles of 6°, 10°, 15°, 18°, and 20.6°. The lines which are most nearly horizontal correspond to an angle of 6°; the steepest lines, to 60°.

A schematic of the experimental set-up in End Station A is shown in Figure II-2. The primary electron beam coming from the linac is directed into beam line A where it is bent through an angle of 24° by a series of precision bending magnets and is focused by sets of quadrupoles. High power slits are situated at the point of maximum momentum dispersion of the beam defining the momentum of the beam in ESA and its momentum spread. For the majority of the data taking, these slits were set to ±.375% acceptance.

Between the momentum analyzing system and the target, the beam passed through two charge monitors each consisting of a ferrite ring with a toroidal winding. Each beam pulse induces a signal in the "toroid" which is proportional to the amount of charge in the pulse. This signal was amplified and digitized and was incremented to provide a measure of the total flux of electrons for a data run. After passing through the toroidal charge monitor, the beam hit the target with a spot size of approximately 2 mm (vertical) x 3 mm (horizontal).

Three targets were used: a liquid hydrogen, a liquid deuterium, and a stainless steel "empty" target used to make subtractions for cell wall scattering. The liquid target cells were 7 inches long, and the liquid was circulated through them in order to eliminate localized beam heating which could cause boiling. The cell pressure and temperature were continually monitored so that the target density could be determined.

The magnetic spectrometer detected particles which scattered through an angle θ relative to the beam; data was taken at angles of 6°, 15°, 18°, and 20.6°. The spectrometer accepts scattered particles which are within a momentum range $\delta = dP/P'$ of plus or minus 2% about its central momentum setting, P' and within a solid angle ($d\Omega$) of approximately 125 microsteradians. ($\Delta\theta_{horizontal} = \pm 4$ milliradians, $\Delta\phi_{vertical} = \pm 8$ milliradians.) Figure II-3 illustrates the notation used in describing the scattered particles' angles and momentum.

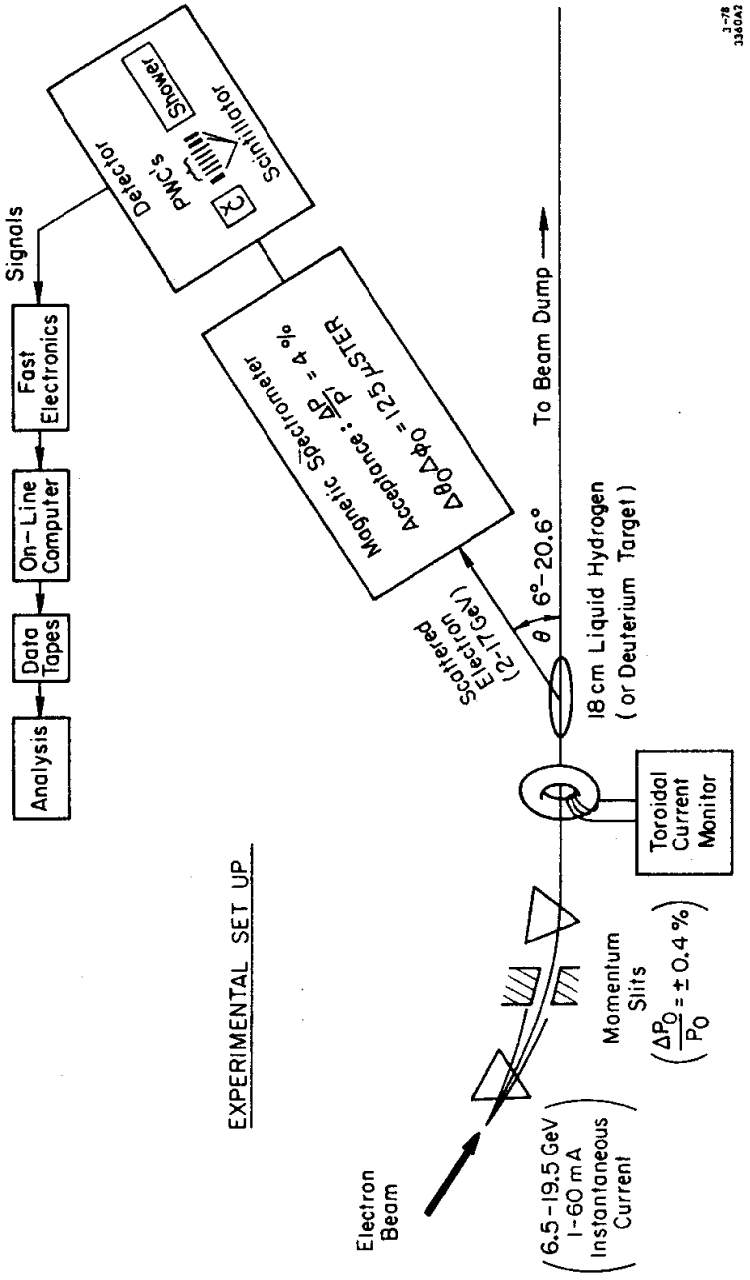

Fig. II-2
A schematic of the experimental set-up showing the main features of the experiment.

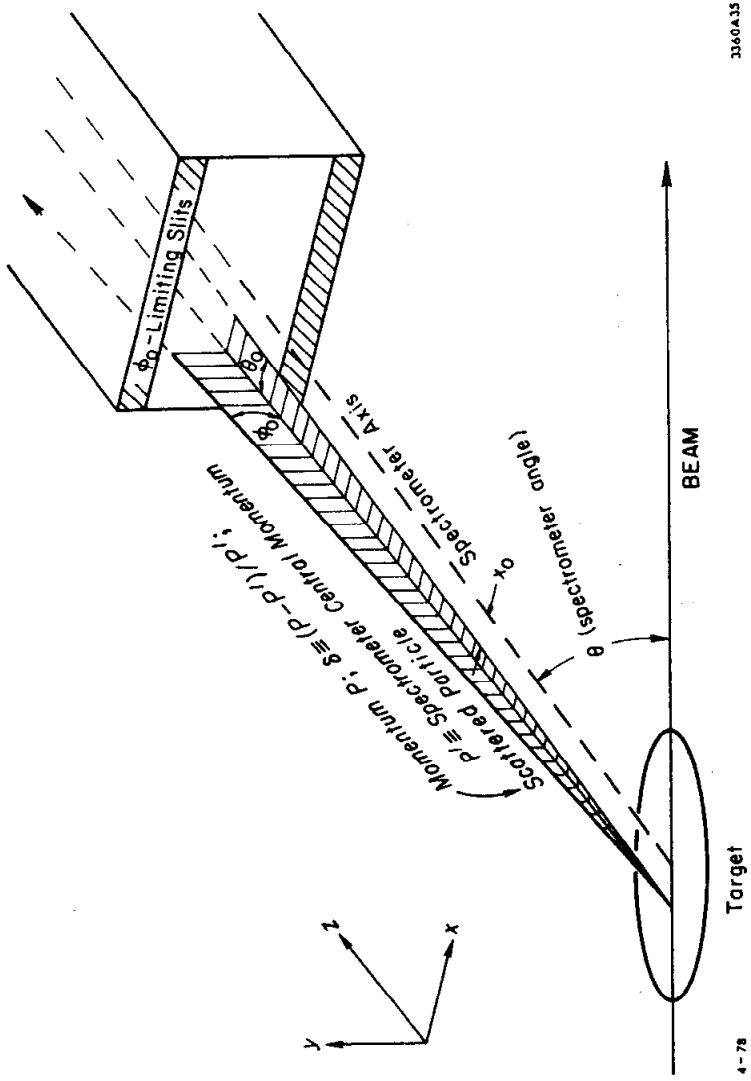

Fig. II-3

Defintion of the scattered electron's momentum and angles. The particle's momentum is measured relative to a calculated central momentum of the spectrometer. The angle ϕ_o is measured relative to a horizontal plane through the spectrometer's axis. θ_o is measured relative to the vertical plane through the spectrometer's axis. X_o is the X position of the scattering vertex at the target.

Those particles within the spectrometer acceptance go through it and enter the concrete shielded detector room, called the "hut". Particles entering the hut traverse a 2 meter atmospheric pressure nitrogen gas Cerenkov counter, a plastic scintillator counter, 5 planes of proportional wire chambers (PWC) with 2 mm wire spacing, 2 more (aperture defining) scintillator counters and, finally, a combination lead glass and lead and scintillator sandwich shower counter.

Particles are identified as electrons on the basis of their pulse heights in the Cerenkov and shower counters. Particle tracks are reconstructed in the PWC system and knowledge of the "optics" of the spectrometer is used to calculate the momentum δ and scattering angle Θ_o, of the event given the track in the hut.

The cross section for given kinematics is then calculated as follows:

$$\frac{d^2\sigma}{d\Omega dP} = \frac{N_{scat}}{N_{in} N_{tgt} (d\Omega dP)}$$

where N_{scat} is the number of electrons whose P and Θ_o fall within the acceptance used in the analysis. N_{in} is the number of beam electrons incident upon the target for the run; N_{tgt} is the density of the target in number of nucleons/cm^2, and $d\Omega dP$ is the size of the acceptance of the spectrometer.

Typically, data is taken in "lines" with fixed E_o and Θ, while the scattered electron's energy E' is varied by changing the momentum setting of the spectrometer. The momentum setting was varied in discrete steps from a maximum energy corresponding to elastic scattering down to a minimum value of 2 GeV. Below this value we did not take data because of the increasing size of several corrections and the falling electron trigger efficiency. For data at low values of the scattered energy, E', additional runs were taken with the polarity of the spectrometer reversed in order to accept positrons and allow corrections for electrons produced in (e^+e^-) charge symmetric processes. All events were logged on tape and subjected to an extensive analysis which is discussed in Chapter 3. We next discuss in some detail the various pieces of apparatus and their operation.

BEAM

The spectrometers are intalled on one of the two high resolution beam lines at SLAC. The accelerator is capable of delivering a high intensity small phase space beam of electrons at energies up to 20 GeV. The maximum current is approximately proportional to the energy and is 5.5×10^{11} electrons per pulse (60 milliamperes instantaneous) at 20 GeV.

The beam consists of a stream of pulses, up to 360 per second. Since each pulse is about 1.5 μseconds long, the maximum "duty" factor of the accelerator is only 5×10^{-4}. The electrons are accelerated down the beam pipe waveguide by microwaves supplied by klystron tubes, so in each pulse there is a fine time structure associated with the microwave frequency of 2856 mHz (10.5 cm). Electrons are bunched in phase with the microwaves, occupying $\pm 5^{\circ}$ of phase giving bunches .3 cm (.01 nsec) long spaced 10.5 cm (.3 nsec) apart. The maximum power in a (20 GeV, 60 mA, 360 pps) beam is .65 megawatts. For a summary of beam parameters, see Table II-1. Also shown are errors in the measurements.

Energy Measurement

The momentum of the beam is determined by the properties of the magnetic analysis system in the A beam line. Those accelerator pulses which are designated for End Station A are shunted $.5^{\circ}$ into the A beam line by pulsed magnets. The beam is then momentum dispersed and collimated to define the central energy and energy spread, and then focused onto our target. The A-line beam transport which accomplishes this consists of 8 dipole magnets and 5 quadrupoles.

As it enters the A-line, the beam size is collimated to 9 mm x 9 mm size by high-power collimators. Further down the line, high-power movable slits are located at the position of maximum momentum dispersion. These slits were set to accept a ±.375% spread in beam energy except during the 10° high resolution scan when they were set to ±.2% of the central momentum.

TABLE II-1

BEAM PARAMETERS

PARAMETER	VALUE	HOW MEASURED	SYSTEMATIC ERROR+
Energy	6.5 GeV to 19.5 GeV	A-line optics, flip coil in identical magnet in series, momentum slits ±.375%	±.1% absolute calibration (.6%)*
Intensity	1-60 ma. instantaneous current	2 toroidal monitors, inter-calibrated with beam and standard capacitor pulse, additional calibration with Faraday cup	±.8% (including .5% allowance for Faraday cup normalization) (±.8%)
Position and Spatial Extent	SPOT: 2 mm (v) x 3 mm (h) angular spread: ±.1 mrad	SEM, "burned" spot on target, spot position on surveyed ZnS screens	1 mm x 1 mm; ±.1 mrad - (±.2%)-18° (±.6%)-6°
Time Structure	1.5 μsec spill	monitored	--
TOTAL ERROR IN CROSS SECTIONS			(1.6%)

+ In parenthesis, we show the error in the cross section due to the error in the particular parameter.

* This is an average over our kinematic range

$$\frac{\Delta\sigma}{\sigma} = (2.5 + 6.5\ X)\ \frac{\Delta E_o}{E_o}\ ;\ \text{where } X = Q^2/2M\nu$$

The central value of the beam momentum is determined by the magnetic field of the bending magnets. The field is measured by a flip coil measuring the magnetic field strength of a ninth magnet, identical with the 8 A-line dipoles and run in series with them. The ninth magnet is located outside the beam area. The central momentum value of the A-beam line is believed known to ±.1%. A change in the incident energy of .1% will change our cross sections by an average of .6% (ranging from about .3% at low values of the scaling variable, X ≈.3, to about .9% at X ≈.8.

Beam Size and Position Measurement

The measurement of the size and position of the beam is important to insure that the beam goes through the center of our target. For example, a beam spot size of σ = 1 mm changes the average target length traversed by about .1%, due to the rounded target ends. If the beam is mis-steered by 1 mm, the effective target length changes by .2%. The incoming angle of the beam must be measured accurately since a .1 mrad mis-steering changes our 18° cross sections by about .2% and the 6° cross sections by .6%.

The beam position was monitored by ZnS screens viewed by remote television cameras which could be observed by the experimenters. Two of the screens were located upstream of the target at 42.3' and 10.9', respectively. During periods of beam set-up, these screens were placed in the beam; during data taking they were removed. The third screen was located 16.7' downstream of the target. It was left in the beam during data taking where it could be used to monitor possible drifts of the beam position. Using the screens, we could position the beam spot to ±1 mm.

Since the distance between screens is approximately 20 m, we could determine possible mis-steering of the beam to be less than plus or minus .1 milliradians. To insure that the position of the target was accurate relative to the beam line defined by the screen, an aluminum oxide screen was mounted on the target assembly itself. The position of the target is accurately known with respect to the

aluminum oxide screen so the target can then be accurately positioned in the beam.

The beam spot size was measured in two ways: in the course of the experiment by a few special runs which monitored the secondary electron emission from a thin wire which was scanned horizontally across the beam, and after the experiment, by exposing raw film to the ends of the target, measuring the residual radiation. Both these methods yield spot sizes of approximately 3 mm (horizontal) and 2 mm (vertical).

Charge Measurement

It is necessary to measure the total number of beam electrons for a data run in order to calculate the cross section. The total charge of each beam pulse was measured by a charge monitor consisting of a toroidally wound ferrite ring through which the beam passed. There were two independent monitors of this design, referred to simply as the "toroids". As the beam pulse passes through a toroid, the changing magnetic flux through the toroidal windings induces a voltage pulse proportional to the amount of charge. This pulse excites an LC circuit with a resonant frequency of 5.25 kHz, causing the circuit to oscillate. After a set sampling time, the peak of the oscillation is amplified and digitized. The output is incremented over the whole run to yield the total charge for the run.

The toroids were calibrated by dumping charge from a standard capacitor through an extra one-turn winding on the toroid. The time constant of the capacitor discharge was similar to the beam pulse length in order to better simulate the beam. The agreement between the two toroids and the standard charge or the capacitor was within ±.5%. An additional calibration using the beam was performed using a Faraday cup located 80' downstream of the target. The beam pulse passed through the toroids and then was contained and its charge measured in the Faraday cup. The toroids agreed with the Faraday cup measurements to ±.5%. The Faraday cup is believed to have an absolute accuracy of ±.5%.[4]

TARGET

Our studies of the proton were made using a target of liquid hydrogen. To study the neutron, we used a deuterium target. The nucleus of deuterium is the simplest nucleus which contains neutrons, and using deuterium minimizes nuclear effects such as the shadowing of single nucleons by the others or the spread in measured cross sections caused by the Fermi motion.

The targets are of the condensation type in which hydrogen or deuterium gas at approximately 2 atmospheres pressure is cooled and condensed by passing it through a coil in thermal contact with a liquid hydrogen reservoir at about 21°K. The resulting liquid is circulated by fans through a closed system, one section of which is a thin walled cell of elliptical cross section. These target cells are approximately seven inches long and one inch wide, constructed out of .0017" thick stainless steel. The target assembly is designed so that each of the target cells can be moved into the beam remotely.

Target Length

To measure the cross section, we need to know the number of nucleons/cm^2 which the beam sees (i.e., the density and the length of the target). The temperature of the liquid in the cells was measured with hydrogen vapor bulb thermometers to an accuracy of ±.1%; knowing the temperature of the liquid allowed us to calculate its density within a systematic uncertainty of ±.3%. The physical length of each cell was measured optically to an accuracy of ±.5% at room temperature and a (.3%) correction was calculated to account for thermal contraction between room temperature and 21°K. For a list of target parameters, see Table II-2.

Throughout the experiment, the target density varied by less than .5%. Some variations were caused by different heat loads sustained by the target for different values of beam power. To dissipate this heat and prevent boiling of the liquid, which would cause large density fluctuations, a fan circulated the liquid at such a speed

TARGET PARAMETERS

PARAMETER	VALUE	HOW MEASURED	SYSTEMATIC ERROR*
Length	6.962" (LH) 6.945" (LD)	Optically, thermal contraction —(.3%) finite beam spot on rounded ends of target-(.3%)	(±.5%)
Temperature	20.4°K (LH) 20.7°K (LD)	Hydrogen vapor bulb termometer	±.1%
Density	.0697(g/cc)(LH) .1684(g/cc)(LD)	Calculated from temperature and pressure	(±.3%)(LH) (±.6%)(LD)
Boiling (heat load from beam)	--	Vary beam currents, repetition rates, target fan speed	--
Purity	0 ± .05% D in H .3 ± .1% H in D	Mass spectrometer analysis of target gas	(.15%)(LD)
TOTAL ERROR IN CROSS SECTIONS			(1%) (LH) (1.3%)(LD)

* cross section error in parentheses

Additional Information:

		Degrees				
		6°	10°	15°	18°	20.6°
"Mock" TGT/cell wall	Fall Spring	5.61 5.28	5.85 5.49	6.17 5.79	6.36 5.97	6.59 6.19
Radiators in Beam ($\times 10^{-2}$ r.l.)	t after (LH) t after (LD)	2.69 2.84	2.31 2.42	1.95 2.03	1.80 1.87	1.70 1.76
	t before (LH) t before (LD)	1.26 1.41	1.26 1.41	1.26 1.41	1.26 1.41	1.26 1.41

Target shape at 16.5 PSI: Width = $.94\sqrt{1-(2Z/L)^{7.3}}$ inches

L = target length

Z = distance from target center along beam line

(≈1m/sec) that each beam pulse strikes fresh liquid. To prove that the data was not suffering from large density variations in the target, special data taking runs were conducted at widely varying values of beam current, repetition rates, and fan speeds. We concluded that target density fluctuations due to boiling were less than ±.5%.

Target Wall Subtractions

In order to extract hydrogen or deuterium cross sections, corrections must be made for those electrons which scatter not from the liquid but from the steel cell walls. This correction is about 5% and is measured by taking data with an empty target cell. In scattering from the liquid target cell walls, an electron will traverse about .02 radiation lengths of liquid before (or after) the scatter, causing it to radiate. To simulate this radiating effect, we constructed a mock empty cell with approximately the same thickness in radiation lengths as the liquid targets (about six times thicker than the actual target cell walls). The material comprising the mock target cell was distributed rather evenly along its length instead of only at the two ends as in the case of the real empty target. Because the spectrometer acceptance falls off with increasing effective target width (and, thus, with increasing spectrometer angle) the ratio of thicknesses of mock to real cell walls (weighted by spectrometer acceptance) grows slightly with increasing angle as shown in Table II-2. For each data point, we took cross sections from the three targets in sequence (hydrogen, deuterium, empty cell) in order that we might make the target wall subtraction for each run.

Radiators in Beam

We must know the thicknesses in radiation length of all the material which the beam passes through in order to do the radiative corrections, which will be discussed in a later chapter. These thicknesses will change with scattering angle since the exiting electron will pass through different thicknesses of liquid and cell

wall according to its angle. Using the known thicknesses of material in the beam and a measured target shape, we calculated the average amount of radiator before (and after) the target center as a function of scattering angle. These are presented in Table II-2 also.

SPECTROMETER

Description

The spectrometer is the heart of our experimental apparatus. With it, we measure the flux of electrons which scatter from the target with a particular value of scattering angle and momentum. The spectrometer is mounted on rails, the axis of the spectrometer points at the target, and the scattering angle is varied by rolling the entire assembly to the desired angle. The momentum of the scattered electrons is varied by changing the currents in its magnets. Dividing scattered flux by the beam flux, target density, and spectrometer acceptance, we are able to calculate the cross section.

The properties of the 20 GeV spectrometer are listed in Table II-3. It is a large (approximately 40 m long) device consisting of 11 magnets; four dipole field bending magnets, ($\approx 5^{o}$ bend), four quadrupoles for focusing, and three sextupoles to correct chromatic aberrations. For a schematic of the spectrometer, see Figure II-4. The magnets are arranged in a vertical S-bend; the first two bending magnets deflect the scattered electrons upward, and the final two deflect them an equal amount downward so that the paths of scattered electrons end up parallel to the floor but above the beam line.

Optical Properties

Let us consider the geometry and the focusing properties of the spectrometer. A scattered electron entering the device has horizontal position X_o, horizontal angle θ_o, and vertical angle ϕ_o relative

SPECTROMETER PARAMETERS

Magnetic Configurations: 11 magnets, 4 bends ($\approx 5^{\circ}$), 4 quadrupoles, 3 sextupoles; "S"-bend (2 bends up, 2 bends down), momentum dispersed in vertical plane, 2 momentum focii--at center and end of spectrometer, θ_o dispersed in horizontal plane, very little mixing of horizontal and vertical planes, 2nd order aberrations reduced by sextupoles.

Dispersions:

$(\theta_o/X) = (.578 + .00164 * E') \text{ mrad/cm}$; 4%

$(\delta/Y) = (.2765 + .0017 * E') \text{ \%/cm}$; 9%

} change from $E' = 2.5$ to $E' = 17.5$ GeV

Resolution of P and θ_o:

	P resolution	θ_o resolution
Uncertainty in X_o, Y_o, ϕ_o	.05%	.06 mrads
Multiple scattering in hut (7.5 GeV)	.02%	.03 mrads
Currents drifting within tolerances	.05%	.02 mrads
PWC granularity (2 mm)	.03%	.06 mrads
Added in quadrature	.08%	.08 mrads
(Multiple scattering in target) (at 7.5 GeV)		+.3 mrads

Tolerances (change in magnet position or current to move track by 1 mm at focal plane):

Magnet	X position	Y position	roll	magnetic current
bends	.5 - 1"	large	.3 - 1 mrad	.12%
quads	.010"*	.018"	.3 - 1 mrad	.1 - .3%
sext	.1"	.2"	≈7 mrad	≈3%

* checked by survey after each angle change

Acceptances:

$\Delta\phi_o$ ±7.99 mrads - set by ϕ_o slits

Nominal Acceptance: $\Delta\theta_o$ +3, -3.75 mrads - software limits

$\Delta\delta$ ±1.75% - software limits

Correction to Nominal Acceptance:: $\frac{\text{"actual"}^*}{\Delta\phi_o \Delta\theta_o \Delta\delta} = 94\%\ (20.6^{\circ}) \rightarrow 98\%\ (6^{\circ})$

* as calculated using a Monte Carlo method and a model of the spectrometer

Systematic Errors: ±4% error due to dispersions
±2% error due to acceptance

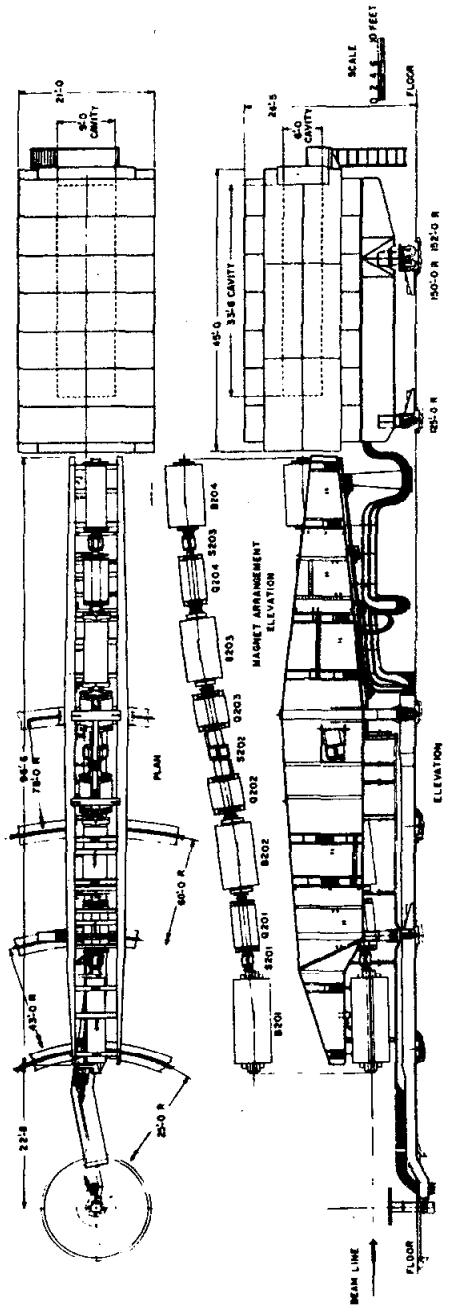

Fig. II-4

20 GeV spectrometer assembly.

to the spectrometer-target center line. The momentum, P, of the scattered particle is measured relative to the spectrometer central momentum P' and is commonly expressed as the percentage offset from the central momentum, $\delta \equiv (P-P')/P'$. The exiting track has positions X and Y and angles θ and ϕ as it passes through the momentum focus located in the detector. See Figure II-3 for an illustration of these quantities.

In the spectrometer a measurement of an event's position and angle at the focus determines the values of X_o, θ_o, ϕ_o and δ. Momentum dispersion occurs in the vertical plane, while events with different incoming θ_o's are dispersed horizontally. At the detector focus, particles of the same momentum are focused to equal values of Y, the vertical displacement, independent of the incoming vertical angle ϕ_o. The vertical angle in the detector, ϕ, depends on ϕ_o as well as momentum, δ. In the horizontal plane, the focusing is line to point; i.e., incoming parallel rays are focused to a point. Thus, the X position in the detector is proportional to the incoming horizontal angle, independent of the event's position at the target, X_o. The horizontal angle in the detector θ, depends upon the initial X_o (at the target) as well as the incoming angle, θ_o. Refer to Figures II-5 and II-6 for a drawing of the focal properties of the spectrometer.

The above descriptions are only correct to first order. The focusing properties of the spectrometer are summarized by a transformation matrix which relates the incoming parameters (X_o, θ_o, ϕ_o, δ) to the track parameters measured at the focal plane of the detector (X, Y, θ, and ϕ). If X_o represents the incoming parameters and X the outgoing, then the expression

$$X_{o_i} = A_{ij}X_j + B_{ikl}X_kX_l$$

is the optical transformation (up to second order) where the A_{ij}'s are the first order optics coefficients and B_{ikl}'s are the second order coefficients. The values of the optics coefficients are given in Table III-1 and summarize our knowledge of the optical properties of the spectrometer. Note that to a good approximation, the vertical and horizontal focusing are decoupled; i.e., X_o and θ_o depend mostly on X and θ, and ϕ_o and δ depend mostly upon Y and ϕ. The optics

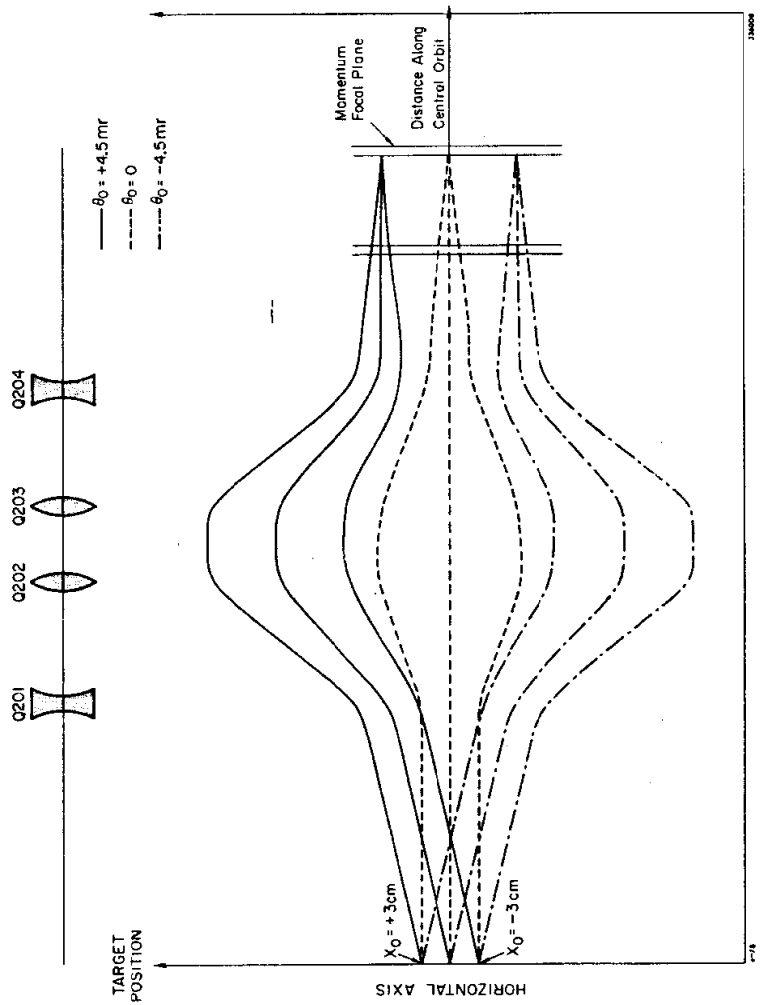

Fig. II-5
Horizontal plane first-order focal properties of the 20 GeV spectrometer.

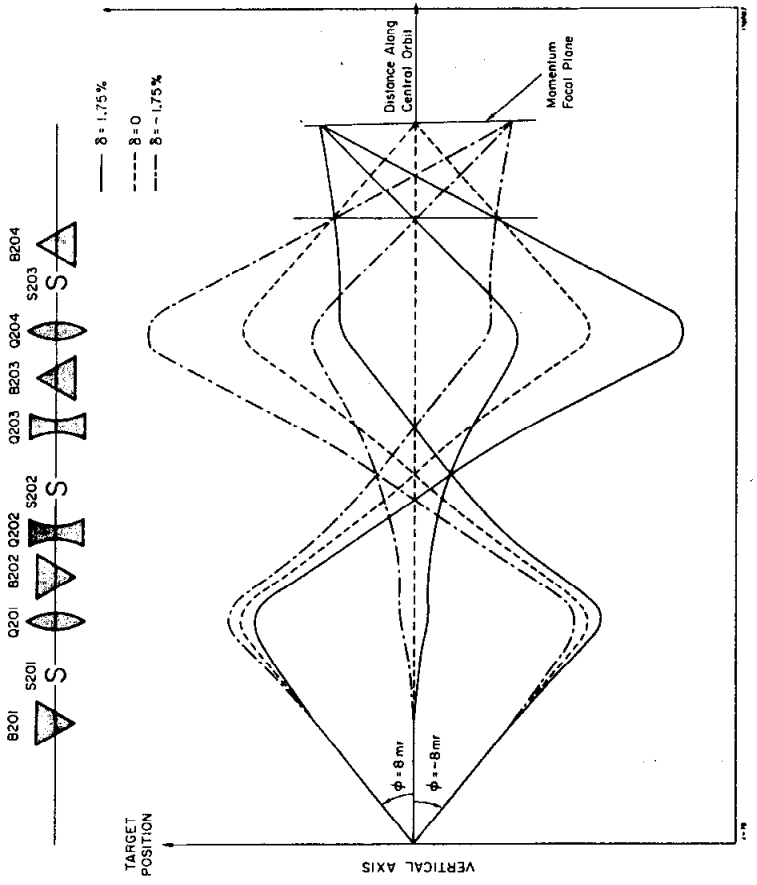

Fig. II-6
Vertical plane first-order focal properties of the 20 GeV spectrometer.

coefficients were measured in 1967 and were partially remeasured in the course of our experiment. For a detailed account of our knowledge of the spectrometer optics and acceptance, see Appendix A-1 and the sub-section on the acceptance and optics in Chapter III.

Resolution

The accuracy of the measurement of Θ_0 and the momentum resolution of the spectrometer determine the mass resolution of the experiment. High resolution is of relevance for W<2 GeV data where narrow resonances are excited in the scattering. Finite resolution arises from a number of factors; lack of knowledge of the optics coefficients, misalignment of magnetic elements, drifts of magnet currents, multiple scattering within the spectrometer, and wire spacing in the PWC's. The theta resolution of the spectrometer is about .1 milliradian, but the dominant source of theta resolution in the experiment arises from multiple scattering in the target of .28 milliradians (at 7.5 GeV). The momentum resolution is about .075%.

Lack of knowledge of the optics coefficients can broaden the momentum (or theta) resolution if two tracks of equal momenta (or theta), but varying in some other quantity, are assigned to different bins because these (unmeasured) quantities affect the final position of the track through the hut. Intrinsically, we do not know Y_0 to better than ±.1 cm, X_0 to ±.5 cm, and ϕ_0 to ±2 mrads. Insofar as X or Y in the hut depends on these quantities, and Θ_0 and δ are calculated from X and Y, then errors will feed through and result in momentum and anglular resolutions of .05% and .06 mrads, respectively.

Multiple scattering in the detector affects the resolution by changing a particle's position (X and Y) at the momentum focus. The amount of material in the detector upstream of the focus is approximately .015 radiation lengths, so that ΔX = .05 cm at $E' = 7.5$ GeV, or a contribution to the momentum and theta resolution of .017% and .03 mrads, respectively. In addition, there are approximately 2.5 x 10^{-2} radiation lengths of material between the center of the target and the spectrometer. This smears Θ_0 by .28 mrads at 7.5 GeV.

Strictly speaking, these effects are not part of the spectrometer resolution, but they contribute to the overall θ_o resolution in the experiment and so are included here.

The currents in the magnets are controlled by regulated power supplies which are subject to small drifts. The currents were read and logged by the computer every 10 minutes, and we used no data in which a magnet's current was outside tolerance. Table II-3 lists these tolerances. A Monte Carlo model of the spectrometer was used to calculate the contribution to the resolution due to drifts within tolerances. The resulting resolution was .045% in momentum and .019 mrad in θ_o.

The wire spacing of the proportional chambers is 2 mm. This means that the X or Y position of a track is known to ±.1 cm. The θ_o resolution due to this is .06 mrads, and the momentum resolution is ±.03%.

Adding the above effects in quadrature, the resolution of the spectrometer as used in this experiment is: momentum .075%; theta .09 mrads.

Acceptance

The acceptance of the spectrometer is the product of its solid angle ($d\theta_o\ d\phi_o$) and its momentum acceptance $d\delta$. The acceptances in δ and θ_o are determined by software limits of ±1.75% and +3, -3.75 milliradians, respectively. The range of ϕ_o is limited by horizontal jaws at the spectrometer entrance to ±8 milliradians. The "nominal" acceptance of the spectrometer is then

$$\text{Acceptance} = d\delta d\theta_o d\phi_o = 3.5\% * 108\ \mu\text{steradians}$$

However, the actual acceptance is limited somewhat further by physical apertures within the spectrometer itself. We used a Monte Carlo simulation of events "swum" through a model of the spectrometer in order to calculate a correction for these apertures. The correction varies with angle (2% at 6° to 6% at 20.6°), and details are presented in Appendix A1.

Systematic Errors Arising From the Spectrometer

Systematic errors in the cross sections due to lack of knowledge of the spectrometer optics or acceptance could be as large as 5% and are described in detail in Appendix A1. Briefly, the two largest sources of error are in the acceptance and in the dispersions. The acceptance is calculated using Monte Carlo methods and is always within 6% of the nominal acceptance. We estimate a possible 2% error in the cross section arising from uncertainities in this calculation.

In first order, the dispersions are the proportionality constants relating δ (or θ_o) to Y (or X). When we set software limits for the acceptance in δ and θ_o, the corresponding limits on X and Y are affected by errors in dispersion. Such errors are reflected in the cross section because the number or counts binned into a certain $\Delta\delta$, $\Delta\theta_o$ bin is proportional to the product $\Delta X \cdot \Delta Y$. We estimate that errors in the θ_o dispersion could be as large as 1%, and in the P disperison 3%, yielding a possible 4% error in the cross section due to lack of knowledge of the spectrometer dispersions. Several smaller effects bring our estimate of the total spectrometer-related systematic error to 5%.

The detector assembly was approximately seven meters long, located in the shielded concrete room at the downstream end of the spectrometer. The entire detector is mounted on two sets of rails and can be moved with the spectrometer to different scattering angles. A layout of the detector arrangement within the shielding hut is given in Figure II-7, and a summary of its construction and performance is outlined in Table II-4. The detector counted the number of particles which passed through the spectrometer, identified those which were electrons, and determined particle trajectories. To accomplish these tasks, the detector assembly consisted of 11 counters; an atmospheric-pressure nitrogen gas Cerenkov counter; three plastic scintillator counters which defined the aperture, TR1, TR2, and TR3; five proportional wire chambers, each with a single plane of wires; a lead glass shower counter 4-radiation lengths thick; and, finally, a 16-radiation length total absorption (TA) shower counter composed of lead sheets interleaved with scintillator. The last 2 counters are designed to sample the showers produced by moving particles. In the 4-radiation length glass counter (called the pre-rad), electrons usually deposit much greater energy than an ionizing particle. The electron deposits its remaining energy in the TA counter, and the signals from the pre-rad and TA are added to give a signal proportional to the electron energy.

The pulse heights of signals from the Cerenkov counter and from the combination of pre-rad and TA were digitized, and cuts placed on their values defined those particles which were electrons. Although some hadrons (mainly, pions) satisfied these "electron" criteria, the hadronic background beneath the electron signal is small and is described in Chapter III under the subsection, "Pion Subtraction".

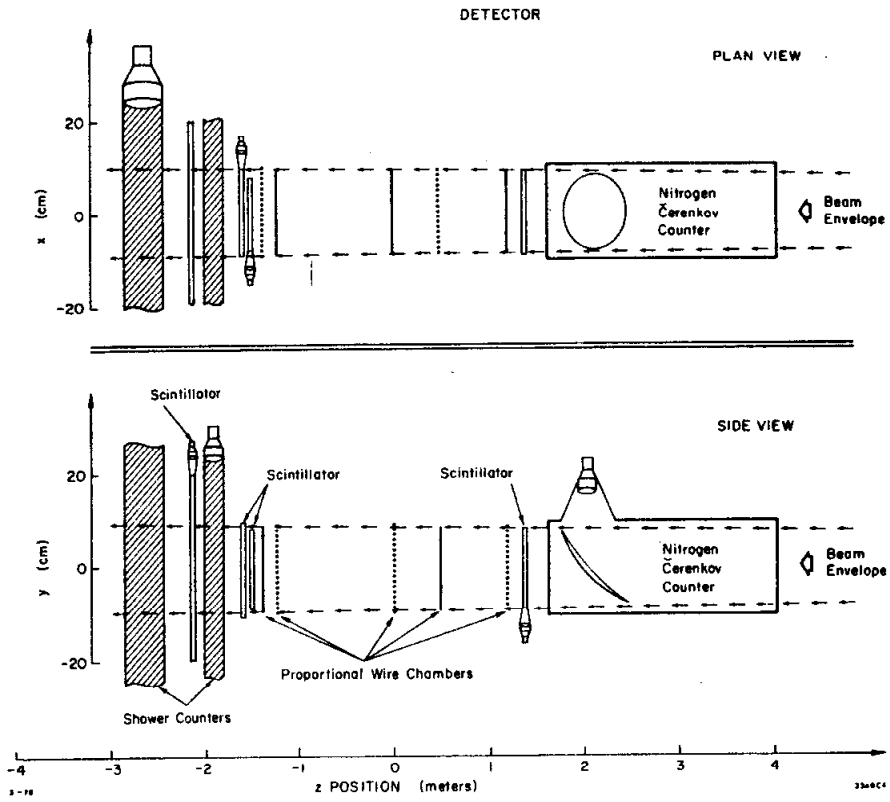

Fig. II-7

A drawing of the detector set-up within the shielded concrete room located behind the spectrometer magnets. The position and size of the counters are shown. There are a total of 460 wires in the proportional wire chamber system.

TABLE II-4

DETECTOR CONSTRUCTION AND PERFORMANCE

Counter		Dimensions	Construction and Comments	Efficiency (electrons)	Efficiency (pions)
Cerenkov		2.4 meters long 12" diameter	Nitrogen gas (atmospheric pressure), spherical mirror, 5" tube,.002" Al windows, σ/μ = .35 (average of 12 photoelectrons per electron event)	>99.8%	Critical momentum (π's) = 5.65 GeV Eff (π's <P crit) ≈.01
TR1		±8.01 cm (Y); ±9.03 cm (X); 3/16" thick	scintillator used in trigger	>99.5%	>99.5%
TR2		±9.13 cm (Y) ±7.91 cm (X) 1/4" thick	scintillator not used in trigger	>99.5%	> 99.5%
TR3		±9.49 cm (Y) ±8.50 cm (X) 1/2" thick	scintillator used in trigger	>99.5%	>99.5%
PWC	Y1	80 wires (2 mm)	4 mm spacing (H.V. to wire plane); 2 mm wire spacing; H.V. 2700 volts, 48 nsec gate; 5 chamber telescope ≈2.5 m long; near momentum focus of spectrometer	individual chamber track inefficiency .5 - 2%; track reconstruction efficiency of system ≈94%	
	X1	96 wires			
	Y2	88 wires			
	X2	96 wires			
	Y3	104 wires			
Shower	Pre-radiator	4.3 r.l. thick 30 cm x 30 cm x 14 cm	Two 5" tubes on 30 cm x 14 cm face, Schott F2 lead glass	>99.8%	≈18%
	Total absorption	16 r.l. thick; 35 x 35 cm	16 layers of lead and Lucite, one 9" tube, 5% decrease of signal size across aperture away from tube, σ/μ (SUM) = 7% at E = 7 GeV	SUM efficiency ≈99.8%	SUM efficiency ≈5%

Briefly, the detector functioned as follows. The master event trigger was a three-fold coincidence between TR1, TR3 and (a greater than minimum ionization) signal from the total absorption counter and the pre-radiator. This signal was a weighted sum of the pre-radiator and total absorption counter outputs and was, in general, well above threshold for incoming electrons. An alternate trigger consisted of a two-fold coincidence between the Cerenkov counter and this sum signal. On receipt of a trigger signal, pulse height information can be used to identify electrons. In addition, each wire of the 5 PWC's was interrogated to determine if it had a voltage pulse in time with the event and, if so, an appropriate bit was set. The computer used these bits of information to reconstruct the track of the detected particle. We proceed with brief descriptions of the individual counters.

Cerenkov Counter

The Cerenkov counter was approximately 2.4 meters long. It was fabricated from a section of aluminum pipe 12 inches in diameter. On either end were vacuum flanges holding thin windows 8 inches in diameter made of .002" aluminum foil. At a distance of approximately 180 cm from the upstream window was a thin mirror which reflected the Cerenkov light through 90 degrees into a 5-inch DVP phototube. The design of the mirror for this counter was determined by Monte Carlo calculations which estimated the light from particles passing through a model of the spectrometer. The radius of curvature of the mirror (69 inches) was adjusted to maximize the amount of light reaching the phototube.

The base of the mirror was formed by a 1/16" thick Lucite sheet which was slump molded to the proper radius. When cold, the front surface of the Lucite was coated with aluminum and magnesium fluoride to form the mirror surface.

A layer of aluminum several thousand angstroms thick was deposited on the mirror by vacuum deposition, and this was followed immediately by the deposition of a 200A° layer of magnesium fluoride.

The magnesium fluoride protects the aluminum and prevents its oxidation or corrosion.

The phototube used was a 58 DVP with a bi-alkali cathode. The face of the tube was coated with a thin layer (.3 mg/cm^2) of p-terphenyl[5] and 140A$^\circ$ of magnesium fluoride. This layer converts ultraviolet photons (1100 to 3600A$^\circ$) into photons of ≈3850A$^\circ$ which are then detected by the phototube. The response of the phototube is effectively shifted towards the ultraviolet by this technique.

In order to be efficient in its electron response and effectively reject pions, a gas Cerenkov counter must be sufficiently long so that ≈50 photons strike the phototube. The choice of a gas is not critical, provided that the number of "knock-on" electrons from pions traveling through the gas is small and that the gas not absorb the Cerenkov light. Nitrogen is an inexpensive, safe, and convenient solution.

The width of the pulse height distribution observed for a sample of electrons is a measure of the fluctuations of the light output of the counter. The ratio of signal width to mean, sigma/mu, was approximately .35 for the Cerenkov counter. Knowing the quantum efficiency of the tube to be ≈20%, this value of the ratio indicates that there were approximately 60 photons incident upon the tube face for each electron, which agrees well with calculations for nitrogen gas. For an illustration of the Cerenkov performance, see Figure II-8.

The Cerenkov counter's inefficiency for detecting electrons (as determined from pure electron samples in elastic peak runs) is displayed versus the position of the cut. Overplotted is the efficiency on pions versus cut position. The pion efficiency was determined during runs in which a 3-radiation length thick lead plate was inserted into the spectrometer to stop electrons and to provide a pure pion sample. The position of the cut chosen for the analysis insured that the Cerenkov counter was ≈99.9% efficient on electrons while still rejecting pions.

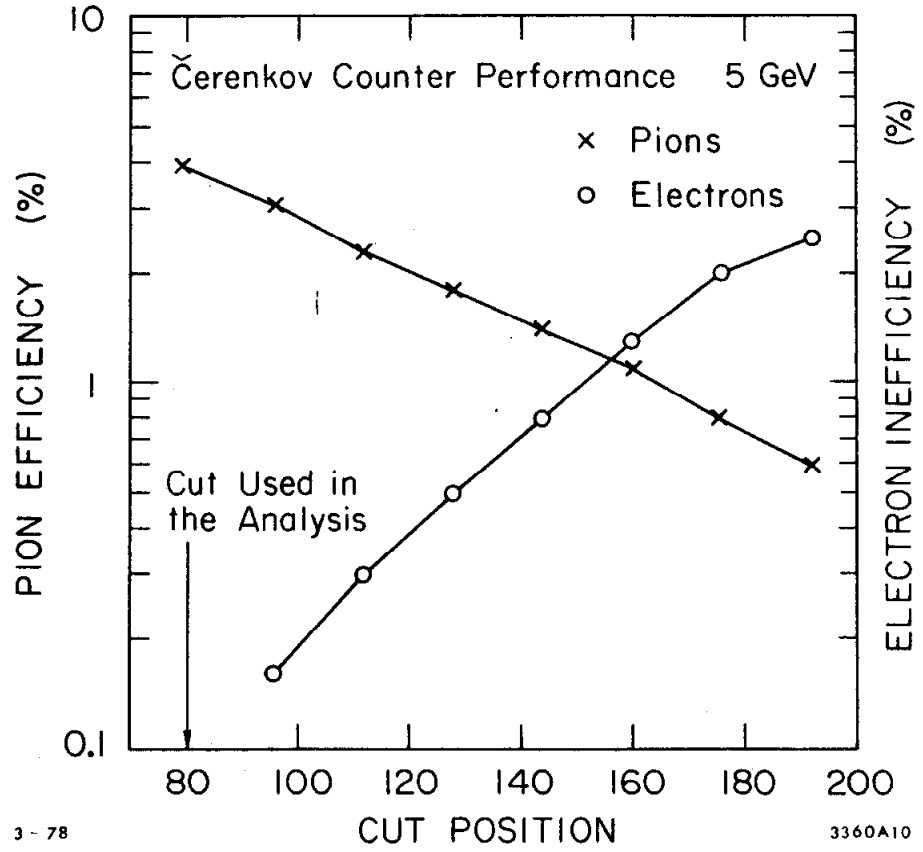

Fig. II-8

The efficiency for pions and inefficiency for electrons for given cuts on the Cerenkov counter pulse height is plotted against the position of the cut (in PHA channel numbers).

Pre-radiator and Total Absorption Shower Counters

The "pre-radiator" is the first element in the total absorption shower counter package. By dividing the shower counter into two parts, we can increase the discrimination between electrons and hadrons of the same momentum. In this experiment, pions form the main background.

Electrons begin to cascade in the counter, and for any particular incident energy there is an optimum length of pre-radiator. The thicker the counter, the larger the electron signal relative to the minimum ionizing hadronic signal. For small thicknesses, the pion signal increases linearly with length; whereas the electron signal, because it is from a cascade mechanism, increases exponentially at first. If the counter is long enough, the pion will interact and possibly charge exchange to produce an electromagnetic cascade. The pre-radiator was designed and constructed to be 4.3 radiation lengths long so that its maximum e/π discrimination would occur in the 2-3 GeV range where we need the best discrimination between pions and electrons.

The pre-radiator was constructed from a block of Schott F2 lead glass 30 cm x 30 cm x 14 cm in size. Two 5-inch 58 DVP phototubes were placed on one of the 14 x 30 cm faces. The glass and phototube were coupled by means of oil which had an index of refraction between that of the lead glass and the tube face. At 3 GeV electron energy, the pre-radiator thickness of 4.3 radiation lengths corresponds closely to "shower maximum", the point in the cascade with the maximum number of secondary particles present. Figure II-9 shows the pre-radiator performance on electrons and pions. Note that for the cut position chosen, the efficiency on electrons is high while still rejecting pions.

Following the pre-radiator is a lead Lucite sandwich counter which absorbs almost all of an electromagnetic shower at these energies. It is referred to as the total absorption (TA) counter, and consists of 16 slabs of lead each 1 radiation length thick and

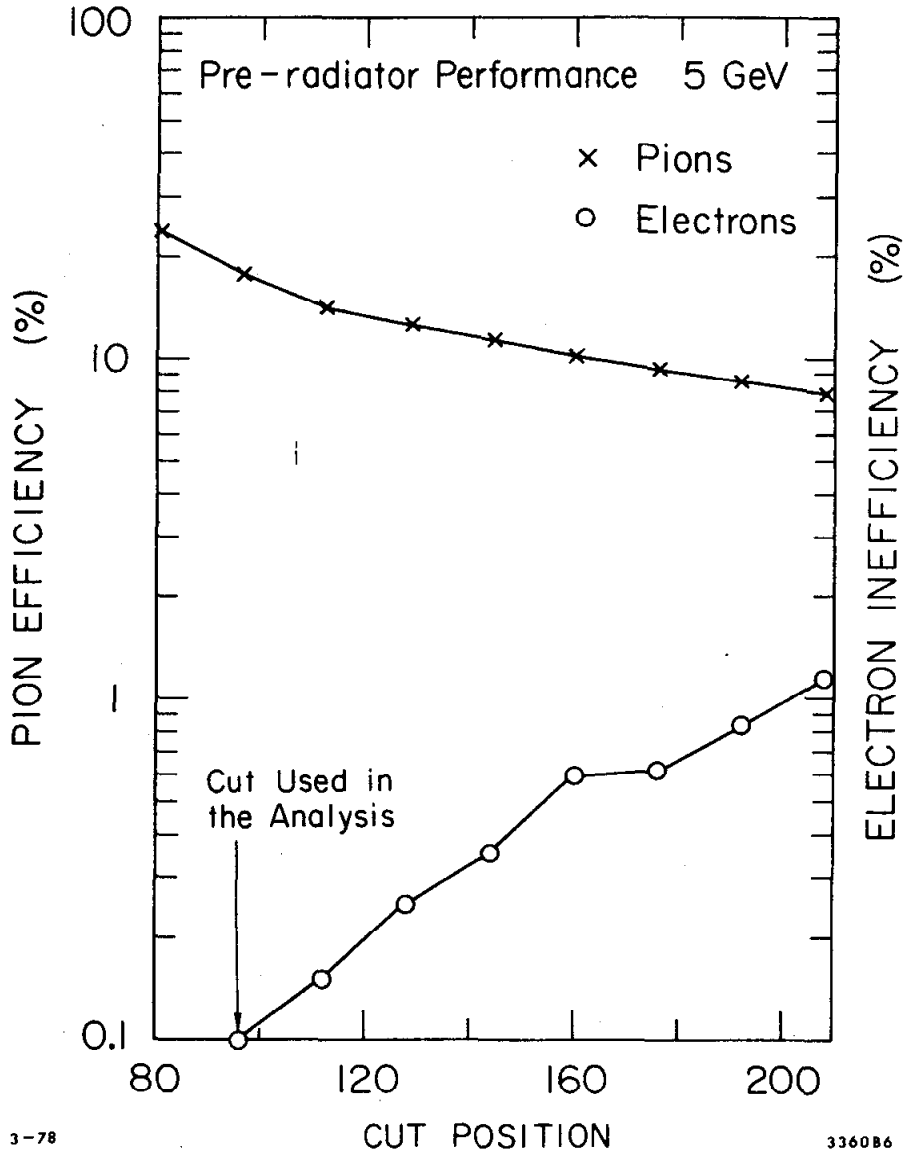

Fig. II-9

The efficiency for pions and inefficiency for electrons of a cut on the pre-radiator pulse height is plotted against the position of the cut.

each followed by a 1/4" thick piece of Lucite. Light pipes conduct the light from the Lucite to a single 9" photo multiplier tube. The response of the counter was dependent on the position of the incoming particle, the main effect being a drop of ≈5% in pulse height for particles entering the counter far from the phototube. This effect was corrected for.

As mentioned earlier, the shower signal used was a sum of the pulses in the pre-radiator and the TA. Because the pre-radiator and the TA were completely different counters constructed from different materials, their responses to electron showers were different. We wanted a summed signal from these two counters to have as narrow an electron peak as possible. In order to produce a narrow peak, the signal output from each counter must be proportional to the energy deposition in that counter. To balance the signals, it was necessary to weight them using different attenuators before summing the two signals in a passive network. The relative weighting was determined empirically by minimizing the ratio of width to mean for the sum signal at an energy of 2.3 GeV. Sigma/mu for the sum was about 7% at 7 GeV. Figure II-10 illustrates the sum counter's efficiency on pions and inefficiency on electrons. At the cut position used in the analysis, the sum is ≈99.9% efficient on electrons yet has a low probability that a pion will produce a signal above the cut.

Scintillator Trigger Counters

There were three scintillator counters, TR1, TR2, and TR3. TR1 was 3/16" thick x 18 cm (horiz.) x 16 cm (vert.). TR2 was 1/4" thick x 15.8 cm (horiz.) x 18.2 cm (vert.). TR3 was 1/2" thick x 17 cm (horiz.) x 19 cm (vert.). TR1 was located immediately behind the Cerenkov counter and preceding the 5 proportional wire chambers. Its thickness was chosen such that it would be greater than 99% efficient on minimum ionizing particles, since it is used in the trigger, yet it had to be as thin as possible to reduce the number of knock-ons produced which would proceed through the wire chambers and confuse the reconstruction of tracks.

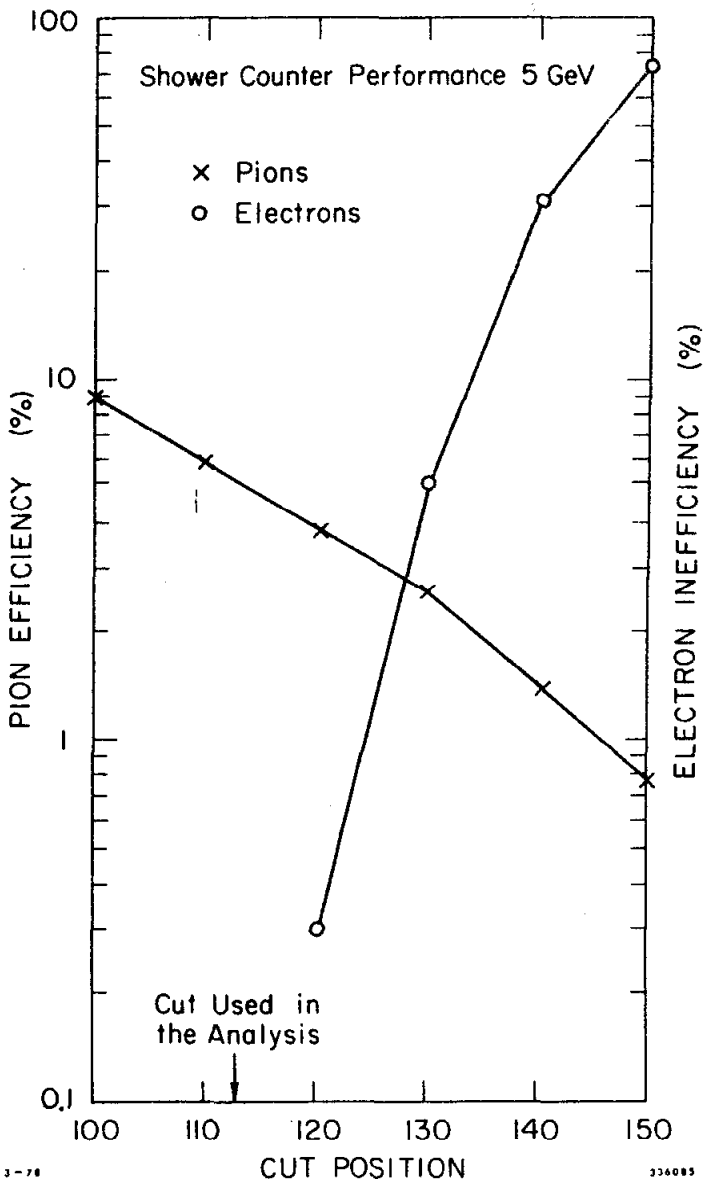

Fig. II-10

The efficiency for pions and inefficiency for electrons of a cut on the "sum" pulse height (which is a sum of both parts of a segmented shower counter) plotted against the position of the cut.

TR2 and TR3 were located immediately behind the proportional wire chambers. TR3 is included in the triple coincidence for the master trigger. Its thickness was chosen such that its efficiency on minimum ionizing tracks would be greater than 99%. The horizontal and vertical dimensions of TR3 were chosen so that this counter would define the aperture and, hence, the solid angle, of the spectrometer. However, deviations of the actual spectrometer from the model used made this only an approximation, although a good one. In the offline analysis, software cuts using wire chamber information actually defined the acceptance.

TR2 is slightly smaller than TR3 and is located immediately before it. It is not used in the master trigger definition. It was used in the on-line efficiency logic during the course of the experiment, primarily to monitor the TR3 efficiency. Since it is smaller than TR3, a track passing through TR1 and TR2 must strike TR3. Counting the percentage of times TR3 fires gives its efficiency.

Trigger Efficiency

The efficiency of the master trigger TR1·TR3·SUM was monitored during the course of the experiment and measured in the offline analysis in the following way. An alternate trigger ($\overline{C}$·SUM) was defined. The number of events in which this alternate trigger fired and the wire chamber tracking information indicated that the particle passed through TR1 and TR3 was counted. From this sample, the percentage of time that the master trigger fired could be obtained. This efficiency was greater than 99.5%.

Proportional Wire Chambers

The proportional wire chambers provided information about the position and angle of a particle's trajectory through the detector. When this was coupled with the optics coefficients of the spectrometer, the scattering angle and the momentum for that particle could be deduced.

There were five wire chambers, each containing one plane of wires. Each chamber was about 20 cm square in aperture, large enough to be greater than the trigger aperture defined by TR3. Each chamber consisted of 80-100 wires spaced 2 mm apart and separated by .4 cm from the high voltage screen. Each wire was connected to a pre-amplifier, and the signal from the pre-amp was typically a few hundred nsec long and .7 volts. The signals were read into a latch in coincidence with a 48 nsec gate. The latches were interrogated and read by the on-line computer.

The inefficiency of each chamber (that is, the number of times a particle passed through and no wires fired) varied from .5% to 2%. Track reconstruction efficiency (dealt with more extensively in the sub-chapter by that name) averaged around 94%.

The average particle fired 3-4 wires as it passed through a chamber. Since the wire spacing was 2 mm, the centroid of the bunch could be determined to better than 1 mm, and this spatial resolution matched well the intrinsic resolution of the spectrometer.

ELECTRONICS

Because of the complexity of information, use of an on-line computer was an essential part of the data gathering. The electronics in this experiment is the link between the analog signals from the detector assembly and the digital information flow into the computer. The electronics was designed to process photomultiplier signals from the detector and decide if the event satisfied certain criteria. If the event satisfies these criteria, a start pulse is sent to the computer which reads in all the event information. We attempt to define the criteria so that electron initiated events are read into the computer with nearly 100% efficiency while the vast majority of those initiated by a hadron are rejected.

Description

There were 12 signals from photomultiplier tubes in the detector; an anode and a dynode signal from each of the six counters. These were the three plastic scintillator counters which defined the aperture (TR1, TR2, and TR3), the Cerenkov counter, two tubes on the 4-radiation length lead glass pre-radiator, and a single tube on the lead-scintillator sandwich total-absorption counter. The anode signals from the two tubes on the pre-radiator were added at the counter, and one signal was sent to the electronics located in the experiment's control center, known as the "counting house"; similarly for the dynodes.

The signals from the anode and dynode of each of the tubes were sent up to the electronics logic circuitry via low-distortion heliac air-core cables with a velocity of propagation of ≈.98C. The cables all were ≈600 nsec long.

Cable lengths were adjusted so that the signals arrived simultaneously at the input to the electronics circuitry in the counting house. These signals were then split with part of the signal going to the pulse height analysers and the other part into discriminators and then into the logic circuits. At this point, the pre-radiator and TA signals are passively summed to form the sum signal. The outputs from the discriminators were used to form various logical quantities. The logic for a master trigger of the system is simple; it is a triple coincidence (C3) between TR1, TR3, and the discriminator output of the sum signal. In the second half of the experiment, this simple trigger was expanded. In addition to the master trigger, a trigger was obtained by a double coincidence of the Cerenkov and sum signals. In this way, we could sample events off-line which contained the second part of the trigger and had a track within the TR1, TR3 aperture and determine the triple coincidence (C3) efficiency.

Firing of the master trigger initiated three separate "gate" pulses of different lengths. One was used to determine whether a number of various discriminator signals had fired simultaneously with the master trigger; a coincidence of this (36 nsec) gate with a particular signal indicated that the signal occured in time with the trigger and an appropriate "flag" bit was set and read by the computer.

A second pulse of 48 nsec was used as a coincidence gate for the pulse height analysers (PHA) on the different counters. The third pulse (40 nsec) was used by the PWC processor unit which read the individual wires firing in time with this gate. There were two identical sets (or levels) of logic circuitry used to produce these gate signals; the second was used in cases where there was a second event occuring during the beam pulse. The losses due to three or more events per pulse were corrected for using a method described in Chapter III, Analysis, in the sub-section on corrections and subtractions (rate effects).

Pedestals

The "pedestal" of a pulse height analyser (PHA) is its digital output (or "channel" number) when there is no input signal in time with its gate.

In order to monitor pedestal drifts, a special circuit was set up which every 10 minutes measured the pulse height from each of the PHA's when no beam was present; i.e., it directly measured the pedestal offset.

RUNNING THE EXPERIMENT

This section describes the data taking procedures followed in the experiment and the procedures for monitoring of the performance of various pieces of equipment.

The measurement of a cross section involved the following steps:

1) Selection of a spectrometer angle. Setting the spectrometer to a new angle involved surveying the magnet positions. Because this survey required three to four hours (and also to facilitate radiative correction calculations), we stayed at one angle during measurements at several different beam energies. For each angle, the survey established a reference line for the spectrometer. The magnets should be in a vertical plane containing this line. The centers of the quadrupoles were always within .008" of this vertical plane; this is within the tolerances (i.e., affecting track positions by less than the resolution). The axis of the spectrometer always pointed to the spectrometer pivot within .03". The roll of the first bending magnet was always less than .16 mrads, well within the tolerance of ≈.6 mrads. The position of the centers of the two ends of the detector was measured to be within 3 mm of the vertical plane through the center of the spectrometer; this could introduce changes in our cross sections as large as 1% due to the offset of the central scattering angle. These offsets were corrected for in the analysis.

(2) Set up the beam parameters. We chose the energy and the energy spread we wanted, and the beam operators adjusted the number and power of the klystrons to deliver a beam of the proper energy into the Beam Switch Yard where the momentum slits defined the spread. Because setting up a beam at a new energy required several hours' time, we ran data at many spectrometer settings for a particular angle and beam energy.

The beam was focused to its nominal spot size at the target (3 mm (h.) x 2 mm (v.)), and steering was adjusted to center the beam on the target. The steering was set up with the aid of three ZnS screens, two upstream of the target and one downstream. This third screen was left in during data taking, allowing the experimenters to observe any changes in the beam position. The beam pulse shape was monitored by displaying the signal from a scintillator located in ESA on an oscilloscope. If beam spill or position deviated from the norm (i.e., a flat pulse 1.5 μsec long), the operators were informed and would remedy the problem.

The toroidal charge monitors were regularly calibrated by dumping a standard charge on a capacitor through an extra one-turn winding on the toroid and were occasionally cross-calibrated with a Faraday cup.

(3) Set the spectrometer momentum. For each beam energy and spectrometer angle setting, data were taken at many different values of the spectrometer momentum setting. A sequence of runs at constant beam energy and spectrometer angle is called a "line" of data. The current setting in the magnets was controlled by the on-line computer. We always established a definite magnetic history for the magnetic values; changing current so that hysteresis effects would not lead to different field strengths for a given current. Our standard procedure was to begin a sequence of runs at high spectrometer momentum and to move down in current. The current in the magnets was continually monitored by the on-line computer which stopped the data taking if the currents were outside tolerances.

(4) Select a target. For each value of beam energy, spectrometer angle and energy, we took data sequentially on the hydrogen, deuterium, and empty target. This minimized errors in the D/H ratio because the runs were taken close together in time, at similar beam conditions, etc.. Since the H_2 and D_2 cells were of identical construction, the empty target run provided data for corrections on both targets.

(5) Initialize computer program. The on-line computer read and logged on tape the initial conditions for a data run: the beam energy, spectrometer angle and energy, target type, etc.. It set all scalers to zero and checked that all monitors were initialized.

Because the nine lines of data taken with the 1.6 GeV spectrometer were taken simultaneously with the 14 lines of 20 GeV spectrometer data, sharing beam and target, the scheduling of the running was a complex chore. The scheduling was arranged beforehand and stored on the on-line computer which prompted the respective experimenters with the next item on the data taking agenda.

6) "Begin the run." There were several different kinds of data flowing into the computer. The first was "event" data which was logged on tape. For each hardware trigger, the computer read the track information from the PWC coincidence latches, the flag bits indicating various discriminator and coincidence signals in time with the event, and particle identification information from the pulse heights of the counter signals. Second, was "pulse" data. For each beam pulse, the computer read the beam charge measured by the toroids. Third, was data for monitoring equipment. At fixed time intervals, the computer read the target temperature, pressure, and position, the central beam energy, drifts of pedestals, and spectrometer magnet currents, etc.

7) Monitoring the experiment's performance. During the course of the experiment, the beam operators tuned the accelerator in order to maintain the beam. The experimenters monitored a number of experimental aspects and the on-line computer made many kinds of on-line checks to identify possible problems.

Our procedures to insure that the counters were performing well were several: regular checks of counter high voltage and gas flow, monitoring of the average pulse heights of the counters versus E′, graphical display of the counters' efficiencies on various on-line "electron" and "not electron" triggers. Counter performance was also monitored by following various ratios of scalers in time. Equipment breakdowns can manifest themselves as sudden shifts in these ratios. For example, a sudden shift in the TR1/TR3 scaler ratios enabled us to find a loss of beam pipe vacuum downstream of the target, which had had little effect on the cross section but had considerably worsened background singles rates.

An important feature of our data running was that we were able to calculate and display cross sections on-line. These were accurate enough to allow us to check them against previous data and assure ourselves that there were no major malfunctions or mistakes.

8) Ending data runs. At the end of a data run, which could be computer controlled by pre-setting the number of electron events desired, the computer read various scalers and the final values of

the various run parameters and stored all this information onto magnetic tape. The data from the approximately 1500 runs was written onto 46 (1650 b.p.i.) tapes, which were condensed and rewritten onto 11 (6250 b.p.i.) high density tapes for the off-line analysis.

9) Special data runs. In addition to the standard data runs, a number of specialized runs were conducted during the course of the experiment. These included "boiling" tests to insure that the target was not suffering from large density fluctuations, "jail bar" runs done to check the θ_o dispersion of the spectrometer, and "scanned" runs in which the spectrometer's central momentum was moved in small steps in order to "scan" a particular missing mass state (elastic and otherwise) across the δ,θ_o acceptance of the spectrometer.

The total time for data collection was ≈8 months with 1700 hours of accelerator time. The analysis of this data is described in the next chapter.

1. E49: A. Bodek (Ph.D. thesis), M.I.T. Laboratory for Nuclear Science, Report No. COO-3069-116 (1972).

E. M. Riordan (Ph.D. thesis), M.I.T. Laboratory for Nuclear Science, Report No. COO-3069-176 (1973).

A. Bodek et al., SLAC-PUB-1327.

E87: E. M. Riordan et al., SLAC-PUB-1634.

2. W. B. Atwood et al., Physics Letters 64B (1976), 479-482; "Electron Scattering off Hydrogen and Deuterium", W. B. Atwood (Ph.D. thesis), SLAC Report No. 185.

3. SLAC User's Handbook.

4. D. E. Yount, "A High Precision Faraday Cup and Quantameter For SLAC," Nucl. Inst. and Meth. 52:1 (1967).

5. E. L. Garwin, Y. Tomkiewicz, D. Trines, "Method for Elimination of Quartz-Face Phototubes in Cerenkov Counters by Use of Wavelength Shifters," Nucl. Instr. and Meth. 107, 365-70 (1973).

OVERVIEW

This chapter describes the analysis of the raw data which results in final cross sections and structure functions. For a flowchart showing the various quantities which enter into the determination of the cross section, see Figure III-1.

The cross section is given by:

$$\frac{d^2\sigma}{d\Omega dE'} = \frac{N_{scat}}{N_{in}N_{tgt.}(d\Omega dE')}$$

We must determine each of the quantities on the righthand side of the equation in order to calculate the cross section. We determine the number of target nucleons from measurements of the length and density of the target. The number of incident beam electrons is measured by the beam charge monitors. The acceptance is calculated with Monte Carlo methods using a ray-tracing program which "swims" particles through a model of the spectrometer. The model is checked by comparing the distribution of Monte Carlo events in scattering angle and momentum with actual data distributions accumulated in the experiment. N_{scat}, the number of scattered electrons, is the number of particles whose pulse heights in the various counters satisfy "electron" criteria and whose momentum and scattering angle (as determined from the positon and angle of the track through the wire chambers) fall within the selected bounds of the acceptance, corrected for a number of effects (dead time, track reconstruction inefficiency, trigger inefficiency, hadron background under the electron signal, etc.)

Each of the approximately 1500 runs are systematically checked for bad data. Examples include runs which had been aborted on-line because 1) the scalers had not been reset, 2) target was out of position, 3) beam was mis-steered, 4) the spectrometer's magnet currents were out of tolerance, etc. For more details, see the "Weeding" section in this chapter. Once the bad runs have been corrected or eliminated, we proceed to the correction for electrons which have

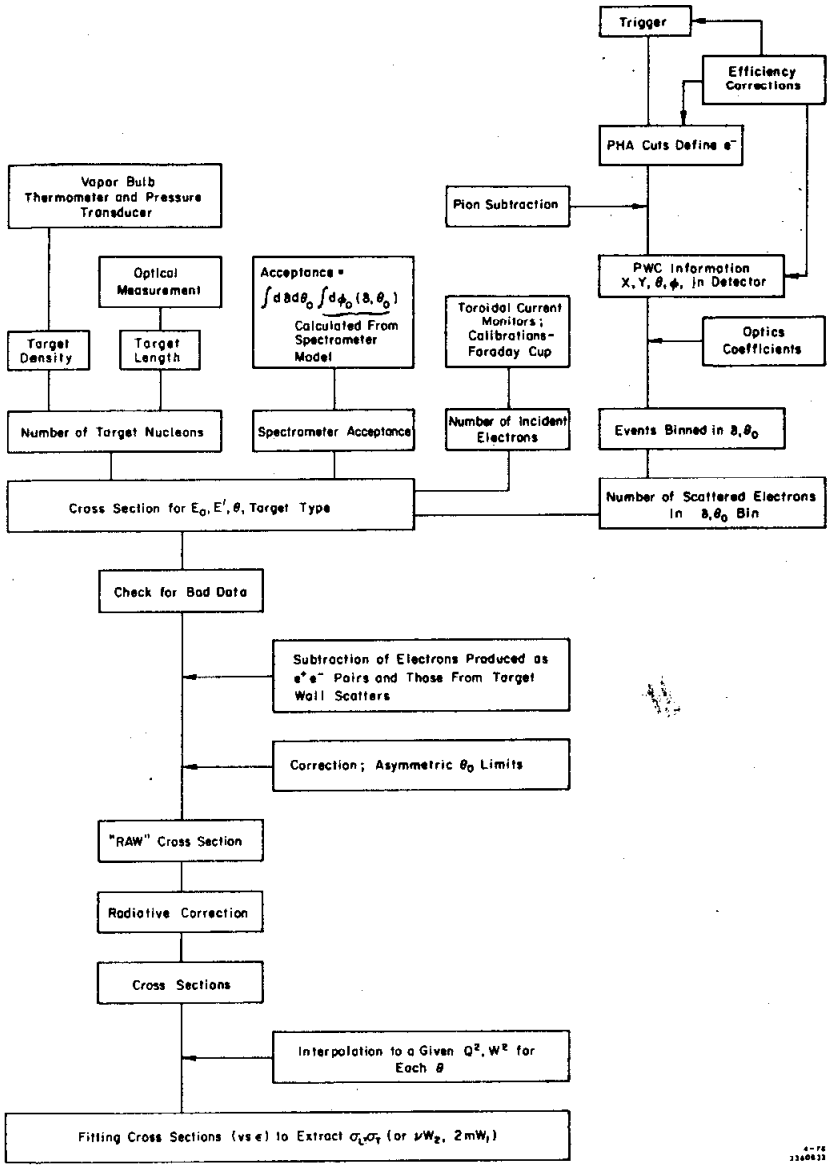

Fig. III-1

A diagram of the analysis used in determining a cross section and extracting the structure functions.

scattered, not from the liquid hydrogen or deuterium, but from the target walls. This correction is made by subtracting from the full target cross section the cross section from runs at the same kinematic point using an empty target cell. A subtraction is also made for those electrons which are produced in the target as e^+e^- pairs by measuring the cross section with the polarity of the spectrometer reversed (in order to count positrons).

The cross sections are then corrected for the effects of asymmetric θ_o limits of the spectrometer acceptance. If there are several runs at the same point or where the kinematics overlap, the measurements must be combined.

The result of this analysis is called the "raw" cross section. It is customary in electron scattering experiments to quote cross sections which have been corrected for radiation of photons during the scattering process rather than the raw cross sections which depend on the detailed experimental set-up.

After applying radiative corrections, we have final hydrogen and deuterium cross sections determined for different values of E_o, E', and θ. The data include cross sections for elastic as well as inelastic scattering. The analysis is the same for both except for slight differences in the radiative corrections. The cross sections are the primary results of the experiment. In order to determine separately the two structure functions, we require cross sections at the same Q^2, W^2 point for different angles. To do this, we must assemble data from several different experiments and, if necessary, interpolate cross sections to common values of Q^2 and W^2. For each angle we find the quantity

$$d^2\sigma/d\Omega dE'/\Gamma \equiv \sigma_t + \varepsilon\sigma_L$$

The structure functions are then determined by a linear fit in ε. In the remainder of this chapter we present a more detailed description of some of the procedures shown in Figure III-1.

ACCEPTANCE AND OPTICS COEFFICIENTS

In this section, the procedures used to obtain the 20 GeV spectrometer's optics coefficients and its acceptance are briefly described. The reader wishing more detailed information should consult Appendix A-1.

In order to determine the differential cross section $d^2\sigma/d\Omega dE'$, two things must be done: 1) decide whether electrons are within the acceptance on the basis of their measured momentum and scattering angle, and 2) calculate the acceptance ($d\Omega\ d\delta$), where $d\Omega$ is the solid angle and $d\delta$ the momentum acceptance of the spectrometer.

Optics Coefficients

In order to do the first, we need a set of optics coefficients which relate the scattered electron's position, angles, and momentum at the target (X_o, θ_o, ϕ_o and δ) to the positions and angles (X, Y, θ, ϕ) as measured by the PWC system located at the spectrometer focus in the detector. The set of optics coefficients actually used for this experiment is given in Table III-1.

These coefficients were obtained from three experimental sources: 1) The spectrometer's optical properties and acceptance were determined in an extensive set of measurements in 1967 in which a low intensity beam was directed into the spectrometer and the actual trajectory of the beam was measured. By fitting the position and angles of trajectories at the spectrometer focus to the incoming positions, angles, and momentum, the transformation matrix for the spectrometer was obtained. The elements of this matrix are the optics coefficients. 2) In the present experiment, data was taken with a set of evenly spaced vertical brass bars at the spectrometer entrance casting a well-defined "shadow" (swaths of constant θ_o) at the focal plane. The θ_o dispersion is adjusted so that these θ_o "swaths" coincide with the (surveyed) positions of the inter-jailbar gaps.

TABLE III-1

OPTICS COEFFICIENTS

1st Order

Incoming Parameters	Position and Angles at P Focus: X	θ	Y	φ
X_o	.0690	-1.622	-.0534	.0179
θ_o	F(E′)*1	-.0328	0.*2	-.0072
δ	.0037	-.0081	F(E′)*3	.0050
φ	.0411	-.0411	-2.138	1.280

*indicates new values; others are old

Higher Order

	XX	Xθ	X	Xφ	θθ	θY	θφ	YY	Yφ	φφ	XXX
X_o	.0060	-.0209	-.0350	.0278	.0156	.0108	-.0118	.0165	-.0229	.0076	-
θ_o	.0050*4	.0098	.0073	-.0058	-.0118	.0114	-.0070	-.0098	.0126	-.0040	.0004*5
δ	.0028	-.0028	-.0024	.0016	-.0030	.0050	-.0030	.0064*6	-.0056	-.0017	-
φ	.0222	-.0729	-.0022	.0018	.0545	.0030	-.0019	.0554	-.0849	.0304	-

*1 (θ_o/X) = .5780 + .00164 * E′; was .6232
*2 (θ_o/Y) was .0310
*3 (δ/Y) = .27653 + .001702 * E′; was .2988
*4 (θ_o/X^2) was -.0025
*5 (θ_o/X^3) was 0.
*6 (δ/Y^2) was .0043

New values used in this experiment; determined from measurements during the experiment.

Offsets of PWC centers relative to spectrometer central ray ($\theta_o, \delta = 0$)

Y offset: Y (.77 cm); was .64 cm

X offset:	6°	10°	15°	18°	20.6°	
At X_1 chamber	(.37,	.60,	.30,	.73,	.54)	- .018 * E′; was .46 cm
At X_2 chamber	(.22,	.52,	.13,	.69,	.44)	- ,018 * E′; was .40 cm

3) The momentum dispersion of the spectrometer can be obtained by observing the position of the elastic peak in the δ,θ_0 focal plane of the spectrometer.

The coefficients we use were determined from all three sources above. They differ somewhat from those obtained by fitting to the 1967 optics data alone; most notably in that the momentum and theta dispersion now appear to be momentum dependent. The change in the cross section using these new coefficients compared with cross sections using the old optics coefficients is a function of E′, given approximately by 0.8(12-E′)%. At E′ = 3 GeV, this constitutes a 7½% change in the cross section.

Because of this change, we carefully checked the new measurements of the optics coefficients (i.e., jailbar runs and elastic peak position studies) as well as reviewing the analysis of the 1967 tests. We found no mistakes in either study. Our best guess is that the difference between the new and the old optics coefficients is most likely due to changes that have occurred either in the spectrometer or its power supplies. We estimate errors in our cross sections as large as 4%, due to possible errors in the dispersions we use. We next discuss the calculation of the spectrometer acceptance.

Acceptance

In determining the acceptance of the spectrometer, we first choose limits on θ_0 and δ (calculated from the position of the particles in the wire chambers). The limits are chosen to correspond to trajectories which pass through the aperture-defining scintillation counters. The limits on ϕ_0 are defined by lead-tungsten slits at the spectrometer entrance (set to ±8 milliradians for the majority of the data taking). The acceptance is not merely the product of the three ranges ($\Delta\theta_0\Delta\phi_0\Delta\delta$) because there are apertures within the spectrometer which cut into this nominal acceptance. In other words, for a given θ_0 and δ, there may be regions of ϕ_0 for

which a particle passes through the ϕ_0 slits but strikes some aperture inside the spectrometer itself. With this in mind, we chose the θ_0 and δ limits such that at least 94% of all events (in a Monte Carlo simulation) which are within the θ_0 and δ limits and within the ϕ_0 slits will traverse the spectrometer without striking an aperture. The correction, therefore, to the nominal acceptance ($\Delta\theta\Delta\phi\Delta\delta$) is always less than 6%. This correction increases with angle (because the projected width of the target grows with spectrometer angle) and is calculated with Monte Carlo methods using a model of the spectrometer. The size of the correction is plotted versus scattering angle in Figure III-2. A detailed study of the model of the spectrometer and the solid angle, described in the Appendix, yields a systematic error of 5% in the cross sections arising from a lack of knowledge of optics coefficients and acceptance.

ELECTRON IDENTIFICATION AND HADRON REJECTION

Electrons were identified and the hadronic background (mainly, pions) was rejected on the basis of the pulse heights from 3 counters: the Cerenkov counter, the pre-radiator (the first segment of a two-part shower counter), and a signal from both parts of the shower counter, called "SUM".

We separate electrons from hadrons by imposing cuts on the pulse heights of the signals from these counters. The electron and hadron pulse height distributions have little overlap, so that the cuts are efficient on electrons yet exclude most of the hadrons. As an illustration of the combined use of the Cerenkov and pre-radiator pulse heights to identify electrons, see Figure III-3, which shows the Cerenkov versus pre-radiator pulse heights for a run at E′ = 3.5 GeV. Noting that the electrons and pions form separate clusters, it is apparent that the optimum cut to separate electrons from pions is not simply a cut on the Cerenkov pulse height and a

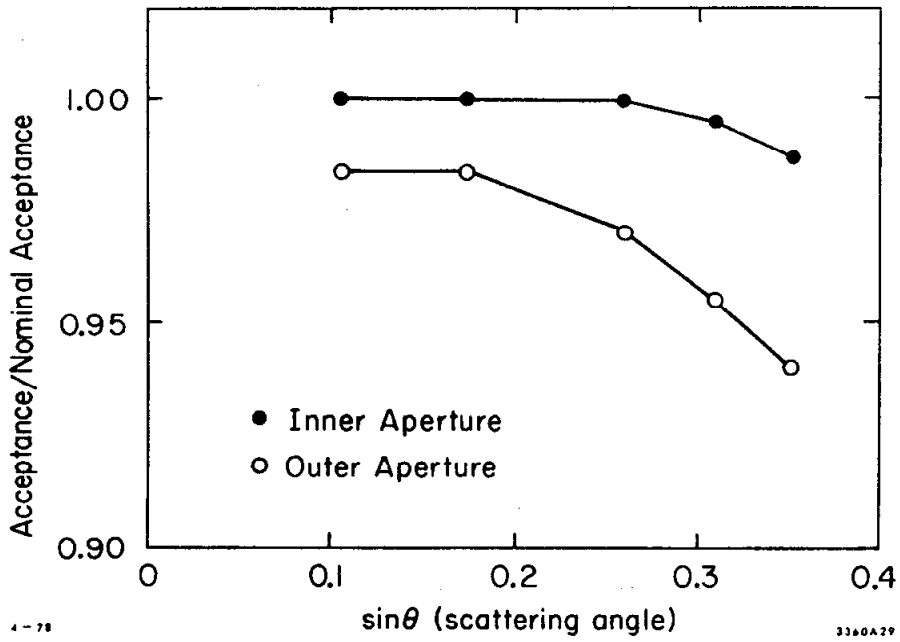

Fig. III-2

A plot of the spectrometer acceptance calculated using Monte Carlo methods, ray tracing, and a magnetic model for the spectrometer, normalized to the nominal acceptance, $\Delta\phi_o \Delta\theta_o \Delta\delta$ = 128 μsteradians * 3.5% momentum acceptance.

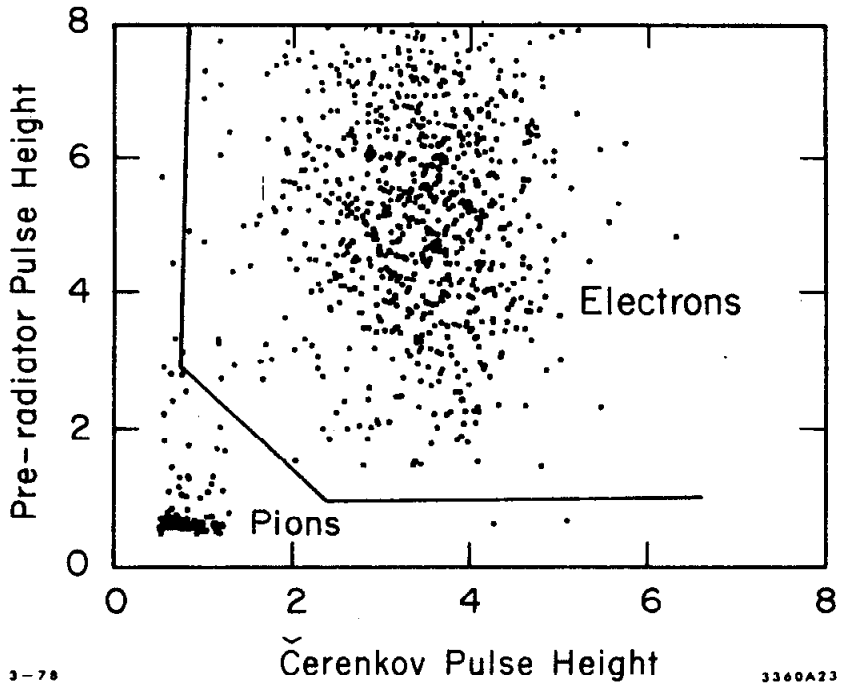

Fig. III-3

A scatterplot of the Cerenkov pulse height versus the pre-radiator pulse height for events from a run at E′=3.5 GeV. Electrons and pions form separate clusters of events. The electron cut we use is shown. It is about 99.8% efficient on electrons and less than 1% efficient for pions with momenta below ≈5.7 GeV. (Pion threshold in nitrogen gas Cerenkov counter is 5.65 GeV.)

second cut on the pre-radiator. Instead, we use the cut shown which separates the electron and pion samples while maintaining high efficiency (>99.8%) for electrons. Because the average pulse height for electrons in the pre-radiator grows only slowly with energy while that in the Cerenkov counter is constant, the same cut was used for all values of the energy.

Some pions give signals in the Cerenkov and pre-radiator which lie above the cut, especially when their momentum is greater than the pion Cerenkov threshold of 5.65 GeV. To reduce the pion contamination still further, we demand a cut on the SUM pulse height. See Figure III-4. The average SUM pulse height for electrons grows approximately linearly with energy, so the cut was dependent on energy and was set to near 3σ below the average pulse height.

These cuts eliminate all but a small fraction of the hadronic background; for most of the kinematic region, less than 1% of the signal was due to hadronic background. The worst contamination occurs when E′ is near 7 GeV, even though the incoming hadron/electron ratio is greater at lower energies reaching 30:1 at E′ = 2.5 GeV. The ratio of hadron triggers/electron triggers is never greater than 4:1 because of the hadron rejection of the trigger. Below 7 GeV, the Cerenkov counter can be used to discriminate against pions. The pion rejection using all the cuts is about 6000:1 below E′ = 5.65 GeV, and rises rapidly to ≈30:1 around E′ = 7 GeV. Above this energy the hadronic background drops rapidly. With a pion rejection of ≈30:1 and a π/E ratio as high as 5:1 at E′ = 7 GeV ($\theta = 6^{o}$, E_{o} = 19.5 GeV), there will be an approximately 16% hadronic contamination. This is the worst case; only 12 runs had hadronic contamination greater than 5%, the majority less than 1%.

Pion Subtraction

This remaining hadronic background (after the cuts) is eliminated by a procedure shown in Figure III-5. We first choose a sample of pions by selecting events with a Cerenkov pulse height less

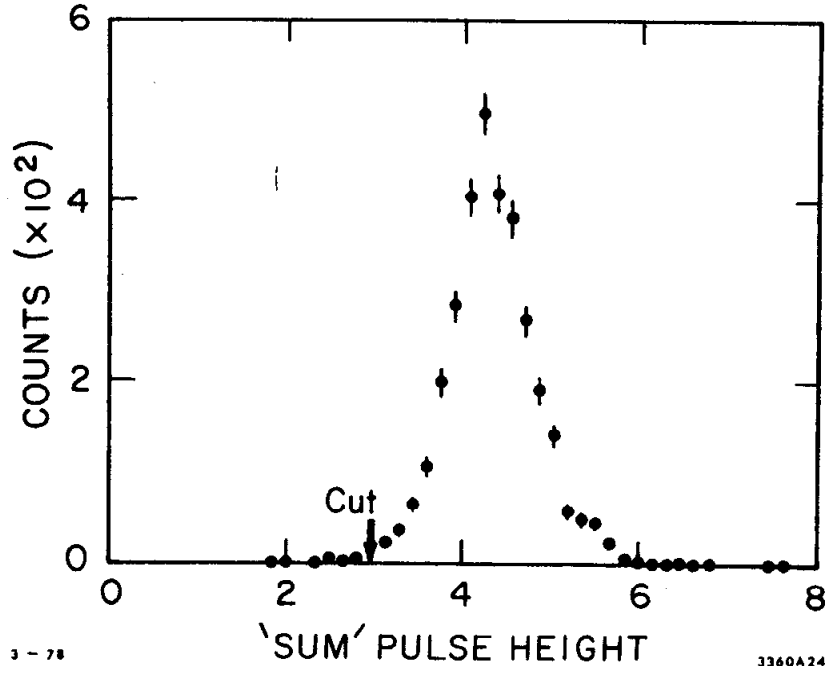

Fig. III-4

A distribution of the "sum" pulse height for events (from a run at momentum 3.5 GeV) which satisfied the electron cuts on the Cerenkov and pre-radiator. The position of a cut defining electrons is shown, and the efficiency of this cut is greater tha 99.5% for electrons.

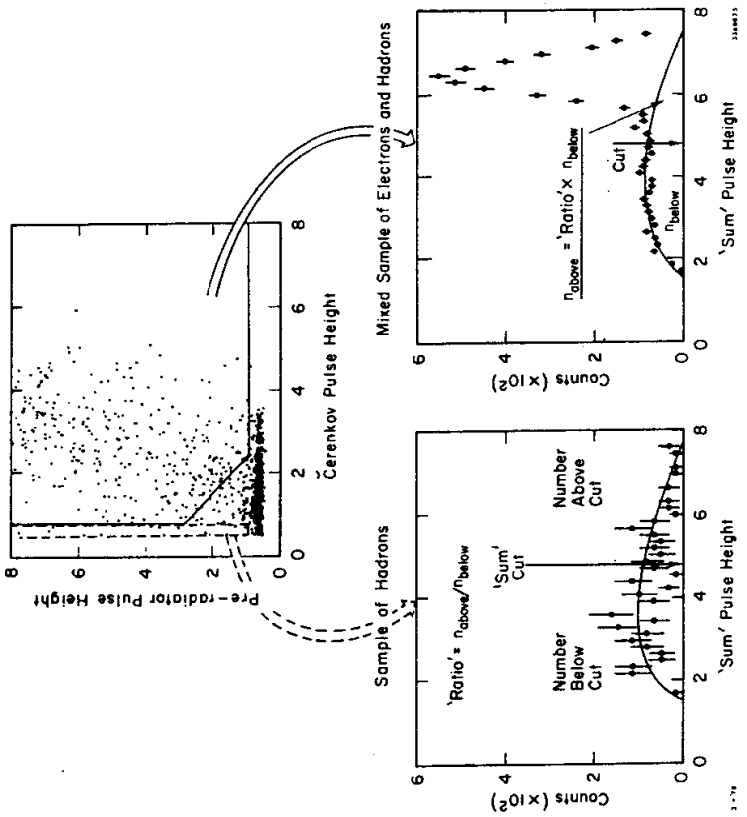

Fig. III-5

An illustration of the method used to estimate the pi background above the electron cut in the shower counter pulse height. The distribution of the background pions' sum pulse height is assumed to be the same as the measured distribution from a sample of pion events below the cut on Cerenkov pulse height.

than the electron cut which occurs in channel 80 (≤.1% of the electrons contaminate this sample). For the sample, we look at the SUM pulse height distribution and determine the "ratio" of the number of events above the SUM cut to those below. Now, for a sample of all the events which lie above the Cerenkov-pre-radiator cut (see Figure III-3), we observe the distribution of the SUM pulse height. Those events below the SUM cut are pions (≤.2% of electrons lie below the SUM cut) and, if we assume that the Cerenkov pulse height is uncorrelated with the SUM and pre-radiator pulse heights, we can estimate that the number of pions above the SUM cut is the previously determined "ratio" times the number below the cut. The assumption that the two samples of pions have the same SUM pulse height distribution is based on the fact that they are both constrained to have pre-radiator pulse heights above the nominal electron cut. This procedure worked badly for runs with few counts, so we interpolated the results of the high statistics runs to correct those with low statistics.

The efficiency on electrons after applying the two cuts (Cerenkov-pre-radiator, and SUM) was measured to be ≥99.5% using pure electron samples from elastic peaks at momenta between 2.2 and 17.5 GeV. The pion contamination was usually less than 1%, and our estimate of 30% for the accuracy of the correction procedure gives a small value for possible systematic errors from particle misidentification. We assigned a possible error of 1% for runs with E′ between 5 and 9 GeV; 2.5% if the angle was 6° or 10° and $E_o \geq 16$ GeV.

TRACK RECONSTRUCTION

There are five proportional wire chambers in the detector hut as shown in Figure II-5. The pattern of proportional wires firing during an event is used to reconstruct the trajectory of particles passing through the spectrometer. Using the spectrometer transfor-

mation matrix, these trajectories determine the momentum (δ) and angle (θ_o) of the scattered particle. In order to assign unique values of δ and θ_o to an event, there must be one, and only one, good track in the X and Y chambers.

There are two X chambers and three Y chambers. The momentum and scattering angle is well-determined if there is one X measurement and two Y measurements of the track (i.e., θ_{hut} is not important in determining θ_o, but ϕ_{hut} is needed to determine δ). Roughly 94% of all electron tracks meet this minimum criteria. Losses arising from chamber inefficiency are very small because of the redundancy in the number of X and Y chambers combined with the high (98%-99%) efficiency of each chamber.

The most common failure to find a single good track arises when two tracks can be fit to the pattern of wires which fired during the event. Table III-2 summarizes the frequency of various patterns. Sometimes such events are associated with two particles coming from the target within the resolving time of the electronics used to read out the wires (48 nsec gate). More often, the second track is the result of low energy particles associated with the event. To account for all these effects, a simple correction can be made based on the ratio of electron triggers to electron triggers with good tracks. As already mentioned, this correction would be about 6%. There is some evidence that this is an over-correction, since for some triggers without good tracks the particle appears to be outside the fiducial volume, and the trigger is formed when the associated particle is detected in TR3. Estimates of the size of this effect (≈1%) can be made by studying the wire chamber pattern in events without good tracks.

To eliminate this over-correction, an alternative inefficiency calculation was used in which the Y (and X) track inefficiencies are calculated separately by demanding a single good track in X (or Y) and observing the fractions of events having a single track in Y (or X). By requiring a good X track with both X chambers firing, the Y track inefficiency calculation suffers less from contamination

TRACK RECONSTRUCTION PARAMETERS

Code Type	%	Comment
1 X trk 1 Y trk	≈93.5%	within 48 ns gate, 1 (and only one) good track in PWC's
1 X trk 2 Y trk	.5%	
1 Y trk 2 X trk	≈2.7%	
2 X trk 2 Y trk	.5%	
1 X trk 0 Y trk	2.2%	some of these are from accidental triggers
1 Y trk 0 X trk	.19%	
0 X trk 0 Y trk	.25%	some of these are from accidental triggers

Selected Y track Configurations

Y track configuration (Y1	Y2	Y3)	Frequency of Occurence	
1	0	0	.02%	Consistent with individual chamber inefficiencies (1-2%)
0	1	0	.005%	
0	0	1	≈1.0%	Larger size probably due to accidental triggers

Summary of the average frequency of various configurations of tracks in the X and the Y proportional wire chambers. In the second half of the table is shown the frequency of occurrence of events with only one Y chamber firing; the larger size of the "001" configuration is an indication of accidental triggers in the event sample (to a level of ≈1%).

by events from outside the fiducial volume. The combined track inefficiency is then given by the product of the X and the Y inefficiencies. Corrections were made for double track events but these are a small effect. This alternate method gave inefficiencies about 1% lower than the simple method described above; i.e., electron triggers/electron triggers with good tracks.

See Figure III-6 for a graph of the PWC correction plotted versus W. The overall inefficiency correction is about 6% with an estimated systematic error as large as 1.5%.

CORRECTIONS AND SUBTRACTIONS

A listing of the sizes of the various corrections applied to the data is given in Table III-3. This sub-chapter briefly describes those corrections which have not been discussed in previous sections.

Rate Effects

High incoming data rates result in inefficiencies or "dead times" in various counters due to the finite recovery time after a count. This effect can be calculated from the dead time of each of the counters and the incoming rate and also can be measured directly. In this experiment, the output signal from the master trigger was split and sent to 4 scalers each having known, fixed dead times of 34, 58, 77, and 108 nsec. The number of events counted by each of these scalers was fit as a function of the known scaler dead time and then an extrapolation to zero gave the rate expected for no dead time. The dead time correction was less than 1% for the 15°, 18°, and 20.6° data and was occasionally as large as 5%-7% for the 6° and 10° data where data rates are higher. The systematic error due to rate effects is estimated to be .5%.

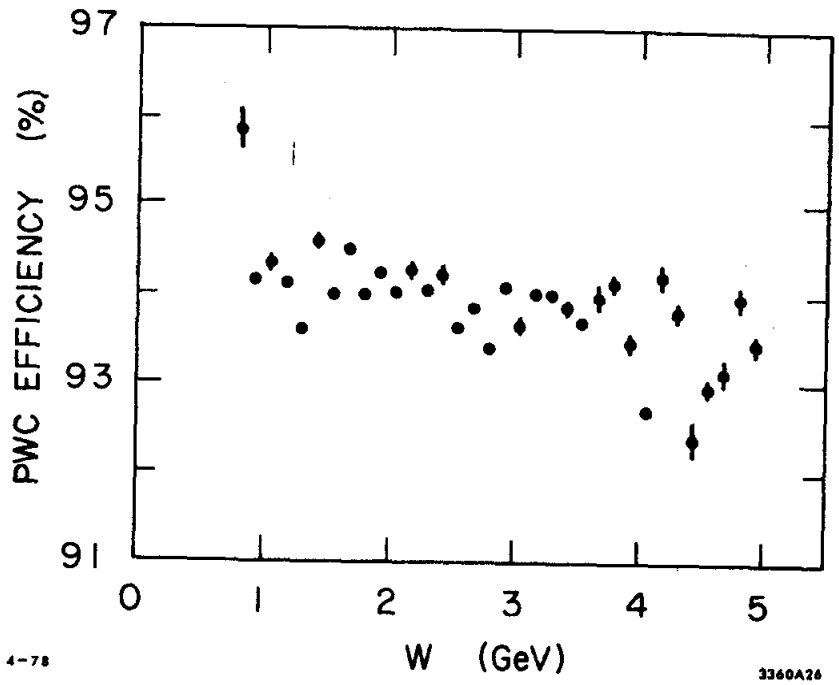

Fig. III-6

A graph of the proportional wire chamber track reconstruction efficiency plotted versus W.

TABLE III-3

TABLE OF CORRECTIONS AND SUBTRACTIONS

Correction	Size	Comments	Systematic Error
Trigger efficiency	.25%	$\leq$1%, 90% of runs $\leq$.5%	.25%
e^+ subtraction	<1% except at low E′	$\geq$5% if W > 2.15 + .14 * E_o; for 6^o if W > 2.5 + .14 * E_o	1.5% if W > W threshold
Empty target subtraction	5%	measured by runs using an empty target cell	1.5%
Dead time correction	$\leq$1% (15^o, 18^o, 20.6^o)	rate dependent, determined for each run by measurement	.5%
PWC track inefficiency	4% - 6%		1.5%
Correction for asymmetric θ_o limits	0 - 6%	Correction: $\frac{.0002}{\sin^2\theta}\frac{1}{(1-x')^2}$: maximum 6% for W = 2 GeV	1%
Correction for hadron contamination of electron signal	<2% for 98% of runs; 5-20% for 6^o and 10^o, 19.5 and 16 GeV, near E′ = 7 GeV	largest at small θ, high E_o, near E′ = 7 GeV; π disc = .00015 for E′ < 5 GeV, .03 for E > 7 GeV $\check{C}$ (π threshold) = 5.65 GeV	1% (5<E′<9) 2.5% for 5<E′<9 GeV, $\theta = 6^o, 10^o$ and E_o > 16 GeV
Radiative Correction	varies .8 + 1.4	Correction : $\frac{1.6 - .36\sin\theta}{\omega'(.29 + .31\sin\theta)}$; $\omega' = 1 + \frac{W^2}{Q^2}$	5%
Target density fluctuations	maximum .5% variation due to beam heating	Varies with beam heat load	.5%
Acceptance/ nominal acceptance	98% (at 6^o) to 94% (at 20.6^o)	largest for large effective target width	1.5%
Variation of (θ_o/X) with E′	4% (2 GeV + 17 GeV)	measured by "jailbar" runs	1%
Variation of (δ/Y) with E′	9% (2 GeV + 17 GeV)	measured by elastic peak positions in δ,θ_o plane	3%

A summary of the sizes of various corrections applied to the data and an estimate of the possible size of the systematic error in the cross section associated with the correction.

Trigger Efficiency

The efficiency of the master trigger (TR1·TR3·SUM) can be estimated using the alternate trigger ($\bar{C}$·SUM). For those events in which the alternate trigger fired, and wire chamber information indicated that the particle passed through TR1, TR3, and the shower counter (all three parts of the triple coincidence), we determined what fraction of the time these events fired the master trigger. This measure of the trigger inefficiency is always less than 1%; for 90% of the runs it is less than .5% with an estimated error of .25%.

Positron Subtraction

A source of background electrons which do not originate from electron hydrogen scattering is due to those electrons which are produced in the target in a charge symmetric way; i.e., as e^+e^- pairs. At our angles, the main source of such pairs is π^o decay.

In order to correct for this, we reversed the polarity of the spectrometer so that it accepted positrons. We measured the positron yield and assumed that this equaled the background yield of electrons. The correction is small except at lowest values of secondary momentum, E′ (or, equivalently, at high values of W). The threshold in W above which the positron subtraction exceeds 5% is given by:

$$W_{threshold}(GeV) = 2.15 + .14 * E_o(GeV), \text{ except for}$$

$$\theta = 6^o \text{ where } W_{threshold} = 2.5 + .14 * E_o$$

The systematic error due to possible problems in the positron subtraction is estimated at 1.5% for $W > W_{threshold}$ and is much smaller for lower W values.

Combining Data and Corrections for "Offset" in Angle

This subsection describes the procedures used to combine data in the resonance region ($W < 2GeV$) and, also, the corrections applied to non-resonance data to account for the asymmetric θ_o limits ($-3.75 < \theta_o < 3.0$ mrads) of the spectrometer acdeptance. In both cases, we correct cross sections for offsets from the central spectrometer angle, θ.

For the resonance region, cross sections were determined for W bins which were 20 MeV wide (considerably smaller than the typical resonance widths). Data was taken by stepping the central momentum, P', of the spectrometer in small increments (compared to the acceptance of $\approx \pm 2\%$) for consecutive runs. In this manner, the W ranges covered by successive runs overlapped each other. This procedure, known as "scanning"[1], ensured that the scattered electrons assigned to a particular W bin came from all parts of the δ, θ_o acceptance, averaging over any acceptance variations across the plane. This ensured that the acceptance for all W bins was the same.

From Figure A1-1, it is obvious that for a particular run the center of a W bin could be offset from $\theta_o = 0$, and this was corrected for. To obtain a single cross section for some W value, cross sections from different runs were combined, correcting each for the offset of the W bin's center from the nominal scattering angle, θ.

For runs outside the resonance region, cross sections for the entire acceptance of the spectrometer were calculated and a correction applied for the offset in θ due to the asymmetric θ_o limits ($-3.75 < \theta_o < 3.0$ mrads). This correction has a maximum size of 6% (occuring at $W = 2$ GeV), and we estimate that its associated systematic error is less than 1%.

WEEDING

After all the data runs had been analysed and the cross sections calculated for each of them, we conducted a systematic check in order to eliminate or correct any bad data. Two techniques were employed to identify runs with problems.

"Outlier" Search

The first was to graph and monitor all quantities which might have an influence on our measured cross section; they were plotted versus run number (in the sequence of data taking), and we hunted for anomalous "outliers" in various distributions or for slow drifts in the values of the quantities. Quantities scanned included flag efficiencies of the various counters, PHA efficiencies, ratio of the signals from the two beam monitors, various correction factors (dead time, PWC inefficiency, pion subtraction), and the average pulse heights in various counters. Runs with anomalous behavior in any of these quantities were scrutinized carefully for possible errors.

Problem Flags

Although the "outlier" search eliminated many flagrant errors due to equipment malfunction, or straightforward mistakes in procedure, a more systematic check was applied to certain areas of the data. A flag was set if a quantity were outside tolerance. Magnet currents were kept within tolerance, target temperature was kept within $\approx 10\%$ ($\approx 2.5\%$ change in the target density) of a reference value, pedestal drifts were monitored and kept within 3 channels (800 channel ADC's), and the goodness of fit for the dead time corrections was monitored. Careful scrutiny of runs having a flag set enabled us to eliminate bad data.

RADIATIVE CORRECTIONS

It is customary to correct electron scattering cross sections for radiation of photons by the electron. In this section, we describe the methods used to do the radiative corrections, the size of the corrections, and possible systematic errors arising from them.

Procedure

In order to radiatively correct the data in this experiment, we followed the same procedures described in Reference 2. Here, we shall sketch the major features of the method and give estimates of the size of possible errors in these procedures. The radiative correction formulas were developed by Tsai[3] and others, and their application to electron scattering data at SLAC was accomplished by Miller[4] and succeeding experimenters.

The first step in correcting the data was the calculation and subtraction of the elastic tails from the inelastic data. The elastic tail was calculated using an exact quantum mechanical formulation for the radiation of a single photon during the scattering process. In addition, corrections are made for real bremsstrahlung in the target before or after the scatter. The formulas require elastic proton form factors $G_E(Q^2)$ and $G_M(Q^2)$ which we obtained from a fit to the world data assuming form factor scaling; $G_E = G_M/\mu_P$. The radiation of multiple soft photons during the scatter was also taken into account. The elastic tail contribution was subtracted, yielding "rare" data (i.e., data which must be corrected further).

This "rare" data was then corrected for radiation in inelastic processes by an iterative method which uses a model for the cross section, calculating the ratio of unradiated/radiated cross sections and then applying this ratio to the "rare" data to obtain the "final" data. In the first iteration, the "rare" data is used as an approximation to the unradiated cross section. The ratio unradiated/

radiated is then calculated at each data point. The "rare" data is then multiplied by this ratio, and the resulting data set is used as the cross section to be radiated. The process is continued until the ratio converges. The "final" data set is formed by multiplying the "rare" data by the radiative correction ratio obtained in this way. Usually, 5 or 6 iterations were sufficient.

In order to avoid excessive computer time, several approximations to the exact radiation formulas were used in the iterative procedure. The peaking approximation in angle assumes that the radiated photon is along the direction of the incoming, or outgoing, electron. If we consider only the radiation of a single (hard) photon, then, in this approximation, the only effect of the radiation is to degrade the energy of the incoming or the outgoing electron. This reduces the radiation calculation from a two-dimensional integration in the Q^2-W^2 plane to two one-dimensional integrations corresponding to radiation from the incoming or outgoing electron, respectively. A second approximation was our use of an "equivalent radiator". Instead of doing exact integrals to correct for radiation associated with the electron scattering, an empirical form identical to the equations for bremsstrahlung was used with an "equivalent radiator" replacing the real radiator. The "equivalent radiator" was adjusted empirically[3] to give agreement between this calculation and the exact treatment. An approximate formula for the equivalent radiator is

$$t_{eq} = \frac{\alpha}{\pi}\left(\ln\left(\frac{Q^2}{m_e^2}\right)-1\right)$$

For $Q^2 = 20$ GeV^2, $t_{eq} = .04$ (compared with real radiators of $\approx .04$ for this experiment). This combination of peaking approximation and the use of equivalent radiators has been checked previously and found to agree with the exact calculation to $\approx 10\%$[4].

Size of Corrections

The ratio of final/raw data for angles of 6°, 15°, *and* 18° *is* presented in Figure III-7. The figure demonstrates that the radiative

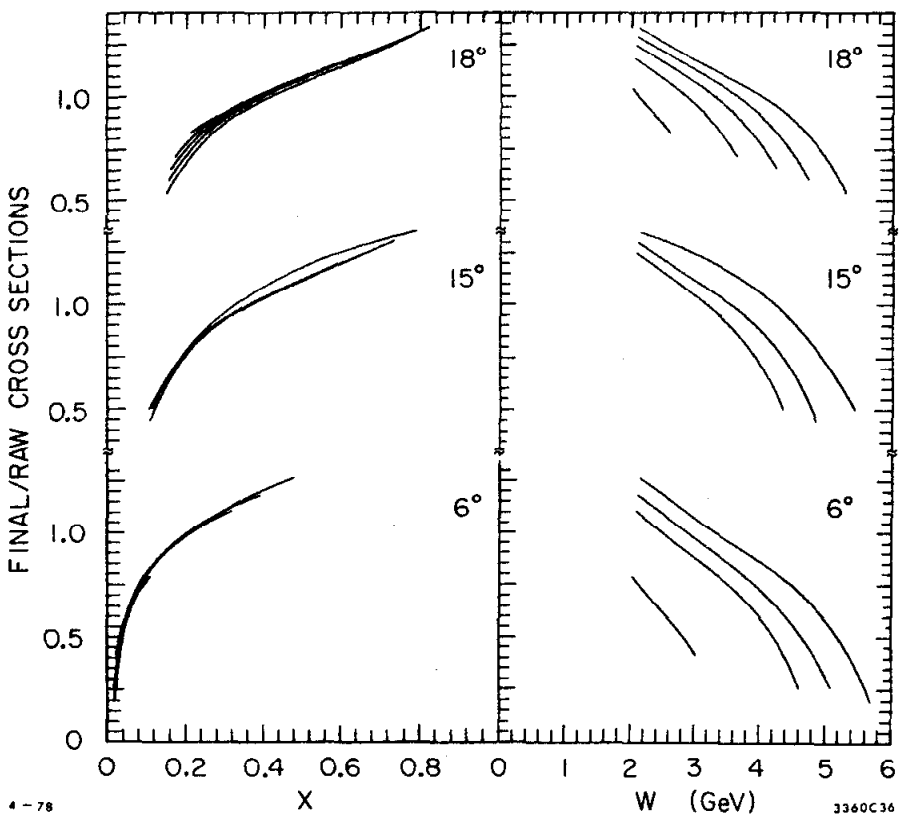

Fig. III-7

A plot of the ratio of radiatively corrected data to "raw" data, plotted against the scaling variable, X, and against the final state mass, W. At each angle, we show the lines for given energy (E_o) corresponding to the data taken in the experiment. For a given angle, the ratio is approximately a single function of X, independent of the different values of beam energy (the different lines).

correction is large, averaging about 25%. The figure indicates that the ratio of final/raw is approximately a function of X only, for each angle, approximated by the following expression:

$$\text{Radiative Correction Ratio} \equiv \text{FINAL/RAW} \simeq \frac{1.6-.36\sin\theta}{\omega'^{(.29+.31\sin\theta)}}; \quad \omega' = 1+\frac{W^2}{Q^2}.$$

Possible errors due to the approximations listed above, coupled with the large size of the corrections, lead us to an estimate of 5% as a possible systematic error in the final cross section due to radiative corrections.

Radiative Corrections to Elastic Peaks

The measured cross section spectrum $d^2\sigma/d\Omega dE'$ shows a sharp peak in E′ due to elastic scattering which is not symmetric but skewed to lower values of E′ because of the energy degradation due to radiation. To radiatively correct the spectrum, an "unfolding" procedure was followed. The contribution to a scattered energy bin from higher energy bins was first calculated and subtracted. The cross section in that bin was then corrected for the number of counts radiated to lower energy bins. In this way, each bin was radiatively corrected. The corrected cross section $d^2\sigma/d\Omega dE'$ is then integrated over E′ from W=.8 GeV to W=1.06 GeV to obtain the elastic cross section $d\sigma/d\Omega$.

SYSTEMATIC ERRORS

Method of Estimation

"Estimated systematic errors" is a redundant phrase[5]. We used a number of methods to help us estimate the systematic error in the cross section. Errors in measured or calculated corrections were assumed to be as large as some fraction of the correction.

Discrepancies in consistency checks (between different subsets of data) set lower bounds on possible errors as did the observation of excessive spread (beyond statistical) in any set of equivalent measurements. Another general method of error analysis consisted of estimating various parameter mis-measurements (like beam energy), and calculating the resulting effect on the cross section. Table III-4 lists the sources and estimated sizes of possible systematic errors.

Correlation Between Errors

Many systematic errors are independent of each other, and the total error can be estimated by adding the various errors in quadrature. Those errors which might be correlated with each other cannot be treated in this way and should simply be summed when the total error is estimated. We group errors into sets where the errors may be correlated but we believe different sets to be independent. Table III-5 shows these sets along with typical values of the systematic errors.

Kinematic Variation

Some errors result in errors of normalization for the entire experiment (e.g., a mis-measurement of the target cell length), while others are strongly dependent on kinematics (e.g., the contamination of the signal by electrons produced as e^+e^- pairs is strongly peaked at low E′). Many of the errors (such as errors in the momentum dispersion) do not fall into either group. For most of the systematic errors, there is a strong possibility of kinematic variation. We believe that the fraction of the total systematic error which is a normalization error for the whole experiment is less than half the total error. We treat the systematic errors on data from different angles and energies as independent when fitting cross sections (to extract structure functions, etc.)

TABLE III-4

SYSTEMATIC ERRORS IN CROSS SECTIONS

Source of Error	Description of Error and Method of Estimation	Size of Systematic Error in Cross Section
Beam Intensity	measured by 2 toroids, monitored with standard capacitor pulse, additional calibration, Faraday cup; all agree within ±.5%, Faraday cup known to ±.5%	±.5% (random) ±.3% (global)
Beam Energy	measured by A-line optics; momentum slits set to ±.375%; absolute calibration ±.1% $\frac{\Delta\sigma}{\sigma} \approx (2.5 + 6.5\ X)\ \frac{\Delta E_o}{E_o}$	±1.2% (random) ± .6% (global)
Beam Steering	SEM; burn spots on target; spot positions on surveyed ZnS screen; steering error ±.1 mrad	±.2% (18°) ±.6% (6°)
Target Length	measured optically; shrinkage correction (.3%); finite beam spot and mis-steering correction (.3%)	±.5%
Target Density	temperature measured to ±.1%; density calculated	±.3% (LH) ±.6% (LD)
Target Purity	hydrogen in LD target	±.15% (LD only)
Spectrometer Acceptance	determined by agreement of model and data	±2%
Offset of Spectrometer Optic Axis	±.3 cm (x); ±.2 cm (y)	±1%
Θ, P dispersions	measure Θ_0 dispersion with "jailbars"; P dispersion with elastic peak positions in δ,ϑ_0 plane	±4%
Trigger efficiency	define alternate trigger to check main trigger	±.5%
PHA efficiency on e^-'s	check on pure sample of electrons at elastic peaks	±.25%
Hadron contamination of electron signal	for events below Ć cut (=all π's), look at PHA distribution on sum; estimate number above cut	1% for 5<E′<9 GeV; except for 6° and 10° (19.5 and 16 GeV) lines it is 2.5%
Rate effects	trigger split into circuits with varying dead time, extrapolated to 0 dead time	.5%

TABLE III-4 (continued)

SYSTEMATIC ERRORS IN CROSS SECTIONS

Source of Error	Description of Error and Method of Estimation	Size of Systematic Error on Cross Section
PWC corrections	correction to (1 good track) is 6%	1.5%
Target Wall Scatters	5% correction	1.5%
e^+e^- production	e^+e^- background >5% above $W_{threshold}$ $W_{thresh} = 2.15 + .14 * E_o(GeV)$ if $\theta=6^o$, $W_{thresh} = 2.5 + .14 * E(GeV)$	1.5% above W_{thresh}
Combining runs, correcting for asymmetric θ_o limits	correction = $\frac{.02\%}{\sin^2\theta/2\ (1-x')^2}$ $\frac{1}{}$ = 2.3% at $x' = .7$, 18^o = 3.3% at $x' = .7$, 15^o	1%
Radiative Corrections	Radiative Correction = $\frac{(1.6 - .36 \sin\theta)}{\omega'-(.29 + .31 \sin\theta)}$, $\omega'=1+\frac{W^2}{Q^2}$ Difference in Correction $(18^o \to 60^o)$ } 28%($\omega'=2.4$) + 20%($\omega'=1$)	5%
Interpolation	Errors estimated from changes in cross section due to different interpolation procedures.	2.5%

TABLE III-5

SYSTEMATIC ERROR SUMMARY

Errors	Uncorrelated Subsets		Error
Beam Intensity	.8%	Beam	1.6%
Beam Energy	.6%		
Beam Angular Spread	.2%		
Target Length	.5%	Target	1%
Target Density	.3%		
Target Purity	.2% (LD)		
Spectrometer Acceptance	2.%	Acceptance	3%
Offset of Spectrometer Optic Axis	1.%		
Uncertainty in θ_o Dispersions	1.%	Dispersions	4%
Uncertainty in P Dispersions	3.%		
Trigger Efficiency	.5%	Electron Counting	3.75%
PHA Efficiency on e^-'s	.25%		
π-subtraction	1.%		
Rate Effects	.5%		
PWC Correction	1.5%		
Target Wall Scattering	1.5%	Electrons (not scattered from target)	3%
e^+e^- Production	1.5%		
Finite Aperture (+ asymmetric θ_o limits)	1.%	θ offset	1%
Interpolation	2.5%	Interpolation	2.5%
			7.5% Average Experimental Systematic Error
Radiative Corrections	5%		

A summary of the major sources of systematic errors grouped into subsets, which we treat independently. Individual errors within subsets are added linearly, but the subset values are added together in quadrature.

CROSS SECTIONS

The set of hydrogen and deuterium cross sections presented in Table III-5 is the primary measurement of the experiment. Data is presented before and after radiative corrections. The table gives both values of the cross section for each energy, scattering angle, and target. The data are presented in columns giving the W value of each data point, the value of the cross section (picobarns/GeV/steradian) and, in parentheses, the statistical counting error and the systematic error for the cross section.

The statistical errors are small (typically, 1-2% for W>2 GeV). This is a reflection of the fact that the duration of data taking was often determined by the 50° and 60° measurements which were being done simultaneously. The systematic errors have been discussed in the previous subsection. They average about 7% over the experiment's range of data and are usually considerably larger than the statistical error on the cross sections.

Figure III-8 is a set of graphs of these cross sections with each "line" of data points at constant E_o and θ plotted versus W. For the graphs of 10° and 15° data, the one 10° line (scaled by a factor of 2) lies at the top; for the combined 18° and 20.6° graphs the single 20.6° line lies at the bottom. For a given angle, the higher energy lines have lower cross sections.

A few features of the cross sections are worth noting. First, for a given angle and W value, the cross sections fall with E_o; similarly, they rise with increasing W except for the lowest angle and energy (6°, 7 GeV) line.

Resonant structure is clearly visible on many of the lines; in particular, structure is apparent in the 15°, 13.3 GeV and 16 GeV lines which are at a Q^2 value of approximately 8 and 10 GeV^2, respectively. Indeed, we see evidence for resonance structure even in the 20.6°, 19.5 GeV line at an average Q^2 of about 18 GeV This is evidence that at least some of the structure seen at low values of Q^2[1] remains as a sizeable fraction of the continuum

Table III-5

HYDROGEN CROSS SECTION

E_0 = 7.00 GeV, θ = 6.00, RAW DATA

W (GEV)	CROSS SECTION		ERRORS	
0.836	-0.308E+05	+- (	0.37E+05,	0.16E+04)
0.856	-0.324E+05	+- (	0.25E+05,	0.17E+04)
0.876	0.194E+04	+- (	0.23E+05,	0.99E+02)
0.896	-0.163E+05	+- (	0.27E+05,	0.83E+03)
0.916	0.576E+07	+- (	0.11E+06,	0.29E+06)
0.935	0.565E+08	+- (	0.33E+06,	0.29E+07)
0.955	0.268E+08	+- (	0.22E+06,	0.14E+07)
0.975	0.654E+07	+- (	0.11E+06,	0.33E+06)
0.995	0.413E+07	+- (	0.91E+05,	0.21E+06)
1.015	0.312E+07	+- (	0.79E+05,	0.16E+06)
1.035	0.249E+07	+- (	0.71E+05,	0.13E+06)
1.055	0.187E+07	+- (	0.64E+05,	0.96E+05)
1.075	0.178E+07	+- (	0.77E+05,	0.91E+05)
1.094	0.205E+07	+- (	0.25E+06,	0.10E+06)
1.134	0.268E+07	+- (	0.30E+06,	0.14E+06)
1.154	0.315E+07	+- (	0.14E+06,	0.16E+06)
1.174	0.429E+07	+- (	0.14E+06,	0.22E+06)
1.194	0.611E+07	+- (	0.17E+06,	0.31E+06)
1.214	0.729E+07	+- (	0.18E+06,	0.37E+06)
1.234	0.723E+07	+- (	0.18E+06,	0.37E+06)
1.254	0.627E+07	+- (	0.17E+06,	0.32E+06)
1.274	0.554E+07	+- (	0.16E+06,	0.28E+06)
1.294	0.497E+07	+- (	0.15E+06,	0.25E+06)
1.314	0.474E+07	+- (	0.16E+06,	0.24E+06)
1.333	0.413E+07	+- (	0.38E+06,	0.21E+06)
1.433	0.315E+07	+- (	0.39E+06,	0.16E+06)
1.453	0.371E+07	+- (	0.92E+05,	0.19E+06)
1.473	0.404E+07	+- (	0.80E+05,	0.21E+06)
1.493	0.464E+07	+- (	0.85E+05,	0.24E+06)
1.513	0.478E+07	+- (	0.86E+05,	0.24E+06)
1.533	0.476E+07	+- (	0.85E+05,	0.24E+06)
1.553	0.451E+07	+- (	0.82E+05,	0.23E+06)
1.573	0.425E+07	+- (	0.85E+05,	0.22E+06)
1.593	0.369E+07	+- (	0.21E+06,	0.19E+06)
1.692	0.515E+07	+- (	0.84E+06,	0.26E+06)
1.712	0.384E+07	+- (	0.92E+05,	0.20E+06)
1.732	0.366E+07	+- (	0.75E+05,	0.19E+06)
1.752	0.355E+07	+- (	0.74E+05,	0.18E+06)
1.772	0.338E+07	+- (	0.71E+05,	0.17E+06)
1.792	0.331E+07	+- (	0.71E+05,	0.17E+06)
1.812	0.344E+07	+- (	0.87E+05,	0.18E+06)
1.832	0.314E+07	+- (	0.13E+07,	0.16E+06)
1.952	0.294E+07	+- (	0.47E+06,	0.15E+06)
1.972	0.276E+07	+- (	0.50E+05,	0.14E+06)
1.992	0.272E+07	+- (	0.44E+05,	0.14E+06)
2.027	0.279E+07	+- (	0.28E+05,	0.14E+06)
2.077	0.298E+07	+- (	0.13E+06,	0.15E+06)
2.258	0.226E+07	+- (	0.22E+05,	0.11E+06)
2.501	0.186E+07	+- (	0.79E+04,	0.93E+05)
2.755	0.172E+07	+- (	0.22E+05,	0.86E+05)
3.003	0.178E+07	+- (	0.26E+05,	0.90E+05)

E_0 = 13.50 GeV, θ = 6.00, RAW DATA

W (GEV)	CROSS SECTION		ERRORS	
1.020	0.598E+05	+- (	0.38E+05,	0.30E+04)
1.039	0.373E+05	+- (	0.84E+04,	0.15E+04)
1.059	0.506E+05	+- (	0.70E+04,	0.25E+04)
1.079	0.459E+05	+- (	0.48E+04,	0.23E+04)
1.099	0.551E+05	+- (	0.44E+04,	0.28E+04)
1.119	0.667E+05	+- (	0.40E+04,	0.34E+04)
1.138	0.726E+05	+- (	0.38E+04,	0.36E+04)
1.158	0.116E+06	+- (	0.47E+04,	0.58E+04)
1.178	0.146E+06	+- (	0.52E+04,	0.73E+04)
1.198	0.201E+06	+- (	0.59E+04,	0.10E+05)
1.218	0.222E+06	+- (	0.62E+04,	0.11E+05)
1.238	0.223E+06	+- (	0.61E+04,	0.11E+05)
1.257	0.214E+06	+- (	0.61E+04,	0.11E+05)
1.277	0.196E+06	+- (	0.57E+04,	0.98E+04)
1.297	0.192E+06	+- (	0.56E+04,	0.97E+04)
1.317	0.194E+06	+- (	0.57E+04,	0.97E+04)
1.337	0.196E+06	+- (	0.54E+04,	0.98E+04)
1.357	0.192E+06	+- (	0.50E+04,	0.96E+04)
1.377	0.204E+06	+- (	0.48E+04,	0.10E+05)

W(GeV)	CROSS SECTION		ERRORS	
1.397	0.210E+06	+- (	0.48E+04,	0.11E+05)
1.417	0.218E+06	+- (	0.51E+04,	0.11E+05)
1.436	0.221E+06	+- (	0.58E+04,	0.11E+05)
1.456	0.264E+06	+- (	0.73E+04,	0.13E+05)
1.476	0.294E+06	+- (	0.82E+04,	0.15E+05)
1.496	0.335E+06	+- (	0.87E+04,	0.17E+05)
1.516	0.334E+06	+- (	0.86E+04,	0.17E+05)
1.536	0.323E+06	+- (	0.84E+04,	0.16E+05)
1.556	0.319E+06	+- (	0.83E+04,	0.16E+05)
1.576	0.291E+06	+- (	0.79E+04,	0.15E+05)
1.596	0.299E+06	+- (	0.80E+04,	0.15E+05)
1.616	0.305E+06	+- (	0.78E+04,	0.15E+05)
1.635	0.328E+06	+- (	0.78E+04,	0.16E+05)
1.655	0.353E+06	+- (	0.78E+04,	0.18E+05)
1.675	0.386E+06	+- (	0.79E+04,	0.19E+05)
1.695	0.390E+06	+- (	0.81E+04,	0.20E+05)
1.715	0.388E+06	+- (	0.81E+04,	0.19E+05)
1.735	0.409E+06	+- (	0.82E+04,	0.21E+05)
1.755	0.380E+06	+- (	0.79E+04,	0.19E+05)
1.775	0.378E+06	+- (	0.78E+04,	0.19E+05)
1.795	0.367E+06	+- (	0.77E+04,	0.18E+05)
1.815	0.372E+06	+- (	0.77E+04,	0.19E+05)
1.835	0.389E+06	+- (	0.79E+04,	0.20E+05)
1.855	0.398E+06	+- (	0.89E+04,	0.20E+05)
1.875	0.414E+06	+- (	0.12E+05,	0.21E+05)
1.895	0.414E+06	+- (	0.19E+05,	0.21E+05)
1.914	0.381E+06	+- (	0.16E+05,	0.19E+05)
1.934	0.370E+06	+- (	0.13E+05,	0.19E+05)
1.954	0.397E+06	+- (	0.12E+05,	0.20E+05)
1.974	0.416E+06	+- (	0.13E+05,	0.21E+05)
1.994	0.412E+06	+- (	0.13E+05,	0.21E+05)
2.029	0.413E+06	+- (	0.78E+04,	0.21E+05)
2.079	0.427E+06	+- (	0.85E+04,	0.21E+05)
2.129	0.493E+06	+- (	0.25E+05,	0.25E+05)
2.504	0.384E+06	+- (	0.44E+04,	0.19E+05)
3.003	0.343E+06	+- (	0.45E+04,	0.18E+05)
3.502	0.313E+06	+- (	0.27E+04,	0.16E+05)
3.752	0.308E+06	+- (	0.38E+04,	0.16E+05)
4.001	0.318E+06	+- (	0.41E+04,	0.16E+05)
4.251	0.364E+06	+- (	0.74E+04,	0.18E+05)
4.501	0.459E+06	+- (	0.11E+05,	0.24E+05)

E_0 = 16.00 GeV, θ = 6.00, RAW DATA

W (GEV)	CROSS SECTION		ERRORS	
0.554	0.240E+03	+- (	0.51E+03,	0.12E+02)
0.573	0.699E+03	+- (	0.64E+03,	0.35E+02)
0.592	-0.366E+03	+- (	0.39E+03,	0.18E+02)
0.611	-0.490E+03	+- (	0.34E+03,	0.25E+02)
0.630	-0.146E+03	+- (	0.31E+03,	0.73E+01)
0.649	-0.120E+03	+- (	0.26E+03,	0.60E+01)
0.688	0.175E+02	+- (	0.24E+03,	0.86E+00)
0.707	-0.135E+02	+- (	0.27E+03,	0.68E+00)
0.727	-0.348E+03	+- (	0.25E+03,	0.17E+02)
0.746	0.278E+02	+- (	0.24E+03,	0.14E+01)
0.766	0.243E+02	+- (	0.22E+03,	0.12E+01)
0.785	0.880E+01	+- (	0.27E+03,	0.44E+00)
0.805	0.263E+03	+- (	0.27E+03,	0.13E+02)
0.825	0.376E+02	+- (	0.26E+03,	0.19E+01)
0.844	-0.125E+03	+- (	0.25E+03,	0.63E+01)
0.864	0.527E+04	+- (	0.60E+03,	0.26E+03)
0.883	0.432E+05	+- (	0.15E+04,	0.22E+04)
0.903	0.118E+06	+- (	0.25E+04,	0.59E+04)
0.923	0.166E+06	+- (	0.29E+04,	0.83E+04)
0.942	0.160E+06	+- (	0.27E+04,	0.80E+04)
0.962	0.126E+06	+- (	0.22E+04,	0.63E+04)
0.982	0.761E+05	+- (	0.16E+04,	0.38E+04)
1.002	0.421E+05	+- (	0.11E+04,	0.21E+04)
1.021	0.250E+05	+- (	0.85E+03,	0.13E+04)
1.041	0.192E+05	+- (	0.71E+03,	0.97E+03)
1.061	0.165E+05	+- (	0.62E+03,	0.83E+03)
1.081	0.154E+05	+- (	0.57E+03,	0.77E+03)
1.100	0.170E+05	+- (	0.59E+03,	0.86E+03)
1.120	0.177E+05	+- (	0.60E+03,	0.89E+03)
1.140	0.233E+05	+- (	0.69E+03,	0.12E+04)
1.160	0.295E+05	+- (	0.78E+03,	0.15E+04)
1.180	0.395E+05	+- (	0.91E+03,	0.20E+04)

5-78

3360848

HYDROGEN CROSS SECTION

W(GeV)	CROSS SECTION		ERRORS	
1.199	0.519E+05	+- (	0.11E+04,	0.26E+04)
1.219	0.622E+05	+- (	0.12E+04,	0.31E+04)
1.239	0.666E+05	+- (	0.13E+04,	0.33E+04)
1.259	0.660E+05	+- (	0.13E+04,	0.33E+04)
1.279	0.654E+05	+- (	0.13E+04,	0.32E+04)
1.299	0.638E+05	+- (	0.13E+04,	0.32E+04)
1.318	0.661E+05	+- (	0.13E+04,	0.33E+04)
1.338	0.691E+05	+- (	0.13E+04,	0.35E+04)
1.358	0.709E+05	+- (	0.13E+04,	0.36E+04)
1.378	0.715E+05	+- (	0.14E+04,	0.36E+04)
1.398	0.720E+05	+- (	0.15E+04,	0.36E+04)
1.418	0.788E+05	+- (	0.17E+04,	0.40E+04)
1.438	0.832E+05	+- (	0.19E+04,	0.42E+04)
1.458	0.944E+05	+- (	0.25E+04,	0.47E+04)
1.477	0.102E+06	+- (	0.35E+04,	0.51E+04)
1.497	0.111E+06	+- (	0.40E+04,	0.56E+04)
1.517	0.125E+06	+- (	0.40E+04,	0.63E+04)
1.537	0.133E+06	+- (	0.40E+04,	0.67E+04)
1.557	0.114E+06	+- (	0.37E+04,	0.57E+04)
1.577	0.115E+06	+- (	0.38E+04,	0.58E+04)
1.597	0.113E+06	+- (	0.40E+04,	0.57E+04)
1.617	0.116E+06	+- (	0.43E+04,	0.58E+04)
1.637	0.121E+06	+- (	0.48E+04,	0.61E+04)
1.656	0.132E+06	+- (	0.54E+04,	0.66E+04)
1.676	0.160E+06	+- (	0.60E+04,	0.80E+04)
1.696	0.169E+06	+- (	0.61E+04,	0.85E+04)
1.716	0.173E+06	+- (	0.62E+04,	0.87E+04)
1.736	0.173E+06	+- (	0.63E+04,	0.87E+04)
1.756	0.173E+06	+- (	0.70E+04,	0.87E+04)
1.776	0.159E+06	+- (	0.80E+04,	0.80E+04)
1.796	0.164E+06	+- (	0.11E+05,	0.82E+04)
1.816	0.162E+06	+- (	0.27E+05,	0.81E+04)
1.856	0.172E+06	+- (	0.31E+05,	0.86E+04)
1.876	0.177E+06	+- (	0.15E+05,	0.89E+04)
1.895	0.176E+06	+- (	0.11E+05,	0.88E+04)
1.915	0.176E+06	+- (	0.90E+04,	0.88E+04)
1.935	0.176E+06	+- (	0.80E+04,	0.89E+04)
1.955	0.176E+06	+- (	0.80E+04,	0.88E+04)
1.975	0.179E+06	+- (	0.81E+04,	0.90E+04)
1.995	0.189E+06	+- (	0.82E+04,	0.95E+04)
2.030	0.190E+06	+- (	0.52E+04,	0.95E+04)
2.080	0.195E+06	+- (	0.53E+04,	0.98E+04)
2.130	0.227E+06	+- (	0.84E+04,	0.11E+05)
2.180	0.143E+06	+- (	0.15E+06,	0.72E+04)
2.254	0.191E+06	+- (	0.26E+04,	0.96E+04)
2.504	0.213E+06	+- (	0.12E+04,	0.11E+05)
2.754	0.210E+06	+- (	0.28E+04,	0.11E+05)
3.004	0.202E+06	+- (	0.18E+04,	0.10E+05)
3.253	0.196E+06	+- (	0.18E+04,	0.98E+04)
3.503	0.190E+06	+- (	0.16E+04,	0.95E+04)
4.002	0.190E+06	+- (	0.22E+04,	0.11E+05)
4.502	0.211E+06	+- (	0.36E+04,	0.12E+05)
4.752	0.254E+06	+- (	0.51E+04,	0.13E+05)
5.001	0.358E+06	+- (	0.91E+04,	0.19E+05)

E_0 = 19.50 GeV, θ = 6.00, RAW DATA

W (GEV)	CROSS SECTION		ERRORS	
0.541	-0.104E+02	+- (	0.62E+02,	0.52E+00)
0.578	0.162E+02	+- (	0.78E+02,	0.81E+00)
0.597	-0.235E+02	+- (	0.57E+02,	0.12E+01)
0.616	0.581E+02	+- (	0.92E+02,	0.29E+01)
0.635	-0.310E+02	+- (	0.73E+02,	0.16E+01)
0.654	-0.533E+02	+- (	0.60E+02,	0.27E+01)
0.673	-0.136E+01	+- (	0.62E+02,	0.68E-01)
0.692	-0.716E+02	+- (	0.59E+02,	0.36E+01)
0.711	-0.903E+01	+- (	0.61E+02,	0.45E+00)
0.731	0.175E+02	+- (	0.68E+02,	0.88E+00)
0.750	-0.363E+02	+- (	0.52E+02,	0.18E+01)
0.769	0.691E+02	+- (	0.62E+02,	0.35E+01)
0.789	0.475E+01	+- (	0.49E+02,	0.24E+00)
0.808	-0.137E+03	+- (	0.89E+02,	0.69E+01)
0.828	-0.462E+02	+- (	0.73E+02,	0.23E+01)
0.847	-0.138E+02	+- (	0.66E+02,	0.69E+00)
0.867	0.521E+03	+- (	0.11E+03,	0.26E+02)
0.886	0.651E+04	+- (	0.30E+03,	0.33E+03)
0.906	0.246E+05	+- (	0.56E+03,	0.12E+04)
0.926	0.364E+05	+- (	0.65E+03,	0.18E+04)
0.945	0.294E+05	+- (	0.57E+03,	0.15E+04)
0.965	0.210E+05	+- (	0.46E+03,	0.11E+04)
0.985	0.164E+05	+- (	0.39E+03,	0.82E+03)
1.004	0.119E+05	+- (	0.33E+03,	0.60E+03)
1.024	0.714E+04	+- (	0.25E+03,	0.36E+03)
1.044	0.429E+04	+- (	0.19E+03,	0.22E+03)

W(GeV)	CROSS SECTION		ERRORS	
1.063	0.359E+04	+- (	0.17E+03,	0.18E+03)
1.083	0.319E+04	+- (	0.15E+03,	0.16E+03)
1.103	0.354E+04	+- (	0.15E+03,	0.18E+03)
1.123	0.397E+04	+- (	0.16E+03,	0.20E+03)
1.142	0.470E+04	+- (	0.17E+03,	0.24E+03)
1.162	0.561E+04	+- (	0.18E+03,	0.28E+03)
1.182	0.770E+04	+- (	0.21E+03,	0.39E+03)
1.202	0.995E+04	+- (	0.24E+03,	0.50E+03)
1.221	0.118E+05	+- (	0.27E+03,	0.59E+03)
1.241	0.127E+05	+- (	0.28E+03,	0.64E+03)
1.261	0.137E+05	+- (	0.30E+03,	0.69E+03)
1.281	0.139E+05	+- (	0.31E+03,	0.70E+03)
1.301	0.150E+05	+- (	0.33E+03,	0.75E+03)
1.320	0.146E+05	+- (	0.34E+03,	0.73E+03)
1.340	0.154E+05	+- (	0.36E+03,	0.77E+03)
1.360	0.161E+05	+- (	0.38E+03,	0.81E+03)
1.380	0.176E+05	+- (	0.38E+03,	0.89E+03)
1.400	0.184E+05	+- (	0.39E+03,	0.93E+03)
1.420	0.197E+05	+- (	0.39E+03,	0.99E+03)
1.439	0.213E+05	+- (	0.41E+03,	0.11E+04)
1.459	0.231E+05	+- (	0.45E+03,	0.12E+04)
1.479	0.274E+05	+- (	0.52E+03,	0.14E+04)
1.499	0.322E+05	+- (	0.59E+03,	0.16E+04)
1.519	0.361E+05	+- (	0.67E+03,	0.18E+04)
1.539	0.356E+05	+- (	0.74E+03,	0.18E+04)
1.559	0.330E+05	+- (	0.83E+03,	0.17E+04)
1.578	0.309E+05	+- (	0.10E+04,	0.16E+04)
1.598	0.336E+05	+- (	0.11E+04,	0.17E+04)
1.618	0.331E+05	+- (	0.11E+04,	0.17E+04)
1.638	0.345E+05	+- (	0.10E+04,	0.17E+04)
1.658	0.402E+05	+- (	0.11E+04,	0.20E+04)
1.678	0.444E+05	+- (	0.12E+04,	0.22E+04)
1.698	0.478E+05	+- (	0.13E+04,	0.24E+04)
1.718	0.483E+05	+- (	0.13E+04,	0.24E+04)
1.738	0.514E+05	+- (	0.15E+04,	0.26E+04)
1.757	0.515E+05	+- (	0.16E+04,	0.26E+04)
1.777	0.505E+05	+- (	0.17E+04,	0.25E+04)
1.797	0.455E+05	+- (	0.18E+04,	0.25E+04)
1.817	0.494E+05	+- (	0.17E+04,	0.25E+04)
1.837	0.545E+05	+- (	0.17E+04,	0.27E+04)
1.857	0.547E+05	+- (	0.17E+04,	0.27E+04)
1.877	0.549E+05	+- (	0.17E+04,	0.28E+04)
1.897	0.548E+05	+- (	0.17E+04,	0.27E+04)
1.917	0.585E+05	+- (	0.17E+04,	0.25E+04)
1.937	0.648E+05	+- (	0.20E+04,	0.32E+04)
1.957	0.616E+05	+- (	0.21E+04,	0.31E+04)
1.976	0.619E+05	+- (	0.23E+04,	0.31E+04)
1.996	0.628E+05	+- (	0.23E+04,	0.32E+04)
2.031	0.669E+05	+- (	0.15E+04,	0.34E+04)
2.081	0.723E+05	+- (	0.16E+04,	0.36E+04)
2.131	0.771E+05	+- (	0.18E+04,	0.39E+04)
2.181	0.783E+05	+- (	0.32E+04,	0.39E+04)
2.255	0.814E+05	+- (	0.83E+03,	0.41E+04)
2.505	0.926E+05	+- (	0.68E+03,	0.46E+04)
2.754	0.977E+05	+- (	0.70E+03,	0.49E+04)
3.003	0.102E+06	+- (	0.68E+03,	0.51E+04)
3.253	0.104E+06	+- (	0.15E+04,	0.52E+04)
3.503	0.100E+06	+- (	0.13E+04,	0.50E+04)
3.752	0.104E+06	+- (	0.16E+04,	0.52E+04)
4.002	0.998E+05	+- (	0.14E+04,	0.50E+04)
4.252	0.101E+06	+- (	0.98E+03,	0.50E+04)
4.502	0.102E+06	+- (	0.99E+03,	0.51E+04)
4.751	0.117E+06	+- (	0.27E+04,	0.65E+04)
5.001	0.123E+06	+- (	0.25E+04,	0.69E+04)
5.251	0.161E+06	+- (	0.37E+04,	0.81E+04)
5.501	0.193E+06	+- (	0.87E+04,	0.10E+05)
5.750	0.379E+06	+- (	0.16E+05,	0.20E+05)

E_0 = 19.50 GeV, θ = 10.00, RAW DATA

W (GEV)	CROSS SECTION		ERRORS	
0.673	0.131E+02	+- (	0.14E+02,	0.66E+00)
0.692	0.101E+02	+- (	0.11E+02,	0.51E+00)
0.711	0.760E+01	+- (	0.81E+01,	0.38E+00)
0.789	0.313E+01	+- (	0.33E+01,	0.16E+00)
0.808	0.260E+01	+- (	0.28E+01,	0.13E+00)
0.828	-0.175E+02	+- (	0.22E+02,	0.87E+00)
0.847	-0.899E+01	+- (	0.13E+02,	0.45E+00)
0.867	0.165E+01	+- (	0.69E+01,	0.83E-01)
0.886	0.646E+02	+- (	0.12E+02,	0.32E+01)
0.906	0.180E+03	+- (	0.16E+02,	0.90E+01)
0.926	0.268E+03	+- (	0.18E+02,	0.13E+02)
0.945	0.249E+03	+- (	0.16E+02,	0.12E+02)
0.965	0.168E+03	+- (	0.13E+02,	0.84E+01)

HYDROGEN CROSS SECTION

W(GeV)	CROSS SECTION		ERRORS	
0.985	0.989E+02	+- (	0.90E+01,	0.49E+01)
1.004	0.543E+02	+- (	0.68E+01,	0.27E+01)
1.024	0.270E+02	+- (	0.62E+01,	0.13E+01)
1.044	0.284E+02	+- (	0.54E+01,	0.14E+01)
1.063	0.315E+02	+- (	0.46E+01,	0.16E+01)
1.083	0.285E+02	+- (	0.49E+01,	0.14E+01)
1.103	0.228E+02	+- (	0.48E+01,	0.11E+01)
1.123	0.230E+02	+- (	0.39E+01,	0.12E+01)
1.142	0.228E+02	+- (	0.45E+01,	0.11E+01)
1.162	0.405E+02	+- (	0.46E+01,	0.20E+01)
1.182	0.540E+02	+- (	0.54E+01,	0.27E+01)
1.202	0.638E+02	+- (	0.47E+01,	0.32E+01)
1.221	0.816E+02	+- (	0.55E+01,	0.41E+01)
1.241	0.903E+02	+- (	0.55E+01,	0.45E+01)
1.261	0.963E+02	+- (	0.53E+01,	0.48E+01)
1.281	0.108E+03	+- (	0.62E+01,	0.54E+01)
1.301	0.118E+03	+- (	0.61E+01,	0.59E+01)
1.320	0.126E+03	+- (	0.61E+01,	0.63E+01)
1.340	0.138E+03	+- (	0.66E+01,	0.69E+01)
1.360	0.166E+03	+- (	0.70E+01,	0.83E+01)
1.380	0.170E+03	+- (	0.71E+01,	0.85E+01)
1.400	0.185E+03	+- (	0.71E+01,	0.92E+01)
1.420	0.194E+03	+- (	0.75E+01,	0.97E+01)
1.439	0.203E+03	+- (	0.79E+01,	0.10E+02)
1.459	0.267E+03	+- (	0.88E+01,	0.13E+02)
1.479	0.316E+03	+- (	0.99E+01,	0.16E+02)
1.499	0.369E+03	+- (	0.11E+02,	0.18E+02)
1.519	0.380E+03	+- (	0.12E+02,	0.19E+02)
1.539	0.377E+03	+- (	0.12E+02,	0.19E+02)
1.559	0.382E+03	+- (	0.12E+02,	0.19E+02)
1.578	0.373E+03	+- (	0.12E+02,	0.19E+02)
1.598	0.358E+03	+- (	0.12E+02,	0.18E+02)
1.618	0.393E+03	+- (	0.13E+02,	0.20E+02)
1.638	0.429E+03	+- (	0.14E+02,	0.21E+02)
1.658	0.494E+03	+- (	0.15E+02,	0.25E+02)
1.678	0.527E+03	+- (	0.16E+02,	0.26E+02)
1.698	0.617E+03	+- (	0.17E+02,	0.31E+02)
1.718	0.695E+03	+- (	0.18E+02,	0.35E+02)
1.738	0.714E+03	+- (	0.18E+02,	0.36E+02)
1.757	0.738E+03	+- (	0.19E+02,	0.37E+02)
1.777	0.684E+03	+- (	0.18E+02,	0.34E+02)
1.797	0.771E+03	+- (	0.20E+02,	0.39E+02)
1.817	0.748E+03	+- (	0.19E+02,	0.37E+02)
1.837	0.791E+03	+- (	0.20E+02,	0.40E+02)
1.857	0.798E+03	+- (	0.21E+02,	0.40E+02)
1.877	0.859E+03	+- (	0.22E+02,	0.43E+02)
1.897	0.908E+03	+- (	0.23E+02,	0.45E+02)
1.917	0.976E+03	+- (	0.24E+02,	0.49E+02)
1.937	0.102E+04	+- (	0.26E+02,	0.51E+02)
1.957	0.103E+04	+- (	0.25E+02,	0.51E+02)
1.976	0.110E+04	+- (	0.26E+02,	0.55E+02)
1.996	0.109E+04	+- (	0.25E+02,	0.55E+02)
2.031	0.126E+04	+- (	0.18E+02,	0.63E+02)
2.081	0.140E+04	+- (	0.21E+02,	0.70E+02)
2.131	0.159E+04	+- (	0.25E+02,	0.80E+02)
2.181	0.170E+04	+- (	0.30E+02,	0.85E+02)
2.231	0.195E+04	+- (	0.41E+02,	0.97E+02)
2.280	0.215E+04	+- (	0.76E+02,	0.11E+03)
2.397	0.253E+04	+- (	0.22E+02,	0.13E+03)
2.699	0.388E+04	+- (	0.22E+02,	0.19E+03)
3.153	0.593E+04	+- (	0.46E+02,	0.30E+03)
3.490	0.765E+04	+- (	0.54E+02,	0.38E+03)
3.963	0.954E+04	+- (	0.63E+02,	0.53E+03)
4.523	0.124E+05	+- (	0.84E+02,	0.70E+03)

E_0=13.30 GeV, θ=15.00, RAW DATA

W (GEV)	CROSS SECTION		ERRORS	
0.588	0.105E+02	+- (	0.11E+02,	0.53E+00)
0.665	0.303E+01	+- (	0.32E+01,	0.15E+00)
0.685	-0.181E+01	+- (	0.51E+01,	0.90E-01)
0.763	0.229E+00	+- (	0.26E+01,	0.11E-01)
0.802	0.240E+00	+- (	0.26E+01,	0.12E-01)
0.822	-0.441E+01	+- (	0.24E+01,	0.22E+00)
0.842	0.125E+01	+- (	0.16E+01,	0.63E-01)
0.861	0.722E+00	+- (	0.22E+01,	0.36E-01)
0.881	0.155E+01	+- (	0.18E+01,	0.78E-01)
0.901	0.216E+02	+- (	0.32E+01,	0.11E+01)
0.921	0.135E+03	+- (	0.73E+01,	0.69E+01)
0.940	0.239E+03	+- (	0.93E+01,	0.12E+02)
0.960	0.199E+03	+- (	0.82E+01,	0.10E+02)
0.980	0.924E+02	+- (	0.53E+01,	0.47E+01)
1.000	0.423E+02	+- (	0.35E+01,	0.22E+01)

5-78

W(GeV)	CROSS SECTION		ERRORS	
1.019	0.289E+02	+- (	0.31E+01,	0.15E+01)
1.039	0.210E+02	+- (	0.26E+01,	0.11E+01)
1.059	0.181E+02	+- (	0.24E+01,	0.92E+00)
1.079	0.214E+02	+- (	0.23E+01,	0.11E+01)
1.099	0.191E+02	+- (	0.22E+01,	0.97E+00)
1.118	0.168E+02	+- (	0.23E+01,	0.86E+00)
1.138	0.214E+02	+- (	0.22E+01,	0.11E+01)
1.158	0.273E+02	+- (	0.24E+01,	0.14E+01)
1.178	0.329E+02	+- (	0.27E+01,	0.17E+01)
1.198	0.396E+02	+- (	0.29E+01,	0.20E+01)
1.218	0.473E+02	+- (	0.30E+01,	0.24E+01)
1.238	0.592E+02	+- (	0.33E+01,	0.30E+01)
1.257	0.626E+02	+- (	0.34E+01,	0.32E+01)
1.277	0.726E+02	+- (	0.35E+01,	0.37E+01)
1.297	0.766E+02	+- (	0.36E+01,	0.39E+01)
1.317	0.840E+02	+- (	0.36E+01,	0.43E+01)
1.337	0.951E+02	+- (	0.41E+01,	0.48E+01)
1.357	0.102E+03	+- (	0.41E+01,	0.52E+01)
1.377	0.110E+03	+- (	0.42E+01,	0.56E+01)
1.397	0.128E+03	+- (	0.44E+01,	0.65E+01)
1.416	0.126E+03	+- (	0.45E+01,	0.64E+01)
1.436	0.144E+03	+- (	0.47E+01,	0.73E+01)
1.456	0.161E+03	+- (	0.49E+01,	0.82E+01)
1.476	0.198E+03	+- (	0.55E+01,	0.10E+02)
1.496	0.242E+03	+- (	0.61E+01,	0.12E+02)
1.516	0.283E+03	+- (	0.65E+01,	0.14E+02)
1.536	0.268E+03	+- (	0.63E+01,	0.14E+02)
1.556	0.265E+03	+- (	0.64E+01,	0.14E+02)
1.576	0.258E+03	+- (	0.63E+01,	0.13E+02)
1.596	0.260E+03	+- (	0.63E+01,	0.13E+02)
1.615	0.269E+03	+- (	0.66E+01,	0.14E+02)
1.635	0.292E+03	+- (	0.69E+01,	0.15E+02)
1.655	0.323E+03	+- (	0.76E+01,	0.16E+02)
1.675	0.367E+03	+- (	0.82E+01,	0.19E+02)
1.695	0.429E+03	+- (	0.93E+01,	0.22E+02)
1.715	0.477E+03	+- (	0.10E+02,	0.24E+02)
1.735	0.505E+03	+- (	0.11E+02,	0.26E+02)
1.755	0.500E+03	+- (	0.11E+02,	0.26E+02)
1.775	0.503E+03	+- (	0.11E+02,	0.26E+02)
1.795	0.515E+03	+- (	0.11E+02,	0.26E+02)
1.815	0.537E+03	+- (	0.11E+02,	0.27E+02)
1.835	0.536E+03	+- (	0.12E+02,	0.27E+02)
1.855	0.581E+03	+- (	0.13E+02,	0.30E+02)
1.875	0.602E+03	+- (	0.14E+02,	0.31E+02)
1.894	0.658E+03	+- (	0.13E+02,	0.34E+02)
1.914	0.691E+03	+- (	0.13E+02,	0.35E+02)
1.934	0.739E+03	+- (	0.13E+02,	0.38E+02)
1.954	0.767E+03	+- (	0.14E+02,	0.39E+02)
1.974	0.804E+03	+- (	0.16E+02,	0.41E+02)
1.994	0.846E+03	+- (	0.18E+02,	0.43E+02)
2.029	0.934E+03	+- (	0.13E+02,	0.48E+02)
2.079	0.102E+04	+- (	0.18E+02,	0.52E+02)
2.126	0.116E+04	+- (	0.12E+02,	0.59E+02)
2.257	0.146E+04	+- (	0.13E+02,	0.74E+02)
2.524	0.224E+04	+- (	0.17E+02,	0.11E+03)
2.915	0.372E+04	+- (	0.19E+02,	0.19E+03)
3.195	0.488E+04	+- (	0.28E+02,	0.25E+03)
3.576	0.648E+04	+- (	0.67E+02,	0.32E+03)
4.003	0.996E+04	+- (	0.18E+03,	0.50E+03)

E_0=16.00 GeV, θ=15.00, RAW DATA

W (GEV)	CROSS SECTION		ERRORS	
0.554	0.513E+01	+- (	0.55E+01,	0.26E+00)
0.611	0.345E+01	+- (	0.37E+01,	0.17E+00)
0.727	0.151E+01	+- (	0.16E+01,	0.75E-01)
0.864	-0.911E-01	+- (	0.29E+01,	0.46E-02)
0.883	0.701E+01	+- (	0.24E+01,	0.35E+00)
0.903	0.328E+02	+- (	0.49E+01,	0.16E+01)
0.923	0.425E+02	+- (	0.53E+01,	0.21E+01)
0.942	0.288E+02	+- (	0.42E+01,	0.14E+01)
0.962	0.180E+02	+- (	0.32E+01,	0.90E+00)
0.982	0.944E+01	+- (	0.27E+01,	0.47E+00)
1.002	0.660E+01	+- (	0.18E+01,	0.33E+00)
1.021	0.184E+01	+- (	0.27E+01,	0.92E-01)
1.041	0.730E+01	+- (	0.18E+01,	0.37E+00)
1.061	0.502E+01	+- (	0.14E+01,	0.25E+00)
1.081	0.364E+01	+- (	0.17E+01,	0.18E+00)
1.100	0.325E+01	+- (	0.11E+01,	0.16E+00)
1.120	0.937E+01	+- (	0.16E+01,	0.47E+00)
1.140	0.463E+01	+- (	0.16E+01,	0.23E+00)
1.160	0.101E+02	+- (	0.19E+01,	0.51E+00)
1.180	0.382E+01	+- (	0.23E+01,	0.19E+00)

3360850

HYDROGEN CROSS SECTION

W(GeV)	CROSS SECTION		ERRORS	
1.199	0.101E+02	+- (	0.20E+01,	0.50E+00)
1.219	0.998E+01	+- (	0.17E+01,	0.50E+00)
1.239	0.126E+02	+- (	0.23E+01,	0.63E+00)
1.259	0.138E+02	+- (	0.22E+01,	0.69E+00)
1.279	0.158E+02	+- (	0.25E+01,	0.79E+00)
1.299	0.188E+02	+- (	0.23E+01,	0.94E+00)
1.318	0.184E+02	+- (	0.27E+01,	0.92E+00)
1.338	0.209E+02	+- (	0.26E+01,	0.10E+01)
1.358	0.252E+02	+- (	0.29E+01,	0.13E+01)
1.378	0.295E+02	+- (	0.31E+01,	0.15E+01)
1.398	0.301E+02	+- (	0.30E+01,	0.15E+01)
1.418	0.332E+02	+- (	0.32E+01,	0.17E+01)
1.438	0.368E+02	+- (	0.30E+01,	0.18E+01)
1.458	0.515E+02	+- (	0.36E+01,	0.26E+01)
1.477	0.582E+02	+- (	0.39E+01,	0.29E+01)
1.497	0.530E+02	+- (	0.36E+01,	0.26E+01)
1.517	0.600E+02	+- (	0.36E+01,	0.30E+01)
1.537	0.595E+02	+- (	0.40E+01,	0.30E+01)
1.557	0.598E+02	+- (	0.37E+01,	0.30E+01)
1.577	0.554E+02	+- (	0.37E+01,	0.28E+01)
1.597	0.625E+02	+- (	0.37E+01,	0.31E+01)
1.617	0.637E+02	+- (	0.37E+01,	0.32E+01)
1.637	0.883E+02	+- (	0.43E+01,	0.42E+01)
1.656	0.897E+02	+- (	0.44E+01,	0.45E+01)
1.676	0.100E+03	+- (	0.46E+01,	0.50E+01)
1.696	0.101E+03	+- (	0.46E+01,	0.51E+01)
1.716	0.120E+03	+- (	0.47E+01,	0.60E+01)
1.736	0.117E+03	+- (	0.46E+01,	0.59E+01)
1.756	0.123E+03	+- (	0.49E+01,	0.61E+01)
1.776	0.121E+03	+- (	0.48E+01,	0.61E+01)
1.796	0.124E+03	+- (	0.50E+01,	0.62E+01)
1.816	0.131E+03	+- (	0.49E+01,	0.66E+01)
1.836	0.140E+03	+- (	0.52E+01,	0.70E+01)
1.856	0.155E+03	+- (	0.53E+01,	0.77E+01)
1.876	0.157E+03	+- (	0.55E+01,	0.79E+01)
1.895	0.165E+03	+- (	0.56E+01,	0.83E+01)
1.915	0.175E+03	+- (	0.59E+01,	0.88E+01)
1.935	0.188E+03	+- (	0.63E+01,	0.94E+01)
1.955	0.216E+03	+- (	0.70E+01,	0.11E+02)
1.975	0.209E+03	+- (	0.73E+01,	0.10E+02)
1.995	0.225E+03	+- (	0.80E+01,	0.11E+02)
2.030	0.243E+03	+- (	0.59E+01,	0.12E+02)
2.080	0.280E+03	+- (	0.85E+01,	0.14E+02)
2.130	0.293E+03	+- (	0.17E+02,	0.15E+02)
2.180	0.303E+03	+- (	0.11E+03,	0.15E+02)
2.275	0.425E+03	+- (	0.56E+01,	0.22E+02)
2.580	0.768E+03	+- (	0.79E+01,	0.39E+02)
2.878	0.124E+04	+- (	0.12E+02,	0.63E+02)
3.310	0.209E+04	+- (	0.19E+02,	0.11E+03)
3.614	0.286E+04	+- (	0.35E+02,	0.15E+03)
4.021	0.397E+04	+- (	0.42E+02,	0.20E+03)
4.469	0.589E+04	+- (	0.81E+02,	0.31E+03)

E_0 = 19.50 GeV, θ = 15.00, RAW DATA

W(GEV)	CROSS SECTION		ERRORS	
1.817	0.233E+02	+- (	0.83E+01,	0.12E+01)
1.837	0.215E+02	+- (	0.85E+01,	0.11E+01)
1.857	0.286E+02	+- (	0.39E+01,	0.14E+01)
1.877	0.315E+02	+- (	0.34E+01,	0.16E+01)
1.897	0.323E+02	+- (	0.30E+01,	0.16E+01)
1.917	0.406E+02	+- (	0.30E+01,	0.20E+01)
1.937	0.422E+02	+- (	0.27E+01,	0.21E+01)
1.957	0.444E+02	+- (	0.26E+01,	0.22E+01)
1.976	0.451E+02	+- (	0.23E+01,	0.23E+01)
1.996	0.495E+02	+- (	0.23E+01,	0.25E+01)
2.031	0.534E+02	+- (	0.15E+01,	0.27E+01)
2.081	0.627E+02	+- (	0.16E+01,	0.31E+01)
2.131	0.706E+02	+- (	0.19E+01,	0.35E+01)
2.181	0.771E+02	+- (	0.24E+01,	0.39E+01)
2.231	0.947E+02	+- (	0.41E+01,	0.47E+01)
2.280	0.802E+02	+- (	0.22E+02,	0.40E+01)
2.313	0.110E+03	+- (	0.12E+01,	0.55E+01)
2.641	0.225E+03	+- (	0.25E+01,	0.11E+02)
2.984	0.409E+03	+- (	0.49E+01,	0.21E+02)
3.316	0.663E+03	+- (	0.76E+01,	0.34E+02)
3.792	0.117E+04	+- (	0.12E+02,	0.60E+02)
4.750	0.282E+04	+- (	0.30E+02,	0.14E+03)
5.028	0.387E+04	+- (	0.57E+02,	0.20E+03)

E_0 = 6.50 GeV, θ = 18.00, RAW DATA

W(GEV)	CROSS SECTION		ERRORS	
0.697	-0.343E+02	+- (	0.50E+02,	0.17E+01)
0.717	-0.180E+02	+- (	0.26E+02,	0.90E+00)
0.737	0.313E+02	+- (	0.25E+02,	0.16E+01)
0.756	0.620E+02	+- (	0.31E+02,	0.31E+01)
0.776	-0.408E+02	+- (	0.21E+02,	0.20E+01)
0.796	0.267E+01	+- (	0.21E+02,	0.13E+00)
0.816	-0.692E+01	+- (	0.15E+02,	0.35E+00)
0.836	0.727E-01	+- (	0.17E+02,	0.36E-02)
0.856	-0.223E+02	+- (	0.12E+02,	0.11E+01)
0.875	-0.732E+01	+- (	0.12E+02,	0.37E+00)
0.895	0.944E+02	+- (	0.20E+02,	0.47E+01)
0.915	0.253E+04	+- (	0.68E+02,	0.13E+03)
0.935	0.181E+05	+- (	0.17E+03,	0.90E+03)
0.955	0.134E+05	+- (	0.14E+03,	0.67E+03)
0.975	0.325E+04	+- (	0.64E+02,	0.16E+03)
0.995	0.188E+04	+- (	0.44E+02,	0.94E+02)
1.015	0.127E+04	+- (	0.33E+02,	0.64E+02)
1.034	0.114E+04	+- (	0.28E+02,	0.57E+02)
1.054	0.992E+03	+- (	0.25E+02,	0.50E+02)
1.074	0.877E+03	+- (	0.24E+02,	0.44E+02)
1.094	0.908E+03	+- (	0.24E+02,	0.45E+02)
1.114	0.106E+04	+- (	0.25E+02,	0.53E+02)
1.134	0.127E+04	+- (	0.27E+02,	0.63E+02)
1.154	0.163E+04	+- (	0.30E+02,	0.81E+02)
1.174	0.222E+04	+- (	0.35E+02,	0.11E+03)
1.194	0.296E+04	+- (	0.44E+02,	0.15E+03)
1.214	0.381E+04	+- (	0.58E+02,	0.19E+03)
1.234	0.413E+04	+- (	0.68E+02,	0.21E+03)
1.253	0.437E+04	+- (	0.76E+02,	0.22E+03)
1.273	0.406E+04	+- (	0.78E+02,	0.20E+03)
1.293	0.415E+04	+- (	0.83E+02,	0.21E+03)
1.313	0.417E+04	+- (	0.92E+02,	0.21E+03)
1.333	0.433E+04	+- (	0.10E+03,	0.22E+03)
1.353	0.459E+04	+- (	0.10E+03,	0.23E+03)
1.373	0.484E+04	+- (	0.10E+03,	0.24E+03)
1.393	0.502E+04	+- (	0.10E+03,	0.25E+03)
1.413	0.555E+04	+- (	0.11E+03,	0.28E+03)
1.433	0.584E+04	+- (	0.11E+03,	0.29E+03)
1.453	0.656E+04	+- (	0.12E+03,	0.33E+03)
1.473	0.734E+04	+- (	0.13E+03,	0.37E+03)
1.493	0.909E+04	+- (	0.17E+03,	0.45E+03)
1.513	0.104E+05	+- (	0.21E+03,	0.52E+03)
1.533	0.981E+04	+- (	0.22E+03,	0.49E+03)
1.553	0.100E+05	+- (	0.24E+03,	0.50E+03)
1.573	0.942E+04	+- (	0.27E+03,	0.47E+03)
1.592	0.863E+04	+- (	0.27E+03,	0.43E+03)
1.612	0.954E+04	+- (	0.28E+03,	0.48E+03)
1.632	0.961E+04	+- (	0.27E+03,	0.48E+03)
1.652	0.108E+05	+- (	0.26E+03,	0.54E+03)
1.672	0.126E+05	+- (	0.27E+03,	0.63E+03)
1.692	0.137E+05	+- (	0.27E+03,	0.69E+03)
1.712	0.150E+05	+- (	0.28E+03,	0.75E+03)
1.732	0.150E+05	+- (	0.28E+03,	0.75E+03)
1.752	0.143E+05	+- (	0.28E+03,	0.71E+03)
1.772	0.145E+05	+- (	0.25E+03,	0.73E+03)
1.792	0.137E+05	+- (	0.20E+03,	0.69E+03)
1.812	0.147E+05	+- (	0.20E+03,	0.74E+03)
1.832	0.153E+05	+- (	0.21E+03,	0.76E+03)
1.852	0.156E+05	+- (	0.24E+03,	0.78E+03)
1.872	0.162E+05	+- (	0.36E+03,	0.81E+03)
1.892	0.179E+05	+- (	0.29E+04,	0.90E+03)
1.952	0.154E+05	+- (	0.11E+04,	0.77E+03)
1.972	0.184E+05	+- (	0.41E+03,	0.92E+03)
1.992	0.189E+05	+- (	0.37E+03,	0.95E+03)
2.027	0.203E+05	+- (	0.26E+03,	0.10E+04)
2.077	0.113E+05	+- (	0.29E+04,	0.56E+03)
2.251	0.243E+05	+- (	0.19E+03,	0.12E+04)
2.252	0.237E+05	+- (	0.26E+03,	0.12E+04)
2.502	0.289E+05	+- (	0.26E+03,	0.14E+04)
2.751	0.319E+05	+- (	0.38E+03,	0.16E+04)

5-78
3360851

HYDROGEN CROSS SECTION

E_0 = 10.40 GeV, θ = 18.00, RAW DATA

W (GEV)	CROSS SECTION		ERRORS	
0.701	0.986E+01	+- (	0.11E+02,	0.50E+00)
0.741	0.464E+01	+- (	0.49E+01,	0.24E+00)
0.800	0.234E+01	+- (	0.25E+01,	0.12E+00)
0.839	0.168E+01	+- (	0.18E+01,	0.86E-01)
0.859	-0.878E+00	+- (	0.50E+01,	0.45E-01)
0.879	-0.124E+01	+- (	0.33E+01,	0.63E-01)
0.898	-0.121E+01	+- (	0.32E+01,	0.62E-01)
0.918	0.594E+02	+- (	0.10E+02,	0.30E+01)
0.938	0.343E+03	+- (	0.22E+02,	0.17E+02)
0.958	0.398E+03	+- (	0.23E+02,	0.20E+02)
0.978	0.173E+03	+- (	0.14E+02,	0.88E+01)
0.997	0.574E+02	+- (	0.83E+01,	0.29E+01)
1.017	0.388E+02	+- (	0.64E+01,	0.20E+01)
1.037	0.356E+02	+- (	0.62E+01,	0.18E+01)
1.057	0.132E+02	+- (	0.49E+01,	0.68E+00)
1.077	0.309E+02	+- (	0.58E+01,	0.16E+01)
1.097	0.253E+02	+- (	0.62E+01,	0.13E+01)
1.117	0.168E+02	+- (	0.60E+01,	0.86E+00)
1.136	0.292E+02	+- (	0.69E+01,	0.15E+01)
1.156	0.296E+02	+- (	0.66E+01,	0.15E+01)
1.176	0.457E+02	+- (	0.83E+01,	0.23E+01)
1.196	0.680E+02	+- (	0.10E+02,	0.35E+01)
1.216	0.805E+02	+- (	0.11E+02,	0.41E+01)
1.236	0.114E+03	+- (	0.12E+02,	0.58E+01)
1.256	0.126E+03	+- (	0.13E+02,	0.64E+01)
1.276	0.102E+03	+- (	0.13E+02,	0.52E+01)
1.295	0.116E+03	+- (	0.15E+02,	0.59E+01)
1.315	0.157E+03	+- (	0.18E+02,	0.80E+01)
1.335	0.140E+03	+- (	0.17E+02,	0.71E+01)
1.355	0.158E+03	+- (	0.16E+02,	0.80E+01)
1.375	0.168E+03	+- (	0.17E+02,	0.86E+01)
1.395	0.204E+03	+- (	0.20E+02,	0.10E+02)
1.415	0.207E+03	+- (	0.20E+02,	0.11E+02)
1.435	0.275E+03	+- (	0.24E+02,	0.14E+02)
1.455	0.222E+03	+- (	0.23E+02,	0.11E+02)
1.475	0.313E+03	+- (	0.27E+02,	0.16E+02)
1.495	0.340E+03	+- (	0.27E+02,	0.17E+02)
1.515	0.370E+03	+- (	0.28E+02,	0.19E+02)
1.534	0.386E+03	+- (	0.31E+02,	0.20E+02)
1.554	0.351E+03	+- (	0.31E+02,	0.18E+02)
1.574	0.376E+03	+- (	0.35E+02,	0.19E+02)
1.594	0.336E+03	+- (	0.32E+02,	0.17E+02)
1.614	0.440E+03	+- (	0.34E+02,	0.22E+02)
1.634	0.426E+03	+- (	0.35E+02,	0.22E+02)
1.654	0.538E+03	+- (	0.41E+02,	0.27E+02)
1.674	0.626E+03	+- (	0.47E+02,	0.32E+02)
1.694	0.600E+03	+- (	0.47E+02,	0.31E+02)
1.714	0.690E+03	+- (	0.44E+02,	0.35E+02)
1.734	0.713E+03	+- (	0.42E+02,	0.36E+02)
1.754	0.716E+03	+- (	0.42E+02,	0.37E+02)
1.774	0.735E+03	+- (	0.42E+02,	0.37E+02)
1.794	0.765E+03	+- (	0.45E+02,	0.39E+02)
1.814	0.771E+03	+- (	0.46E+02,	0.39E+02)
1.834	0.865E+03	+- (	0.50E+02,	0.44E+02)
1.853	0.871E+03	+- (	0.55E+02,	0.44E+02)
1.873	0.915E+03	+- (	0.63E+02,	0.47E+02)
1.893	0.917E+03	+- (	0.79E+02,	0.47E+02)
1.913	0.107E+04	+- (	0.12E+03,	0.54E+02)
1.933	0.884E+03	+- (	0.23E+03,	0.45E+02)
1.973	0.830E+03	+- (	0.28E+03,	0.42E+02)
1.993	0.103E+04	+- (	0.13E+03,	0.53E+02)
2.028	0.144E+04	+- (	0.58E+02,	0.73E+02)
2.078	0.149E+04	+- (	0.55E+02,	0.76E+02)
2.128	0.178E+04	+- (	0.75E+02,	0.91E+02)
2.178	0.178E+04	+- (	0.42E+03,	0.91E+02)
2.306	0.231E+04	+- (	0.42E+02,	0.12E+03)
2.656	0.384E+04	+- (	0.75E+02,	0.19E+03)
2.904	0.521E+04	+- (	0.72E+02,	0.26E+03)
3.237	0.690E+04	+- (	0.84E+02,	0.35E+03)
3.607	0.101E+05	+- (	0.19E+03,	0.50E+03)

E_0 = 13.30 GeV, θ = 18.00 RAW DATA

W (GEV)	CROSS SECTION		ERRORS	
1.476	0.747E+02	+- (	0.31E+02,	0.38E+01)
1.496	0.497E+02	+- (	0.18E+02,	0.25E+01)
1.516	0.530E+02	+- (	0.13E+02,	0.27E+01)
1.536	0.647E+02	+- (	0.11E+02,	0.33E+01)
1.556	0.663E+02	+- (	0.90E+01,	0.34E+01)
1.576	0.491E+02	+- (	0.71E+01,	0.25E+01)

W(GeV)	CROSS SECTION		ERRORS	
1.596	0.655E+02	+- (	0.66E+01,	0.33E+01)
1.615	0.715E+02	+- (	0.62E+01,	0.36E+01)
1.635	0.622E+02	+- (	0.57E+01,	0.32E+01)
1.655	0.728E+02	+- (	0.53E+01,	0.37E+01)
1.675	0.935E+02	+- (	0.61E+01,	0.48E+01)
1.695	0.108E+03	+- (	0.60E+01,	0.55E+01)
1.715	0.123E+03	+- (	0.65E+01,	0.63E+01)
1.735	0.134E+03	+- (	0.67E+01,	0.68E+01)
1.755	0.136E+03	+- (	0.70E+01,	0.70E+01)
1.775	0.133E+03	+- (	0.68E+01,	0.68E+01)
1.795	0.128E+03	+- (	0.66E+01,	0.65E+01)
1.815	0.123E+03	+- (	0.66E+01,	0.62E+01)
1.835	0.139E+03	+- (	0.69E+01,	0.71E+01)
1.855	0.148E+03	+- (	0.69E+01,	0.75E+01)
1.875	0.162E+03	+- (	0.72E+01,	0.83E+01)
1.894	0.164E+03	+- (	0.78E+01,	0.84E+01)
1.914	0.172E+03	+- (	0.81E+01,	0.88E+01)
1.934	0.198E+03	+- (	0.88E+01,	0.10E+02)
1.954	0.208E+03	+- (	0.90E+01,	0.11E+02)
1.974	0.215E+03	+- (	0.96E+01,	0.11E+02)
1.994	0.237E+03	+- (	0.11E+02,	0.12E+02)
2.029	0.241E+03	+- (	0.10E+02,	0.12E+02)
2.079	0.320E+03	+- (	0.93E+02,	0.16E+02)
2.182	0.361E+03	+- (	0.44E+01,	0.18E+02)
2.463	0.659E+03	+- (	0.91E+01,	0.34E+02)
2.735	0.105E+04	+- (	0.10E+02,	0.53E+02)
3.130	0.182E+04	+- (	0.21E+02,	0.93E+02)
3.404	0.249E+04	+- (	0.33E+02,	0.12E+03)
3.767	0.360E+04	+- (	0.57E+02,	0.18E+03)
4.159	0.573E+04	+- (	0.12E+03,	0.30E+03)

E_0 = 16.00 GeV, θ = 18.00, RAW DATA

W (GEV)	CROSS SECTION		ERRORS	
1.756	0.215E+02	+- (	0.65E+01,	0.11E+01)
1.776	0.291E+02	+- (	0.47E+01,	0.15E+01)
1.796	0.301E+02	+- (	0.34E+01,	0.15E+01)
1.816	0.294E+02	+- (	0.29E+01,	0.15E+01)
1.836	0.348E+02	+- (	0.28E+01,	0.18E+01)
1.856	0.399E+02	+- (	0.27E+01,	0.20E+01)
1.876	0.428E+02	+- (	0.26E+01,	0.22E+01)
1.895	0.429E+02	+- (	0.24E+01,	0.22E+01)
1.915	0.453E+02	+- (	0.25E+01,	0.23E+01)
1.935	0.478E+02	+- (	0.26E+01,	0.24E+01)
1.955	0.492E+02	+- (	0.26E+01,	0.25E+01)
1.975	0.583E+02	+- (	0.28E+01,	0.30E+01)
1.995	0.570E+02	+- (	0.27E+01,	0.29E+01)
2.030	0.671E+02	+- (	0.21E+01,	0.34E+01)
2.080	0.759E+02	+- (	0.35E+01,	0.39E+01)
2.130	0.784E+02	+- (	0.15E+02,	0.40E+01)
2.187	0.996E+02	+- (	0.14E+01,	0.51E+01)
2.491	0.198E+03	+- (	0.25E+01,	0.10E+02)
2.807	0.369E+03	+- (	0.40E+01,	0.19E+02)
3.111	0.602E+03	+- (	0.77E+01,	0.31E+02)
3.543	0.106E+04	+- (	0.12E+02,	0.54E+02)
3.839	0.153E+04	+- (	0.20E+02,	0.77E+02)
4.225	0.232E+04	+- (	0.36E+02,	0.12E+03)
4.634	0.374E+04	+- (	0.79E+02,	0.20E+03)

E_0 = 19.50 GeV, θ = 18.00, RAW DATA

W (GEV)	CROSS SECTION		ERRORS	
1.598	0.105E+02	+- (	0.11E+02,	0.53E+00)
1.618	0.557E+01	+- (	0.59E+01,	0.28E+00)
1.638	0.329E+01	+- (	0.35E+01,	0.16E+00)
1.658	0.638E+01	+- (	0.39E+01,	0.32E+00)
1.678	0.103E+02	+- (	0.41E+01,	0.51E+00)
1.698	0.845E+01	+- (	0.32E+01,	0.42E+00)
1.718	0.553E+01	+- (	0.27E+01,	0.28E+00)
1.738	0.731E+01	+- (	0.22E+01,	0.37E+00)
1.757	0.578E+01	+- (	0.18E+01,	0.29E+00)
1.777	0.899E+01	+- (	0.20E+01,	0.45E+00)
1.797	0.526E+01	+- (	0.14E+01,	0.26E+00)
1.817	0.106E+02	+- (	0.19E+01,	0.53E+00)
1.837	0.580E+01	+- (	0.15E+01,	0.29E+00)
1.857	0.813E+01	+- (	0.14E+01,	0.41E+00)
1.877	0.858E+01	+- (	0.15E+01,	0.44E+00)
1.897	0.101E+02	+- (	0.16E+01,	0.52E+00)
1.917	0.897E+01	+- (	0.14E+01,	0.46E+00)
1.937	0.122E+02	+- (	0.16E+01,	0.62E+00)

HYDROGEN CROSS SECTION

W(GeV)	CROSS SECTION		ERRORS	
1.957	0.113E+02	+- (	0.15E+01,	0.58E+00)
1.976	0.113E+02	+- (	0.16E+01,	0.5E+00)
1.996	0.126E+02	+- (	0.17E+01,	0.65E+00)
2.031	0.157E+02	+- (	0.13E+01,	0.80E+00)
2.081	0.123E+02	+- (	0.14E+01,	0.63E+00)
2.131	0.187E+02	+- (	0.23E+01,	0.9GE+00)
2.181	0.245E+02	+- (	0.45E+01,	0.13E+01)
2.228	0.259E+02	+- (	0.71E+00,	0.13E+01)
2.516	0.522E+02	+- (	0.12E+01,	0.27E+01)
2.858	0.108E+03	+- (	0.19E+01,	0.55E+01)
3.212	0.201E+03	+- (	0.30E+01,	0.10E+02)
3.549	0.344E+03	+- (	0.50E+01,	0.18E+02)
4.021	0.650E+03	+- (	0.12E+02,	0.33E+02)
4.341	0.886E+03	+- (	0.15E+02,	0.4GE+02)
4.754	0.142E+04	+- (	0.27E+02,	0.71E+02)
5.183	0.258E+04	+- (	0.55E+02,	0.13E+03)

E_0 = 19.50 GeV, θ = 20.60, RAW DATA

W(GEV)	CROSS SECTION		ERRORS	
0.711	0.555E+00	+- (	0.59E+00,	0.2GE-01)
0.906	0.203E+00	+- (	0.22E+00,	0.10E-01)
0.926	0.188E+00	+- (	0.20E+00,	0.96E-02)
0.965	0.809E+00	+- (	0.39E+00,	0.4 E-01)
0.985	0.616E+00	+- (	0.61E+00,	0.3 E-01)
1.004	0.443E+00	+- (	0.37E+00,	0.23E-01)
1.044	0.143E+00	+- (	0.15E+00,	0.73E-02)
1.063	0.141E+00	+- (	0.15E+00,	0.72E-02)
1.123	0.266E+00	+- (	0.20E+00,	0.14E-01)
1.182	0.127E+00	+- (	0.14E+00,	0.65E-02)
1.241	0.251E+00	+- (	0.29E+00,	0.13E-01)
1.261	0.862E-01	+- (	0.36E+00,	0.4GE-02)
1.281	0.293E+00	+- (	0.22E+00,	0.15E-01)
1.301	0.155E+00	+- (	0.17E+00,	0.79E-02)
1.340	0.341E+00	+- (	0.40E+00,	0.17E-01)
1.360	0.769E+00	+- (	0.41E+00,	0.39E-01)
1.380	0.210E+00	+- (	0.22E+00,	0.11E-01)
1.400	0.466E+00	+- (	0.35E+00,	0.24E-01)
1.420	0.783E+00	+- (	0.48E+00,	0.40E-01)
1.439	0.890E+00	+- (	0.55E+00,	0.45E-01)
1.459	0.682E+00	+- (	0.51E+00,	0.35E-01)
1.479	0.805E+00	+- (	0.86E+00,	0.41E-01)
1.499	0.161E+01	+- (	0.86E+00,	0.82E-01)
1.519	0.144E+01	+- (	0.77E+00,	0.73E-01)
1.539	0.131E+01	+- (	0.70E+00,	0.67E-01)
1.559	0.312E+00	+- (	0.59E+00,	0.16E-01)
1.578	0.619E+00	+- (	0.47E+00,	0.32E-01)
1.598	0.917E+00	+- (	0.56E+00,	0.47E-01)
1.618	0.942E+00	+- (	0.73E+00,	0.48E-01)
1.638	0.119E+01	+- (	0.64E+00,	0.61E-01)
1.658	0.118E+01	+- (	0.63E+00,	0.60E-01)
1.678	0.205E+01	+- (	0.83E+00,	0.10E+00)
1.698	0.124E+01	+- (	0.78E+00,	0.63E-01)
1.718	0.126E+01	+- (	0.67E+00,	0.64E-01)
1.738	0.253E+01	+- (	0.11E+01,	0.13E+00)
1.757	0.383E+01	+- (	0.13E+01,	0.20E+00)
1.777	0.236E+01	+- (	0.95E+00,	0.12E+00)
1.797	0.200E+01	+- (	0.75E+00,	0.10E+00)
1.817	0.283E+01	+- (	0.78E+00,	0.14E+00)
1.837	0.354E+01	+- (	0.77E+00,	0.18E+00)
1.857	0.358E+01	+- (	0.70E+00,	0.18E+00)
1.877	0.234E+01	+- (	0.61E+00,	0.12E+00)
1.897	0.341E+01	+- (	0.67E+00,	0.17E+00)
1.917	0.312E+01	+- (	0.52E+00,	0.16E+00)
1.937	0.414E+01	+- (	0.55E+00,	0.21E+00)
1.957	0.381E+01	+- (	0.52E+00,	0.19E+00)
1.976	0.519E+01	+- (	0.56E+00,	0.26E+00)
1.996	0.525E+01	+- (	0.60E+00,	0.27E+00)
2.031	0.584E+01	+- (	0.38E+00,	0.30E+00)
2.081	0.677E+01	+- (	0.41E+00,	0.35E+00)
2.131	0.740E+01	+- (	0.49E+00,	0.38E+00)
2.181	0.910E+01	+- (	0.82E+00,	0.46E+00)
2.231	0.134E+02	+- (	0.27E+01,	0.6GE+00)
2.345	0.138E+02	+- (	0.35E+00,	0.70E+00)
2.643	0.298E+02	+- (	0.64E+00,	0.15E+01)
2.995	0.638E+02	+- (	0.12E+01,	0.33E+01)
3.354	0.124E+03	+- (	0.21E+01,	0.63E+01)
3.692	0.223E+03	+- (	0.33E+01,	0.11E+02)
4.158	0.410E+03	+- (	0.55E+01,	0.21E+02)
4.470	0.611E+03	+- (	0.78E+01,	0.31E+02)
4.865	0.101E+04	+- (	0.14E+02,	0.5 E+02)
5.268	0.185E+04	+- (	0.51E+02,	0.97E+02)

5-78

E_0 = 7.00 GeV, θ = 6.00, FINAL DATA

W(GEV)	CROSS SECTION		ERRORS	
1.094	0.122E+07	+- (	0.48E+06,	0.62E+05)
1.134	0.259E+07	+- (	0.52E+06,	0.13E+06)
1.154	0.348E+07	+- (	0.24E+06,	0.18E+06)
1.174	0.549E+07	+- (	0.24E+06,	0.28E+06)
1.194	0.864E+07	+- (	0.26E+06,	0.44E+06)
1.214	0.105E+08	+- (	0.30E+06,	0.5 E+06)
1.234	0.977E+07	+- (	0.27E+06,	0.50E+06)
1.254	0.772E+07	+- (	0.23E+06,	0.40E+06)
1.274	0.634E+07	+- (	0.21E+06,	0.32E+06)
1.294	0.543E+07	+- (	0.19E+06,	0.28E+06)
1.314	0.504E+07	+- (	0.19E+06,	0.26E+06)
1.333	0.425E+07	+- (	0.46E+06,	0.22E+06)
1.433	0.311E+07	+- (	0.46E+06,	0.16E+06)
1.453	0.383E+07	+- (	0.11E+06,	0.20E+06)
1.473	0.436E+07	+- (	0.98E+05,	0.22E+06)
1.493	0.528E+07	+- (	0.11E+06,	0.27E+06)
1.513	0.532E+07	+- (	0.11E+06,	0.27E+06)
1.533	0.496E+07	+- (	0.97E+05,	0.25E+06)
1.553	0.448E+07	+- (	0.90E+05,	0.23E+06)
1.573	0.413E+07	+- (	0.91E+05,	0.21E+06)
1.593	0.350E+07	+- (	0.22E+06,	0.18E+06)
1.692	0.540E+07	+- (	0.95E+06,	0.28E+06)
1.712	0.374E+07	+- (	0.99E+05,	0.19E+06)
1.732	0.341E+07	+- (	0.77E+05,	0.17E+06)
1.752	0.324E+07	+- (	0.74E+05,	0.17E+06)
1.772	0.304E+07	+- (	0.71E+05,	0.16E+06)
1.792	0.295E+07	+- (	0.70E+05,	0.15E+06)
1.812	0.307E+07	+- (	0.85E+05,	0.16E+06)
1.832	0.276E+07	+- (	0.12E+07,	0.14E+06)
1.952	0.246E+07	+- (	0.44E+06,	0.12E+06)
1.972	0.228E+07	+- (	0.46E+05,	0.12E+06)
1.992	0.222E+07	+- (	0.40E+05,	0.11E+06)
2.027	0.226E+07	+- (	0.25E+05,	0.12E+06)
2.077	0.239E+07	+- (	0.12E+06,	0.12E+06)
2.258	0.166E+07	+- (	0.18E+05,	0.84E+05)
2.501	0.122E+07	+- (	0.62E+04,	0.61E+05)
2.755	0.974E+06	+- (	0.16E+05,	0.49E+05)
3.003	0.819E+06	+- (	0.17E+05,	0.41E+05)

E_0 = 13.50 GeV, θ = 6.00, FINAL DATA

W(GEV)	CROSS SECTION		ERRORS	
1.099	0.231E+05	+- (	0.98E+04,	0.12E+04)
1.119	0.548E+05	+- (	0.82E+04,	0.27E+04)
1.138	0.712E+05	+- (	0.73E+04,	0.36E+04)
1.158	0.156E+06	+- (	0.87E+04,	0.78E+04)
1.178	0.215E+06	+- (	0.95E+04,	0.1 E+05)
1.198	0.318E+06	+- (	0.11E+05,	0.1GE+05)
1.218	0.352E+06	+- (	0.11E+05,	0.18E+05)
1.238	0.337E+06	+- (	0.10E+05,	0.17E+05)
1.257	0.307E+06	+- (	0.97E+04,	0.15E+05)
1.277	0.268E+06	+- (	0.88E+04,	0.13E+05)
1.297	0.257E+06	+- (	0.84E+04,	0.13E+05)
1.317	0.255E+06	+- (	0.83E+04,	0.13E+05)
1.337	0.256E+06	+- (	0.78E+04,	0.13E+05)
1.357	0.249E+06	+- (	0.72E+04,	0.13E+05)
1.377	0.266E+06	+- (	0.69E+04,	0.13E+05)
1.397	0.274E+06	+- (	0.68E+04,	0.14E+05)
1.417	0.286E+06	+- (	0.72E+04,	0.14E+05)
1.436	0.291E+06	+- (	0.82E+04,	0.15E+05)
1.456	0.356E+06	+- (	0.10E+05,	0.18E+05)
1.476	0.409E+06	+- (	0.12E+05,	0.21E+05)
1.496	0.483E+06	+- (	0.13E+05,	0.24E+05)
1.516	0.473E+06	+- (	0.13E+05,	0.24E+05)
1.536	0.430E+06	+- (	0.12E+05,	0.22E+05)
1.556	0.408E+06	+- (	0.11E+05,	0.20E+05)
1.576	0.366E+06	+- (	0.10E+05,	0.18E+05)
1.596	0.375E+06	+- (	0.10E+05,	0.19E+05)
1.616	0.384E+06	+- (	0.10E+05,	0.19E+05)
1.635	0.418E+06	+- (	0.10E+05,	0.21E+05)
1.655	0.459E+06	+- (	0.10E+05,	0.23E+05)
1.675	0.515E+06	+- (	0.11E+05,	0.26E+05)
1.695	0.524E+06	+- (	0.11E+05,	0.26E+05)
1.715	0.502E+06	+- (	0.11E+05,	0.25E+05)
1.735	0.508E+06	+- (	0.10E+05,	0.26E+05)
1.755	0.464E+06	+- (	0.99E+04,	0.23E+05)
1.775	0.458E+06	+- (	0.97E+04,	0.23E+05)
1.795	0.443E+06	+- (	0.96E+04,	0.22E+05)
1.815	0.448E+06	+- (	0.95E+04,	0.22E+05)

3360853

HYDROGEN CROSS SECTION

W(GeV)	CROSS SECTION		ERRORS	
1.835	0.467E+06	+- (	0.97E+04,	0.23E+05)
1.855	0.475E+06	+- (	0.11E+05,	0.24E+05)
1.875	0.492E+06	+- (	0.14E+05,	0.25E+05)
1.895	0.489E+06	+- (	0.23E+05,	0.25E+05)
1.914	0.447E+06	+- (	0.20E+05,	0.22E+05)
1.934	0.431E+06	+- (	0.15E+05,	0.22E+05)
1.954	0.460E+06	+- (	0.15E+05,	0.23E+05)
1.974	0.480E+06	+- (	0.15E+05,	0.24E+05)
1.994	0.472E+06	+- (	0.15E+05,	0.24E+05)
2.029	0.468E+06	+- (	0.90E+04,	0.23E+05)
2.079	0.477E+06	+- (	0.97E+04,	0.24E+05)
2.504	0.385E+06	+- (	0.45E+04,	0.19E+05)
3.003	0.306E+06	+- (	0.42E+04,	0.16E+05)
3.502	0.245E+06	+- (	0.22E+04,	0.13E+05)
3.752	0.220E+06	+- (	0.29E+04,	0.11E+05)
4.001	0.199E+06	+- (	0.30E+04,	0.10E+05)
4.251	0.190E+06	+- (	0.49E+04,	0.96E+04)
4.501	0.174E+06	+- (	0.68E+04,	0.91E+04)

E_0 = 16.00 GeV, θ = 6.00, FINAL DATA

W (GEV)	CROSS SECTION		ERRORS	
1.100	0.699E+04	+- (	0.14E+04,	0.35E+03)
1.120	0.111E+05	+- (	0.13E+04,	0.56E+03)
1.140	0.241E+05	+- (	0.14E+04,	0.12E+04)
1.160	0.374E+05	+- (	0.15E+04,	0.19E+04)
1.180	0.573E+05	+- (	0.17E+04,	0.29E+04)
1.199	0.811E+05	+- (	0.20E+04,	0.41E+04)
1.219	0.987E+05	+- (	0.22E+04,	0.50E+04)
1.239	0.103E+06	+- (	0.22E+04,	0.52E+04)
1.259	0.977E+05	+- (	0.22E+04,	0.49E+04)
1.279	0.939E+05	+- (	0.21E+04,	0.47E+04)
1.299	0.895E+05	+- (	0.20E+04,	0.45E+04)
1.318	0.920E+05	+- (	0.20E+04,	0.46E+04)
1.338	0.958E+05	+- (	0.20E+04,	0.48E+04)
1.358	0.980E+05	+- (	0.20E+04,	0.49E+04)
1.378	0.986E+05	+- (	0.20E+04,	0.50E+04)
1.398	0.993E+05	+- (	0.22E+04,	0.50E+04)
1.418	0.109E+06	+- (	0.25E+04,	0.55E+04)
1.438	0.116E+06	+- (	0.29E+04,	0.58E+04)
1.458	0.134E+06	+- (	0.37E+04,	0.67E+04)
1.477	0.149E+06	+- (	0.54E+04,	0.75E+04)
1.497	0.168E+06	+- (	0.63E+04,	0.84E+04)
1.517	0.186E+06	+- (	0.61E+04,	0.94E+04)
1.537	0.187E+06	+- (	0.58E+04,	0.94E+04)
1.557	0.154E+06	+- (	0.52E+04,	0.77E+04)
1.577	0.153E+06	+- (	0.53E+04,	0.77E+04)
1.597	0.149E+06	+- (	0.54E+04,	0.75E+04)
1.617	0.154E+06	+- (	0.59E+04,	0.77E+04)
1.637	0.163E+06	+- (	0.66E+04,	0.82E+04)
1.656	0.180E+06	+- (	0.76E+04,	0.91E+04)
1.676	0.225E+06	+- (	0.86E+04,	0.11E+05)
1.696	0.241E+06	+- (	0.89E+04,	0.12E+05)
1.716	0.237E+06	+- (	0.86E+04,	0.12E+05)
1.736	0.228E+06	+- (	0.85E+04,	0.11E+05)
1.756	0.224E+06	+- (	0.93E+04,	0.11E+05)
1.776	0.205E+06	+- (	0.10E+05,	0.10E+05)
1.796	0.210E+06	+- (	0.14E+05,	0.11E+05)
1.816	0.208E+06	+- (	0.35E+05,	0.10E+05)
1.856	0.219E+06	+- (	0.40E+05,	0.11E+05)
1.876	0.224E+06	+- (	0.20E+05,	0.11E+05)
1.895	0.221E+06	+- (	0.14E+05,	0.11E+05)
1.915	0.221E+06	+- (	0.11E+05,	0.11E+05)
1.935	0.220E+06	+- (	0.10E+05,	0.11E+05)
1.955	0.218E+06	+- (	0.10E+05,	0.11E+05)
1.975	0.221E+06	+- (	0.10E+05,	0.11E+05)
1.995	0.231E+06	+- (	0.10E+05,	0.12E+05)
2.030	0.230E+06	+- (	0.68E+04,	0.12E+05)
2.080	0.234E+06	+- (	0.64E+04,	0.12E+05)
2.254	0.220E+06	+- (	0.30E+04,	0.11E+05)
2.504	0.231E+06	+- (	0.14E+04,	0.12E+05)
2.754	0.215E+06	+- (	0.29E+04,	0.11E+05)
3.004	0.196E+06	+- (	0.18E+04,	0.98E+04)
3.253	0.180E+06	+- (	0.17E+04,	0.90E+04)
3.503	0.165E+06	+- (	0.14E+04,	0.83E+04)
4.002	0.145E+06	+- (	0.18E+04,	0.81E+04)
4.502	0.126E+06	+- (	0.25E+04,	0.71E+04)
4.752	0.122E+06	+- (	0.32E+04,	0.61E+04)
5.001	0.120E+06	+- (	0.50E+04,	0.63E+04)

5-78

E_0 = 19.50 GeV, θ = 6.00, FINAL DATA

W (GEV)	CROSS SECTION		ERRORS	
1.103	0.159E+04	+- (	0.39E+03,	0.80E+02)
1.123	0.300E+04	+- (	0.34E+03,	0.15E+03)
1.142	0.486E+04	+- (	0.35E+03,	0.24E+03)
1.162	0.692E+04	+- (	0.36E+03,	0.35E+03)
1.182	0.112E+05	+- (	0.41E+03,	0.56E+03)
1.202	0.155E+05	+- (	0.46E+03,	0.78E+03)
1.221	0.186E+05	+- (	0.50E+03,	0.94E+03)
1.241	0.198E+05	+- (	0.50E+03,	0.99E+03)
1.261	0.209E+05	+- (	0.52E+03,	0.10E+04)
1.281	0.209E+05	+- (	0.52E+03,	0.10E+04)
1.301	0.223E+05	+- (	0.54E+03,	0.11E+04)
1.320	0.214E+05	+- (	0.55E+03,	0.11E+04)
1.340	0.225E+05	+- (	0.58E+03,	0.11E+04)
1.360	0.236E+05	+- (	0.59E+03,	0.12E+04)
1.380	0.258E+05	+- (	0.60E+03,	0.13E+04)
1.400	0.270E+05	+- (	0.60E+03,	0.14E+04)
1.420	0.290E+05	+- (	0.61E+03,	0.15E+04)
1.439	0.315E+05	+- (	0.65E+03,	0.16E+04)
1.459	0.346E+05	+- (	0.71E+03,	0.17E+04)
1.479	0.421E+05	+- (	0.82E+03,	0.21E+04)
1.499	0.511E+05	+- (	0.97E+03,	0.26E+04)
1.519	0.569E+05	+- (	0.11E+04,	0.29E+04)
1.539	0.530E+05	+- (	0.11E+04,	0.27E+04)
1.559	0.470E+05	+- (	0.12E+04,	0.24E+04)
1.578	0.434E+05	+- (	0.14E+04,	0.22E+04)
1.598	0.471E+05	+- (	0.16E+04,	0.24E+04)
1.618	0.465E+05	+- (	0.15E+04,	0.23E+04)
1.638	0.489E+05	+- (	0.15E+04,	0.25E+04)
1.658	0.580E+05	+- (	0.16E+04,	0.29E+04)
1.678	0.656E+05	+- (	0.18E+04,	0.33E+04)
1.698	0.717E+05	+- (	0.20E+04,	0.36E+04)
1.718	0.703E+05	+- (	0.20E+04,	0.35E+04)
1.738	0.719E+05	+- (	0.21E+04,	0.36E+04)
1.757	0.707E+05	+- (	0.22E+04,	0.36E+04)
1.777	0.689E+05	+- (	0.23E+04,	0.35E+04)
1.797	0.674E+05	+- (	0.25E+04,	0.34E+04)
1.817	0.672E+05	+- (	0.24E+04,	0.34E+04)
1.837	0.740E+05	+- (	0.24E+04,	0.37E+04)
1.857	0.740E+05	+- (	0.23E+04,	0.37E+04)
1.877	0.740E+05	+- (	0.23E+04,	0.37E+04)
1.897	0.735E+05	+- (	0.23E+04,	0.37E+04)
1.917	0.781E+05	+- (	0.24E+04,	0.39E+04)
1.937	0.862E+05	+- (	0.26E+04,	0.43E+04)
1.957	0.815E+05	+- (	0.29E+04,	0.41E+04)
1.976	0.816E+05	+- (	0.31E+04,	0.41E+04)
1.996	0.826E+05	+- (	0.31E+04,	0.41E+04)
2.031	0.871E+05	+- (	0.20E+04,	0.44E+04)
2.081	0.932E+05	+- (	0.20E+04,	0.47E+04)
2.131	0.984E+05	+- (	0.24E+04,	0.49E+04)
2.181	0.990E+05	+- (	0.41E+04,	0.50E+04)
2.255	0.101E+06	+- (	0.10E+04,	0.51E+04)
2.505	0.109E+06	+- (	0.81E+03,	0.55E+04)
2.754	0.109E+06	+- (	0.79E+03,	0.55E+04)
3.003	0.108E+06	+- (	0.72E+03,	0.54E+04)
3.253	0.105E+06	+- (	0.15E+04,	0.53E+04)
3.503	0.963E+05	+- (	0.13E+04,	0.48E+04)
3.752	0.951E+05	+- (	0.15E+04,	0.48E+04)
4.002	0.873E+05	+- (	0.13E+04,	0.44E+04)
4.252	0.832E+05	+- (	0.84E+03,	0.42E+04)
4.502	0.784E+05	+- (	0.80E+03,	0.40E+04)
4.751	0.826E+05	+- (	0.21E+04,	0.46E+04)
5.001	0.757E+05	+- (	0.18E+04,	0.42E+04)
5.251	0.825E+05	+- (	0.23E+04,	0.41E+04)
5.501	0.662E+05	+- (	0.48E+04,	0.35E+04)
5.750	0.683E+05	+- (	0.75E+04,	0.36E+04)

E_0 = 19.50 GeV, θ = 10.00, FINAL DATA

W (GEV)	CROSS SECTION		ERRORS	
1.103	0.584E+01	+- (	0.11E+02,	0.29E+00)
1.123	0.102E+02	+- (	0.83E+01,	0.51E+00)
1.142	0.127E+02	+- (	0.90E+01,	0.63E+00)
1.162	0.494E+02	+- (	0.90E+01,	0.25E+01)
1.182	0.761E+02	+- (	0.10E+02,	0.38E+01)
1.202	0.946E+02	+- (	0.87E+01,	0.47E+01)
1.221	0.126E+03	+- (	0.99E+01,	0.63E+01)
1.241	0.139E+03	+- (	0.98E+01,	0.69E+01)

3360854

HYDROGEN CROSS SECTION

W(GeV)	CROSS SECTION		ERRORS	
1.261	0.146E+03	+- (	0.91E+01,	0.73E+01)
1.281	0.164E+03	+- (	0.10E+02,	0.82E+01)
1.301	0.178E+03	+- (	0.10E+02,	0.89E+01)
1.320	0.190E+03	+- (	0.99E+01,	0.95E+01)
1.340	0.208E+03	+- (	0.11E+02,	0.10E+02)
1.360	0.252E+03	+- (	0.11E+02,	0.13E+02)
1.380	0.257E+03	+- (	0.11E+02,	0.13E+02)
1.400	0.279E+03	+- (	0.11E+02,	0.14E+02)
1.420	0.294E+03	+- (	0.12E+02,	0.15E+02)
1.439	0.308E+03	+- (	0.13E+02,	0.15E+02)
1.459	0.412E+03	+- (	0.14E+02,	0.21E+02)
1.479	0.497E+03	+- (	0.16E+02,	0.25E+02)
1.499	0.594E+03	+- (	0.18E+02,	0.30E+02)
1.519	0.606E+03	+- (	0.19E+02,	0.30E+02)
1.539	0.571E+03	+- (	0.18E+02,	0.29E+02)
1.559	0.557E+03	+- (	0.18E+02,	0.28E+02)
1.578	0.537E+03	+- (	0.18E+02,	0.27E+02)
1.598	0.514E+03	+- (	0.18E+02,	0.26E+02)
1.618	0.566E+03	+- (	0.19E+02,	0.28E+02)
1.638	0.623E+03	+- (	0.21E+02,	0.31E+02)
1.658	0.724E+03	+- (	0.22E+02,	0.36E+02)
1.678	0.785E+03	+- (	0.24E+02,	0.39E+02)
1.698	0.936E+03	+- (	0.26E+02,	0.47E+02)
1.718	0.105E+04	+- (	0.27E+02,	0.52E+02)
1.738	0.104E+04	+- (	0.27E+02,	0.52E+02)
1.757	0.105E+04	+- (	0.27E+02,	0.52E+02)
1.777	0.961E+03	+- (	0.26E+02,	0.48E+02)
1.797	0.108E+04	+- (	0.28E+02,	0.54E+02)
1.817	0.105E+04	+- (	0.27E+02,	0.52E+02)
1.837	0.111E+04	+- (	0.28E+02,	0.55E+02)
1.857	0.111E+04	+- (	0.29E+02,	0.56E+02)
1.877	0.119E+04	+- (	0.31E+02,	0.60E+02)
1.897	0.126E+04	+- (	0.32E+02,	0.63E+02)
1.917	0.135E+04	+- (	0.33E+02,	0.67E+02)
1.937	0.140E+04	+- (	0.34E+02,	0.70E+02)
1.957	0.141E+04	+- (	0.35E+02,	0.70E+02)
1.976	0.151E+04	+- (	0.35E+02,	0.75E+02)
1.996	0.149E+04	+- (	0.35E+02,	0.74E+02)
2.031	0.170E+04	+- (	0.24E+02,	0.85E+02)
2.081	0.187E+04	+- (	0.28E+02,	0.94E+02)
2.131	0.212E+04	+- (	0.34E+02,	0.11E+03)
2.181	0.224E+04	+- (	0.40E+02,	0.11E+03)
2.231	0.255E+04	+- (	0.54E+02,	0.13E+03)
2.280	0.280E+04	+- (	0.99E+02,	0.14E+03)
2.397	0.323E+04	+- (	0.28E+02,	0.16E+03)
2.699	0.474E+04	+- (	0.28E+02,	0.24E+03)
3.153	0.670E+04	+- (	0.52E+02,	0.34E+03)
3.490	0.812E+04	+- (	0.58E+02,	0.41E+03)
3.963	0.921E+04	+- (	0.62E+02,	0.52E+03)
4.523	0.106E+05	+- (	0.73E+02,	0.60E+03)

E_0 = 13.30 GeV, θ = 15.00, FINAL DATA

W (GEV)	CROSS SECTION		ERRORS	
1.099	0.117E+02	+- (	0.46E+01,	0.60E+00)
1.118	0.915E+01	+- (	0.43E+01,	0.47E+00)
1.138	0.192E+02	+- (	0.47E+01,	0.98E+00)
1.158	0.309E+02	+- (	0.43E+01,	0.16E+01)
1.178	0.413E+02	+- (	0.47E+01,	0.21E+01)
1.198	0.534E+02	+- (	0.49E+01,	0.27E+01)
1.218	0.663E+02	+- (	0.52E+01,	0.34E+01)
1.238	0.854E+02	+- (	0.54E+01,	0.44E+01)
1.257	0.898E+02	+- (	0.58E+01,	0.46E+01)
1.277	0.104E+03	+- (	0.56E+01,	0.53E+01)
1.297	0.109E+03	+- (	0.57E+01,	0.56E+01)
1.317	0.119E+03	+- (	0.56E+01,	0.61E+01)
1.337	0.135E+03	+- (	0.62E+01,	0.69E+01)
1.357	0.144E+03	+- (	0.62E+01,	0.73E+01)
1.377	0.155E+03	+- (	0.62E+01,	0.79E+01)
1.397	0.181E+03	+- (	0.65E+01,	0.92E+01)
1.416	0.177E+03	+- (	0.66E+01,	0.90E+01)
1.436	0.203E+03	+- (	0.70E+01,	0.10E+02)
1.456	0.231E+03	+- (	0.73E+01,	0.12E+02)
1.476	0.292E+03	+- (	0.83E+01,	0.15E+02)
1.496	0.366E+03	+- (	0.96E+01,	0.19E+02)
1.516	0.416E+03	+- (	0.98E+01,	0.21E+02)
1.536	0.370E+03	+- (	0.89E+01,	0.19E+02)
1.556	0.355E+03	+- (	0.87E+01,	0.18E+02)
1.576	0.342E+03	+- (	0.86E+01,	0.17E+02)
1.596	0.344E+03	+- (	0.86E+01,	0.18E+02)
1.615	0.358E+03	+- (	0.89E+01,	0.18E+02)
1.635	0.390E+03	+- (	0.94E+01,	0.20E+02)
1.655	0.435E+03	+- (	0.10E+02,	0.22E+02)

W(GeV)	CROSS SECTION		ERRORS	
1.675	0.501E+03	+- (	0.11E+02,	0.26E+02)
1.695	0.601E+03	+- (	0.13E+02,	0.31E+02)
1.715	0.671E+03	+- (	0.15E+02,	0.34E+02)
1.735	0.684E+03	+- (	0.15E+02,	0.35E+02)
1.755	0.656E+03	+- (	0.14E+02,	0.33E+02)
1.775	0.650E+03	+- (	0.14E+02,	0.33E+02)
1.795	0.662E+03	+- (	0.15E+02,	0.34E+02)
1.815	0.690E+03	+- (	0.15E+02,	0.35E+02)
1.835	0.687E+03	+- (	0.16E+02,	0.35E+02)
1.855	0.746E+03	+- (	0.17E+02,	0.38E+02)
1.875	0.773E+03	+- (	0.18E+02,	0.39E+02)
1.894	0.843E+03	+- (	0.17E+02,	0.43E+02)
1.914	0.885E+03	+- (	0.17E+02,	0.45E+02)
1.934	0.945E+03	+- (	0.17E+02,	0.48E+02)
1.954	0.980E+03	+- (	0.18E+02,	0.50E+02)
1.974	0.103E+04	+- (	0.20E+02,	0.52E+02)
1.994	0.108E+04	+- (	0.22E+02,	0.55E+02)
2.029	0.118E+04	+- (	0.17E+02,	0.60E+02)
2.079	0.128E+04	+- (	0.23E+02,	0.65E+02)
2.126	0.134E+04	+- (	0.14E+02,	0.74E+02)
2.257	0.176E+04	+- (	0.16E+02,	0.90E+02)
2.524	0.257E+04	+- (	0.20E+02,	0.13E+03)
2.915	0.396E+04	+- (	0.20E+02,	0.20E+03)
3.195	0.489E+04	+- (	0.28E+02,	0.25E+03)
3.576	0.590E+04	+- (	0.62E+02,	0.29E+03)
4.003	0.769E+04	+- (	0.14E+03,	0.38E+03)

E_0 = 16.00 GeV, θ = 15.00, FINAL DATA

W (GEV)	CROSS SECTION		ERRORS	
1.199	0.145E+02	+- (	0.35E+01,	0.73E+00)
1.219	0.144E+02	+- (	0.31E+01,	0.72E+00)
1.239	0.188E+02	+- (	0.40E+01,	0.94E+00)
1.259	0.206E+02	+- (	0.37E+01,	0.10E+01)
1.279	0.234E+02	+- (	0.41E+01,	0.12E+01)
1.299	0.279E+02	+- (	0.37E+01,	0.14E+01)
1.318	0.269E+02	+- (	0.42E+01,	0.13E+01)
1.338	0.304E+02	+- (	0.41E+01,	0.15E+01)
1.358	0.368E+02	+- (	0.45E+01,	0.18E+01)
1.378	0.431E+02	+- (	0.47E+01,	0.22E+01)
1.398	0.436E+02	+- (	0.45E+01,	0.22E+01)
1.418	0.483E+02	+- (	0.48E+01,	0.24E+01)
1.438	0.538E+02	+- (	0.45E+01,	0.27E+01)
1.458	0.765E+02	+- (	0.54E+01,	0.38E+01)
1.477	0.883E+02	+- (	0.60E+01,	0.44E+01)
1.497	0.821E+02	+- (	0.60E+01,	0.41E+01)
1.517	0.907E+02	+- (	0.56E+01,	0.45E+01)
1.537	0.847E+02	+- (	0.58E+01,	0.42E+01)
1.557	0.823E+02	+- (	0.52E+01,	0.41E+01)
1.577	0.754E+02	+- (	0.51E+01,	0.38E+01)
1.597	0.852E+02	+- (	0.51E+01,	0.43E+01)
1.617	0.870E+02	+- (	0.52E+01,	0.43E+01)
1.637	0.116E+03	+- (	0.60E+01,	0.58E+01)
1.656	0.124E+03	+- (	0.62E+01,	0.62E+01)
1.676	0.141E+03	+- (	0.65E+01,	0.70E+01)
1.696	0.145E+03	+- (	0.67E+01,	0.73E+01)
1.716	0.174E+03	+- (	0.69E+01,	0.87E+01)
1.736	0.164E+03	+- (	0.65E+01,	0.82E+01)
1.756	0.166E+03	+- (	0.68E+01,	0.83E+01)
1.776	0.162E+03	+- (	0.65E+01,	0.81E+01)
1.796	0.164E+03	+- (	0.67E+01,	0.82E+01)
1.816	0.174E+03	+- (	0.65E+01,	0.87E+01)
1.836	0.186E+03	+- (	0.70E+01,	0.93E+01)
1.856	0.205E+03	+- (	0.72E+01,	0.10E+02)
1.876	0.209E+03	+- (	0.74E+01,	0.10E+02)
1.895	0.219E+03	+- (	0.75E+01,	0.11E+02)
1.915	0.232E+03	+- (	0.79E+01,	0.12E+02)
1.935	0.249E+03	+- (	0.84E+01,	0.12E+02)
1.955	0.285E+03	+- (	0.93E+01,	0.14E+02)
1.975	0.275E+03	+- (	0.97E+01,	0.14E+02)
1.995	0.296E+03	+- (	0.11E+02,	0.15E+02)
2.030	0.318E+03	+- (	0.78E+01,	0.16E+02)
2.080	0.364E+03	+- (	0.11E+02,	0.19E+02)
2.130	0.378E+03	+- (	0.22E+02,	0.19E+02)
2.275	0.532E+03	+- (	0.71E+01,	0.27E+02)
2.580	0.918E+03	+- (	0.95E+01,	0.47E+02)
2.878	0.141E+04	+- (	0.14E+02,	0.72E+02)
3.310	0.219E+04	+- (	0.20E+02,	0.11E+03)
3.614	0.283E+04	+- (	0.35E+02,	0.14E+03)
4.021	0.355E+04	+- (	0.38E+02,	0.18E+03)
4.469	0.440E+04	+- (	0.64E+02,	0.23E+03)

5-78
3360855

HYDROGEN CROSS SECTION

E = 19.50 GeV, θ = 15.00, FINAL DATA

W (GEV)	CROSS SECTION		ERRORS	
1.917	0.552E+02	+- (	0.41E+01,	0.28E+01)
1.937	0.574E+02	+- (	0.37E+01,	0.29E+01)
1.957	0.603E+02	+- (	0.36E+01,	0.30E+01)
1.976	0.611E+02	+- (	0.32E+01,	0.31E+01)
1.996	0.671E+02	+- (	0.31E+01,	0.34E+01)
2.031	0.720E+02	+- (	0.21E+01,	0.36E+01)
2.081	0.841E+02	+- (	0.22E+01,	0.42E+01)
2.131	0.938E+02	+- (	0.25E+01,	0.47E+01)
2.181	0.102E+03	+- (	0.32E+01,	0.51E+01)
2.231	0.124E+03	+- (	0.54E+01,	0.62E+01)
2.313	0.142E+03	+- (	0.16E+01,	0.71E+01)
2.681	0.279E+03	+- (	0.31E+01,	0.14E+02)
2.984	0.483E+03	+- (	0.58E+01,	0.25E+02)
3.316	0.745E+03	+- (	0.86E+01,	0.38E+02)
3.792	0.122E+04	+- (	0.12E+02,	0.62E+02)
4.750	0.232E+04	+- (	0.25E+02,	0.12E+03)
5.028	0.279E+04	+- (	0.44E+02,	0.15E+03)

E_0 = 6.50 GeV, θ = 18.00, FINAL DATA

W (GEV)	CROSS SECTION		ERRORS	
1.094	0.393E+03	+- (	0.43E+02,	0.20E+02)
1.114	0.729E+03	+- (	0.42E+02,	0.36E+02)
1.134	0.114E+04	+- (	0.45E+02,	0.57E+02)
1.154	0.179E+04	+- (	0.49E+02,	0.89E+02)
1.174	0.278E+04	+- (	0.57E+02,	0.14E+03)
1.194	0.392E+04	+- (	0.70E+02,	0.20E+03)
1.214	0.514E+04	+- (	0.86E+02,	0.26E+03)
1.234	0.544E+04	+- (	0.99E+02,	0.27E+03)
1.253	0.561E+04	+- (	0.11E+03,	0.28E+03)
1.273	0.503E+04	+- (	0.11E+03,	0.25E+03)
1.293	0.502E+04	+- (	0.11E+03,	0.25E+03)
1.313	0.497E+04	+- (	0.12E+03,	0.25E+03)
1.333	0.512E+04	+- (	0.13E+03,	0.26E+03)
1.353	0.541E+04	+- (	0.13E+03,	0.27E+03)
1.373	0.571E+04	+- (	0.13E+03,	0.29E+03)
1.393	0.593E+04	+- (	0.13E+03,	0.30E+03)
1.413	0.663E+04	+- (	0.14E+03,	0.33E+03)
1.433	0.706E+04	+- (	0.14E+03,	0.35E+03)
1.453	0.811E+04	+- (	0.15E+03,	0.41E+03)
1.473	0.933E+04	+- (	0.18E+03,	0.47E+03)
1.493	0.118E+05	+- (	0.24E+03,	0.59E+03)
1.513	0.133E+05	+- (	0.26E+03,	0.66E+03)
1.533	0.120E+05	+- (	0.27E+03,	0.60E+03)
1.553	0.117E+05	+- (	0.30E+03,	0.59E+03)
1.573	0.108E+05	+- (	0.32E+03,	0.54E+03)
1.592	0.980E+04	+- (	0.32E+03,	0.49E+03)
1.612	0.109E+05	+- (	0.33E+03,	0.54E+03)
1.632	0.110E+05	+- (	0.32E+03,	0.55E+03)
1.652	0.126E+05	+- (	0.31E+03,	0.63E+03)
1.672	0.150E+05	+- (	0.33E+03,	0.75E+03)
1.692	0.168E+05	+- (	0.33E+03,	0.84E+03)
1.712	0.182E+05	+- (	0.34E+03,	0.91E+03)
1.732	0.174E+05	+- (	0.33E+03,	0.87E+03)
1.752	0.159E+05	+- (	0.33E+03,	0.80E+03)
1.772	0.160E+05	+- (	0.28E+03,	0.80E+03)
1.792	0.150E+05	+- (	0.22E+03,	0.75E+03)
1.812	0.160E+05	+- (	0.23E+03,	0.80E+03)
1.832	0.166E+05	+- (	0.24E+03,	0.83E+03)
1.852	0.169E+05	+- (	0.26E+03,	0.85E+03)
1.872	0.176E+05	+- (	0.40E+03,	0.88E+03)
1.972	0.196E+05	+- (	0.45E+03,	0.98E+03)
1.992	0.201E+05	+- (	0.40E+03,	0.10E+04)
2.027	0.213E+05	+- (	0.28E+03,	0.11E+04)
2.251	0.237E+05	+- (	0.19E+03,	0.12E+04)
2.252	0.232E+05	+- (	0.26E+03,	0.12E+04)
2.502	0.256E+05	+- (	0.24E+03,	0.13E+04)
2.751	0.246E+05	+- (	0.32E+03,	0.12E+04)

E_0 = 10.40 GeV, θ = 18.00, FINAL DATA

W (GEV)	CROSS SECTION		ERRORS	
1.097	0.967E+01	+- (	0.12E+02,	0.49E+00)
1.117	-0.255E+01	+- (	0.11E+02,	0.13E+00)
1.136	0.219E+02	+- (	0.12E+02,	0.11E+01)
1.156	0.247E+02	+- (	0.11E+02,	0.13E+01)
1.176	0.536E+02	+- (	0.14E+02,	0.27E+01)

W(GeV)	CROSS SECTION		ERRORS	
1.196	0.912E+02	+- (	0.17E+02,	0.47E+01)
1.216	0.110E+03	+- (	0.17E+02,	0.56E+01)
1.236	0.159E+03	+- (	0.19E+02,	0.81E+01)
1.256	0.172E+03	+- (	0.20E+02,	0.88E+01)
1.276	0.133E+03	+- (	0.20E+02,	0.68E+01)
1.295	0.151E+03	+- (	0.22E+02,	0.77E+01)
1.315	0.207E+03	+- (	0.25E+02,	0.1E+02)
1.335	0.181E+03	+- (	0.24E+02,	0.92E+01)
1.355	0.204E+03	+- (	0.22E+02,	0.10E+02)
1.375	0.218E+03	+- (	0.24E+02,	0.1E+02)
1.395	0.268E+03	+- (	0.27E+02,	0.14E+02)
1.415	0.273E+03	+- (	0.28E+02,	0.14E+02)
1.435	0.370E+03	+- (	0.33E+02,	0.19E+02)
1.455	0.301E+03	+- (	0.33E+02,	0.15E+02)
1.475	0.440E+03	+- (	0.39E+02,	0.22E+02)
1.495	0.485E+03	+- (	0.39E+02,	0.25E+02)
1.515	0.522E+03	+- (	0.41E+02,	0.27E+02)
1.534	0.519E+03	+- (	0.43E+02,	0.26E+02)
1.554	0.453E+03	+- (	0.41E+02,	0.23E+02)
1.574	0.477E+03	+- (	0.45E+02,	0.24E+02)
1.594	0.422E+03	+- (	0.42E+02,	0.22E+02)
1.614	0.556E+03	+- (	0.44E+02,	0.28E+02)
1.634	0.542E+03	+- (	0.46E+02,	0.26E+02)
1.654	0.695E+03	+- (	0.54E+02,	0.35E+02)
1.674	0.827E+03	+- (	0.63E+02,	0.42E+02)
1.694	0.811E+03	+- (	0.65E+02,	0.41E+02)
1.714	0.928E+03	+- (	0.60E+02,	0.47E+02)
1.734	0.917E+03	+- (	0.55E+02,	0.47E+02)
1.754	0.892E+03	+- (	0.54E+02,	0.46E+02)
1.774	0.904E+03	+- (	0.53E+02,	0.46E+02)
1.794	0.937E+03	+- (	0.56E+02,	0.48E+02)
1.814	0.943E+03	+- (	0.57E+02,	0.48E+02)
1.834	0.106E+04	+- (	0.62E+02,	0.54E+02)
1.853	0.107E+04	+- (	0.69E+02,	0.54E+02)
1.873	0.112E+04	+- (	0.78E+02,	0.57E+02)
1.893	0.112E+04	+- (	0.98E+02,	0.57E+02)
1.913	0.130E+04	+- (	0.15E+03,	0.66E+02)
2.028	0.172E+04	+- (	0.70E+02,	0.88E+02)
2.078	0.176E+04	+- (	0.66E+02,	0.90E+02)
2.128	0.209E+04	+- (	0.89E+02,	0.1E+03)
2.306	0.261E+04	+- (	0.48E+02,	0.13E+03)
2.656	0.401E+04	+- (	0.79E+02,	0.20E+03)
2.904	0.513E+04	+- (	0.72E+02,	0.26E+03)
3.237	0.617E+04	+- (	0.77E+02,	0.31E+03)
3.607	0.753E+04	+- (	0.15E+03,	0.38E+03)

E_0 = 13.30 GeV, θ = 18.00, FINAL DATA

W (GEV)	CROSS SECTION		ERRORS	
1.476	0.112E+03	+- (	0.48E+02,	0.57E+01)
1.496	0.748E+02	+- (	0.27E+02,	0.38E+01)
1.516	0.787E+02	+- (	0.20E+02,	0.40E+01)
1.536	0.919E+02	+- (	0.16E+02,	0.47E+01)
1.556	0.904E+02	+- (	0.13E+02,	0.46E+01)
1.576	0.653E+02	+- (	0.96E+01,	0.33E+01)
1.596	0.870E+02	+- (	0.90E+01,	0.44E+01)
1.615	0.952E+02	+- (	0.84E+01,	0.49E+01)
1.635	0.832E+02	+- (	0.78E+01,	0.42E+01)
1.655	0.987E+02	+- (	0.73E+01,	0.50E+01)
1.675	0.130E+03	+- (	0.85E+01,	0.66E+01)
1.695	0.153E+03	+- (	0.87E+01,	0.78E+01)
1.715	0.174E+03	+- (	0.92E+01,	0.88E+01)
1.735	0.182E+03	+- (	0.91E+01,	0.93E+01)
1.755	0.179E+03	+- (	0.92E+01,	0.91E+01)
1.775	0.172E+03	+- (	0.89E+01,	0.88E+01)
1.795	0.165E+03	+- (	0.86E+01,	0.84E+01)
1.815	0.158E+03	+- (	0.86E+01,	0.80E+01)
1.835	0.179E+03	+- (	0.90E+01,	0.91E+01)
1.855	0.190E+03	+- (	0.89E+01,	0.97E+01)
1.875	0.208E+03	+- (	0.94E+01,	0.1E+02)
1.894	0.211E+03	+- (	0.10E+02,	0.1E+02)
1.914	0.221E+03	+- (	0.11E+02,	0.11E+02)
1.934	0.254E+03	+- (	0.11E+02,	0.13E+02)
1.954	0.265E+03	+- (	0.12E+02,	0.14E+02)
1.974	0.274E+03	+- (	0.12E+02,	0.14E+02)
1.994	0.301E+03	+- (	0.14E+02,	0.15E+02)
2.029	0.305E+03	+- (	0.13E+02,	0.16E+02)
2.182	0.444E+03	+- (	0.55E+01,	0.23E+02)
2.463	0.769E+03	+- (	0.11E+02,	0.39E+02)
2.735	0.116E+04	+- (	0.11E+02,	0.59E+02)
3.130	0.187E+04	+- (	0.22E+02,	0.96E+02)
3.408	0.242E+04	+- (	0.33E+02,	0.12E+03)
3.767	0.316E+04	+- (	0.52E+02,	0.16E+03)
4.159	0.412E+04	+- (	0.97E+02,	0.22E+03)

5-78

3360856

HYDROGEN CROSS SECTION

E_0= 16.00 GeV, θ = 18.00, FINAL DATA

W (GEV)	CROSS SECTION		ERRORS	
1.756	0.291E+02	+- (	0.89E+01,	0.15E+01)
1.776	0.390E+02	+- (	0.63E+01,	0.20E+01)
1.796	0.401E+02	+- (	0.46E+01,	0.20E+01)
1.816	0.392E+02	+- (	0.39E+01,	0.20E+01)
1.836	0.464E+02	+- (	0.38E+01,	0.24E+01)
1.856	0.533E+02	+- (	0.37E+01,	0.27E+01)
1.876	0.572E+02	+- (	0.34E+01,	0.25E+01)
1.895	0.572E+02	+- (	0.33E+01,	0.29E+01)
1.915	0.603E+02	+- (	0.34E+01,	0.31E+01)
1.935	0.635E+02	+- (	0.34E+01,	0.32E+01)
1.955	0.652E+02	+- (	0.34E+01,	0.33E+01)
1.975	0.771E+02	+- (	0.37E+01,	0.39E+01)
1.995	0.751E+02	+- (	0.36E+01,	0.38E+01)
2.030	0.881E+02	+- (	0.26E+01,	0.45E+01)
2.080	0.980E+02	+- (	0.45E+01,	0.50E+01)
2.187	0.127E+03	+- (	0.18E+01,	0.65E+01)
2.491	0.239E+03	+- (	0.30E+01,	0.12E+02)
2.807	0.426E+03	+- (	0.47E+01,	0.22E+02)
3.111	0.662E+03	+- (	0.65E+01,	0.34E+02)
3.543	0.109E+04	+- (	0.12E+02,	0.55E+02)
3.839	0.147E+04	+- (	0.19E+02,	0.73E+02)
4.225	0.199E+04	+- (	0.32E+02,	0.99E+02)
4.634	0.256E+04	+- (	0.60E+02,	0.13E+03)

E_0= 19.50 GeV, θ = 18.00, FINAL DATA

W (GEV)	CROSS SECTION		ERRORS	
1.598	0.153E+02	+- (	0.16E+02,	0.76E+00)
1.618	0.803E+01	+- (	0.87E+01,	0.40E+00)
1.638	0.475E+01	+- (	0.52E+01,	0.24E+00)
1.658	0.936E+01	+- (	0.58E+01,	0.47E+00)
1.678	0.153E+02	+- (	0.62E+01,	0.77E+00)
1.698	0.129E+02	+- (	0.49E+01,	0.64E+00)
1.718	0.841E+01	+- (	0.41E+01,	0.42E+00)
1.738	0.107E+02	+- (	0.33E+01,	0.53E+00)
1.757	0.814E+01	+- (	0.25E+01,	0.41E+00)
1.777	0.125E+02	+- (	0.28E+01,	0.63E+00)
1.797	0.726E+01	+- (	0.20E+01,	0.36E+00)
1.817	0.147E+02	+- (	0.26E+01,	0.74E+00)
1.837	0.800E+01	+- (	0.20E+01,	0.40E+00)
1.857	0.112E+02	+- (	0.20E+01,	0.57E+00)
1.877	0.119E+02	+- (	0.21E+01,	0.60E+00)
1.897	0.140E+02	+- (	0.22E+01,	0.71E+00)
1.917	0.124E+02	+- (	0.19E+01,	0.63E+00)
1.937	0.168E+02	+- (	0.23E+01,	0.85E+00)
1.957	0.155E+02	+- (	0.21E+01,	0.79E+00)
1.976	0.155E+02	+- (	0.21E+01,	0.79E+00)
1.996	0.173E+02	+- (	0.23E+01,	0.88E+00)
2.031	0.214E+02	+- (	0.18E+01,	0.11E+01)
2.081	0.165E+02	+- (	0.19E+01,	0.84E+00)
2.131	0.251E+02	+- (	0.32E+01,	0.13E+01)
2.181	0.325E+02	+- (	0.61E+01,	0.17E+01)
2.228	0.340E+02	+- (	0.94E+00,	0.17E+01)
2.516	0.656E+02	+- (	0.15E+01,	0.33E+01)
2.858	0.129E+03	+- (	0.23E+01,	0.66E+01)
3.212	0.230E+03	+- (	0.35E+01,	0.12E+02)
3.549	0.374E+03	+- (	0.55E+01,	0.19E+02)
4.021	0.653E+03	+- (	0.12E+02,	0.33E+02)
4.341	0.835E+03	+- (	0.18E+02,	0.42E+02)
4.754	0.119E+04	+- (	0.23E+02,	0.59E+02)
5.183	0.169E+04	+- (	0.40E+02,	0.88E+02)

E_0 = 19.50 GeV, θ = 20.60, FINAL DATA

W (GEV)	CROSS SECTION		ERRORS	
1.123	0.413E+00	+- (	0.40E+00,	0.21E-01)
1.182	0.155E+00	+- (	0.25E+00,	0.79E-02)
1.241	0.369E+00	+- (	0.51E+00,	0.19E-01)
1.261	0.871E-01	+- (	0.59E+00,	0.48E-02)
1.281	0.417E+00	+- (	0.35E+00,	0.21E-01)
1.301	0.194E+00	+- (	0.26E+00,	0.99E-02)
1.340	0.472E+00	+- (	0.60E+00,	0.24E-01)
1.360	0.111E+01	+- (	0.62E+00,	0.57E-01)
1.380	0.276E+00	+- (	0.34E+00,	0.14E-01)
1.400	0.658E+00	+- (	0.53E+00,	0.34E-01)
1.420	0.114E+01	+- (	0.72E+00,	0.58E-01)

W(GeV)	CROSS SECTION		ERRORS	
1.439	0.131E+01	+- (	0.83E+00,	0.67E-01)
1.459	0.101E+01	+- (	0.79E+00,	0.52E-01)
1.479	0.123E+01	+- (	0.13E+01,	0.63E-01)
1.499	0.253E+01	+- (	0.14E+01,	0.13E+00)
1.519	0.224E+01	+- (	0.12E+01,	0.11E+00)
1.539	0.195E+01	+- (	0.11E+01,	0.99E-01)
1.559	0.424E+00	+- (	0.86E+00,	0.22E-01)
1.578	0.850E+00	+- (	0.66E+00,	0.43E-01)
1.598	0.126E+01	+- (	0.80E+00,	0.64E-01)
1.618	0.130E+01	+- (	0.10E+01,	0.66E-01)
1.638	0.167E+01	+- (	0.91E+00,	0.85E-01)
1.658	0.167E+01	+- (	0.91E+00,	0.85E-01)
1.678	0.297E+01	+- (	0.12E+01,	0.15E+00)
1.698	0.183E+01	+- (	0.12E+01,	0.93E-01)
1.718	0.186E+01	+- (	0.10E+01,	0.95E-01)
1.738	0.363E+01	+- (	0.16E+01,	0.19E+00)
1.757	0.531E+01	+- (	0.18E+01,	0.27E+00)
1.777	0.322E+01	+- (	0.13E+01,	0.16E+00)
1.797	0.271E+01	+- (	0.10E+01,	0.14E+00)
1.817	0.384E+01	+- (	0.11E+01,	0.20E+00)
1.837	0.480E+01	+- (	0.11E+01,	0.24E+00)
1.857	0.486E+01	+- (	0.96E+00,	0.25E+00)
1.877	0.316E+01	+- (	0.84E+00,	0.16E+00)
1.897	0.462E+01	+- (	0.92E+00,	0.24E+00)
1.917	0.422E+01	+- (	0.71E+00,	0.22E+00)
1.937	0.561E+01	+- (	0.75E+00,	0.29E+00)
1.957	0.514E+01	+- (	0.70E+00,	0.26E+00)
1.976	0.700E+01	+- (	0.77E+00,	0.36E+00)
1.996	0.707E+01	+- (	0.81E+00,	0.36E+00)
2.031	0.783E+01	+- (	0.51E+00,	0.40E+00)
2.081	0.900E+01	+- (	0.55E+00,	0.46E+00)
2.131	0.977E+01	+- (	0.66E+00,	0.50E+00)
2.181	0.119E+02	+- (	0.11E+01,	0.61E+00)
2.385	0.176E+02	+- (	0.85E+00,	0.90E+00)
2.683	0.366E+02	+- (	0.79E+00,	0.19E+01)
2.995	0.747E+02	+- (	0.15E+01,	0.38E+01)
3.354	0.138E+03	+- (	0.24E+01,	0.70E+01)
3.692	0.236E+03	+- (	0.36E+01,	0.12E+02)
4.158	0.399E+03	+- (	0.54E+01,	0.20E+02)
4.470	0.552E+03	+- (	0.72E+01,	0.28E+02)
4.865	0.798E+03	+- (	0.11E+02,	0.40E+02)
5.268	0.107E+04	+- (	0.35E+02,	0.56E+02)

5-78
3360857

DEUTERIUM CROSS SECTION

E_0 = 7.00 GeV, θ = 6.00, RAW DATA

W(GEV)	CROSS SECTION		ERRORS	
0.836	0.129E+07	+- (	0.16E+06,	0.66E+05)
0.856	0.203E+07	+- (	0.12E+06,	0.10E+06)
0.876	0.397E+07	+- (	0.16E+06,	0.20E+06)
0.896	0.788E+07	+- (	0.22E+06,	0.40E+06)
0.916	0.152E+08	+- (	0.30E+06,	0.76E+06)
0.935	0.229E+08	+- (	0.36E+06,	0.12E+07)
0.955	0.229E+08	+- (	0.36E+06,	0.12E+07)
0.975	0.178E+08	+- (	0.31E+06,	0.91E+06)
0.995	0.116E+08	+- (	0.25E+06,	0.55E+06)
1.015	0.801E+07	+- (	0.21E+06,	0.41E+06)
1.035	0.591E+07	+- (	0.18E+06,	0.30E+06)
1.055	0.471E+07	+- (	0.16E+06,	0.24E+06)
1.075	0.449E+07	+- (	0.20E+06,	0.23E+06)
1.094	0.383E+07	+- (	0.57E+06,	0.20E+06)
1.114	0.540E+07	+- (	0.45E+06,	0.28E+06)
1.154	0.668E+07	+- (	0.21E+06,	0.34E+06)
1.174	0.759E+07	+- (	0.20E+06,	0.39E+06)
1.194	0.918E+07	+- (	0.22E+06,	0.47E+06)
1.214	0.106E+08	+- (	0.23E+06,	0.54E+06)
1.234	0.110E+08	+- (	0.23E+06,	0.56E+06)
1.254	0.105E+08	+- (	0.23E+06,	0.54E+06)
1.274	0.958E+07	+- (	0.22E+06,	0.49E+06)
1.294	0.923E+07	+- (	0.21E+06,	0.47E+06)
1.314	0.854E+07	+- (	0.22E+06,	0.44E+06)
1.333	0.896E+07	+- (	0.59E+06,	0.46E+06)
1.433	0.612E+07	+- (	0.56E+06,	0.31E+06)
1.453	0.664E+07	+- (	0.13E+06,	0.34E+06)
1.473	0.704E+07	+- (	0.11E+06,	0.36E+06)
1.493	0.711E+07	+- (	0.11E+06,	0.36E+06)
1.513	0.742E+07	+- (	0.11E+06,	0.38E+06)
1.533	0.748E+07	+- (	0.11E+06,	0.38E+06)
1.553	0.751E+07	+- (	0.11E+06,	0.38E+06)
1.573	0.751E+07	+- (	0.12E+06,	0.38E+06)
1.593	0.698E+07	+- (	0.29E+06,	0.36E+06)
1.692	0.659E+07	+- (	0.77E+06,	0.34E+06)
1.712	0.621E+07	+- (	0.93E+05,	0.32E+06)
1.732	0.623E+07	+- (	0.78E+05,	0.32E+06)
1.752	0.625E+07	+- (	0.78E+05,	0.32E+06)
1.772	0.616E+07	+- (	0.77E+05,	0.31E+06)
1.792	0.586E+07	+- (	0.75E+05,	0.30E+06)
1.812	0.610E+07	+- (	0.91E+05,	0.31E+06)
1.832	0.573E+07	+- (	0.14E+07,	0.29E+06)
1.952	0.431E+07	+- (	0.58E+06,	0.22E+06)
1.972	0.481E+07	+- (	0.68E+05,	0.25E+06)
1.992	0.480E+07	+- (	0.60E+05,	0.24E+06)
2.027	0.492E+07	+- (	0.38E+05,	0.25E+06)
2.077	0.512E+07	+- (	0.18E+06,	0.26E+06)
2.258	0.398E+07	+- (	0.27E+05,	0.20E+06)
2.501	0.337E+07	+- (	0.19E+05,	0.17E+06)
2.755	0.302E+07	+- (	0.26E+05,	0.15E+06)
3.003	0.304E+07	+- (	0.32E+05,	0.15E+06)

E_0 = 13.50 GeV, θ = 6.00, RAW DATA

W(GEV)	CROSS SECTION		ERRORS	
1.317	0.275E+06	+- (	0.11E+06,	0.14E+05)
1.337	0.294E+06	+- (	0.23E+05,	0.15E+05)
1.357	0.322E+06	+- (	0.15E+05,	0.16E+05)
1.377	0.299E+06	+- (	0.11E+05,	0.15E+05)
1.397	0.334E+06	+- (	0.92E+04,	0.17E+05)
1.417	0.354E+06	+- (	0.88E+04,	0.16E+05)
1.436	0.344E+06	+- (	0.87E+04,	0.17E+05)
1.456	0.371E+06	+- (	0.89E+04,	0.15E+05)
1.476	0.410E+06	+- (	0.93E+04,	0.21E+05)
1.496	0.438E+06	+- (	0.96E+04,	0.22E+05)
1.516	0.432E+06	+- (	0.95E+04,	0.22E+05)
1.536	0.472E+06	+- (	0.98E+04,	0.24E+05)
1.556	0.471E+06	+- (	0.97E+04,	0.24E+05)
1.576	0.495E+06	+- (	0.99E+04,	0.25E+05)
1.596	0.518E+06	+- (	0.10E+05,	0.26E+05)
1.616	0.504E+06	+- (	0.97E+04,	0.25E+05)
1.635	0.531E+06	+- (	0.98E+04,	0.27E+05)
1.655	0.522E+06	+- (	0.95E+04,	0.26E+05)
1.675	0.535E+06	+- (	0.95E+04,	0.27E+05)
1.695	0.553E+06	+- (	0.98E+04,	0.28E+05)
1.715	0.561E+06	+- (	0.99E+04,	0.28E+05)
1.735	0.589E+06	+- (	0.10E+05,	0.29E+05)
1.755	0.571E+06	+- (	0.98E+04,	0.29E+05)
1.775	0.603E+06	+- (	0.10E+05,	0.30E+05)
1.795	0.601E+06	+- (	0.10E+05,	0.30E+05)
1.815	0.617E+06	+- (	0.10E+05,	0.31E+05)
1.835	0.614E+06	+- (	0.10E+05,	0.31E+05)
1.855	0.646E+06	+- (	0.11E+05,	0.32E+05)
1.875	0.637E+06	+- (	0.15E+05,	0.32E+05)
1.895	0.653E+06	+- (	0.26E+05,	0.33E+05)
1.914	0.619E+06	+- (	0.25E+05,	0.31E+05)
1.934	0.581E+06	+- (	0.19E+05,	0.29E+05)
1.954	0.635E+06	+- (	0.19E+05,	0.32E+05)
1.974	0.635E+06	+- (	0.19E+05,	0.32E+05)
1.994	0.649E+06	+- (	0.19E+05,	0.32E+05)
2.029	0.673E+06	+- (	0.12E+05,	0.34E+05)
2.079	0.702E+06	+- (	0.13E+05,	0.35E+05)
2.129	0.766E+06	+- (	0.38E+05,	0.38E+05)
2.504	0.669E+06	+- (	0.76E+04,	0.33E+05)
3.003	0.668E+06	+- (	0.74E+04,	0.31E+05)
3.502	0.572E+06	+- (	0.61E+04,	0.29E+05)
3.752	0.560E+06	+- (	0.57E+04,	0.29E+05)
4.001	0.574E+06	+- (	0.82E+04,	0.29E+05)
4.251	0.619E+06	+- (	0.13E+05,	0.31E+05)
4.501	0.752E+06	+- (	0.20E+05,	0.39E+05)

E_0 = 16.00 GeV, θ = 6.00, RAW DATA

W(GEV)	CROSS SECTION		ERRORS	
0.535	0.970E+03	+- (	0.13E+04,	0.46E+02)
0.554	0.243E+04	+- (	0.15E+04,	0.12E+03)
0.573	0.948E+04	+- (	0.25E+04,	0.47E+03)
0.592	0.800E+04	+- (	0.21E+04,	0.40E+03)
0.611	0.696E+04	+- (	0.18E+04,	0.35E+03)
0.630	0.860E+04	+- (	0.17E+04,	0.43E+03)
0.649	0.601E+04	+- (	0.13E+04,	0.30E+03)
0.669	0.879E+04	+- (	0.14E+04,	0.44E+03)
0.688	0.989E+04	+- (	0.14E+04,	0.49E+03)
0.707	0.113E+05	+- (	0.14E+04,	0.56E+03)
0.727	0.128E+05	+- (	0.14E+04,	0.64E+03)
0.746	0.176E+05	+- (	0.15E+04,	0.88E+03)
0.766	0.200E+05	+- (	0.15E+04,	0.10E+04)
0.785	0.267E+05	+- (	0.18E+04,	0.13E+04)
0.805	0.306E+05	+- (	0.18E+04,	0.15E+04)
0.825	0.371E+05	+- (	0.20E+04,	0.19E+04)
0.844	0.532E+05	+- (	0.24E+04,	0.27E+04)
0.864	0.545E+05	+- (	0.24E+04,	0.27E+04)
0.883	0.647E+05	+- (	0.26E+04,	0.32E+04)
0.903	0.702E+05	+- (	0.26E+04,	0.35E+04)
0.923	0.779E+05	+- (	0.27E+04,	0.39E+04)
0.942	0.845E+05	+- (	0.26E+04,	0.42E+04)
0.962	0.823E+05	+- (	0.24E+04,	0.41E+04)
0.982	0.775E+05	+- (	0.22E+04,	0.39E+04)
1.002	0.703E+05	+- (	0.20E+04,	0.35E+04)
1.021	0.649E+05	+- (	0.18E+04,	0.32E+04)
1.041	0.620E+05	+- (	0.16E+04,	0.31E+04)
1.061	0.574E+05	+- (	0.15E+04,	0.29E+04)
1.081	0.545E+05	+- (	0.14E+04,	0.27E+04)
1.100	0.536E+05	+- (	0.13E+04,	0.27E+04)
1.120	0.572E+05	+- (	0.14E+04,	0.29E+04)
1.140	0.591E+05	+- (	0.14E+04,	0.30E+04)
1.160	0.652E+05	+- (	0.15E+04,	0.33E+04)
1.180	0.734E+05	+- (	0.16E+04,	0.37E+04)
1.199	0.758E+05	+- (	0.17E+04,	0.38E+04)
1.219	0.824E+05	+- (	0.18E+04,	0.41E+04)
1.239	0.855E+05	+- (	0.18E+04,	0.43E+04)
1.259	0.924E+05	+- (	0.19E+04,	0.46E+04)
1.279	0.940E+05	+- (	0.19E+04,	0.47E+04)
1.299	0.956E+05	+- (	0.19E+04,	0.48E+04)

6 – 78
3360860

DEUTERIUM CROSS SECTION

E_0 = 16.00 GeV, θ = 6.00, RAW DATA

1.318	0.105E+06	+- (	0.19E+04,	0.52E+04)
1.338	0.103E+06	+- (	0.19E+04,	0.52E+04)
1.358	0.111E+06	+- (	0.19E+04,	0.55E+04)
1.378	0.115E+06	+- (	0.20E+04,	0.56E+04)
1.398	0.121E+06	+- (	0.22E+04,	0.60E+04)
1.418	0.128E+06	+- (	0.24E+04,	0.64E+04)
1.438	0.133E+06	+- (	0.27E+04,	0.67E+04)
1.458	0.145E+06	+- (	0.32E+04,	0.73E+04)
1.477	0.156E+06	+- (	0.40E+04,	0.78E+04)
1.497	0.153E+06	+- (	0.41E+04,	0.76E+04)
1.517	0.163E+06	+- (	0.41E+04,	0.81E+04)
1.537	0.177E+06	+- (	0.42E+04,	0.86E+04)
1.557	0.171E+06	+- (	0.41E+04,	0.86E+04)
1.577	0.191E+06	+- (	0.46E+04,	0.95E+04)
1.597	0.189E+06	+- (	0.50E+04,	0.95E+04)
1.617	0.197E+06	+- (	0.57E+04,	0.99E+04)
1.637	0.207E+06	+- (	0.70E+04,	0.10E+05)
1.656	0.191E+06	+- (	0.89E+04,	0.95E+04)
1.676	0.220E+06	+- (	0.10E+05,	0.11E+05)
1.696	0.217E+06	+- (	0.10E+05,	0.11E+05)
1.716	0.229E+06	+- (	0.10E+05,	0.11E+05)
1.736	0.253E+06	+- (	0.11E+05,	0.13E+05)
1.756	0.215E+06	+- (	0.11E+05,	0.11E+05)
1.776	0.263E+06	+- (	0.15E+05,	0.13E+05)
1.796	0.248E+06	+- (	0.19E+05,	0.12E+05)
1.816	0.245E+06	+- (	0.48E+05,	0.12E+05)
1.856	0.200E+06	+- (	0.35E+05,	0.10E+05)
1.876	0.258E+06	+- (	0.20E+05,	0.13E+05)
1.895	0.267E+06	+- (	0.14E+05,	0.13E+05)
1.915	0.276E+06	+- (	0.12E+05,	0.14E+05)
1.935	0.273E+06	+- (	0.11E+05,	0.14E+05)
1.955	0.279E+06	+- (	0.11E+05,	0.14E+05)
1.975	0.279E+06	+- (	0.11E+05,	0.14E+05)
1.995	0.294E+06	+- (	0.11E+05,	0.15E+05)
2.030	0.309E+06	+- (	0.70E+04,	0.15E+05)
2.080	0.321E+06	+- (	0.72E+04,	0.16E+05)
2.130	0.347E+06	+- (	0.11E+05,	0.17E+05)
2.180	0.335E+06	+- (	0.24E+05,	0.17E+05)
2.254	0.336E+06	+- (	0.26E+04,	0.17E+05)
2.504	0.359E+06	+- (	0.27E+04,	0.18E+05)
2.754	0.358E+06	+- (	0.29E+04,	0.18E+05)
3.004	0.356E+06	+- (	0.32E+04,	0.18E+05)
3.253	0.348E+06	+- (	0.27E+04,	0.17E+05)
3.503	0.344E+06	+- (	0.26E+04,	0.17E+05)
4.002	0.346E+06	+- (	0.27E+04,	0.19E+05)
4.502	0.385E+06	+- (	0.43E+04,	0.22E+05)
4.752	0.447E+06	+- (	0.74E+04,	0.22E+05)
5.001	0.584E+06	+- (	0.15E+05,	0.30E+05)

E_0 = 19.50 GeV, θ = 6.00, RAW DATA

W(GEV)	CROSS SECTION		ERRORS	
0.541	0.130E+04	+- (	0.31E+03,	0.65E+02)
0.559	0.780E+03	+- (	0.25E+03,	0.39E+02)
0.578	0.146E+04	+- (	0.26E+03,	0.73E+02)
0.597	0.128E+04	+- (	0.23E+03,	0.64E+02)
0.616	0.187E+04	+- (	0.26E+03,	0.93E+02)
0.635	0.187E+04	+- (	0.25E+03,	0.94E+02)
0.654	0.185E+04	+- (	0.23E+03,	0.92E+02)
0.673	0.248E+04	+- (	0.25E+03,	0.12E+03)
0.692	0.239E+04	+- (	0.23E+03,	0.12E+03)
0.711	0.308E+04	+- (	0.25E+03,	0.15E+03)
0.731	0.328E+04	+- (	0.24E+03,	0.16E+03)
0.750	0.410E+04	+- (	0.26E+03,	0.20E+03)
0.769	0.436E+04	+- (	0.27E+03,	0.22E+03)
0.789	0.557E+04	+- (	0.30E+03,	0.28E+03)
0.808	0.676E+04	+- (	0.33E+03,	0.34E+03)
0.828	0.696E+04	+- (	0.33E+03,	0.35E+03)
0.847	0.910E+04	+- (	0.37E+03,	0.46E+03)
0.867	0.938E+04	+- (	0.37E+03,	0.47E+03)
0.886	0.109E+05	+- (	0.39E+03,	0.55E+03)
0.906	0.125E+05	+- (	0.41E+03,	0.63E+03)
0.926	0.141E+05	+- (	0.43E+03,	0.70E+03)
0.945	0.140E+05	+- (	0.42E+03,	0.70E+03)
0.965	0.151E+05	+- (	0.43E+03,	0.75E+03)
0.985	0.141E+05	+- (	0.41E+03,	0.71E+03)
1.004	0.143E+05	+- (	0.40E+03,	0.72E+03)
1.024	0.144E+05	+- (	0.39E+03,	0.72E+03)
1.044	0.132E+05	+- (	0.37E+03,	0.66E+03)
1.063	0.128E+05	+- (	0.36E+03,	0.64E+03)
1.083	0.131E+05	+- (	0.35E+03,	0.66E+03)
1.103	0.121E+05	+- (	0.33E+03,	0.61E+03)
1.123	0.129E+05	+- (	0.34E+03,	0.64E+03)
1.142	0.131E+05	+- (	0.34E+03,	0.66E+03)
1.162	0.136E+05	+- (	0.34E+03,	0.68E+03)
1.182	0.157E+05	+- (	0.37E+03,	0.79E+03)
1.202	0.160E+05	+- (	0.39E+03,	0.80E+03)
1.221	0.172E+05	+- (	0.42E+03,	0.86E+03)
1.241	0.185E+05	+- (	0.45E+03,	0.92E+03)
1.261	0.193E+05	+- (	0.48E+03,	0.96E+03)
1.281	0.212E+05	+- (	0.53E+03,	0.11E+04)
1.301	0.209E+05	+- (	0.57E+03,	0.10E+04)
1.320	0.230E+05	+- (	0.65E+03,	0.11E+04)
1.340	0.235E+05	+- (	0.75E+03,	0.12E+04)
1.360	0.266E+05	+- (	0.81E+03,	0.13E+04)
1.380	0.273E+05	+- (	0.80E+03,	0.14E+04)
1.400	0.293E+05	+- (	0.61E+03,	0.15E+04)
1.420	0.318E+05	+- (	0.83E+03,	0.16E+04)
1.439	0.337E+05	+- (	0.86E+03,	0.17E+04)
1.459	0.345E+05	+- (	0.90E+03,	0.17E+04)
1.479	0.373E+05	+- (	0.97E+03,	0.19E+04)
1.499	0.412E+05	+- (	0.11E+04,	0.21E+04)
1.519	0.432E+05	+- (	0.11E+04,	0.22E+04)
1.539	0.439E+05	+- (	0.12E+04,	0.22E+04)
1.559	0.472E+05	+- (	0.14E+04,	0.24E+04)
1.578	0.471E+05	+- (	0.15E+04,	0.24E+04)
1.598	0.508E+05	+- (	0.16E+04,	0.25E+04)
1.618	0.518E+05	+- (	0.15E+04,	0.26E+04)
1.638	0.527E+05	+- (	0.15E+04,	0.26E+04)
1.658	0.576E+05	+- (	0.16E+04,	0.29E+04)
1.678	0.606E+05	+- (	0.16E+04,	0.30E+04)
1.698	0.623E+05	+- (	0.17E+04,	0.31E+04)
1.718	0.628E+05	+- (	0.18E+04,	0.31E+04)
1.738	0.679E+05	+- (	0.20E+04,	0.34E+04)
1.757	0.681E+05	+- (	0.22E+04,	0.34E+04)
1.777	0.740E+05	+- (	0.26E+04,	0.37E+04)
1.797	0.721E+05	+- (	0.27E+04,	0.36E+04)
1.817	0.748E+05	+- (	0.27E+04,	0.37E+04)
1.837	0.778E+05	+- (	0.26E+04,	0.39E+04)
1.857	0.756E+05	+- (	0.25E+04,	0.40E+04)
1.877	0.849E+05	+- (	0.26E+04,	0.42E+04)
1.897	0.848E+05	+- (	0.26E+04,	0.42E+04)
1.917	0.875E+05	+- (	0.26E+04,	0.44E+04)
1.937	0.941E+05	+- (	0.29E+04,	0.47E+04)
1.957	0.922E+05	+- (	0.31E+04,	0.46E+04)
1.976	0.968E+05	+- (	0.35E+04,	0.48E+04)
1.996	0.996E+05	+- (	0.35E+04,	0.50E+04)
2.031	0.101E+06	+- (	0.22E+04,	0.51E+04)
2.081	0.105E+06	+- (	0.23E+04,	0.53E+04)
2.131	0.120E+06	+- (	0.27E+04,	0.60E+04)
2.181	0.120E+06	+- (	0.48E+04,	0.60E+04)
2.255	0.125E+06	+- (	0.12E+04,	0.63E+04)
2.505	0.150E+06	+- (	0.12E+04,	0.75E+04)
2.754	0.162E+06	+- (	0.13E+04,	0.81E+04)
3.003	0.170E+06	+- (	0.17E+04,	0.85E+04)
3.253	0.174E+06	+- (	0.15E+04,	0.87E+04)
3.503	0.177E+06	+- (	0.13E+04,	0.88E+04)
3.752	0.180E+06	+- (	0.16E+04,	0.90E+04)
4.002	0.179E+06	+- (	0.24E+04,	0.89E+04)
4.252	0.179E+06	+- (	0.14E+04,	0.90E+04)
4.502	0.188E+06	+- (	0.21E+04,	0.11E+05)
4.751	0.206E+06	+- (	0.41E+04,	0.12E+05)
5.001	0.230E+06	+- (	0.41E+04,	0.13E+05)
5.251	0.279E+06	+- (	0.66E+04,	0.14E+05)
5.501	0.363E+06	+- (	0.14E+05,	0.19E+05)
5.750	0.615E+06	+- (	0.31E+05,	0.32E+05)

DEUTERIUM CROSS SECTION

E_0 = 13.30 GeV, θ = 15.00, RAW DATA

W (GEV)	CROSS SECTION		ERRORS	
1.516	0.496E+03	+- (	0.21E+03,	0.25E+02)
1.536	0.193E+03	+- (	0.81E+02,	0.99E+01)
1.556	0.429E+03	+- (	0.93E+02,	0.22E+02)
1.576	0.496E+03	+- (	0.84E+02,	0.25E+02)
1.596	0.356E+03	+- (	0.62E+02,	0.18E+02)
1.615	0.415E+03	+- (	0.60E+02,	0.21E+02)
1.635	0.448E+03	+- (	0.59E+02,	0.23E+02)
1.655	0.563E+03	+- (	0.66E+02,	0.29E+02)
1.675	0.626E+03	+- (	0.69E+02,	0.32E+02)
1.695	0.607E+03	+- (	0.68E+02,	0.31E+02)
1.715	0.569E+03	+- (	0.59E+02,	0.29E+02)
1.735	0.637E+03	+- (	0.48E+02,	0.32E+02)
1.755	0.661E+03	+- (	0.41E+02,	0.34E+02)
1.775	0.689E+03	+- (	0.37E+02,	0.35E+02)
1.795	0.694E+03	+- (	0.33E+02,	0.35E+02)
1.815	0.812E+03	+- (	0.33E+02,	0.41E+02)
1.835	0.743E+03	+- (	0.32E+02,	0.38E+02)
1.855	0.892E+03	+- (	0.33E+02,	0.45E+02)
1.875	0.888E+03	+- (	0.29E+02,	0.45E+02)
1.894	0.943E+03	+- (	0.26E+02,	0.48E+02)
1.914	0.950E+03	+- (	0.24E+02,	0.48E+02)
1.934	0.104E+04	+- (	0.23E+02,	0.53E+02)
1.954	0.112E+04	+- (	0.25E+02,	0.57E+02)
1.974	0.115E+04	+- (	0.26E+02,	0.59E+02)
1.994	0.123E+04	+- (	0.28E+02,	0.63E+02)
2.029	0.132E+04	+- (	0.20E+02,	0.67E+02)
2.079	0.146E+04	+- (	0.27E+02,	0.74E+02)
2.126	0.166E+04	+- (	0.12E+02,	0.85E+02)
2.257	0.213E+04	+- (	0.18E+02,	0.11E+03)
2.524	0.330E+04	+- (	0.23E+02,	0.17E+03)
2.915	0.573E+04	+- (	0.32E+02,	0.29E+03)
3.195	0.790E+04	+- (	0.39E+02,	0.40E+03)
3.576	0.110E+05	+- (	0.96E+02,	0.55E+03)
4.003	0.170E+05	+- (	0.23E+03,	0.85E+03)

E_0 = 16.00 GeV, θ = 15.00, RAW DATA

W(GEV)	CROSS SECTION		ERRORS	
0.535	0.768E+01	+- (	0.81E+01,	0.38E+00)
0.554	0.661E+01	+- (	0.70E+01,	0.33E+00)
0.592	0.504E+01	+- (	0.53E+01,	0.25E+00)
0.611	0.176E+02	+- (	0.94E+01,	0.85E+00)
0.630	0.778E+01	+- (	0.58E+01,	0.39E+00)
0.649	0.334E+01	+- (	0.35E+01,	0.17E+00)
0.669	0.289E+01	+- (	0.30E+01,	0.14E+00)
0.688	0.100E+02	+- (	0.53E+01,	0.5CE+00)
0.707	0.658E+01	+- (	0.40E+01,	0.33E+00)
0.727	0.116E+02	+- (	0.50E+01,	0.56E+00)
0.746	0.341E+01	+- (	0.25E+01,	0.17E+00)
0.766	0.228E+02	+- (	0.62E+01,	0.11E+01)
0.785	0.952E+01	+- (	0.38E+01,	0.46E+00)
0.805	0.110E+02	+- (	0.39E+01,	0.55E+00)
0.825	0.178E+02	+- (	0.56E+01,	0.89E+00)
0.844	0.106E+02	+- (	0.35E+01,	0.53E+00)
0.864	0.152E+02	+- (	0.48E+01,	0.76E+00)
0.883	0.187E+02	+- (	0.43E+01,	0.93E+00)
0.903	0.236E+02	+- (	0.46E+01,	0.12E+01)
0.923	0.149E+02	+- (	0.35E+01,	0.75E+00)
0.942	0.117E+02	+- (	0.30E+01,	0.58E+00)
0.962	0.202E+02	+- (	0.38E+01,	0.1CE+01)
0.982	0.111E+02	+- (	0.30E+01,	0.5CE+00)
1.002	0.205E+02	+- (	0.36E+01,	0.1CE+01)
1.021	0.168E+02	+- (	0.38E+01,	0.84E+00)
1.041	0.178E+02	+- (	0.31E+01,	0.89E+00)
1.061	0.202E+02	+- (	0.32E+01,	0.1CE+01)
1.081	0.232E+02	+- (	0.34E+01,	0.12E+01)
1.100	0.227E+02	+- (	0.32E+01,	0.11E+01)
1.120	0.252E+02	+- (	0.33E+01,	0.13E+01)
1.140	0.258E+02	+- (	0.34E+01,	0.13E+01)
1.160	0.266E+02	+- (	0.33E+01,	0.13E+01)
1.180	0.262E+02	+- (	0.36E+01,	0.13E+01)

W(GEV)	CROSS SECTION		ERRORS	
1.199	0.266E+02	+- (	0.32E+01,	0.13E+01)
1.219	0.324E+02	+- (	0.35E+01,	0.16E+01)
1.239	0.308E+02	+- (	0.35E+01,	0.15E+01)
1.259	0.357E+02	+- (	0.36E+01,	0.18E+01)
1.279	0.366E+02	+- (	0.37E+01,	0.18E+01)
1.299	0.421E+02	+- (	0.38E+01,	0.21E+01)
1.318	0.440E+02	+- (	0.39E+01,	0.22E+01)
1.338	0.472E+02	+- (	0.39E+01,	0.24E+01)
1.358	0.489E+02	+- (	0.40E+01,	0.24E+01)
1.378	0.560E+02	+- (	0.43E+01,	0.28E+01)
1.398	0.559E+02	+- (	0.42E+01,	0.28E+01)
1.418	0.549E+02	+- (	0.41E+01,	0.27E+01)
1.438	0.695E+02	+- (	0.44E+01,	0.35E+01)
1.458	0.701E+02	+- (	0.44E+01,	0.35E+01)
1.477	0.812E+02	+- (	0.48E+01,	0.41E+01)
1.497	0.785E+02	+- (	0.47E+01,	0.39E+01)
1.517	0.812E+02	+- (	0.45E+01,	0.41E+01)
1.537	0.842E+02	+- (	0.48E+01,	0.42E+01)
1.557	0.105E+03	+- (	0.51E+01,	0.53E+01)
1.577	0.102E+03	+- (	0.51E+01,	0.51E+01)
1.597	0.113E+03	+- (	0.53E+01,	0.57E+01)
1.617	0.116E+03	+- (	0.53E+01,	0.58E+01)
1.637	0.125E+03	+- (	0.55E+01,	0.63E+01)
1.656	0.131E+03	+- (	0.56E+01,	0.66E+01)
1.676	0.132E+03	+- (	0.56E+01,	0.66E+01)
1.696	0.143E+03	+- (	0.58E+01,	0.72E+01)
1.716	0.157E+03	+- (	0.59E+01,	0.79E+01)
1.736	0.168E+03	+- (	0.61E+01,	0.84E+01)
1.756	0.168E+03	+- (	0.62E+01,	0.84E+01)
1.776	0.170E+03	+- (	0.62E+01,	0.85E+01)
1.796	0.191E+03	+- (	0.65E+01,	0.96E+01)
1.816	0.205E+03	+- (	0.65E+01,	0.10E+02)
1.836	0.209E+03	+- (	0.66E+01,	0.10E+02)
1.856	0.227E+03	+- (	0.66E+01,	0.11E+02)
1.876	0.238E+03	+- (	0.67E+01,	0.12E+02)
1.895	0.250E+03	+- (	0.67E+01,	0.12E+02)
1.915	0.260E+03	+- (	0.69E+01,	0.13E+02)
1.935	0.287E+03	+- (	0.72E+01,	0.14E+02)
1.955	0.288E+03	+- (	0.74E+01,	0.14E+02)
1.975	0.316E+03	+- (	0.80E+01,	0.16E+02)
1.995	0.312E+03	+- (	0.83E+01,	0.16E+02)
2.030	0.356E+03	+- (	0.61E+01,	0.18E+02)
2.080	0.389E+03	+- (	0.82E+01,	0.20E+02)
2.130	0.430E+03	+- (	0.16E+02,	0.22E+02)
2.180	0.462E+03	+- (	0.10E+03,	0.24E+02)
2.275	0.625E+03	+- (	0.75E+01,	0.32E+02)
2.580	0.112E+04	+- (	0.10E+02,	0.57E+02)
2.878	0.182E+04	+- (	0.15E+02,	0.93E+02)
3.310	0.325E+04	+- (	0.29E+02,	0.17E+03)
3.614	0.451E+04	+- (	0.38E+02,	0.23E+03)
4.021	0.670E+04	+- (	0.53E+02,	0.34E+03)
4.469	0.104E+05	+- (	0.17E+03,	0.54E+03)

E_0 = 19.50 GeV, θ = 15.00, RAW DATA

W(GEV)	CROSS SECTION		ERRORS	
1.817	0.489E+02	+- (	0.15E+02,	0.24E+01)
1.837	0.339E+02	+- (	0.70E+01,	0.17E+01)
1.857	0.476E+02	+- (	0.61E+01,	0.24E+01)
1.877	0.490E+02	+- (	0.51E+01,	0.24E+01)
1.897	0.567E+02	+- (	0.48E+01,	0.28E+01)
1.917	0.550E+02	+- (	0.42E+01,	0.28E+01)
1.937	0.618E+02	+- (	0.40E+01,	0.31E+01)
1.957	0.627E+02	+- (	0.38E+01,	0.31E+01)
1.976	0.655E+02	+- (	0.35E+01,	0.33E+01)
1.996	0.764E+02	+- (	0.36E+01,	0.38E+01)
2.031	0.765E+02	+- (	0.23E+01,	0.39E+01)
2.081	0.907E+02	+- (	0.24E+01,	0.45E+01)
2.131	0.997E+02	+- (	0.27E+01,	0.5CE+01)
2.181	0.110E+03	+- (	0.35E+01,	0.55E+01)
2.231	0.135E+03	+- (	0.61E+01,	0.68E+01)
2.280	0.172E+03	+- (	0.41E+02,	0.86E+01)
2.313	0.159E+03	+- (	0.16E+01,	0.8CE+01)
2.641	0.325E+03	+- (	0.31E+01,	0.16E+02)
2.984	0.580E+03	+- (	0.56E+01,	0.3CE+02)
3.316	0.992E+03	+- (	0.10E+02,	0.51E+02)
3.792	0.182E+04	+- (	0.15E+02,	0.93E+02)

6-78

3360862

DEUTERIUM CROSS SECTION

E_0 = 6.50 GeV, θ=18.00, RAW DATA

W(GEV)	CROSS SECTION		ERRORS	
0.677	0.881E+03	+- (	0.35E+03,	0.45E+02)
0.697	0.344E+03	+- (	0.15E+03,	0.18E+02)
0.717	0.367E+03	+- (	0.12E+03,	0.16E+02)
0.737	0.106E+04	+- (	0.16E+03,	0.53E+02)
0.756	0.109E+04	+- (	0.15E+03,	0.54E+02)
0.776	0.926E+03	+- (	0.13E+03,	0.46E+02)
0.796	0.116E+04	+- (	0.14E+03,	0.56E+02)
0.816	0.146E+04	+- (	0.14E+03,	0.73E+02)
0.836	0.139E+04	+- (	0.13E+03,	0.69E+02)
0.856	0.181E+04	+- (	0.14E+03,	0.91E+02)
0.875	0.188E+04	+- (	0.14E+03,	0.94E+02)
0.895	0.253E+04	+- (	0.17E+03,	0.13E+03)
0.915	0.305E+04	+- (	0.17E+03,	0.15E+03)
0.935	0.319E+04	+- (	0.17E+03,	0.16E+03)
0.955	0.309E+04	+- (	0.17E+03,	0.15E+03)
0.975	0.350E+04	+- (	0.17E+03,	0.17E+03)
0.995	0.405E+04	+- (	0.14E+03,	0.20E+03)
1.015	0.370E+04	+- (	0.96E+02,	0.18E+03)
1.034	0.371E+04	+- (	0.74E+02,	0.19E+03)
1.054	0.365E+04	+- (	0.63E+02,	0.18E+03)
1.074	0.358E+04	+- (	0.57E+02,	0.18E+03)
1.094	0.345E+04	+- (	0.53E+02,	0.17E+03)
1.114	0.349E+04	+- (	0.51E+02,	0.17E+03)
1.134	0.370E+04	+- (	0.50E+02,	0.18E+03)
1.154	0.396E+04	+- (	0.50E+02,	0.20E+03)
1.174	0.432E+04	+- (	0.52E+02,	0.22E+03)
1.194	0.470E+04	+- (	0.57E+02,	0.23E+03)
1.214	0.507E+04	+- (	0.65E+02,	0.25E+03)
1.234	0.553E+04	+- (	0.76E+02,	0.28E+03)
1.253	0.588E+04	+- (	0.87E+02,	0.29E+03)
1.273	0.630E+04	+- (	0.98E+02,	0.32E+03)
1.293	0.656E+04	+- (	0.11E+03,	0.33E+03)
1.313	0.692E+04	+- (	0.12E+03,	0.35E+03)
1.333	0.706E+04	+- (	0.12E+03,	0.35E+03)
1.353	0.716E+04	+- (	0.11E+03,	0.36E+03)
1.373	0.804E+04	+- (	0.12E+03,	0.40E+03)
1.393	0.844E+04	+- (	0.12E+03,	0.42E+03)
1.413	0.923E+04	+- (	0.13E+03,	0.46E+03)
1.433	0.997E+04	+- (	0.13E+03,	0.50E+03)
1.453	0.106E+05	+- (	0.14E+03,	0.53E+03)
1.473	0.111E+05	+- (	0.15E+03,	0.56E+03)
1.493	0.123E+05	+- (	0.19E+03,	0.61E+03)
1.513	0.130E+05	+- (	0.23E+03,	0.65E+03)
1.533	0.132E+05	+- (	0.25E+03,	0.66E+03)
1.553	0.131E+05	+- (	0.27E+03,	0.65E+03)
1.573	0.139E+05	+- (	0.29E+03,	0.69E+03)
1.592	0.136E+05	+- (	0.30E+03,	0.68E+03)
1.612	0.150E+05	+- (	0.32E+03,	0.75E+03)
1.632	0.163E+05	+- (	0.30E+03,	0.81E+03)
1.652	0.169E+05	+- (	0.27E+03,	0.84E+03)
1.672	0.180E+05	+- (	0.28E+03,	0.9CE+03)
1.692	0.188E+05	+- (	0.29E+03,	0.94E+03)
1.712	0.197E+05	+- (	0.30E+03,	0.99E+03)
1.732	0.204E+05	+- (	0.31E+03,	0.1CE+04)
1.752	0.210E+05	+- (	0.35E+03,	0.11E+04)
1.772	0.217E+05	+- (	0.30E+03,	0.11E+04)
1.792	0.221E+05	+- (	0.22E+03,	0.11E+04)
1.812	0.235E+05	+- (	0.23E+03,	0.12E+04)
1.832	0.244E+05	+- (	0.24E+03,	0.12E+04)
1.852	0.248E+05	+- (	0.26E+03,	0.12E+04)
1.872	0.253E+05	+- (	0.39E+03,	0.13E+04)
1.892	0.234E+05	+- (	0.28E+04,	0.12E+04)
1.952	0.292E+05	+- (	0.12E+04,	0.15E+04)
1.972	0.267E+05	+- (	0.43E+03,	0.14E+04)
1.992	0.303E+05	+- (	0.39E+03,	0.15E+04)
2.027	0.321E+05	+- (	0.28E+03,	0.16E+04)
2.077	0.358E+05	+- (	0.42E+04,	0.18E+04)
2.252	0.395E+05	+- (	0.27E+03,	0.20E+04)
2.502	0.482E+05	+- (	0.34E+03,	0.24E+04)
2.751	0.566E+05	+- (	0.49E+03,	0.28E+04)

E_0 = 10.40, θ = 18.00, RAW DATA

W(GEV)	CROSS SECTION		ERRORS	
0.701	0.457E+02	+- (	0.24E+02,	0.23E+01)
0.721	0.299E+02	+- (	0.16E+02,	0.15E+01)
0.741	0.376E+02	+- (	0.15E+02,	0.19E+01)
0.760	0.454E+02	+- (	0.14E+02,	0.23E+01)
0.780	0.429E+02	+- (	0.13E+02,	0.22E+01)
0.800	0.489E+02	+- (	0.12E+02,	0.25E+01)
0.819	0.569E+02	+- (	0.12E+02,	0.29E+01)
0.839	0.740E+02	+- (	0.13E+02,	0.38E+01)
0.859	0.960E+02	+- (	0.14E+02,	0.48E+01)
0.879	0.740E+02	+- (	0.12E+02,	0.38E+01)
0.898	0.907E+02	+- (	0.13E+02,	0.46E+01)
0.918	0.906E+02	+- (	0.13E+02,	0.46E+01)
0.938	0.106E+03	+- (	0.13E+02,	0.54E+01)
0.958	0.105E+03	+- (	0.13E+02,	0.54E+01)
0.978	0.105E+03	+- (	0.12E+02,	0.53E+01)
0.997	0.109E+03	+- (	0.12E+02,	0.55E+01)
1.017	0.111E+03	+- (	0.11E+02,	0.57E+01)
1.037	0.124E+03	+- (	0.12E+02,	0.63E+01)
1.057	0.123E+03	+- (	0.12E+02,	0.63E+01)
1.077	0.118E+03	+- (	0.12E+02,	0.60E+01)
1.097	0.118E+03	+- (	0.12E+02,	0.6CE+01)
1.117	0.130E+03	+- (	0.14E+02,	0.66E+01)
1.136	0.132E+03	+- (	0.14E+02,	0.67E+01)
1.156	0.108E+03	+- (	0.13E+02,	0.55E+01)
1.176	0.153E+03	+- (	0.16E+02,	0.78E+01)
1.196	0.148E+03	+- (	0.16E+02,	0.76E+01)
1.216	0.164E+03	+- (	0.16E+02,	0.84E+01)
1.236	0.194E+03	+- (	0.17E+02,	0.95E+01)
1.256	0.206E+03	+- (	0.18E+02,	0.10E+02)
1.276	0.237E+03	+- (	0.21E+02,	0.12E+02)
1.295	0.234E+03	+- (	0.21E+02,	0.12E+02)
1.315	0.205E+03	+- (	0.20E+02,	0.10E+02)
1.335	0.271E+03	+- (	0.22E+02,	0.14E+02)
1.355	0.300E+03	+- (	0.22E+02,	0.15E+02)
1.375	0.255E+03	+- (	0.20E+02,	0.13E+02)
1.395	0.339E+03	+- (	0.24E+02,	0.17E+02)
1.415	0.332E+03	+- (	0.24E+02,	0.17E+02)
1.435	0.403E+03	+- (	0.27E+02,	0.21E+02)
1.455	0.380E+03	+- (	0.28E+02,	0.19E+02)
1.475	0.410E+03	+- (	0.29E+02,	0.21E+02)
1.495	0.443E+03	+- (	0.29E+02,	0.23E+02)
1.515	0.441E+03	+- (	0.30E+02,	0.22E+02)
1.534	0.452E+03	+- (	0.33E+02,	0.23E+02)
1.554	0.495E+03	+- (	0.37E+02,	0.25E+02)
1.574	0.653E+03	+- (	0.46E+02,	0.33E+02)
1.594	0.642E+03	+- (	0.44E+02,	0.33E+02)
1.614	0.669E+03	+- (	0.42E+02,	0.34E+02)
1.634	0.666E+03	+- (	0.44E+02,	0.34E+02)
1.654	0.779E+03	+- (	0.48E+02,	0.4CE+02)
1.674	0.852E+03	+- (	0.51E+02,	0.43E+02)
1.694	0.844E+03	+- (	0.51E+02,	0.43E+02)
1.714	0.100E+04	+- (	0.49E+02,	0.51E+02)
1.734	0.925E+03	+- (	0.44E+02,	0.47E+02)
1.754	0.104E+04	+- (	0.47E+02,	0.53E+02)
1.774	0.102E+04	+- (	0.46E+02,	0.52E+02)
1.794	0.114E+04	+- (	0.50E+02,	0.58E+02)
1.814	0.126E+04	+- (	0.53E+02,	0.64E+02)
1.834	0.113E+04	+- (	0.52E+02,	0.5EE+02)
1.853	0.137E+04	+- (	0.63E+02,	0.7CE+02)
1.873	0.136E+04	+- (	0.70E+02,	0.69E+02)
1.893	0.150E+04	+- (	0.92E+02,	0.77E+02)
1.913	0.134E+04	+- (	0.12E+03,	0.6EE+02)
1.933	0.184E+04	+- (	0.30E+03,	0.94E+02)
1.973	0.159E+04	+- (	0.41E+03,	0.81E+02)
1.993	0.184E+04	+- (	0.18E+03,	0.94E+02)
2.028	0.205E+04	+- (	0.74E+02,	0.1CE+03)
2.078	0.217E+04	+- (	0.71E+02,	0.11E+03)
2.128	0.268E+04	+- (	0.98E+02,	0.14E+03)
2.178	0.283E+04	+- (	0.55E+03,	0.14E+03)
2.306	0.343E+04	+- (	0.66E+02,	0.17E+03)
2.656	0.592E+04	+- (	0.12E+03,	0.3CE+03)
2.904	0.822E+04	+- (	0.93E+02,	0.41E+03)
3.237	0.119E+05	+- (	0.13E+03,	0.6CE+03)
3.607	0.179E+05	+- (	0.20E+03,	0.9CE+03)

DEUTERIUM CROSS SECTION

E_0 = 13.30 GeV, θ = 18.00, RAW DATA

W (GEV)	CROSS SECTION		ERRORS	
1.436	0.539E+02	+- (	0.60E+02,	0.27E+01)
1.456	0.183E+02	+- (	0.17E+02,	0.93E+00)
1.476	0.768E+02	+- (	0.20E+02,	0.35E+01)
1.496	0.459E+02	+- (	0.12E+02,	0.23E+01)
1.516	0.584E+02	+- (	0.11E+02,	0.3CE+01)
1.536	0.830E+02	+- (	0.10E+02,	0.42E+01)
1.556	0.824E+02	+- (	0.87E+01,	0.42E+01)
1.576	0.849E+02	+- (	0.79E+01,	0.43E+01)
1.596	0.965E+02	+- (	0.74E+01,	0.48E+01)
1.615	0.130E+03	+- (	0.78E+01,	0.66E+01)
1.635	0.106E+03	+- (	0.68E+01,	0.54E+01)
1.655	0.127E+03	+- (	0.67E+01,	0.65E+01)
1.675	0.129E+03	+- (	0.68E+01,	0.66E+01)
1.695	0.142E+03	+- (	0.67E+01,	0.72E+01)
1.715	0.155E+03	+- (	0.71E+01,	0.79E+01)
1.735	0.163E+03	+- (	0.73E+01,	0.83E+01)
1.755	0.175E+03	+- (	0.79E+01,	0.89E+01)
1.775	0.169E+03	+- (	0.78E+01,	0.86E+01)
1.795	0.179E+03	+- (	0.79E+01,	0.91E+01)
1.815	0.195E+03	+- (	0.83E+01,	0.99E+01)
1.835	0.207E+03	+- (	0.84E+01,	0.11E+02)
1.855	0.222E+03	+- (	0.83E+01,	0.11E+02)
1.875	0.229E+03	+- (	0.85E+01,	0.12E+02)
1.894	0.261E+03	+- (	0.96E+01,	0.13E+02)
1.914	0.265E+03	+- (	0.99E+01,	0.14E+02)
1.934	0.295E+03	+- (	0.11E+02,	0.15E+02)
1.954	0.293E+03	+- (	0.11E+02,	0.15E+02)
1.974	0.318E+03	+- (	0.11E+02,	0.16E+02)
1.994	0.331E+03	+- (	0.13E+02,	0.17E+02)
2.025	0.351E+03	+- (	0.12E+02,	0.18E+02)
2.079	0.557E+03	+- (	0.12E+03,	0.30E+02)
2.182	0.519E+03	+- (	0.43E+01,	0.26E+02)
2.463	0.931E+03	+- (	0.87E+01,	0.47E+02)
2.735	0.159E+04	+- (	0.15E+02,	0.81E+02)
3.130	0.282E+04	+- (	0.30E+02,	0.14E+03)
3.404	0.406E+04	+- (	0.46E+02,	0.2CE+03)
3.767	0.607E+04	+- (	0.67E+02,	0.3CE+03)
4.159	0.582E+04	+- (	0.16E+03,	0.51E+03)

E_0 = 16.00 GeV, θ = 18.00, RAW DATA

W (GEV)	CROSS SECTION		ERRORS	
1.736	0.445E+02	+- (	0.33E+02,	0.22E+01)
1.756	0.305E+02	+- (	0.85E+01,	0.16E+01)
1.776	0.494E+02	+- (	0.68E+01,	0.25E+01)
1.796	0.432E+02	+- (	0.48E+01,	0.22E+01)
1.816	0.432E+02	+- (	0.41E+01,	0.22E+01)
1.836	0.475E+02	+- (	0.38E+01,	0.24E+01)
1.856	0.564E+02	+- (	0.37E+01,	0.29E+01)
1.876	0.623E+02	+- (	0.36E+01,	0.32E+01)
1.895	0.615E+02	+- (	0.34E+01,	0.31E+01)
1.915	0.665E+02	+- (	0.35E+01,	0.34E+01)
1.935	0.661E+02	+- (	0.35E+01,	0.34E+01)
1.955	0.702E+02	+- (	0.36E+01,	0.3EE+01)
1.975	0.825E+02	+- (	0.39E+01,	0.42E+01)
1.995	0.857E+02	+- (	0.39E+01,	0.44E+01)
2.030	0.981E+02	+- (	0.30E+01,	0.5CE+01)
2.080	0.106E+03	+- (	0.48E+01,	0.54E+01)
2.130	0.141E+03	+- (	0.24E+02,	0.72E+01)
2.187	0.139E+03	+- (	0.17E+01,	0.71E+01)
2.491	0.264E+03	+- (	0.27E+01,	0.14E+02)
2.807	0.535E+03	+- (	0.40E+01,	0.27E+02)
3.111	0.897E+03	+- (	0.95E+01,	0.46E+02)
3.543	0.169E+04	+- (	0.15E+02,	0.86E+02)
3.835	0.245E+04	+- (	0.31E+02,	0.12E+03)
4.225	0.387E+04	+- (	0.47E+02,	0.19E+03)
4.634	0.657E+04	+- (	0.10E+03,	0.34E+03)

E_0 = 19.50 GeV, θ = 18.00, RAW DATA

W (GEV)	CROSS SECTION		ERRORS	
1.618	0.832E+01	+- (	0.62E+01,	0.42E+00)
1.638	0.258E+01	+- (	0.27E+01,	0.13E+00)
1.658	0.701E+01	+- (	0.37E+01,	0.35E+00)
1.678	0.131E+02	+- (	0.38E+01,	0.65E+00)
1.698	0.753E+01	+- (	0.28E+01,	0.38E+00)
1.718	0.142E+02	+- (	0.36E+01,	0.71E+00)
1.738	0.679E+01	+- (	0.21E+01,	0.34E+00)
1.757	0.108E+02	+- (	0.23E+01,	0.54E+00)
1.777	0.995E+01	+- (	0.20E+01,	0.50E+00)
1.797	0.596E+01	+- (	0.19E+01,	0.50E+00)
1.817	0.846E+01	+- (	0.16E+01,	0.42E+00)
1.837	0.133E+02	+- (	0.20E+01,	0.66E+00)
1.857	0.127E+02	+- (	0.18E+01,	0.65E+00)
1.877	0.121E+02	+- (	0.17E+01,	0.62E+00)
1.897	0.155E+02	+- (	0.18E+01,	0.79E+00)
1.917	0.144E+02	+- (	0.17E+01,	0.73E+00)
1.937	0.216E+02	+- (	0.21E+01,	0.11E+01)
1.957	0.167E+02	+- (	0.18E+01,	0.85E+00)
1.976	0.211E+02	+- (	0.20E+01,	0.11E+01)
1.996	0.179E+02	+- (	0.19E+01,	0.91E+00)
2.031	0.207E+02	+- (	0.14E+01,	0.11E+01)
2.081	0.257E+02	+- (	0.19E+01,	0.13E+01)
2.131	0.277E+02	+- (	0.27E+01,	0.14E+01)
2.181	0.311E+02	+- (	0.47E+01,	0.16E+01)
2.228	0.371E+02	+- (	0.81E+00,	0.19E+01)
2.516	0.757E+02	+- (	0.14E+01,	0.39E+01)
2.858	0.153E+03	+- (	0.22E+01,	0.78E+01)
3.212	0.295E+03	+- (	0.33E+01,	0.15E+02)
3.549	0.504E+03	+- (	0.64E+01,	0.26E+02)
4.021	0.996E+03	+- (	0.13E+02,	0.51E+02)
4.341	0.144E+04	+- (	0.19E+02,	0.72E+02)
4.754	0.243E+04	+- (	0.44E+02,	0.12E+03)
5.183	0.445E+04	+- (	0.97E+02,	0.23E+03)

E_0 = 19.50 GeV, θ = 20.60, RAW DATA

W (GEV)	CROSS SECTION		ERRORS	
1.777	0.211E+01	+- (	0.22E+01,	0.11E+00)
1.797	0.212E+01	+- (	0.13E+01,	0.11E+00)
1.817	0.628E+01	+- (	0.17E+01,	0.32E+00)
1.837	0.473E+01	+- (	0.12E+01,	0.24E+00)
1.857	0.409E+01	+- (	0.94E+00,	0.21E+00)
1.877	0.548E+01	+- (	0.10E+01,	0.28E+00)
1.897	0.526E+01	+- (	0.92E+00,	0.27E+00)
1.917	0.764E+01	+- (	0.95E+00,	0.39E+00)
1.937	0.622E+01	+- (	0.79E+00,	0.32E+00)
1.957	0.778E+01	+- (	0.85E+00,	0.40E+00)
1.976	0.860E+01	+- (	0.86E+00,	0.44E+00)
1.996	0.899E+01	+- (	0.90E+00,	0.46E+00)
2.031	0.975E+01	+- (	0.58E+00,	0.5CE+00)
2.081	0.126E+02	+- (	0.67E+00,	0.64E+00)
2.131	0.111E+02	+- (	0.73E+00,	0.57E+00)
2.181	0.148E+02	+- (	0.12E+01,	0.76E+00)
2.231	0.102E+02	+- (	0.29E+01,	0.52E+00)
2.345	0.223E+02	+- (	0.54E+00,	0.11E+01)
2.643	0.435E+02	+- (	0.13E+01,	0.22E+01)

E_0 = 7.00 GeV, θ = 6.00, FINAL DATA

W (GEV)	CROSS SECTION		ERRORS	
1.075	0.208E+07	+- (	0.43E+06,	0.11E+06)
1.094	0.174E+07	+- (	0.11E+07,	0.85E+05)
1.134	0.559E+07	+- (	0.77E+06,	0.28E+06)
1.154	0.806E+07	+- (	0.36E+06,	0.41E+06)
1.174	0.984E+07	+- (	0.33E+06,	0.5CE+06)
1.194	0.126E+08	+- (	0.36E+06,	0.64E+06)
1.214	0.147E+08	+- (	0.37E+06,	0.75E+06)
1.234	0.147E+08	+- (	0.35E+06,	0.75E+06)
1.254	0.133E+08	+- (	0.32E+06,	0.68E+06)
1.274	0.115E+08	+- (	0.29E+06,	0.58E+06)
1.294	0.107E+08	+- (	0.27E+06,	0.54E+06)
1.314	0.961E+07	+- (	0.28E+06,	0.49E+06)
1.333	0.100E+08	+- (	0.74E+06,	0.51E+06)

6—78

3360864

DEUTERIUM CROSS SECTION

E_0 = 16.00 GeV, θ = 6.00, FINAL DATA

W(GEV)	CROSS SECTION		ERRORS	
1.081	0.264E+05	+- (	0.32E+04,	0.13E+04)
1.100	0.347E+05	+- (	0.28E+04,	0.17E+04)
1.120	0.506E+05	+- (	0.27E+04,	0.25E+04)
1.140	0.606E+05	+- (	0.27E+04,	0.30E+04)
1.160	0.770E+05	+- (	0.28E+04,	0.38E+04)
1.180	0.950E+05	+- (	0.29E+04,	0.47E+04)
1.199	0.101E+06	+- (	0.29E+04,	0.50E+04)
1.219	0.113E+06	+- (	0.30E+04,	0.56E+04)
1.239	0.118E+06	+- (	0.31E+04,	0.59E+04)
1.259	0.130E+06	+- (	0.32E+04,	0.65E+04)
1.279	0.132E+06	+- (	0.31E+04,	0.66E+04)
1.299	0.134E+06	+- (	0.30E+04,	0.67E+04)
1.318	0.148E+06	+- (	0.30E+04,	0.74E+04)
1.338	0.146E+06	+- (	0.29E+04,	0.73E+04)
1.358	0.158E+06	+- (	0.30E+04,	0.79E+04)
1.378	0.164E+06	+- (	0.31E+04,	0.82E+04)
1.398	0.172E+06	+- (	0.33E+04,	0.86E+04)
1.418	0.183E+06	+- (	0.37E+04,	0.92E+04)
1.438	0.191E+06	+- (	0.41E+04,	0.95E+04)
1.458	0.208E+06	+- (	0.48E+04,	0.10E+05)
1.477	0.224E+06	+- (	0.59E+04,	0.11E+05)
1.497	0.218E+06	+- (	0.61E+04,	0.11E+05)
1.517	0.231E+06	+- (	0.60E+04,	0.12E+05)
1.537	0.250E+06	+- (	0.62E+04,	0.13E+05)
1.557	0.241E+06	+- (	0.60E+04,	0.12E+05)
1.577	0.268E+06	+- (	0.67E+04,	0.13E+05)
1.597	0.265E+06	+- (	0.72E+04,	0.13E+05)
1.617	0.275E+06	+- (	0.82E+04,	0.14E+05)
1.637	0.288E+06	+- (	0.10E+05,	0.14E+05)
1.656	0.263E+06	+- (	0.13E+05,	0.13E+05)
1.676	0.303E+06	+- (	0.14E+05,	0.15E+05)
1.696	0.296E+06	+- (	0.14E+05,	0.15E+05)
1.716	0.311E+06	+- (	0.14E+05,	0.16E+05)
1.876	0.335E+06	+- (	0.26E+05,	0.17E+05)
1.895	0.346E+06	+- (	0.19E+05,	0.17E+05)
1.915	0.355E+06	+- (	0.15E+05,	0.18E+05)
1.935	0.349E+06	+- (	0.14E+05,	0.17E+05)
1.955	0.355E+06	+- (	0.14E+05,	0.18E+05)
1.975	0.354E+06	+- (	0.14E+05,	0.18E+05)
1.995	0.370E+06	+- (	0.14E+05,	0.19E+05)
2.030	0.386E+06	+- (	0.88E+04,	0.19E+05)
2.080	0.396E+06	+- (	0.89E+04,	0.20E+05)
2.130	0.423E+06	+- (	0.13E+05,	0.21E+05)
2.504	0.399E+06	+- (	0.31E+04,	0.20E+05)
2.754	0.374E+06	+- (	0.31E+04,	0.19E+05)
3.004	0.349E+06	+- (	0.31E+04,	0.17E+05)
3.253	0.323E+06	+- (	0.26E+04,	0.16E+05)
3.503	0.304E+06	+- (	0.23E+04,	0.15E+05)
4.002	0.272E+06	+- (	0.22E+04,	0.15E+05)
4.502	0.247E+06	+- (	0.30E+04,	0.14E+05)
4.752	0.240E+06	+- (	0.48E+04,	0.12E+05)
5.001	0.232E+06	+- (	0.82E+04,	0.12E+05)

E_0 = 19.50 GeV, θ = 6.00, FINAL DATA

W(GEV)	CROSS SECTION		ERRORS	
1.083	0.953E+04	+- (	0.88E+03,	0.46E+03)
1.103	0.873E+04	+- (	0.71E+03,	0.44E+03)
1.123	0.118E+05	+- (	0.68E+03,	0.59E+03)
1.142	0.136E+05	+- (	0.66E+03,	0.68E+03)
1.162	0.155E+05	+- (	0.66E+03,	0.76E+03)
1.182	0.201E+05	+- (	0.70E+03,	0.10E+04)
1.202	0.211E+05	+- (	0.71E+03,	0.11E+04)
1.221	0.234E+05	+- (	0.74E+03,	0.12E+04)
1.241	0.259E+05	+- (	0.78E+03,	0.13E+04)
1.261	0.275E+05	+- (	0.82E+03,	0.14E+04)
1.281	0.307E+05	+- (	0.90E+03,	0.15E+04)
1.301	0.304E+05	+- (	0.95E+03,	0.15E+04)
1.320	0.338E+05	+- (	0.11E+04,	0.17E+04)
1.340	0.347E+05	+- (	0.12E+04,	0.17E+04)
1.360	0.397E+05	+- (	0.13E+04,	0.20E+04)
1.380	0.408E+05	+- (	0.13E+04,	0.20E+04)
1.400	0.439E+05	+- (	0.13E+04,	0.22E+04)
1.433	0.647E+07	+- (	0.68E+06,	0.33E+06)
1.453	0.708E+07	+- (	0.15E+06,	0.36E+06)
1.473	0.754E+07	+- (	0.13E+06,	0.38E+06)
1.493	0.760E+07	+- (	0.13E+06,	0.39E+06)
1.513	0.791E+07	+- (	0.13E+06,	0.40E+06)
1.533	0.793E+07	+- (	0.13E+06,	0.40E+06)
1.553	0.792E+07	+- (	0.12E+06,	0.40E+06)
1.573	0.787E+07	+- (	0.13E+06,	0.40E+06)
1.593	0.723E+07	+- (	0.32E+06,	0.37E+06)
1.692	0.657E+07	+- (	0.82E+06,	0.34E+06)
1.712	0.611E+07	+- (	0.99E+05,	0.31E+06)
1.732	0.606E+07	+- (	0.82E+05,	0.31E+06)
1.752	0.605E+07	+- (	0.81E+05,	0.31E+06)
1.772	0.590E+07	+- (	0.79E+05,	0.30E+06)
1.792	0.554E+07	+- (	0.76E+05,	0.28E+06)
1.812	0.574E+07	+- (	0.92E+05,	0.29E+06)
1.952	0.372E+07	+- (	0.55E+06,	0.19E+06)
1.972	0.417E+07	+- (	0.63E+05,	0.21E+06)
1.992	0.413E+07	+- (	0.55E+05,	0.21E+06)
2.027	0.418E+07	+- (	0.35E+05,	0.21E+06)
2.077	0.430E+07	+- (	0.16E+06,	0.21E+06)
2.258	0.308E+07	+- (	0.22E+05,	0.15E+06)
2.501	0.238E+07	+- (	0.15E+05,	0.12E+06)
2.755	0.190E+07	+- (	0.19E+05,	0.95E+05)
3.003	0.163E+07	+- (	0.22E+05,	0.81E+05)

E_0 = 13.50 GeV, θ = 6.00, FINAL DATA

W(GEV)	CROSS SECTION		ERRORS	
1.337	0.398E+06	+- (	0.34E+05,	0.20E+05)
1.357	0.439E+06	+- (	0.22E+05,	0.22E+05)
1.377	0.403E+06	+- (	0.16E+05,	0.20E+05)
1.397	0.454E+06	+- (	0.14E+05,	0.23E+05)
1.417	0.482E+06	+- (	0.13E+05,	0.24E+05)
1.436	0.467E+06	+- (	0.13E+05,	0.23E+05)
1.456	0.506E+06	+- (	0.12E+05,	0.25E+05)
1.476	0.560E+06	+- (	0.13E+05,	0.28E+05)
1.496	0.597E+06	+- (	0.14E+05,	0.30E+05)
1.516	0.585E+06	+- (	0.13E+05,	0.29E+05)
1.536	0.638E+06	+- (	0.14E+05,	0.32E+05)
1.556	0.632E+06	+- (	0.14E+05,	0.32E+05)
1.576	0.663E+06	+- (	0.14E+05,	0.33E+05)
1.596	0.692E+06	+- (	0.14E+05,	0.35E+05)
1.616	0.669E+06	+- (	0.13E+05,	0.33E+05)
1.635	0.703E+06	+- (	0.13E+05,	0.35E+05)
1.655	0.687E+06	+- (	0.13E+05,	0.34E+05)
1.675	0.700E+06	+- (	0.13E+05,	0.35E+05)
1.695	0.720E+06	+- (	0.13E+05,	0.36E+05)
1.715	0.725E+06	+- (	0.13E+05,	0.36E+05)
1.735	0.756E+06	+- (	0.13E+05,	0.38E+05)
1.755	0.728E+06	+- (	0.13E+05,	0.36E+05)
1.775	0.764E+06	+- (	0.13E+05,	0.38E+05)
1.795	0.757E+06	+- (	0.13E+05,	0.38E+05)
1.815	0.771E+06	+- (	0.13E+05,	0.39E+05)
1.835	0.763E+06	+- (	0.13E+05,	0.38E+05)
1.855	0.798E+06	+- (	0.14E+05,	0.40E+05)
1.875	0.783E+06	+- (	0.19E+05,	0.39E+05)
1.895	0.798E+06	+- (	0.32E+05,	0.40E+05)
2.504	0.667E+06	+- (	0.79E+04,	0.34E+05)
3.003	0.550E+06	+- (	0.68E+04,	0.28E+05)
3.502	0.460E+06	+- (	0.51E+04,	0.23E+05)
3.752	0.416E+06	+- (	0.45E+04,	0.21E+05)
4.001	0.384E+06	+- (	0.61E+04,	0.20E+05)
4.251	0.354E+06	+- (	0.87E+04,	0.18E+05)
4.501	0.334E+06	+- (	0.12E+05,	0.17E+05)

DEUTERIUM CROSS SECTION

E_0=19.50 GeV, θ=6.00, FINAL DATA

W(GEV)	CROSS SECTION		ERRORS	
1.420	0.479E+05	+- (	0.13E+04,	0.24E+04)
1.439	0.509E+05	+- (	0.14E+04,	0.25E+04)
1.459	0.520E+05	+- (	0.14E+04,	0.26E+04)
1.479	0.561E+05	+- (	0.15E+04,	0.28E+04)
1.499	0.619E+05	+- (	0.17E+04,	0.31E+04)
1.519	0.648E+05	+- (	0.18E+04,	0.32E+04)
1.539	0.655E+05	+- (	0.19E+04,	0.33E+04)
1.559	0.702E+05	+- (	0.21E+04,	0.35E+04)
1.578	0.697E+05	+- (	0.23E+04,	0.35E+04)
1.598	0.751E+05	+- (	0.24E+04,	0.38E+04)
1.618	0.763E+05	+- (	0.23E+04,	0.38E+04)
1.638	0.772E+05	+- (	0.22E+04,	0.39E+04)
1.658	0.843E+05	+- (	0.23E+04,	0.42E+04)
1.678	0.893E+05	+- (	0.24E+04,	0.44E+04)
1.698	0.902E+05	+- (	0.26E+04,	0.45E+04)
1.718	0.903E+05	+- (	0.27E+04,	0.45E+04)
1.738	0.892E+05	+- (	0.29E+04,	0.45E+04)
1.757	0.969E+05	+- (	0.32E+04,	0.48E+04)
1.777	0.105E+06	+- (	0.37E+04,	0.52E+04)
1.797	0.101E+06	+- (	0.39E+04,	0.51E+04)
1.817	0.105E+06	+- (	0.38E+04,	0.52E+04)
1.837	0.108E+06	+- (	0.36E+04,	0.54E+04)
1.857	0.110E+06	+- (	0.35E+04,	0.55E+04)
1.877	0.117E+06	+- (	0.36E+04,	0.59E+04)
1.897	0.117E+06	+- (	0.36E+04,	0.58E+04)
1.917	0.120E+06	+- (	0.36E+04,	0.60E+04)
1.937	0.128E+06	+- (	0.40E+04,	0.64E+04)
1.957	0.125E+06	+- (	0.43E+04,	0.62E+04)
1.976	0.131E+06	+- (	0.38E+04,	0.65E+04)
1.996	0.134E+06	+- (	0.44E+04,	0.67E+04)
2.031	0.135E+06	+- (	0.30E+04,	0.67E+04)
2.081	0.139E+06	+- (	0.30E+04,	0.70E+04)
2.131	0.157E+06	+- (	0.36E+04,	0.78E+04)
2.181	0.155E+06	+- (	0.62E+04,	0.78E+04)
2.255	0.160E+06	+- (	0.15E+04,	0.80E+04)
2.505	0.181E+06	+- (	0.15E+04,	0.90E+04)
2.754	0.185E+06	+- (	0.15E+04,	0.92E+04)
3.003	0.184E+06	+- (	0.19E+04,	0.92E+04)
3.253	0.176E+06	+- (	0.16E+04,	0.88E+04)
3.503	0.171E+06	+- (	0.13E+04,	0.86E+04)
3.752	0.166E+06	+- (	0.15E+04,	0.83E+04)
4.002	0.157E+06	+- (	0.22E+04,	0.79E+04)
4.252	0.150E+06	+- (	0.12E+04,	0.75E+04)
4.502	0.149E+06	+- (	0.17E+04,	0.83E+04)
4.751	0.151E+06	+- (	0.32E+04,	0.84E+04)
5.001	0.151E+06	+- (	0.30E+04,	0.84E+04)
5.251	0.155E+06	+- (	0.42E+04,	0.77E+04)
5.501	0.153E+06	+- (	0.80E+04,	0.80E+04)
5.750	0.160E+06	+- (	0.15E+05,	0.83E+04)

E_0=13.30 GeV, θ=15.00, FINAL DATA

W(GEV)	CROSS SECTION		ERRORS	
1.516	0.691E+03	+- (	0.29E+03,	0.35E+02)
1.536	0.260E+03	+- (	0.12E+03,	0.13E+02)
1.556	0.589E+03	+- (	0.13E+03,	0.30E+02)
1.576	0.680E+03	+- (	0.12E+03,	0.35E+02)
1.596	0.482E+03	+- (	0.87E+02,	0.25E+02)
1.615	0.502E+03	+- (	0.84E+02,	0.25E+02)
1.635	0.605E+03	+- (	0.82E+02,	0.31E+02)
1.655	0.761E+03	+- (	0.91E+02,	0.39E+02)
1.675	0.843E+03	+- (	0.95E+02,	0.43E+02)
1.695	0.815E+03	+- (	0.93E+02,	0.42E+02)
1.715	0.760E+03	+- (	0.80E+02,	0.39E+02)
1.735	0.850E+03	+- (	0.66E+02,	0.43E+02)
1.755	0.879E+03	+- (	0.65E+02,	0.45E+02)
1.775	0.914E+03	+- (	0.49E+02,	0.47E+02)
1.795	0.918E+03	+- (	0.45E+02,	0.47E+02)
1.815	0.107E+04	+- (	0.44E+02,	0.55E+02)
1.835	0.975E+03	+- (	0.42E+02,	0.50E+02)
1.855	0.117E+04	+- (	0.43E+02,	0.60E+02)
1.875	0.116E+04	+- (	0.38E+02,	0.59E+02)
1.894	0.123E+04	+- (	0.35E+02,	0.63E+02)
1.914	0.123E+04	+- (	0.32E+02,	0.63E+02)
1.934	0.135E+04	+- (	0.31E+02,	0.69E+02)
1.954	0.144E+04	+- (	0.32E+02,	0.73E+02)
1.974	0.148E+04	+- (	0.34E+02,	0.76E+02)
1.994	0.157E+04	+- (	0.37E+02,	0.80E+02)
2.029	0.168E+04	+- (	0.25E+02,	0.86E+02)
2.079	0.184E+04	+- (	0.34E+02,	0.94E+02)
2.126	0.207E+04	+- (	0.15E+02,	0.11E+03)
2.251	0.260E+04	+- (	0.22E+02,	0.13E+03)
2.524	0.392E+04	+- (	0.27E+02,	0.20E+03)
2.915	0.616E+04	+- (	0.35E+02,	0.31E+03)
3.195	0.803E+04	+- (	0.40E+02,	0.41E+03)
3.576	0.102E+05	+- (	0.54E+02,	0.51E+03)
4.003	0.135E+05	+- (	0.19E+03,	0.67E+03)

E_0=16.00 GeV, θ=15.00, FINAL DATA

W(GEV)	CROSS SECTION		ERRORS	
1.199	0.378E+02	+- (	0.56E+01,	0.19E+01)
1.219	0.466E+02	+- (	0.59E+01,	0.23E+01)
1.239	0.431E+02	+- (	0.57E+01,	0.22E+01)
1.259	0.505E+02	+- (	0.58E+01,	0.25E+01)
1.279	0.514E+02	+- (	0.58E+01,	0.26E+01)
1.299	0.597E+02	+- (	0.59E+01,	0.30E+01)
1.318	0.623E+02	+- (	0.61E+01,	0.31E+01)
1.338	0.671E+02	+- (	0.60E+01,	0.34E+01)
1.358	0.695E+02	+- (	0.62E+01,	0.35E+01)
1.378	0.802E+02	+- (	0.65E+01,	0.40E+01)
1.398	0.798E+02	+- (	0.63E+01,	0.40E+01)
1.418	0.780E+02	+- (	0.62E+01,	0.39E+01)
1.438	0.996E+02	+- (	0.66E+01,	0.50E+01)
1.458	0.100E+03	+- (	0.66E+01,	0.50E+01)
1.477	0.116E+03	+- (	0.71E+01,	0.58E+01)
1.497	0.111E+03	+- (	0.69E+01,	0.56E+01)
1.517	0.114E+03	+- (	0.66E+01,	0.57E+01)
1.537	0.118E+03	+- (	0.70E+01,	0.59E+01)
1.557	0.147E+03	+- (	0.73E+01,	0.74E+01)
1.577	0.143E+03	+- (	0.73E+01,	0.71E+01)
1.597	0.158E+03	+- (	0.75E+01,	0.79E+01)
1.617	0.161E+03	+- (	0.75E+01,	0.80E+01)
1.637	0.173E+03	+- (	0.77E+01,	0.86E+01)
1.656	0.181E+03	+- (	0.79E+01,	0.91E+01)
1.676	0.182E+03	+- (	0.79E+01,	0.91E+01)
1.696	0.196E+03	+- (	0.81E+01,	0.98E+01)
1.716	0.216E+03	+- (	0.82E+01,	0.11E+02)
1.736	0.240E+03	+- (	0.84E+01,	0.12E+02)
1.756	0.229E+03	+- (	0.86E+01,	0.11E+02)
1.776	0.231E+03	+- (	0.85E+01,	0.12E+02)
1.796	0.259E+03	+- (	0.90E+01,	0.13E+02)
1.816	0.278E+03	+- (	0.90E+01,	0.14E+02)
1.836	0.263E+03	+- (	0.90E+01,	0.14E+02)
1.856	0.306E+03	+- (	0.90E+01,	0.15E+02)
1.876	0.319E+03	+- (	0.91E+01,	0.16E+02)
1.895	0.334E+03	+- (	0.91E+01,	0.17E+02)
1.915	0.348E+03	+- (	0.92E+01,	0.17E+02)
1.935	0.382E+03	+- (	0.97E+01,	0.19E+02)
1.955	0.361E+03	+- (	0.99E+01,	0.18E+02)
1.975	0.418E+03	+- (	0.11E+02,	0.21E+02)
1.995	0.411E+03	+- (	0.11E+02,	0.21E+02)
2.030	0.467E+03	+- (	0.81E+01,	0.23E+02)
2.080	0.506E+03	+- (	0.11E+02,	0.26E+02)
2.130	0.556E+03	+- (	0.20E+02,	0.28E+02)
2.275	0.788E+03	+- (	0.95E+01,	0.40E+02)
2.580	0.135E+04	+- (	0.12E+02,	0.65E+02)
2.878	0.209E+04	+- (	0.17E+02,	0.11E+03)
3.310	0.345E+04	+- (	0.31E+02,	0.18E+03)
3.614	0.452E+04	+- (	0.39E+02,	0.23E+03)
4.021	0.612E+04	+- (	0.49E+02,	0.31E+03)
4.469	0.802E+04	+- (	0.14E+03,	0.42E+03)

E_0= 19.50 GeV, θ=15.00, FINAL DATA

W(GEV)	CROSS SECTION		ERRORS	
1.417	0.666E+02	+- (	0.21E+02,	0.33E+01)
1.437	0.459E+02	+- (	0.96E+01,	0.23E+01)
1.457	0.646E+02	+- (	0.84E+01,	0.32E+01)
1.477	0.664E+02	+- (	0.71E+01,	0.33E+01)
1.497	0.768E+02	+- (	0.66E+01,	0.38E+01)
1.517	0.745E+02	+- (	0.58E+01,	0.37E+01)
1.537	0.836E+02	+- (	0.55E+01,	0.42E+01)
1.557	0.847E+02	+- (	0.51E+01,	0.42E+01)
1.576	0.882E+02	+- (	0.47E+01,	0.44E+01)
1.596	0.103E+03	+- (	0.48E+01,	0.51E+01)
2.031	0.105E+03	+- (	0.31E+01,	0.53E+01)
2.081	0.121E+03	+- (	0.33E+01,	0.60E+01)
2.131	0.132E+03	+- (	0.36E+01,	0.66E+01)
2.181	0.145E+03	+- (	0.47E+01,	0.72E+01)
2.231	0.177E+03	+- (	0.80E+01,	0.89E+01)
2.313	0.207E+03	+- (	0.20E+01,	0.10E+02)
2.441	0.405E+03	+- (	0.39E+01,	0.20E+02)
2.984	0.687E+03	+- (	0.67E+01,	0.35E+02)
3.316	0.112E+04	+- (	0.12E+02,	0.57E+02)
3.752	0.190E+04	+- (	0.16E+02,	0.97E+02)

6-78

3360866

DEUTERIUM CROSS SECTION

E_0 = 6.50 GeV, θ=18.00, FINAL DATA

W(GEV)	CROSS SECTION		ERRORS	
1.154	0.403E+04	+- (	0.75E+02,	0.20E+03)
1.174	0.470E+04	+- (	0.79E+02,	0.24E+03)
1.194	0.534E+04	+- (	0.84E+02,	0.27E+03)
1.214	0.592E+04	+- (	0.94E+02,	0.30E+03)
1.234	0.659E+04	+- (	0.11E+03,	0.33E+03)
1.253	0.705E+04	+- (	0.12E+03,	0.35E+03)
1.273	0.766E+04	+- (	0.14E+03,	0.38E+03)
1.293	0.792E+04	+- (	0.15E+03,	0.40E+03)
1.313	0.837E+04	+- (	0.16E+03,	0.42E+03)
1.333	0.853E+04	+- (	0.16E+03,	0.43E+03)
1.353	0.862E+04	+- (	0.15E+03,	0.43E+03)
1.373	0.975E+04	+- (	0.15E+03,	0.49E+03)
1.393	0.102E+05	+- (	0.16E+03,	0.51E+03)
1.413	0.113E+05	+- (	0.17E+03,	0.56E+03)
1.433	0.122E+05	+- (	0.17E+03,	0.61E+03)
1.453	0.130E+05	+- (	0.18E+03,	0.65E+03)
1.473	0.137E+05	+- (	0.20E+03,	0.68E+03)
1.493	0.150E+05	+- (	0.25E+03,	0.75E+03)
1.513	0.157E+05	+- (	0.29E+03,	0.79E+03)
1.533	0.158E+05	+- (	0.31E+03,	0.79E+03)
1.553	0.156E+05	+- (	0.33E+03,	0.78E+03)
1.573	0.164E+05	+- (	0.36E+03,	0.82E+03)
1.592	0.160E+05	+- (	0.37E+03,	0.80E+03)
1.612	0.177E+05	+- (	0.39E+03,	0.89E+03)
1.632	0.192E+05	+- (	0.37E+03,	0.96E+03)
1.652	0.198E+05	+- (	0.33E+03,	0.99E+03)
1.672	0.211E+05	+- (	0.34E+03,	0.11E+04)
1.692	0.219E+05	+- (	0.35E+03,	0.11E+04)
1.712	0.228E+05	+- (	0.35E+03,	0.11E+04)
1.732	0.235E+05	+- (	0.37E+03,	0.12E+04)
1.752	0.241E+05	+- (	0.42E+03,	0.12E+04)
1.772	0.247E+05	+- (	0.35E+03,	0.12E+04)
1.792	0.250E+05	+- (	0.26E+03,	0.12E+04)
1.812	0.264E+05	+- (	0.26E+03,	0.13E+04)
1.832	0.272E+05	+- (	0.28E+03,	0.14E+04)
1.852	0.276E+05	+- (	0.30E+03,	0.14E+04)
1.872	0.279E+05	+- (	0.44E+03,	0.14E+04)
1.952	0.316E+05	+- (	0.14E+04,	0.16E+04)
1.972	0.308E+05	+- (	0.47E+03,	0.15E+04)
1.992	0.324E+05	+- (	0.43E+03,	0.16E+04)
2.027	0.340E+05	+- (	0.30E+03,	0.17E+04)
2.252	0.392E+05	+- (	0.28E+03,	0.20E+04)
2.502	0.438E+05	+- (	0.32E+03,	0.22E+04)
2.751	0.458E+05	+- (	0.42E+03,	0.23E+04)

E_0 = 10.40 GeV, θ = 18.00 FINAL DATA

W(GEV)	CROSS SECTION		ERRORS	
1.176	0.178E+03	+- (	0.26E+02,	0.91E+01)
1.196	0.173E+03	+- (	0.25E+02,	0.88E+01)
1.216	0.198E+03	+- (	0.24E+02,	0.10E+02)
1.236	0.244E+03	+- (	0.26E+02,	0.12E+02)
1.256	0.262E+03	+- (	0.28E+02,	0.13E+02)
1.276	0.308E+03	+- (	0.31E+02,	0.16E+02)
1.295	0.302E+03	+- (	0.31E+02,	0.15E+02)
1.315	0.259E+03	+- (	0.29E+02,	0.13E+02)
1.335	0.354E+03	+- (	0.32E+02,	0.18E+02)
1.355	0.394E+03	+- (	0.31E+02,	0.20E+02)
1.375	0.330E+03	+- (	0.29E+02,	0.17E+02)
1.395	0.447E+03	+- (	0.34E+02,	0.23E+02)
1.415	0.438E+03	+- (	0.34E+02,	0.22E+02)
1.435	0.516E+03	+- (	0.38E+02,	0.27E+02)
1.455	0.505E+03	+- (	0.39E+02,	0.26E+02)
1.475	0.547E+03	+- (	0.40E+02,	0.28E+02)
1.495	0.587E+03	+- (	0.40E+02,	0.30E+02)
1.515	0.579E+03	+- (	0.41E+02,	0.30E+02)
1.534	0.589E+03	+- (	0.45E+02,	0.30E+02)
1.554	0.644E+03	+- (	0.49E+02,	0.33E+02)
1.574	0.852E+03	+- (	0.61E+02,	0.43E+02)
1.594	0.835E+03	+- (	0.59E+02,	0.42E+02)
1.614	0.868E+03	+- (	0.56E+02,	0.44E+02)
1.634	0.862E+03	+- (	0.58E+02,	0.44E+02)

W(GEV)	CROSS SECTION		ERRORS	
1.654	0.101E+04	+- (	0.64E+02,	0.51E+02)
1.674	0.110E+04	+- (	0.68E+02,	0.56E+02)
1.694	0.108E+04	+- (	0.67E+02,	0.55E+02)
1.714	0.128E+04	+- (	0.64E+02,	0.65E+02)
1.734	0.118E+04	+- (	0.56E+02,	0.60E+02)
1.754	0.131E+04	+- (	0.60E+02,	0.67E+02)
1.774	0.129E+04	+- (	0.59E+02,	0.66E+02)
1.794	0.143E+04	+- (	0.64E+02,	0.73E+02)
1.814	0.157E+04	+- (	0.68E+02,	0.80E+02)
1.834	0.141E+04	+- (	0.66E+02,	0.72E+02)
1.853	0.170E+04	+- (	0.79E+02,	0.86E+02)
1.873	0.168E+04	+- (	0.87E+02,	0.86E+02)
1.893	0.185E+04	+- (	0.11E+03,	0.94E+02)
1.913	0.164E+04	+- (	0.15E+03,	0.84E+02)
1.933	0.225E+04	+- (	0.37E+03,	0.11E+03)
1.973	0.193E+04	+- (	0.5CE+03,	0.98E+02)
1.993	0.222E+04	+- (	0.22E+03,	0.11E+03)
2.028	0.246E+04	+- (	0.90E+02,	0.13E+03)
2.078	0.258E+04	+- (	0.85E+02,	0.13E+03)
2.128	0.316E+04	+- (	0.12E+03,	0.16E+03)
2.306	0.389E+04	+- (	0.76E+02,	0.20E+03)
2.656	0.625E+04	+- (	0.12E+03,	0.31E+03)
2.904	0.819E+04	+- (	0.98E+02,	0.41E+03)
3.237	0.108E+05	+- (	0.12E+03,	0.54E+03)
3.607	0.139E+05	+- (	0.17E+03,	0.69E+03)

E_0 = 13.30 GeV, θ = 18.00, FINAL DATA

W(GEV)	CROSS SECTION		ERRORS	
1.536	0.113E+03	+- (	0.14E+02,	0.56E+01)
1.556	0.112E+03	+- (	0.12E+02,	0.57E+01)
1.576	0.115E+03	+- (	0.11E+02,	0.59E+01)
1.596	0.131E+03	+- (	0.10E+02,	0.67E+01)
1.615	0.177E+03	+- (	0.11E+02,	0.90E+01)
1.635	0.143E+03	+- (	0.95E+01,	0.73E+01)
1.655	0.171E+03	+- (	0.93E+01,	0.87E+01)
1.675	0.174E+03	+- (	0.93E+01,	0.89E+01)
1.695	0.190E+03	+- (	0.92E+01,	0.97E+01)
1.715	0.208E+03	+- (	0.96E+01,	0.11E+02)
1.735	0.217E+03	+- (	0.99E+01,	0.11E+02)
1.755	0.233E+03	+- (	0.11E+02,	0.12E+02)
1.775	0.223E+03	+- (	0.10E+02,	0.11E+02)
1.795	0.236E+03	+- (	0.11E+02,	0.12E+02)
1.815	0.256E+03	+- (	0.11E+02,	0.13E+02)
1.835	0.270E+03	+- (	0.11E+02,	0.14E+02)
1.855	0.289E+03	+- (	0.11E+02,	0.15E+02)
1.875	0.297E+03	+- (	0.11E+02,	0.15E+02)
1.894	0.338E+03	+- (	0.13E+02,	0.17E+02)
1.914	0.342E+03	+- (	0.13E+02,	0.17E+02)
1.934	0.379E+03	+- (	0.14E+02,	0.19E+02)
1.954	0.375E+03	+- (	0.14E+02,	0.19E+02)
1.974	0.406E+03	+- (	0.15E+02,	0.21E+02)
1.994	0.421E+03	+- (	0.16E+02,	0.21E+02)
2.029	0.444E+03	+- (	0.16E+02,	0.23E+02)
2.182	0.639E+03	+- (	0.53E+01,	0.33E+02)
2.463	0.109E+04	+- (	0.10E+02,	0.56E+02)
2.735	0.178E+04	+- (	0.17E+02,	0.91E+02)
3.130	0.293E+04	+- (	0.31E+02,	0.15E+03)
3.404	0.397E+04	+- (	0.45E+02,	0.20E+03)
3.767	0.538E+04	+- (	0.61E+02,	0.27E+03)
4.159	0.727E+04	+- (	0.12E+03,	0.38E+03)

E_0 = 16.00 GeV, θ = 18.00, FINAL DATA

W(GEV)	CROSS SECTION		ERRORS	
1.796	0.587E+02	+- (	0.67E+01,	0.30E+01)
1.816	0.585E+02	+- (	0.56E+01,	0.30E+01)
1.836	0.640E+02	+- (	0.52E+01,	0.33E+01)
1.856	0.759E+02	+- (	0.51E+01,	0.39E+01)
1.876	0.836E+02	+- (	0.48E+01,	0.43E+01)
1.895	0.822E+02	+- (	0.46E+01,	0.42E+01)
1.915	0.886E+02	+- (	0.47E+01,	0.45E+01)
1.935	0.878E+02	+- (	0.47E+01,	0.45E+01)
1.955	0.929E+02	+- (	0.48E+01,	0.47E+01)
1.975	0.109E+03	+- (	0.51E+01,	0.56E+01)
1.995	0.113E+03	+- (	0.52E+01,	0.57E+01)
2.030	0.128E+03	+- (	0.40E+01,	0.65E+01)
2.080	0.137E+03	+- (	0.62E+01,	0.70E+01)
2.187	0.177E+03	+- (	0.22E+01,	0.90E+01)
2.491	0.345E+03	+- (	0.33E+01,	0.18E+02)
2.807	0.621E+03	+- (	0.47E+01,	0.32E+02)
3.111	0.991E+03	+- (	0.11E+02,	0.51E+02)
3.543	0.173E+04	+- (	0.15E+02,	0.88E+02)
3.839	0.235E+04	+- (	0.31E+02,	0.12E+03)
4.225	0.333E+04	+- (	0.42E+02,	0.17E+03)
4.634	0.464E+04	+- (	0.77E+02,	0.24E+03)

6-78

3360867

DEUTERIUM CROSS SECTION

E_0 = 19.50 GeV, θ = 18.00, FINAL DATA

W (GEV)	CROSS SECTION		ERRORS	
1.658	0.101E+02	+- (	0.54E+01,	0.51E+00)
1.678	0.145E+02	+- (	0.55E+01,	0.73E+00)
1.698	0.108E+02	+- (	0.41E+01,	0.54E+00)
1.718	0.204E+02	+- (	0.52E+01,	0.10E+01)
1.738	0.963E+01	+- (	0.30E+01,	0.48E+00)
1.757	0.154E+02	+- (	0.34E+01,	0.77E+00)
1.777	0.140E+02	+- (	0.29E+01,	0.70E+00)
1.797	0.140E+02	+- (	0.27E+01,	0.70E+00)
1.817	0.118E+02	+- (	0.23E+01,	0.59E+00)
1.837	0.185E+02	+- (	0.28E+01,	0.93E+00)
1.857	0.177E+02	+- (	0.25E+01,	0.90E+00)
1.877	0.168E+02	+- (	0.24E+01,	0.86E+00)
1.897	0.215E+02	+- (	0.26E+01,	0.11E+01)
1.917	0.198E+02	+- (	0.24E+01,	0.10E+01)
1.937	0.297E+02	+- (	0.29E+01,	0.15E+01)
1.957	0.229E+02	+- (	0.25E+01,	0.12E+01)
1.976	0.288E+02	+- (	0.28E+01,	0.15E+01)
1.996	0.243E+02	+- (	0.26E+01,	0.12E+01)
2.031	0.281E+02	+- (	0.20E+01,	0.14E+01)
2.081	0.346E+02	+- (	0.26E+01,	0.18E+01)
2.131	0.370E+02	+- (	0.36E+01,	0.19E+01)
2.181	0.412E+02	+- (	0.63E+01,	0.21E+01)
2.228	0.488E+02	+- (	0.11E+01,	0.25E+01)
2.516	0.956E+02	+- (	0.18E+01,	0.49E+01)
2.858	0.185E+03	+- (	0.26E+01,	0.94E+01)
3.212	0.338E+03	+- (	0.38E+01,	0.17E+02)
3.549	0.550E+03	+- (	0.71E+01,	0.28E+02)
4.021	0.100E+04	+- (	0.13E+02,	0.51E+02)
4.341	0.136E+04	+- (	0.18E+02,	0.66E+02)
4.754	0.205E+04	+- (	0.39E+02,	0.10E+03)
5.183	0.299E+04	+- (	0.72E+02,	0.16E+03)

E_0 = 19.50 GeV, θ = 20.60, FINAL DATA

W (GEV)	CROSS SECTION		ERRORS	
1.817	0.103E+02	+- (	0.27E+01,	0.52E+00)
1.837	0.753E+01	+- (	0.19E+01,	0.38E+00)
1.857	0.637E+01	+- (	0.15E+01,	0.32E+00)
1.877	0.840E+01	+- (	0.16E+01,	0.43E+00)
1.897	0.793E+01	+- (	0.14E+01,	0.40E+00)
1.917	0.114E+02	+- (	0.14E+01,	0.58E+00)
1.937	0.911E+01	+- (	0.12E+01,	0.46E+00)
1.957	0.113E+02	+- (	0.12E+01,	0.58E+00)
1.976	0.123E+02	+- (	0.12E+01,	0.63E+00)
1.996	0.127E+02	+- (	0.13E+01,	0.65E+00)
2.031	0.135E+02	+- (	0.81E+00,	0.69E+00)
2.081	0.171E+02	+- (	0.91E+00,	0.87E+00)
2.131	0.148E+02	+- (	0.98E+00,	0.76E+00)
2.181	0.195E+02	+- (	0.16E+01,	0.99E+00)
2.345	0.290E+02	+- (	0.70E+00,	0.15E+01)
2.643	0.507E+02	+- (	0.15E+01,	0.26E+01)

6-78

3360B68

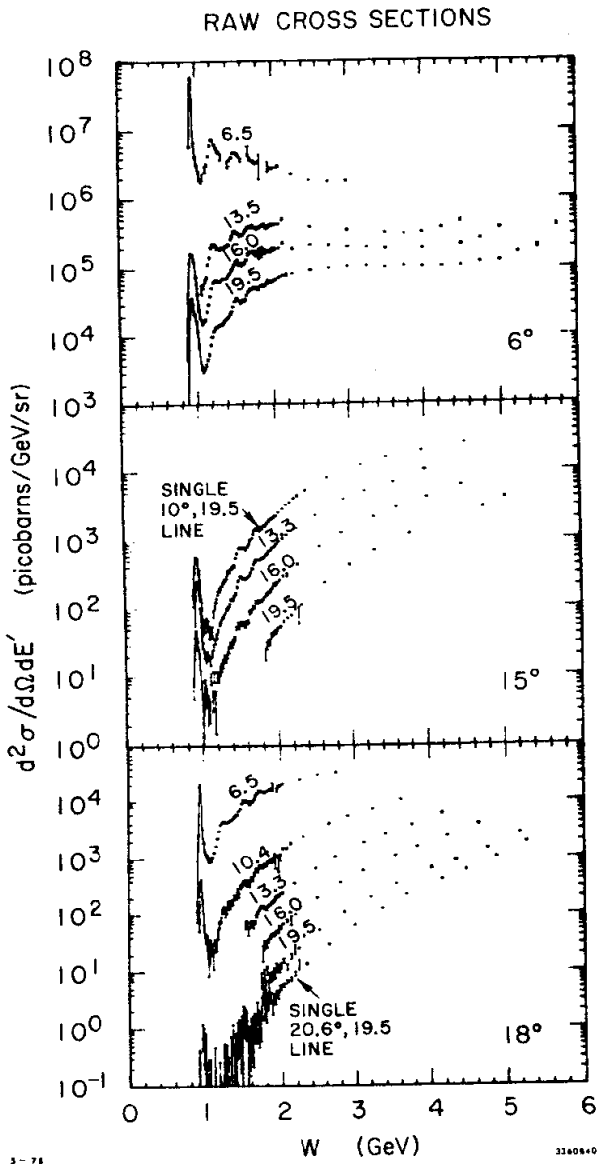

Fig. III-8

A plot of the differential cross section $d^2\sigma/d\Omega dE'$ as a function of final state mass W in GeV. The beam energy and scattering angles of the data are indicated. Resonant structure is evident below W≈2 GeV.

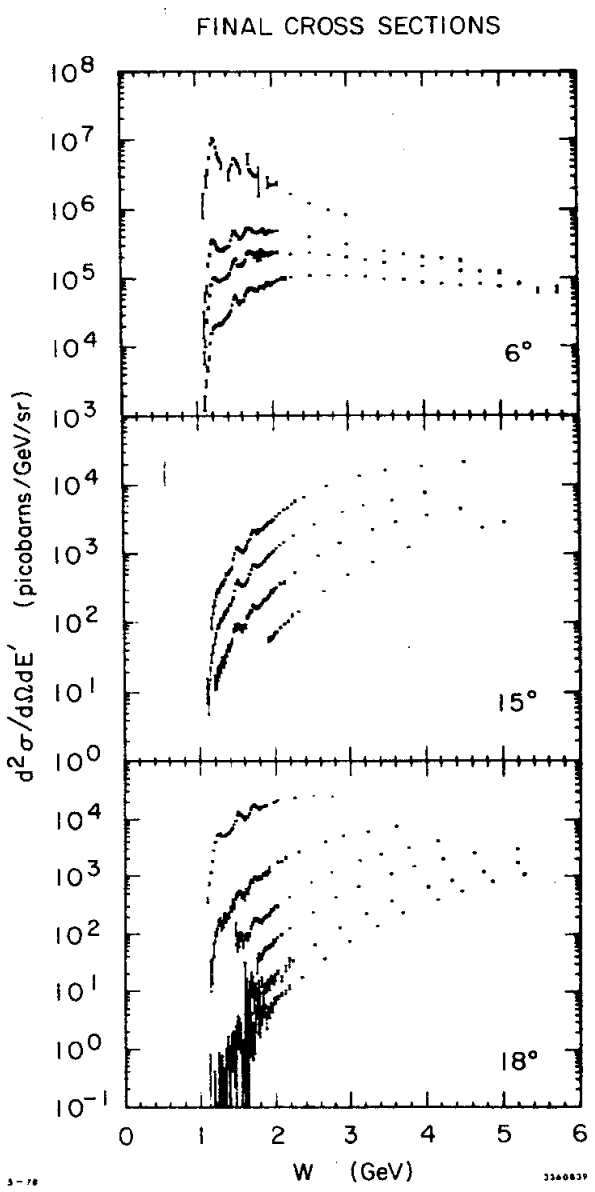

background even at Q^2=18 GeV . There is a clearly discernible elastic peak (≈8 counts) in the 20.6°, 19.5 GeV line at a Q^2 value of 21 GeV^2. Our elastic scattering results will be presented in the next chapter.

Note that the cross section, $d^2\sigma/d\Omega dE'$ varies over a range of 10^8 for the range of data in the experiment, reflecting the wide kinematic coverage from large angle, high energy (20.6°, 19.5 GeV) data to small angle, low energy (6°, 7 GeV) data.

Another obvious feature of the data are the fluctuations occurring near W=2 GeV. These fluctuations are an instrumental effect arising from the fact that W bins near 2 GeV have counts coming only from an edge of the δ,θ_o acceptance, i.e., they are not "scanned". (See Chapter III, "Corrections for Offset Aperture".) The fluctuations are consistent with a ≈±10% uncertainty in the acceptance of individual W bins in the δ,θ_o plane.

The next section describes how we interpolate our cross sections (and those from other experiments) so that they can be used to extract the proton's structure functions.

INTERPOLATION

Since the cross section is given by the expression, $\Gamma * (\sigma_T+\varepsilon\sigma_L)$ a single measurement of the cross section at some Q^2, W^2 point will not determine σ_L and σ_T separately. However, we can separately determine σ_L and σ_T if we measure the cross section for one value of Q^2, W^2, but at different θ's (i.e., different values of ε).

In practice, there are very few exact "crossover" points where we took data from different angles at the same value of Q^2 and W^2. We set up a grid of points in the Q^2, W^2 plane where we want to determine separately σ_L and σ_T. Choosing one of these grid points, we interpolate the cross sections to that point from any angle whose

data range covers that point. After dividing the cross sections by Γ, they are fit to first order in ε.[6] The ε=0 intercept is σ_T and the ε=1 value of the fit is $\sigma_T+\sigma_L$; the slope being proportional to $R \equiv \sigma_L/\sigma_T$. In this manner, σ_L/σ_T is determined at each of the Q^2,W^2 points selected. The interpolation methods are now discussed.

Description of Interpolation Procedure

In order to use low order polynomials (1st and 2nd order) to do the interpolations, the main variations have been taken out. The first step in the interpolation procedure, then, was to divide each of the cross sections (for all angles and energies) by a single function (of E_o, E', and θ) which fits our data to about 20% in the W>2 GeV region; thus producing a set of "normalized" cross sections. We interpolate in the set of normalized values; multiplying the interpolated value at each grid point by the normalizing function to obtain the interpolated cross section.

The set of grid points (to which the interpolations are done) must have approximately the same density in the Q^2,W^2 plane as the data points. If there are too few points, we do not utilize all the data; if too many, we use the same data many times. The correlation[7] between two grid point values is proportional to the fractional contribution to their values from common data. If two grid points use the same set of data in the interpolation, they are 100% correlated; if they depend on no common data, the correlation between them is 0. To minimize this correlation, we chose a set of grid points in the Q^2,W^2 plane with a spacing of 3 GeV^2. The correlation between neighboring grid points for the 18° data was about 10% and for the 60° data was about 30% (reflecting the lower density of the large angle data).

For an illustration of the interpolation method, see Figure III-9. The figure demonstrates how cross sections (for a given θ) are interpolated to a grid point. As stated before, data for a particular scattering angle, θ, is taken in runs at constant E_o;

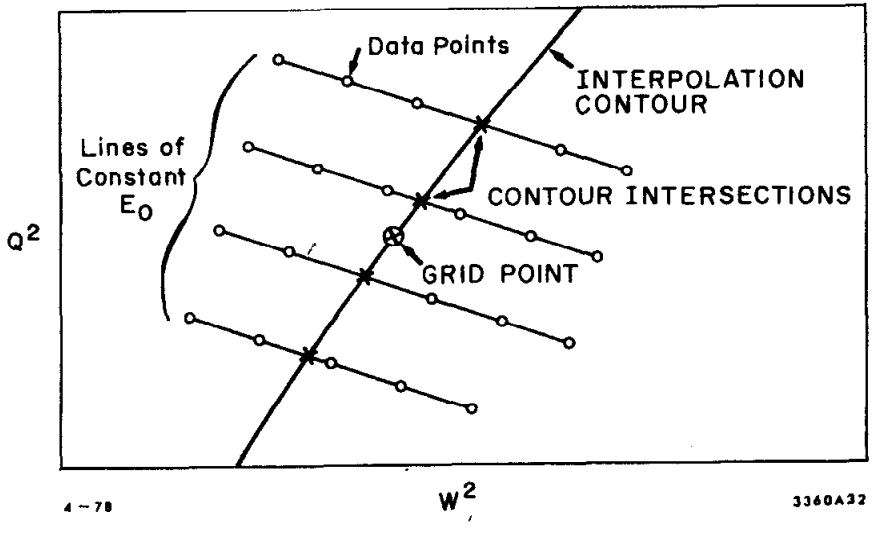

Fig. III-9

Sketch of the procedures used to interpolate cross sections from data at a single angle to a selected Q^2,W^2 "grid" point. Using data which has been multiplied by factors which greatly reduce the kinematic variation, the interpolation proceeds along the E_0 lines to intersection points, then along the interpolation contour to a grid point.

i.e., in "lines" in the Q^2,W^2 plane. Cross sections can be interpolated along the E_0 lines, but in order to interpolate to the grid point (which, in general, does not lie on one of the E_0 lines), it is necessary to choose a second contour of interpolation.

The method we used to interpolate the normalized cross sections along the E_0 lines to the contour intersection points was to fit and evaluate the fit at the contour intersection points. Then the interpolated values at these intersections were themselves interpolated along the chosen contour to the position of the grid point. Our standard procedure included the following: (1) 2 to 4 data points (within ΔW=.5 GeV of the contour intersections) were used in the interpolation along the E_0 lines; (2) 2nd order fits were used for the case of 4 data points; otherwise, linear fits were used; (3) the interpolation contours were chosen to be straight lines in the Q^2,W^2 plane originating at Q^2=0, W^2=4 GeV^2; (4) for W<2 GeV, these contours were constant W lines; (5) only the two nearest intersection points were used in the interpolation along the second contour. As these procedures were rather arbitrary, we investigated the change in the interpolated value of the cross section due to changing these procedures and concluded that systematic errors in the cross sections due to interpolations could be as large as 2.5%.

There was one exception to our general rule of no data extrapolations. Because there was only one "line" of 20.6° data (that with E=19.5), we were forced to fit the normalized cross section along the line and to extrapolate <u>off</u> the E_0 line to preselected grid points at specified values of Q^2 and W^2. We fit along the line to a function of X' and extrapolated off the line using a function of ν. We used for the variation of the cross section with ν, that obtained from two nearby 18° "lines". We extrapolated no further than 1.4 GeV in ν, nor changed the value of the cross section (due to the extrapolation) by more than 1.8%.

Checks on the Procedure

We employed a direct test to see that the interpolation procedure was giving reasonable answers. We checked that for those grid points which fell between two lines of data that the interpolated values lay between the data as it should. This was accomplished by overplotting the two lines of data along with the interpolated values, versus W. An example is shown in Figure III-10. This check was performed on all the data, and it was verified that the interpolation scheme was performing adequately.

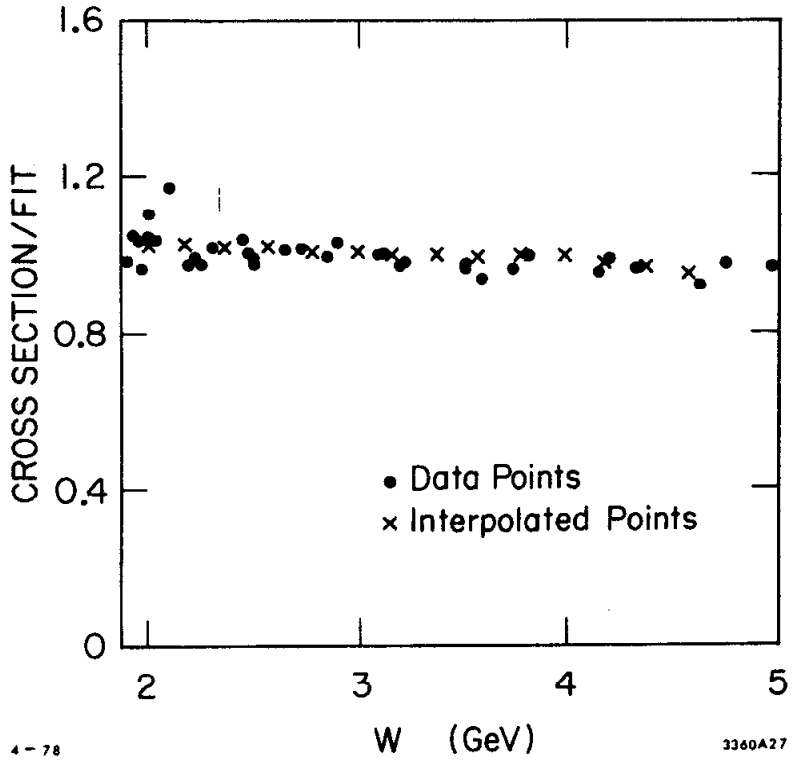

Fig. III-10

Illustration of the agreement between interpolated points and measured cross sections. Data points from two adjacent E_0 lines are overplotted with interpolated values from grid points located between the two lines.

CHAPTER III - REFERENCES

1. S. Stein et al., "Electron Scattering at 4 degrees With Energies of 4.5 GeV-20 GeV," Phys. Rev. D12, 1884 (1975).

2. W. B. Atwood et al., Physics Letters 64B (1976), 479-482; "Electron Scattering off Hydrogen and Deuterium", W. B. Atwood (Ph.D. thesis), SLAC Report No. 185.

   Luke W. Mo and Yung-Su Tsai, "Radiative Corrections to Elastic and Inelastic ep and mu p Scattering", Rev. Mod. Phys. 41, 205-35 (1969).

3. Luke W. Mo and Yung-Su Tsai, "Inelastic e p and mu p Scattering", Rev. Mod. Phys. 41, 205-35 (1969).

4. G. Miller (Ph.D. thesis), SLAC Report No. 129 (1971).

5. Private communication, H. De Staebler.

6. The errors used when fitting versus epsilon were the quadratic sum of the statistical and systematic errors. The systematic error assigned to this experiment's cross sections averaged at about 7½% and has been described in a previous section. The systematic error on the 50° and 60° data was obtained from W. B. Atwood's thesis, SLAC Report No. 185, and was parameterized as: $(5.8+.032*W^4)\%$. A systematic error of 5.5% was assigned to the M.I.T. cross sections.

7. The grid point values, G_i, can be expressed as a weighted sum of the data point values, D_i,

$$G_i = W_{ij}D_j$$

where the weights are determined from the values of the interpolation fits. The correlation matrix of the grid point $(C_G)_{ij}$ can then be expressed in the following form:

$$(C_G)_{ij} = W_{ik}(\sigma_D)_{kl}W_{lj}^t$$

when σ_D is the correlation matrix for the data points. Since the statistical errors on the data points are uncorrelated $(\sigma_D)_{kl}=0$ for $k\neq l$. Therefore

$$(C_G)_{ij} = W_{ik}(\sigma_D)_{kk}W_{kj}^t$$

is the correlation matrix for the grid points with $(C_G)_{ii}$ being the error squared on the i^{th} grid point.

In previous chapters, we have described how the cross sections and their systematic errors were extracted from the measurements. The most obvious feature of the inelastic data is the slow fall-off of the cross sections with Q^2 compared with elastic cross sections, as expected if the electron is scattering from point-like objects within the proton. To determine proton structure functions[1], it is necessary to separate the two independent structure functions, σ_T and σ_L, or the equivalent pair, W_1 and νW_2, by comparing cross sections at the same W^2,Q^2 but differing angles.

By combining our cross section measurements with those taken at 50° and 60° using the 1.6 GeV spectrometer[2] and with previous measurements[3] by various combinations of SLAC and MIT groups, we can extract σ_T and σ_L from the cross sections. The extraction is accomplished by interpolating cross sections from different angles to common Q^2,W^2 points. Recall that the differential cross section can be expressed as $\Gamma * (\sigma_T+\varepsilon\sigma_L)$. Dividing each of the interpolated cross sections by

$$\Gamma \equiv \left(\frac{e^2}{4\pi^2}\,\frac{2KE'}{Q^2E_o(1-\varepsilon)}\right)$$

we then fit the remainder, $(\sigma_T+\varepsilon\sigma_L)$ to a linear function of $\varepsilon,\equiv(1/(1+2\tan^2\theta/2(1+\nu^2/Q^2))$. The $\varepsilon=0$ intercept yields σ_T and the $\varepsilon=1$ intercept yields the sum, $\sigma_T+\sigma_L$.

We can perform the extraction of the structure functions using data from this experiment and the data at 50° and 60°, or by using a combined set of data from various SLAC and MIT measurements. Figure IV-1 is a plot of interpolated cross sections from several independent experiments. Each of the sub-graphs is at a particular Q^2,W^2 point, and in each the differential cross sections $d^2\sigma/d\Omega dE'$ divided by their flux factor, Γ, are plotted against the epsilon value corresponding to the angle. Large angle data gives low values of epsilon (the green points are 50° and 60° data from this experiment). The blue points are the cross sections taken with the 20 GeV spectrometer

Fig. IV-1

Graphs of photo absorption cross sections, $d^2\sigma/d\Omega dE'/\Gamma \equiv (\sigma_T + \epsilon\sigma_L)$, plotted against the polarization parameter, ϵ, for various Q^2, W^2 points. Data from different experiments are included: red points are MIT-SLAC (experiment E87), black points are MIT-SLAC (E49), blue points are SLAC (E89-20 GeV spectrometer), and the green points are SLAC (E89-1.6 GeV spectrometer). For purposes of comparison, scales on individual graphs have been adjusted so that a diagonal line would correspond to $\sigma_L/\sigma_T = .5$

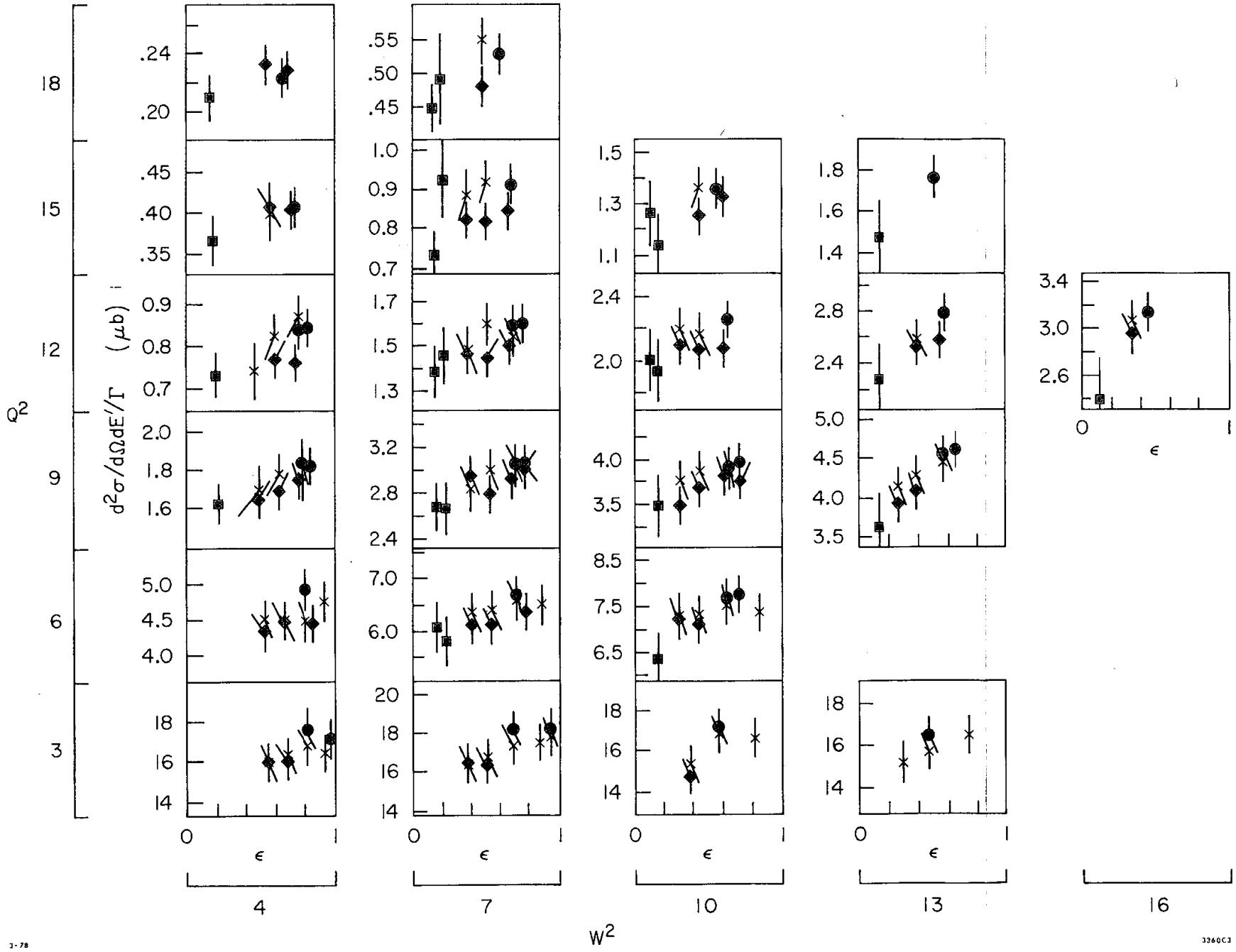
Q^2
$d^2\sigma/d\Omega dE'/\Gamma$ (μb)
W^2
ϵ
3
6
9
12
15
18
4
7
10
13
16

in this experiment. The red points are from an MIT-SLAC (SFG) experiment (E87)[3] which used the 8 GeV spectrometer, and the black points are from an earlier MIT[4] experiment (E49), also using the 8 GeV spectrometer.

As mentioned above, the ε=0 intercept of a straight line fit is σ_T and the ε=1 intercept is $\sigma_T+\sigma_L$, so the slope of a line through the data is proportional to σ_L/σ_T. If σ_L/σ_T=0, the points should lie on a line with no slope. For purposes of comparison, scales on individual graphs have been adjusted so that a diagonal corresponds to σ_L/σ_T=.5. Before presenting results on σ_L/σ_T, we note a few features of the data.

Notice that the E89 (20 GeV spectrometer) data is consistently higher than the MIT data where they overlap. In fact, the E89 (20) data (blue) is, on the average, 5.5% higher than the MIT (E87) data (red) and 3% higher than the MIT (E49) data (black). These differences are large and of concern to us, but a careful study unveiled no obvious errors in our data. The various data are consistent within an estimated 8% relative systematic error between our experiment and those of MIT.

It is difficult to detect normalization differences betwen the E89 (20 GeV spectrometer) data and E89 (1.6 GeV spectrometer) data (green) taken at 50° and 60° because there is no overlap in angle. One procedure is to compare elastic cross sections (which will be presented later in the chapter) at the same value of Q^2. To make this comparison requires an assumption about the behavior of G_E/G_M (the ratio of the "electric" to "magnetic" elastic form factors) which is the elastic analogue of σ_L/σ_T. If we assume that $\mu_p G_E/G_M$=1, i.e., "form factor scaling", then the E89 (20) elastic cross sections are 5% higher than those for E89 (1.6).

σ_L/σ_T

Values for $R=\sigma_L/\sigma_T$ are obtained from straight line fits to each of the graphs in the figure. When fitting, the errors used were those

shown in the graph which are the combined systematic and statistical errors,[5] added in quadrature. The values of $R=\sigma_L/\sigma_T$ at each Q^2, W^2 point are presented in Table IV-1. The errors on σ_L/σ_T quoted are those from the fitting program and take into account the correlation of the errors on σ_L and σ_T. The errors on individual points (the combination of statistical and systematic errors) are treated as if they were uncorrelated when fitting, even those from the same experiment. Although this is not rigorously true, it is a reasonable approximation, since we estimate that the proportion of systematic error which represents an overall normalization error (independent of kinematics) is less than 50%.

In addition to the values of σ_L/σ_T extracted using all the data in Figure IV-1, in Table IV-1 we also present values of σ_L/σ_T and the corresponding systematic errors obtained from E89 (green and blue) data alone. The average value of R over the entire Q^2, W^2 range, using the combined data set (all data in Figure IV-1) is .21. Using only the data from E89 (20 and 1.6), the average value of R obtained is .30. The systematic error on either of these average values is estimated as ±.1. This error of .1 is approximately the same size as the minimum error of an individual point. This is a reflection of the fact that combining individual measurements does not reduce the error, when systematic errors dominate. The errors are consistent with the observation that if we allow the E89 (1.6) data to increase by its systematic error everywhere, the average value of R decreases from .21 to .13. The values of R that we report are consistent with an earlier measurement of MIT[4] of .14 ±.06 using the (red and black) data shown in Figure IV-1, although with slightly different radiative corrections and interpolation methods. As can be seen in Figure IV-1, the individual data points are quite consistent with each other; it is, then, not surprising that the value for R is also consistent.

The quantity $R \equiv (\sigma_L/\sigma_T)$ is interesting because it is a measure of the spin of the constituents of the proton. In naive parton models.

TABLE IV-1

Q^2-W^2 GRID E89 DATA ONLY

Q^2	W^2	R	dR	νW_2	$d\nu W_2$	$2MW_1$	$d2MW_1$
0.6000E+01	0.7000E+01	0.2502E+00	0.1815E+00	0.1678E+00	0.1347E-01	0.3101E+00	0.2604E-01
0.6000E+01	0.1000E+02	0.4463E+00	0.2706E+00	0.2543E+00	0.1759E-01	0.4840E+00	0.6338E-01
0.9000E+01	0.4000E+01	0.2237E+00	0.1583E+00	0.3216E-01	0.1759E-02	0.4303E-01	0.4041E-02
0.9000E+01	0.7000E+01	0.2722E+00	0.1505E+00	0.9249E-01	0.5017E-02	0.1391E+00	0.1107E-01
0.9000E+01	0.1000E+02	0.2642E+00	0.2431E+00	0.1560E+00	0.1148E-01	0.2725E+00	0.3583E-01
0.9000E+01	0.1300E+02	0.5450E+00	0.3572E+00	0.2273E+00	0.1928E-01	0.3697E+00	0.5831E-01
0.1200E+02	0.4000E+01	0.2647E+00	0.1782E+00	0.1639E-01	0.9305E-03	0.1935E-01	0.2013E-02
0.1200E+02	0.7000E+01	0.2364E+00	0.1544E+00	0.5383E-01	0.3028E-02	0.7420E-01	0.6234E-02
0.1200E+02	0.1000E+02	0.2994E+00	0.2171E+00	0.1040E+00	0.9566E-02	0.1543E+00	0.1458E-01
0.1200E+02	0.1300E+02	0.5468E+00	0.4165E+00	0.1647E+00	0.1738E-01	0.2296E+00	0.3813E-01
0.1200E+02	0.1600E+02	0.1014E+01	0.7556E+00	0.2444E+00	0.3881E-01	0.2901E+00	0.6419E-01
0.1500E+02	0.4000E+01	0.2013E+00	0.2213E+00	0.8486E-02	0.6814E-03	0.9906E-02	0.1037E-02
0.1500E+02	0.7000E+01	0.3528E+00	0.2079E+00	0.3484E-01	0.2900E-02	0.4056E-01	0.3687E-02
0.1500E+02	0.1000E+02	0.3362E+00	0.2709E+00	0.7097E-01	0.8479E-02	0.9316E-01	0.9519E-02
0.1500E+02	0.1300E+02	0.5656E+00	0.5004E+00	0.1200E+00	0.1744E-01	0.1485E+00	0.2623E-01
0.1800E+02	0.4000E+01	0.1353E+00	0.2193E+00	0.4849E-02	0.4595E-03	0.5723E-02	0.5646E-03
0.1800E+02	0.7000E+01	0.3770E+00	0.2564E+00	0.2195E-01	0.2334E-02	0.2369E-01	0.2369E-02

$x-\nu$ GRID E89 DATA ONLY

Q^2	W^2	R	dR	νW_2	$d\nu W_2$	$2MW_1$	$d2MW_1$
0.8042E+01	0.4097E+01	0.2044E+00	0.1541E+00	0.4262E-01	0.2242E-02	0.6061E-01	0.5684E-02
0.7264E+01	0.4875E+01	0.2767E+00	0.1466E+00	0.7344E-01	0.3651E-02	0.1071E+00	0.8693E-02
0.6434E+01	0.5705E+01	0.3373E+00	0.1920E+00	0.1179E+00	0.8742E-02	0.1819E+00	0.1617E-01
0.5630E+01	0.6510E+01	0.3591E+00	0.2002E+00	0.1692E+00	0.1315E-01	0.2880E+00	0.2567E-01
0.2815E+01	0.9324E+01	0.1539E+00	0.2642E+00	0.3394E+00	0.1682E-01	0.1269E+01	0.2278E+00
0.1083E+02	0.4128E+01	0.2232E+00	0.1599E+00	0.2250E-01	0.1198E-02	0.2852E-01	0.2719E-02
0.1005E+02	0.4901E+01	0.1281E+00	0.1481E+00	0.3766E-01	0.2039E-02	0.5509E-01	0.5177E-02
0.9080E+01	0.5874E+01	0.2089E+00	0.1389E+00	0.6681E-01	0.3544E-02	0.9948E-01	0.7723E-02
0.8042E+01	0.6912E+01	0.3099E+00	0.1576E+00	0.1098E+00	0.5870E-02	0.1676E+00	0.1384E-01
0.7037E+01	0.7917E+01	0.2295E+00	0.1512E+00	0.1588E+00	0.9030E-02	0.2906E+00	0.2364E-01
0.5630E+01	0.9324E+01	0.3935E+00	0.2519E+00	0.2502E+00	0.1677E-01	0.4938E+00	0.6274E-01
0.1299E+02	0.4777E+01	0.1564E+00	0.1695E+00	0.1998E-01	0.1150E-02	0.2607E-01	0.2759E-02
0.1206E+02	0.5705E+01	0.2472E+00	0.1566E+00	0.3529E-01	0.1921E-02	0.4551E-01	0.3961E-02
0.1090E+02	0.6873E+01	0.2766E+00	0.1583E+00	0.6330E-01	0.3506E-02	0.8719E-01	0.7349E-02
0.9651E+01	0.8118E+01	0.3417E+00	0.1680E+00	0.1063E+00	0.6000E-02	0.1552E+00	0.1307E-01
0.8444E+01	0.9324E+01	0.2095E+00	0.2240E+00	0.1535E+00	0.1096E-01	0.2803E+00	0.3556E-01
0.6756E+01	0.1101E+02	0.4989E+00	0.3010E+00	0.2525E+00	0.1861E-01	0.4563E+00	0.6370E-01
0.1516E+02	0.5427E+01	0.2643E+00	0.2063E+00	0.1905E-01	0.1313E-02	0.2228E-01	0.2121E-02
0.1407E+02	0.6510E+01	0.2933E+00	0.1992E+00	0.3415E-01	0.2796E-02	0.4169E-01	0.3865E-02
0.1271E+02	0.7872E+01	0.2926E+00	0.1953E+00	0.6112E-01	0.5135E-02	0.8174E-01	0.7068E-02
0.1126E+02	0.9324E+01	0.3178E+00	0.1765E+00	0.1025E+00	0.6226E-02	0.1500E+00	0.1323E-01
0.9852E+01	0.1073E+02	0.2889E+00	0.2626E+00	0.1527E+00	0.1186E-01	0.2580E+00	0.3570E-01
0.7881E+01	0.1270E+02	0.5853E+00	0.3541E+00	0.2544E+00	0.2078E-01	0.4299E+00	0.6593E-01
0.1287E+02	0.1053E+02	0.2883E+00	0.2269E+00	0.1004E+00	0.9650E-02	0.1486E+00	0.1478E-01
0.1126E+02	0.1214E+02	0.4461E+00	0.3811E+00	0.1588E+00	0.1650E-01	0.2367E+00	0.3818E-01
0.9007E+01	0.1439E+02	0.6874E+00	0.4308E+00	0.2594E+00	0.2384E-01	0.4084E+00	0.7106E-01
0.1013E+02	0.1608E+02	0.1163E+01	0.7820E+00	0.2950E+00	0.3660E-01	0.3600E+00	0.8769E-01

Q^2-W^2 GRID COMBINED DATA SET

Q^2	W^2	R	dR	νW_2	$d\nu W_2$	$2MW_1$	$d2MW_1$
0.3000E+01	0.4000E+01	0.1750E+00	0.1482E+00	0.1829E+00	0.5679E-02	0.4070E+00	0.4191E-01
0.3000E+01	0.7000E+01	0.1947E+00	0.1104E+00	0.2905E+00	0.9540E-02	0.8132E+00	0.5668E-01
0.3000E+01	0.1000E+02	0.3196E+00	0.2264E+00	0.3412E+00	0.2416E-01	0.1120E+01	0.1218E+00
0.3000E+01	0.1300E+02	0.1742E+00	0.2179E+00	0.3533E+00	0.3188E-01	0.1587E+01	0.1647E+00
0.6000E+01	0.4000E+01	0.1574E+00	0.1775E+00	0.6923E-01	0.3077E-02	0.1140E+00	0.1321E-01
0.6000E+01	0.7000E+01	0.1529E+00	0.1059E+00	0.1591E+00	0.6473E-02	0.3189E+00	0.1882E-01
0.6000E+01	0.1000E+02	0.1752E+00	0.1202E+00	0.2343E+00	0.1113E-01	0.5488E+00	0.3408E-01
0.9000E+01	0.4000E+01	0.2223E+00	0.1413E+00	0.3154E-01	0.1354E-02	0.4225E-01	0.3407E-02
0.9000E+01	0.7000E+01	0.2113E+00	0.1160E+00	0.9032E-01	0.3633E-02	0.1426E+00	0.8906E-02
0.9000E+01	0.1000E+02	0.2058E+00	0.1372E+00	0.1515E+00	0.7782E-02	0.2773E+00	0.1896E-01
0.9000E+01	0.1300E+02	0.4506E+00	0.1924E+00	0.2225E+00	0.1453E-01	0.3855E+00	0.2849E-01
0.1200E+02	0.4000E+01	0.2752E+00	0.1668E+00	0.1617E-01	0.7240E-03	0.1893E-01	0.1790E-02
0.1200E+02	0.7000E+01	0.2025E+00	0.1273E+00	0.5257E-01	0.2468E-02	0.7451E-01	0.4912E-02
0.1200E+02	0.1000E+02	0.1540E+00	0.1591E+00	0.9698E-01	0.7389E-02	0.1619E+00	0.1114E-01
0.1200E+02	0.1300E+02	0.4168E+00	0.3203E+00	0.1553E+00	0.1649E-01	0.2362E+00	0.2983E-01
0.1200E+02	0.1600E+02	0.8781E+00	0.6461E+00	0.2422E+00	0.4119E-01	0.3082E+00	0.5550E-01
0.1500E+02	0.4000E+01	0.1928E+00	0.1968E+00	0.8536E-02	0.5894E-03	0.1004E-01	0.1077E-02
0.1500E+02	0.7000E+01	0.2390E+00	0.1620E+00	0.3295E-01	0.2164E-02	0.4188E-01	0.3047E-02
0.1500E+02	0.1000E+02	0.2824E+00	0.2245E+00	0.6871E-01	0.6130E-02	0.9398E-01	0.8834E-02
0.1500E+02	0.1300E+02	0.5656E+00	0.5004E+00	0.1200E+00	0.1744E-01	0.1485E+00	0.2623E-01
0.1800E+02	0.4000E+01	0.1580E+00	0.1925E+00	0.4996E-02	0.3763E-03	0.5781E-02	0.5911E-03
0.1800E+02	0.7000E+01	0.3688E+00	0.2495E+00	0.2179E-01	0.2038E-02	0.2366E-01	0.2356E-02

$x-\nu$ GRID COMBINED DATA SET

Q^2	W^2	R	dR	νW_2	$d\nu W_2$	$2MW_1$	$d2MW_1$
0.2252E+01	0.4258E+01	0.2640E+00	0.2391E+00	0.2523E+00	0.8673E-02	0.6239E+00	0.1018E+00
0.4825E+01	0.4499E+01	0.2644E+00	0.1927E+00	0.1212E+00	0.5165E-02	0.2078E+00	0.2419E-01
0.4222E+01	0.5102E+01	0.2161E+00	0.1816E+00	0.1695E+00	0.8192E-02	0.3368E+00	0.3638E-01
0.3378E+01	0.5947E+01	0.2015E+00	0.1697E+00	0.2392E+00	0.1212E-01	0.5808E+00	0.5673E-01
0.2815E+01	0.6510E+01	0.2489E+00	0.1229E+00	0.2688E+00	0.9340E-02	0.7902E+00	0.5881E-01
0.2111E+01	0.7213E+01	0.2964E+00	0.1612E+00	0.3391E+00	0.1223E-01	0.1155E+01	0.1122E+00
0.8042E+01	0.4097E+01	0.1696E+00	0.1250E+00	0.4126E-01	0.1617E-02	0.6042E-01	0.4560E-02
0.7264E+01	0.4875E+01	0.2444E+00	0.1123E+00	0.7150E-01	0.2349E-02	0.1070E+00	0.6969E-02
0.6434E+01	0.5705E+01	0.2185E+00	0.1154E+00	0.1121E+00	0.4249E-02	0.1897E+00	0.1229E-01
0.5630E+01	0.6510E+01	0.2123E+00	0.1130E+00	0.1599E+00	0.6230E-02	0.3050E+00	0.1897E-01
0.4504E+01	0.7636E+01	0.2094E+00	0.1564E+00	0.2389E+00	0.1275E-01	0.5556E+00	0.4620E-01
0.3753E+01	0.8386E+01	0.1475E+00	0.1416E+00	0.2841E+00	0.1586E-01	0.8203E+00	0.6144E-01
0.2815E+01	0.9324E+01	0.3113E+00	0.1443E+00	0.3366E+00	0.1240E-01	0.1107E+01	0.9116E-01
0.1083E+02	0.4128E+01	0.2443E+00	0.1531E+00	0.2227E-01	0.9663E-03	0.2775E-01	0.2457E-02
0.1005E+02	0.4901E+01	0.1795E+00	0.1263E+00	0.3745E-01	0.1485E-02	0.5239E-01	0.3903E-02
0.9080E+01	0.5874E+01	0.2380E+00	0.1207E+00	0.6645E-01	0.2566E-02	0.9663E-01	0.6382E-02
0.8042E+01	0.6912E+01	0.2230E+00	0.1192E+00	0.1067E+00	0.4287E-02	0.1745E+00	0.1122E-01
0.7037E+01	0.7917E+01	0.1594E+00	0.1144E+00	0.1533E+00	0.6864E-02	0.2975E+00	0.1818E-01
0.5630E+01	0.9324E+01	0.1774E+00	0.1196E+00	0.2335E+00	0.1085E-01	0.5455E+00	0.3403E-01
0.4691E+01	0.1026E+02	0.7620E-01	0.1439E+00	0.2723E+00	0.1739E-01	0.8228E+00	0.6370E-01
0.3519E+01	0.1144E+02	0.2431E+00	0.2061E+00	0.3356E+00	0.2518E-01	0.1147E+01	0.1131E+00
0.2346E+01	0.1261E+02	0.3441E+00	0.2344E+00	0.3623E+00	0.1702E-01	0.1685E+01	0.2343E+00
0.1299E+02	0.4777E+01	0.2538E+00	0.1572E+00	0.2000E-01	0.9367E-03	0.2406E-01	0.2064E-02
0.1206E+02	0.5705E+01	0.2536E+00	0.1353E+00	0.3488E-01	0.1549E-02	0.4476E-01	0.3160E-02
0.1090E+02	0.6873E+01	0.2479E+00	0.1226E+00	0.6251E-01	0.2563E-02	0.8808E-01	0.5634E-02
0.9651E+01	0.8118E+01	0.2064E+00	0.1178E+00	0.1018E+00	0.4535E-02	0.1653E+00	0.9962E-02
0.8444E+01	0.9324E+01	0.1334E+00	0.1301E+00	0.1482E+00	0.7813E-02	0.2888E+00	0.1979E-01
0.6756E+01	0.1101E+02	0.2191E+00	0.1411E+00	0.2324E+00	0.1297E-01	0.5164E+00	0.3427E-01
0.5630E+01	0.1214E+02	0.2600E+00	0.1987E+00	0.2863E+00	0.1840E-01	0.7291E+00	0.7300E-01
0.4222E+01	0.1355E+02	0.2212E+00	0.1822E+00	0.3380E+00	0.2392E-01	0.1165E+01	0.9920E-01
0.1516E+02	0.5427E+01	0.1944E+00	0.1730E+00	0.1779E-01	0.1196E-02	0.2203E-01	0.1896E-02
0.1407E+02	0.6510E+01	0.1799E+00	0.1555E+00	0.3197E-01	0.2094E-02	0.4277E-01	0.3168E-02
0.1271E+02	0.7872E+01	0.2214E+00	0.1567E+00	0.5900E-01	0.3888E-02	0.8351E-01	0.5836E-02
0.1126E+02	0.9324E+01	0.2063E+00	0.1357E+00	0.9889E-01	0.5524E-02	0.1581E+00	0.1010E-01
0.9852E+01	0.1073E+02	0.3104E+00	0.1733E+00	0.1530E+00	0.9486E-02	0.2544E+00	0.1958E-01
0.7881E+01	0.1270E+02	0.3086E+00	0.1582E+00	0.2358E+00	0.1393E-01	0.4827E+00	0.3290E-01
0.4926E+01	0.1566E+02	0.2021E+00	0.1812E+00	0.3358E+00	0.2543E-01	0.1167E+01	0.9555E-01
0.1732E+02	0.6077E+01	0.1884E+00	0.2210E+00	0.1628E-01	0.1517E-02	0.1995E-01	0.2078E-02
0.1608E+02	0.7314E+01	0.3003E+00	0.2235E+00	0.3082E-01	0.2689E-02	0.3688E-01	0.3515E-02
0.1453E+02	0.8870E+01	0.4307E-01	0.1826E+00	0.5174E-01	0.5396E-02	0.8465E-01	0.6619E-02
0.1287E+02	0.1053E+02	0.1427E+00	0.1650E+00	0.9302E-01	0.7522E-02	0.1552E+00	0.1094E-01
0.1126E+02	0.1214E+02	0.4088E+00	0.2674E+00	0.1572E+00	0.1613E-01	0.2406E+00	0.2262E-01
0.9007E+01	0.1439E+02	0.5715E+00	0.3009E+00	0.2551E+00	0.2177E-01	0.4312E+00	0.4916E-01
0.1634E+02	0.9869E+01	0.1582E+00	0.2971E+00	0.5339E-01	0.8712E-02	0.7785E-01	0.8133E-02
0.1448E+02	0.1174E+02	0.1971E+00	0.3379E+00	0.9422E-01	0.1684E-01	0.1487E+00	0.1689E-01
0.1267E+02	0.1355E+02	0.2316E+00	0.3476E+00	0.1408E+00	0.2189E-01	0.2445E+00	0.3277E-01
0.1013E+02	0.1608E+02	0.8256E+00	0.5052E+00	0.2842E+00	0.3801E-01	0.4108E+00	0.6172E-01

5-78

3360359

spin ½ partons give rise to small values of R, which decrease rapidly with increasing Q^2. Early observations[6] that $R \simeq 1/5$ supported the idea that the electron is scattering from spin ½ partons and were evidence against early vector meson dominance models[7] which predicted large values for R, growing with Q^2. In response to the need for better measurements of R, two independent experimental programs were undertaken; the MIT experiment which hoped to keep systematic errors small by using only one spectrometer, and "E89" which hoped to increase the accuracy by increasing the range of available ε. More recent predictions based upon QCD[8] are somewhat smaller than the earlier measurements and also are less than the previously reported MIT[4] data ($R \simeq .14$). The disagreement is even more marked in the present experiment where R is found to be $\simeq .30 \pm .1$. The models make detailed predictions of not only the size but also the kinematic variation of R. To study possible kinematic trends, we have plotted the values of R against several common variables, Q^2, W^2, X', and ν, and present the results in Figure IV-2.

Plotted on each graph are the R values we obtain using E89 (20 and 1.6) data only and those from the combined data set, which lie somewhat lower. The error given is the minimum error for the individual measurements within a bin. R shows no noticeable trends outside its systematic errors versus either X' or Q^2. On the Q^2 graph are overplotted two theoretical predictions; one (the lower line) from an early QCD paper[8], and the second from a paper[9] which the author modified the earlier QCD results with dynamical effects, giving rise to an increase of the average $P_\perp^2$ of the struck quark with increasing Q^2. In either case, the prediction shown is for $X = .6$ which is the average X for our data. Since early parton calculations had shown $R \simeq 4P_\perp^2/Q^2$[10], it is not surprising that if $P_\perp^2$ grows with Q^2, the calculated R will be more nearly constant than if $P_\perp$ is constant or assumed to be negligible[11].

If the apparent constancy of the experimental value for R versus Q^2 is due to increasing $P_\perp$ of the struck quark, then the simple formula $R \simeq 4P_\perp^2/Q^2$ gives rise to an estimate that (at $Q^2 = 20$ GeV^2 and $R \simeq .2$) the average $P_\perp$ of the struck parton is approximately 1 GeV. This is consistent with the $P_\perp$ of the dimuon pairs[12] produced in hadron

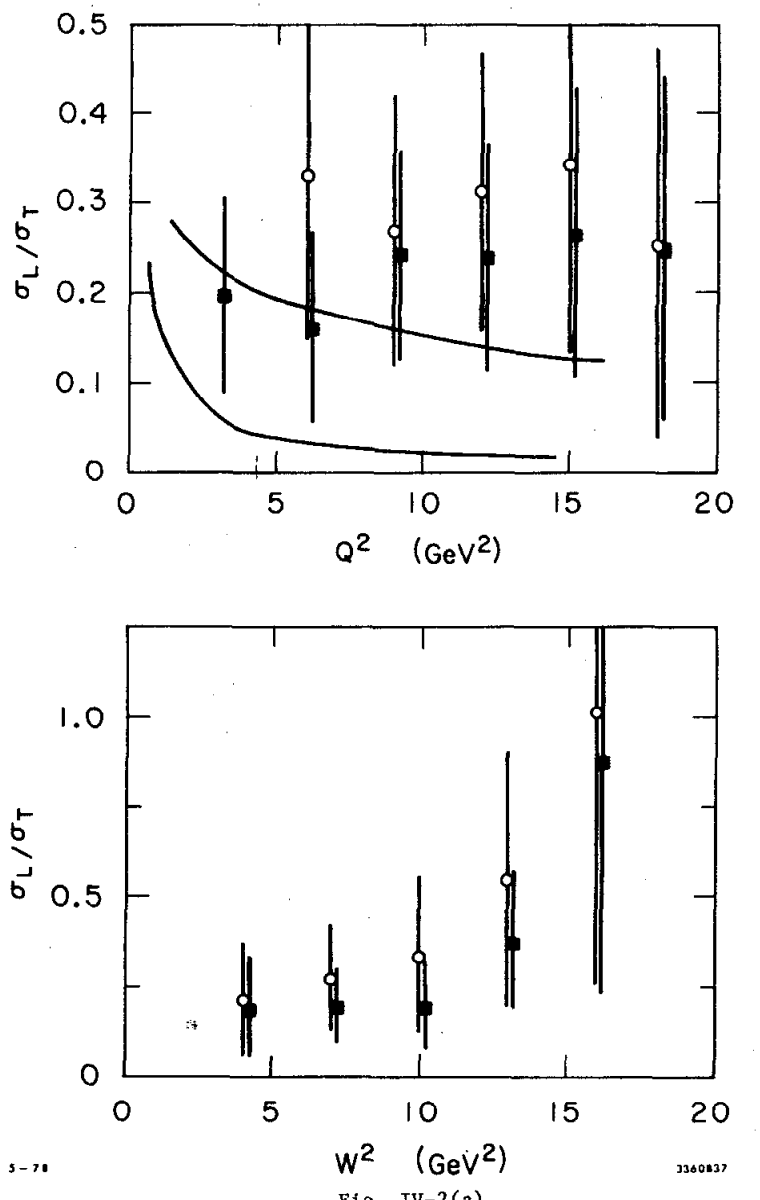

Fig. IV-2(a)

Graphs of $R(\equiv\sigma_L/\sigma_T)$ versus 4 kinematic variables: Q^2, W^2, ν, and X'. The open circles are obtained using data from this experiment only (i.e., the blue and green points in Fig. IV-1). The dark squares are from the combined data set. The errors shown for any particular bin are equal to the smallest systematic error of any individual point which contributes to that bin. The lines shown on the graph of R versus Q^2 are from two recent QCD calculations[8,9].

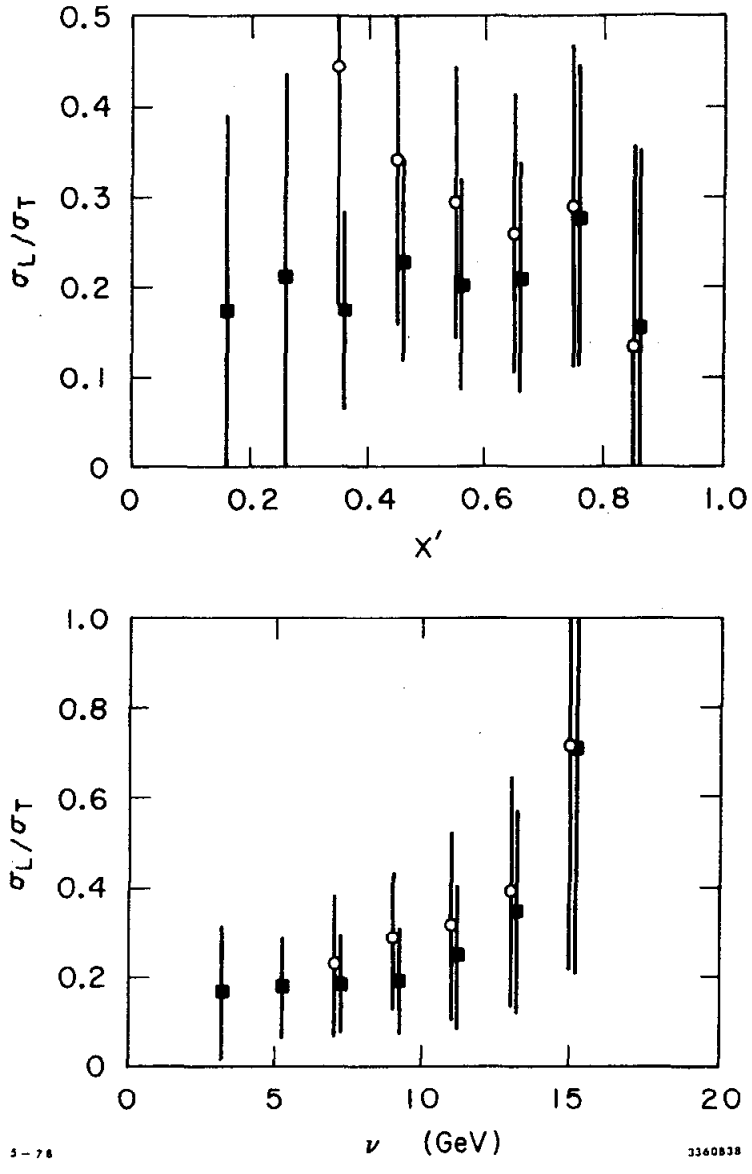

Fig. IV-2(b)

collisions at Fermilab. Both processes may arise from a common dynamical origin; at any rate, the value of R may reflect dynamics as well as the spin structure of the proton.

Turning our attention now to the graphs of R versus W^2 and ν, we see some evidence that the data may be rising with increasing W or ν. We have taken a conservative viewpoint regarding systematic errors and have not combined errors within a bin but have plotted the smallest error on the individual points contributing to a bin. To study this rise more closely, consider the $W^2 = 16$, $Q^2 = 10$ sub-graph in Figure IV-1. In order to reduce R to .2, the 1.6 GeV (50^o) data (green) would have to rise by 20%. If it rises by a full systematic error (14%), the value of R only decreases to .4. It is our feeling that a 20% error in the data is improbable, and therefore the rise may be siginificant. The effect is most pronounced near the edge of our kinematical acceptance, which urges caution in the interpretation, but further measurements in this region are warranted.

Our conclusions on the experimental value for σ_L/σ_T are the following. 1) R is not consistent with zero; our best estimate for the average value of R is $R = .21 \pm .1$. These results are somewhat higher than theory, although higher-order corrections to the theory have recently reduced the disagreement. 2) There is no evidence for a fall-off of R with Q^2 or X', and there is some evidence for a rise with ν or W^2.

$2mW_1$ and νW_2

The results of the fits to the interpolated cross sections in Figure IV-1 can be used to determine νW_2 and $2MW_1$, instead of σ_L and σ_T. Approximate scaling for νW_2 and $2MW_1$ is expected in parton models and was first observed some years ago [13]. Today, studies of scaling behavior have been refined to the study of small violations of scaling which have been seen in electron and muon data [14]. To understand the recent interpretations of scaling behavior, it may be helpful to review the basic assumptions of the naive parton models and discuss what modifications to these assumptions are made in more recent theories.

Scaling in parton models is a consequence of electrons scattering quasi-elastically from single partons. The assumptions inherent in this simple view are the following:

1) The electron scatters incoherently from a single parton. This will not be true at low $Q^2 (\lesssim 2\ GeV^2)$ where the "turn-off" of scaling can be interpreted as a decrease in the probability for incoherent scattering relative to elastic (i.e., coherent) scattering. The incoherent scattering approximation ("impulse" approximation) is assumed to be valid at higher values of Q^2. (However, Blankenbecler [15] points out that taking into account scattering from di-quark states, which are neglected in the impulse approximation, can yield the right magnitude of scaling violation seen at SLAC.)

2) Choice of scaling variable. The assumption thet the parton has fraction X of the proton's momentum implies a definition of X, the scaling variable. Our experiments are not in the asymptotic region ($Q^2, \nu \to \infty$) where masses and binding energies are negligible compared to Q^2 and ν. Studying deviations of the experimental scaling variable from the asymptotic form may give information about binding energies and masses of the quarks. However, the amount of scaling deviation observed is linked to the choice of variable. In principle, it is always possible to eliminate scaling violations by arbitrarily choosing as a definition of

scaling variable the contours in the Q^2, W^2 plane of constant νW_2 or $2MW_1$. The important point here is that the size of the scaling violations is dependent on the choice of scaling variable.

3) Partons have no structure. The structure functions νW_2 and $2MW_1$ should depend only on the probability of a parton having a fraction X of the proton's momentum; this probability is assumed in the simple model to be independent of Q^2.

While these assumptions gave good qualitative agreement with early measurements of scaling, they are not in quantitative agreement with present measurements, nor do they take into account known theoretical corrections. Quantum Chromo Dynamics has attempted a much more sophisticated approach to a physically similar model and a large literature exists on the subject. In QCD, one can calculate the Q^2 dependence of the structure functions which arise from "radiation-like" diagrams in which the struck parton can radiate some of its energy by emitting gluons. This Q^2 dependence should manifest itself as a fall-off of the structure functions with $\ln(Q^2)$ at large values of X (>.3) and a rise at small values (<.2) of X.

To investigate these possible effects, we present the νW_2 and $2MW_1$ data in such a way that small scaling deviations are evident. To see small deviations, it is useful to study νW_2 and $2MW_1$ at fixed values of the scaling variable. To do this, we set up a different grid for interpolation in the Q^2,W^2 plane.

Grid points were located at intersections of constant ν contours with constant scaling variable contours. Because a detailed testing of scaling must include a study of the effects of choice of scaling variable, we chose 3 separate grids: an X-ν, X'-ν, and ξ-ν grid, where X is the Bjorken scaling variable $Q^2/2M\nu$, X' is the Bloom-Gilman variable $Q^2/(2M\nu + M^2)$ and ξ is, due to Nachtmann, $Q^2/M(\nu + \sqrt{\nu^2 + Q^2})$. Table IV-1 tabulates the structure function values for the X - ν grid. One way to display the results is shown in Figure IV-3. In these graphs, νW_2 (or $2MW_1$) is plotted against Q^2. Data points which lie along the roughly constant lines are from constant values of X (or X' or ξ), and the values of the scaling variable for a particular line are indicated. "Scaling" in a variable gives values of νW_2 or $2mW_1$, which do not change with Q^2, so that data points in the graphs should lie on horizontal lines for perfect scaling. The data tend to decrease with increasing Q^2 for the X-ν grid; less so for

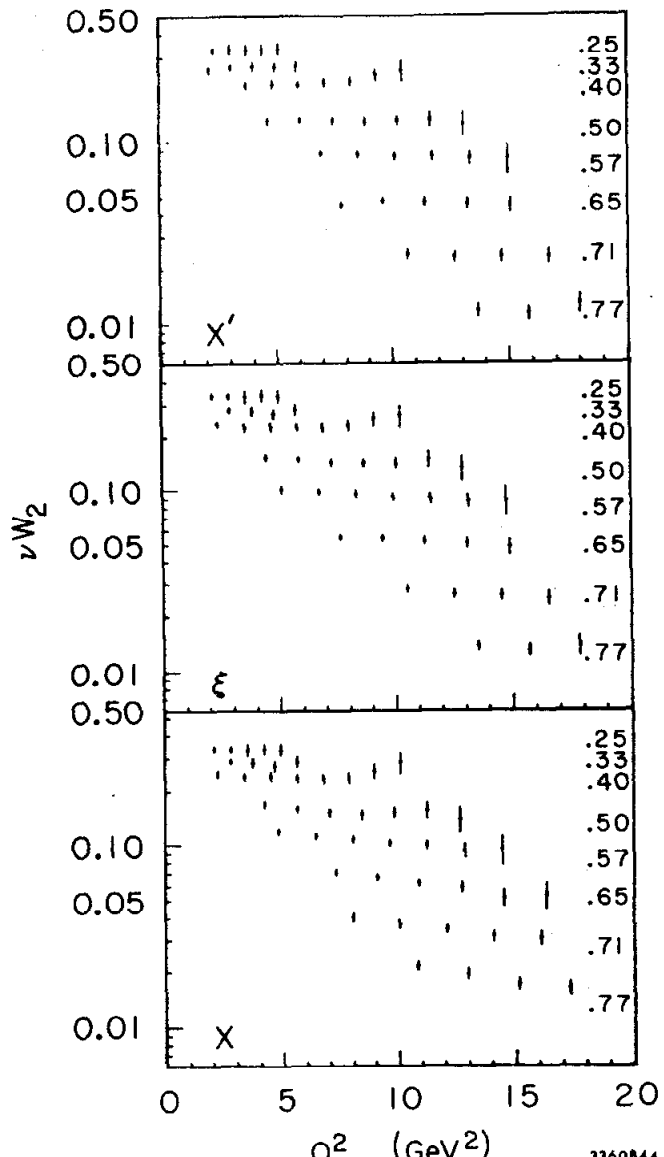

Fig. IV-3(a)

Plots of νW_2 and $2mW_1$ versus Q^2. The groupings of data points at (approximately) constant values of the structure function consist of points all at a constant value of scaling variable; the value is indicated by the column of numbers on the righthand side. The 3 sub-graphs correspond to 3 choices of scaling variable: X′, ξ, and X. Scaling violations manifest themselves as slopes of lines through the points at a constant value of the scaling variable.

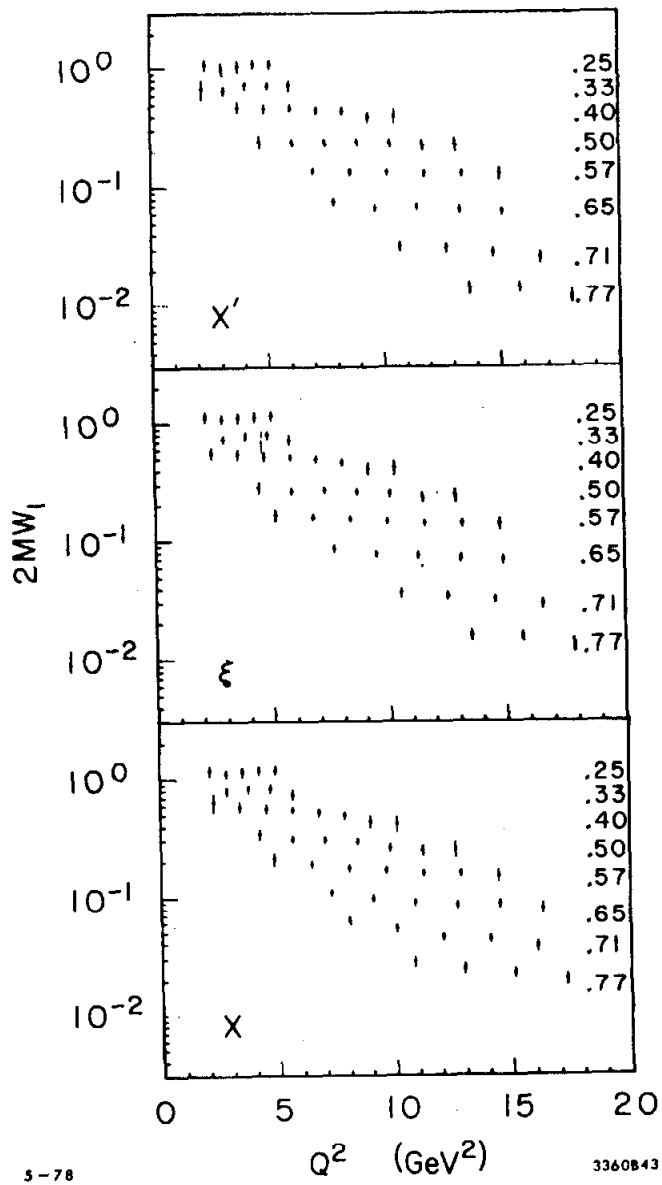

Fig. IV-3(b)

the $X' - \nu$ and $\xi - \nu$. Note, also, that the slope seems smaller at low values of X (X',ξ). The two highest Q^2 points for X = .4 show peculiar behavior; on the νW_2 plots they seem anomalously high and on the $2MW_1$ plots, low. This coincides with the observation of large values of σ_L/σ_T in this region and could be due to systematic errors in this region of the Q^2, W^2 plane. (To bring these high Q^2 points into line with the lower Q^2 points at X = .4 would necessitate moving the 50°, 60° data up by ≈8%, changing the value of R at the highest W^2 points by ≈ .27; i. e., .87 → .6.)

A parameterization of the scaling violation is presented in Figure IV-4. In Figure IV-3, each group of data points at constant scaling variable is fit to a form $a(1+bQ^2)$. In Figure IV-4, the value b (i. e., the slope with Q^2 is plotted for different values of scaling variable. The νW_2 data show little slope with Q^2 for the variable X' (i. e., the data scale well in X') but show more of a trend with ξ and still more with X. The $2MW_1$ data are not consistent with scaling in any of the three variables. For the variables X, both $2MW_1$ and νW_2 show a pattern of increasing fall-off with Q^2 at larger values of X. The fall-off (for constant X) of W_1 and νW_2 at large values of X (≈.7) is characterized by a slope $b \approx .03/GeV^2$.

These results can be compared with a summary of MIT and SLAC (E89-1.6 GeV spectrometer) data presented in 1975[16]. At that time, the νW_2 results presented were from MIT-SLAC (SFG) separated data (i. e, the red and black points) while the $2mW_1$ results were obtained from the 50° and 60° data (green points) assuming R = .18. As in the present analysis, νW_2 and $2mW_1$ were fit to functions of the scaling variable multiplied by $1+bQ^2$ to allow for Q^2 dependence. In that analysis, for νW_2 and for the scaling variable X, the slope parameter, b, had average value $\langle b\rangle_x = -.029 \pm .001$, and for the variable X', $\langle b\rangle_{x'} = .011 \pm .001$. For $2MW_1$, the average slope parameter for the variable X' was found to be $\langle b\rangle_{x'} = -.011 \pm .001$. No average value was presented for the variable X because of the poor fits of the assumed parameterization to the data, but the average slope (as estimated for an X ≅ .6 graph of the Q^2 slope of $2MW_1$) was approximately $\langle b\rangle_x \approx -.03$.

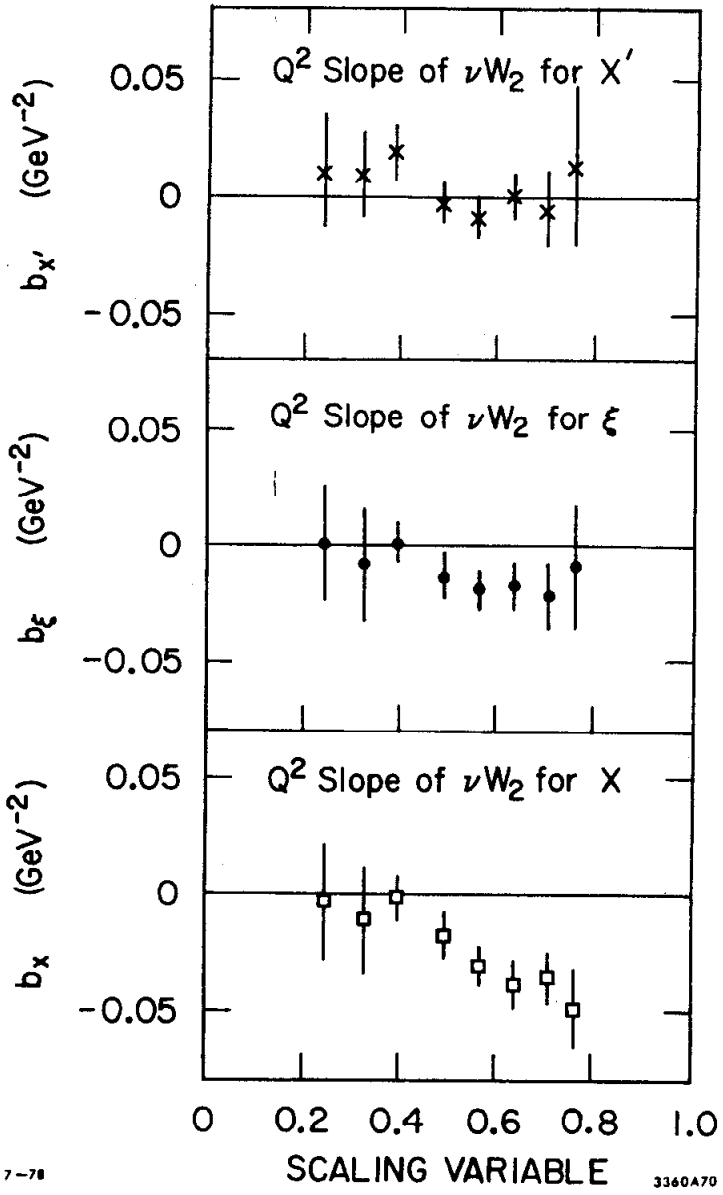

Fig. IV-4(a)

A plot of the values of slopes in Q^2 from fits to the data of Figure IV-3. A first-order fit in Q^2 is made to all points at a constant value of the indicated scaling variable. In part A of this figure, the fitted slopes in Q^2 of νW_2 are displayed versus the scaling variables; part B is a similar plot for $2mW_1$. Scaling violations show up as a non-zero value for the slopes.

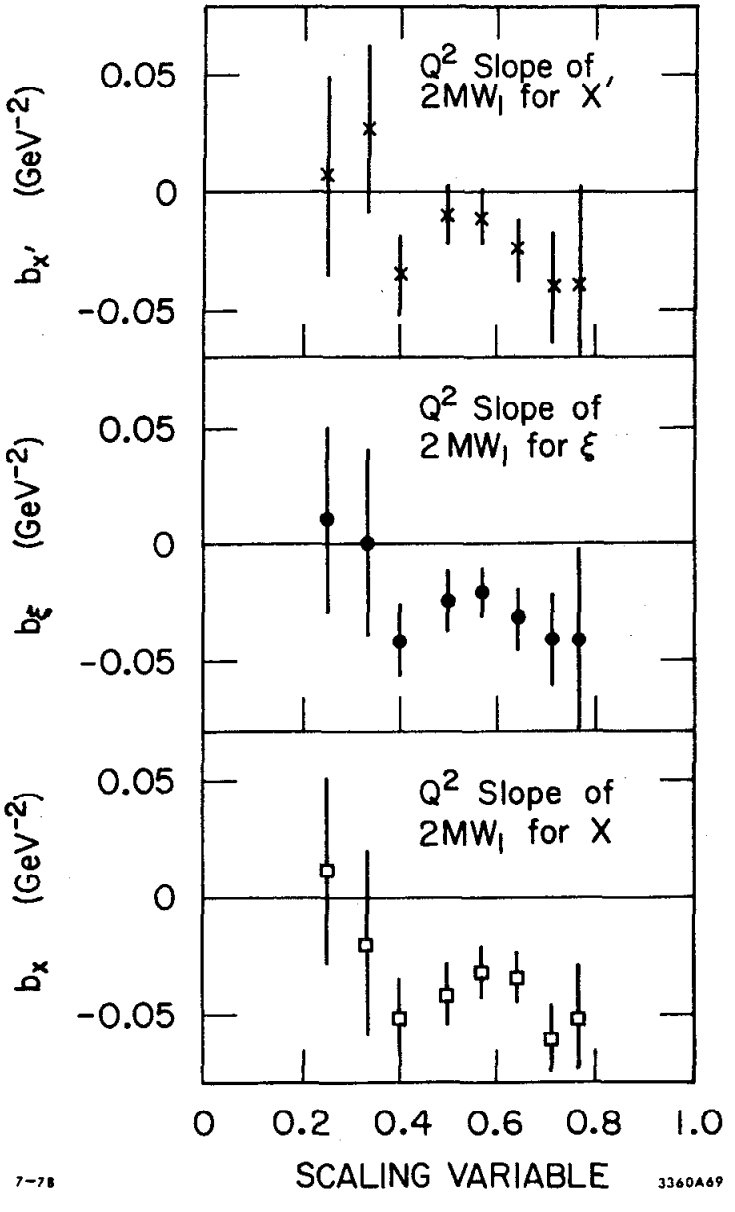

Fig. IV-4(b)

In the present analysis (using the combined data set and averaging over the data of Figure IV-4), we obtain $\langle b \rangle_X = -.021 \pm .003$, and $\langle b \rangle_{X'} = .0003 \pm .004$ for νW_2. For $2MW_1$ we obtain $\langle b \rangle_X = -.029 \pm .004$ and $\langle b \rangle_{X'} = -0.016 \pm .005$. For νW_2 our results show somewhat less dependence on Q^2 (for both X and X') than had the previously reported data. However, for $2MW_1$ our data show a steeper slope with Q^2 than the previous data. The differences may arise from the fact that the older analysis assumed a constant value for R, whereas in the combined data set, R is rising with ν. For a constant value of the scaling variable, νW_2 will fall off more slowly with Q^2 (and/or $2MW_1$ faster) if R increases with ν. If we leave out of the combined data set the points at high W where R is large (i.e., x = .4) we obtain for the combined data set $\langle b \rangle_{X'} = -.001 \pm .005$ and $\langle b \rangle_X = -.023 \pm 003$ for νW_2. Leaving out the X = .4 causes $2MW_1$ values to change in the opposite direction; for this case $\langle b \rangle_X = -.028 \pm .004$ and $\langle b \rangle_{X'} = -.014 \pm .005$. These values agree better with the previous experimental summary. Using the 1975 summary of the data, it was concluded that νW_2 did not scale in X'. This seems not so when one includes the data from this experiment. In any case, the Bloom-Gilman variable plays a smaller role in the theoretical analysis of scaling nowadays, so that the question of scaling in X' is of limited interest. (Note that the treatment of errors in the older analysis was based on statistical behavior so that the errors obtained in the fits were considerably smaller than here.)

Now that we have established that the present analysis is consistent with the previous results, we look in more detail at the pattern of scaling violation. Asymptotically free gauge theories predict increasing fall-off with Q^2 for large values of X. Recent muon scattering[14] data see νW_2 rising with Q^2 (i.e., a positive slope) at low values of X (X = .2). Our data do not extend below X = .25; however, our data do seem consistent with a steeper Q^2 dependence of the structure functions at higher values of the scaling variable, in agreement with qualitative ideas of the recent theories. This is apparent in the graphs of the slopes of νW_2 and $2MW_1$ at constant X, which decrease from ≈0 at X = .25 to ≈-.03 at X = .77.

In QCD theories, the variation of the scaling functions with Q^2 is expected to be logarithmic; i. e., $\nu W_2(X,Q^2) = \nu W_2(x) * (1 + b \ln Q^2)$.

In Figure IV-5, the derivative of $\partial F/\partial \ln Q^2$ for νW_2 and $2MW_1$ is plotted against the scaling variable for each of the 3 scaling variables. Calculations[17] based upon asymptotically free gauge theories predict that this derivative should be positive for small X ($X < .2$) and negative for large X ($X > .3$). Our data are consistent with these ideas, showing some tendency for a fall off the derivative as the scaling variable increases from .25 (especially for X), but by themselves do not offer much support to such theories.

Our conclusions regarding the scaling behavior of νW_2 and $2mW_1$ are the following:

1) νW_2 is consistent with scaling in X' but shows a fall-off with increasing Q^2 for the scaling variable ξ and a greater fall-off ($\approx 2.5\%/GeV^2$) for the variable X. $2MW_1$ is not consistent with scaling in any of the 3 variables.

2) Because of theoretical uncertainties in the choice of scaling variable, it is more important to study the general pattern of scaling violation than to focus in detail on scaling in a single choice of variable. Our observations are consistent with a steeper Q^2 fall-off at larger values of the scaling variable, as in QCD, but the data cannot be said to require such behavior. Only in combination with the rising values of νW_2 with increasing Q^2 that are observed in muon scattering is there evidence for the behavior suggested by asymptotic freedom.

ELASTIC SCATTERING RESULTS

During the course of the experiment, we measured the elastic cross section at different values of Q^2 ranging from .5 to 21 GeV^2. The beam energy, angle, and Q^2 are presented in Table IV-2 along with the radiatively corrected cross section and its statistical error and the average W value of the peak. The systematic error on these cross sections is estimated as ≈5%. Also listed is the value of the structure function G_M calculated from the cross sections assuming "form factor scaling"; i. e., $\mu_p G_E = G_M$.

In Figure IV-6, we plot this extracted G_M multiplied by $(Q^2)^2$ versus Q^2 along with the assembled world data from a plot in W. B. Atwood's thesis[2]. This curve seems to approach a constant value and is consistent with an asymptotic $1/Q^4$ behavior for G_M.

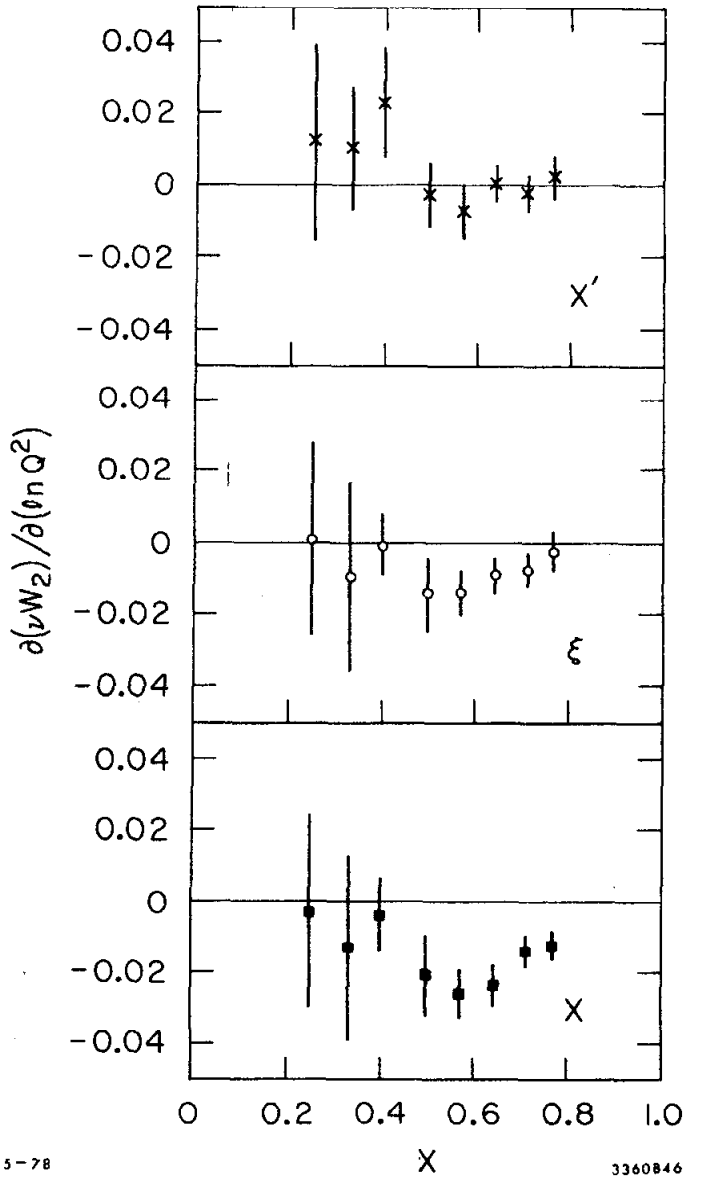

Fig. IV-5(a)

A plot of the slope of the structure function in $(\ln Q^2)$ for fixed value of the scaling variable. Plots for 3 different choices of scaling variable are shown. Part A shows the slope of νW_2; part B the slope of $2mW_1$.

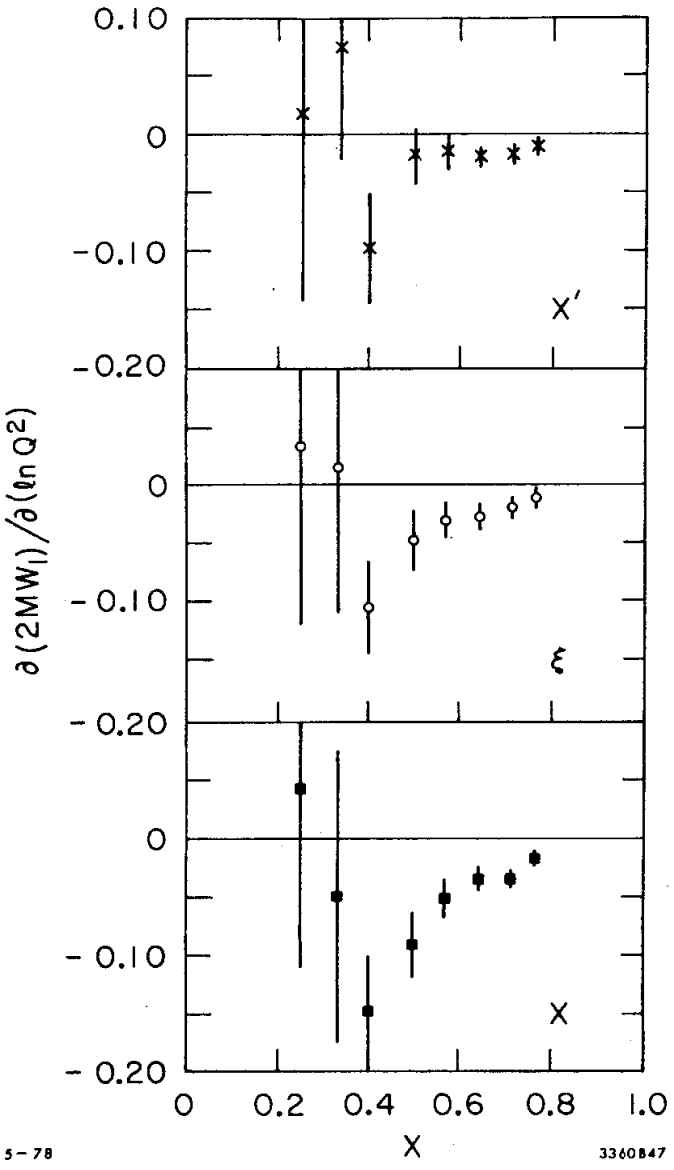

Fig. IV-5(b)

E_o	θ	Q^2	$\frac{d\sigma}{d\Omega}$	$G_M/\mu_p * Q^4$ (+)	W(GeV)
19.5	6.	3.74	$(.524\pm.007)\times10^{-32}$	.372±.0025	.9405±.0006
7.	6.	.52	$(.297\pm.0018)\times10^{-29}$	.091±.0003	.9374±.0002
16.	6.	2.57	$(.243\pm.003)\times10^{-31}$	.331±.002	.9335±.0005
13.3	15.	8.13	$(.170\pm.006)\times10^{-34}$	.418±.007	.9413±.0016
16.0	15.	11.00	$(.362\pm.036)\times10^{-35}$	.417±.021	.9301±.0051
6.5	18.	3.09	$(.917\pm.013)\times10^{-33}$	.352±.0025	.9404±.0006
10.4	18.	6.86	$(.247\pm.020)\times10^{-34}$	.416±.017	.9422±.0031
19.5	20.6	20.90	$(.414\pm.170)\times10^{-37}$	.379±.078	.9691±.0160

Q^2	$(\mu_p G_E/G_M)^2$	G_M (EXTRACTED) (ǂ) * Q^4/μ_p
2.5	2.30±1.4	.299±.03
3.0	2.33±1.6	.325±.03
4.0	2.30±2.5	.360±.04
5.0	2.29±3.4	.382±.04
10.0	.97±5.6	.418±.04

(+) This G_M calculated from the cross section assuming $G_M=\mu_p G_E$

(ǂ) This G_M is extracted using 50°, 60° cross sections with smaller angle data (6°, 15°, and 18°) from 20 GeV spectrometer

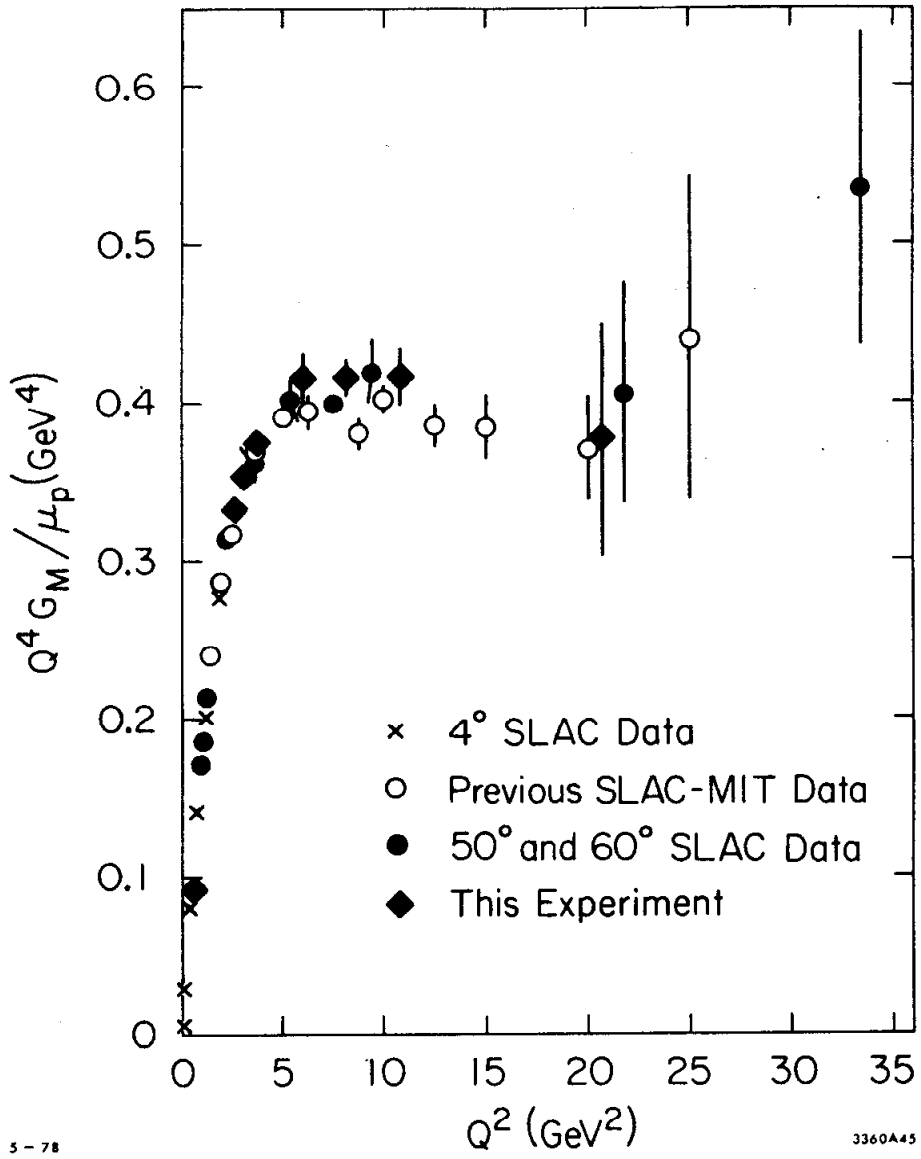

Fig. IV-6

A graph of the value of the G_M structure function from several different experiments, extracted from the measured cross section by assuming $G_E = G_M/\mu p$. The structure function, G_M, multiplied by Q^4 seems to approach a constant, indicating a $1/Q^4$ behavior at large Q^2.

In the parton model, the structure function G_E and G_M are related to the momentum distributiom of the partons which comprise the proton. In electron scattering, the virtual photon strikes a single parton, imparting 4-momentum squared, Q^2, to it. In order for the proton to remain intact, there must be subsequent momentum transfers from the struck parton to the other partons in order that their relative momentum remain small. Each momentum transfer multiplies the amplitude by a factor $1/Q^2$; so the total power of $(1/Q^2)$ in the structure function is an indication of the number of constituents. This simple picture is preserved in more sophisticated calculations. Experimentally, the structure function, G_M, approaches a $(1/Q^2)^2$ behavior, implying 3 charged partons. In Table IV-2 are also presented values for G_M extracted from large (50° and 60°) angle data and smaller angle (6°, 15°, 18°, and 20.6°) data. The error bars are systematic, arising from an estimate of a 5% systematic error in the elastic cross sections.

SUMMARY

Our results are the following:

1) It would be difficult to reconcile the data with the hypothesis that R is equal to zero in this kinematic region. Our best value for R comes from the "combined" data set and gives $R = .21 \pm .1$.

2) R may be increasing with increasing W^2 or ν.

3) νW_2 and $2MW_1$ exhibit a scale breaking whose pattern is not inconsistent with the predictions of QCD. At $X \simeq .7$ νW_2 and $2MW_1$ decrease by about 3%/GeV^2 as Q^2 increases.

4) Values of G_M extracted from elastic cross sections approach a $1/Q^4$ dependence above $Q^2 \simeq 5$ GeV^2.

CHAPTER IV - REFERENCES

1. Note that under the assumptions of Lorentz invariance, one photon exchange, and parity conservation, the cross section for unpolarized electron proton scattering can be written in its most general form as a function representing scattering from a structureless spin ½ particle multiplied by a factor which includes two (and only two) independent structure functions.
2. W. B. Atwood et al., Physics Letters 64B (1976), 479-482; "Electron Scattering off Hydrogen and Deuterium", W. B. Atwood (Ph.D. thesis), SLAC Report No. 185.
3. E49: A. Bodek (Ph.D. thesis), M.I.T. Laboratory for Nuclear Science, Report No. COO-3069-116 (1972).
   E. M. Riordan (Ph.D. thesis), M.I.T. Laboratory for Nuclear Science, Report No. COO-3069-176 (1973).
   A. Bodek et al., SLAC-PUB-1327.
   E87: E. M. Riordan et al., SLAC-PUB-1634.
4. E. M. Riordan et al., SLAC-PUB-1634.
5. The systematic error assigned to this experiment's cross section averaged at about 7½% and has been described in a previous section. The systematic error on the 50° and 60° data was obtained from W. B. Atwood's thesis, SLAC Report No. 185, and was parameterized as: $(5.8 + .032*W^4)\%$. A systematic error of 5.5% was assigned to the M.I.T. cross sections.
6. G. Miller (Ph.D. thesis), SLAC Report No. 129 (1971).
7. VDM: "Vector-Meson Dominance - Present Status and Future Prospects," by J. J. Sakurai, 1969 International Conference on Electron and Photon Interactions at High Energies, Daresburg, England.
8. A. DeRujula et al., Ann. Phys. 103 (1977), 315-353.
9. Kwang Je Kim, "Impulse Approximation in QCD, Parton's P_T-Distribution and Application to Deep Inelastic Process", Mainz Univ. Preprint MZ-TH 78/1, Jan. 1978.
10. R. P. Feynman, Photon Hadron Interactions, W. A. Benjamin, Inc., 1972.

11. In Ref. 7, the authors assume that P_T^2 is negligible compared to Q^2 and/or W^2.
12. D. C. Ham et al., Phys. Rev. Letters 37, 1374-1377 (1976).
    D. M. Kaplan et al., Farmilab Pub. 77-107-Exp. (Feb. 1978)
13. E. D. Bloom et al., Phys. Rev. Letters 23, 930 (1969)
    M. Breidenback et al., Phys. Rev. Letters 23, 935 (1969).
14. H. L. Anderson et al., Phys. Rev. Letters 37, 4-7 (1976).
    H. L. Anderson et al., Phys. Rev. Letters 38, 1450-1454 (1977).
15. I. A. Schmidt and R. Blankenbecler, Phys. Rev. D16, 1318-1326 (1977).
16. R. E. Taylor, "Inelastic Electron-Nucleon Scattering Experiments," invited paper published in the Conference Proceedings of the International Symposium on Lepton and Photon Interactions, Stanford University, Stanford, Cal., August 21-27, 1975.
17. Porter W. Johnson and Wu-hi Tung, Illinois Inst. of Tech., Preprint: Print-77-0382, "Precise Treatment of Operator Mixing in Application of Asymptotically Free Theories to Deep Inelastic Scattering."

APPENDIX I

SPECTROMETER ACCEPTANCE AND OPTICS COEFFICIENTS

INTRODUCTION

The optical properties of the 20 GeV spectrometer were determined in a series of experimental tests in the winter of 1967 and 1968. Subsequently, experimenters have used these results to calculate their cross sections. This experiment used a range of ϕ_o=(±8 mrads) and a projected target width X_o (±3 cm), much larger values than previous experiments, in order to get reasonable counting rates at the larger angles. For these reasons, we expected errors related to the spectrometer acceptance to be large (≳3%) compared to most errors in the experiment. So we devoted some data taking and considerable analysis to checking the optical properties of the spectrometer.

The solid angle acceptance, $d\Omega$, of the spectrometer is about 128 microsteradians (±8 mrads in vertical angle, ϕ_o, and ±4 mrads in the horizontal angle, θ_o), and the momentum acceptance, $d\delta$, is approximately ±2%. For a definition of these angle and momentum variables, see Figure II-3. In order to determine the differential cross section $d^2\sigma/d\Omega dE'$, it is necessary to count the number of scattered electrons which have momentum, δ, and angle θ_o, within the acceptance limits (-3.75 mrad < θ_o < 3.0 mrads) and ($|\delta|$ < 1.75%). It is also necessary to calculate the acceptance, $d\Omega d\delta$, for the spectrometer. For the case of the resonance region (W<2 GeV), where one calculates cross sections for individual W bins (see Figure A1-1), it is necessary to know δ and θ_o of each particle, in order to bin the event in W.

A particle's δ and θ_o are calculated from the position and angle of its track through the wire chambers, using a matrix transformation whose elements are referred to as optics coefficients. In our notation, an individual coefficient is denoted A/B where B is the measured variable in the detector and A the calculated variable. For instance,

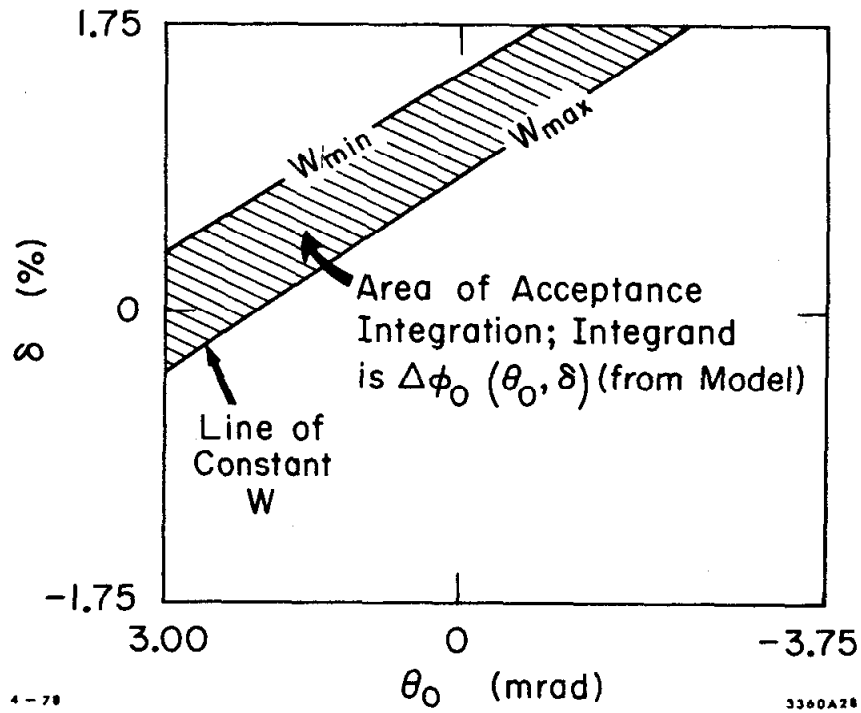

Fig. A1-1

A sketch of the position of a W bin in the δ, θ_o plane. To calculate the acceptance for a W bin, we integrate the calculated ϕ_o acceptance over the δ, θ_o range covered by the W bin.

(θ_o/X) is the coefficient of X in the expansion $\theta_o=(\theta_o/X)\cdot X + (\theta_o/Y)\cdot Y$ + ...etc. The determination of the optics coefficients is discussed in the first subsection of this Appendix.

The acceptance $(d\Omega d\delta)$ is the product of the range in θ_o, δ, and ϕ_o covered by scattered particles. For W<2 GeV, it is the product of these ranges subtended by a single W bin (again, see Figure A1-1). The ranges of acceptance for θ_o and δ are determined by limits used in the analysis program since these quantities are measured with good resolution. The ϕ_o acceptance is defined by lead-tungsten slits[1] at the entrance to the spectrometer. For the majority of data taking, the ϕ_o slits were set to ±8 mrads. For a given θ_o and δ within the software limits, not all particles which enter the spectrometer within the ϕ_o slits pass through the spectrometer because some of them strike apertures inside the spectrometer. Averaged over the whole δ and θ_o acceptance, the fraction is calculated to be less than 6% (Figure A1-2 shows the corrected acceptance/nominal acceptance versus scattering angle). To make this acceptance correction, we employ a model of the spectrometer which divides each magnetic element into several sections and "swims" the particles through each section using appropriate matrix transformations. At the end of each section, the particle's position is checked to see if it has struck an aperture. A Monte Carlo generation of many such events averaged over target position allows us to fit the ϕ_o acceptance as a function of θ_o and δ. The details of the model are presented in the second subsection of this appendix.

As a guide to the appendix, the reader may refer to Figure A1-3 which outlines the logic of the solid angle investigations. The flowchart illustrates the connections between the various data and how they were used to determine the optics coefficients and the acceptance of the spectrometer. The left side shows the inputs to the Monte Carlo model used to calculate the ϕ_o acceptance, while the right side demonstrates how the optical properties are determined. Let us first consider the information available about the optics of the spectrometer.

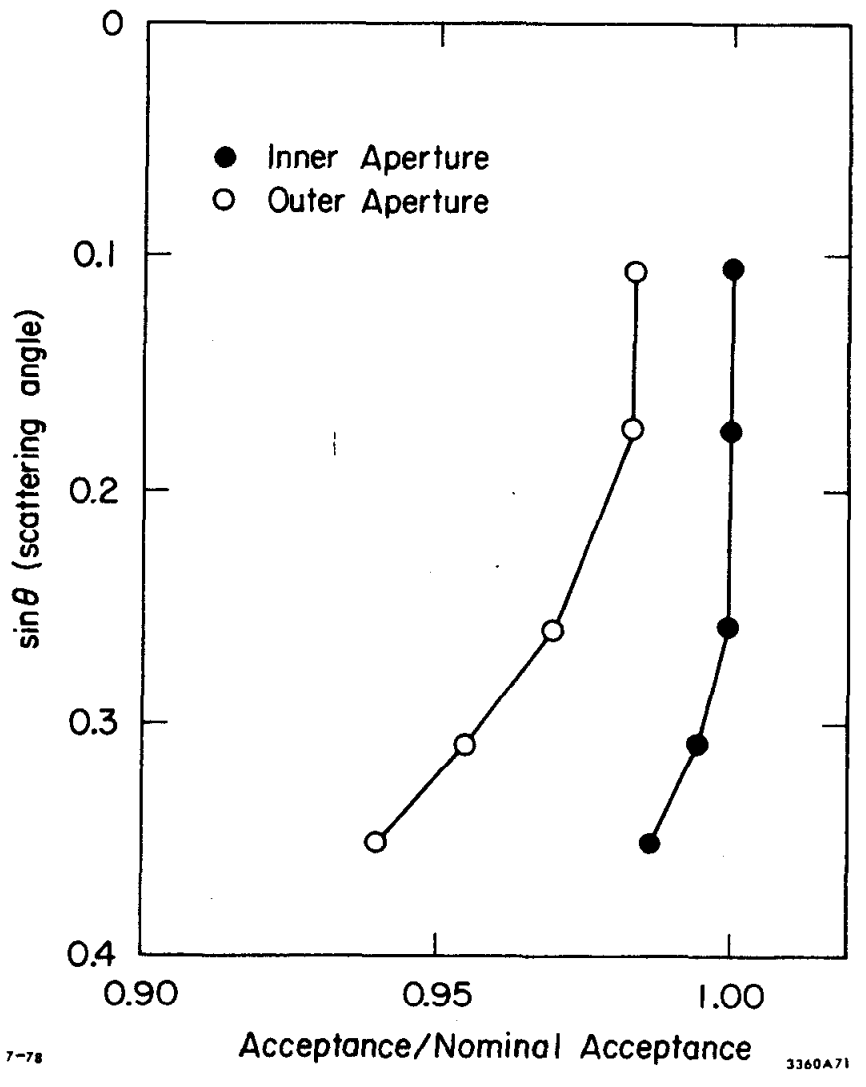

Fig. A1-2

A graph of the acceptance calculated by the model, normalized to its nominal value $(\Delta\theta_o\Delta\phi_o\Delta\delta)$, plotted versus the scattering angle. The "outer" aperture is used in the analysis; the "inner" is used for consistency checks of the spectrometer acceptance (see Figure A1-17). The maximum correction to the nominal acceptance is 6%.

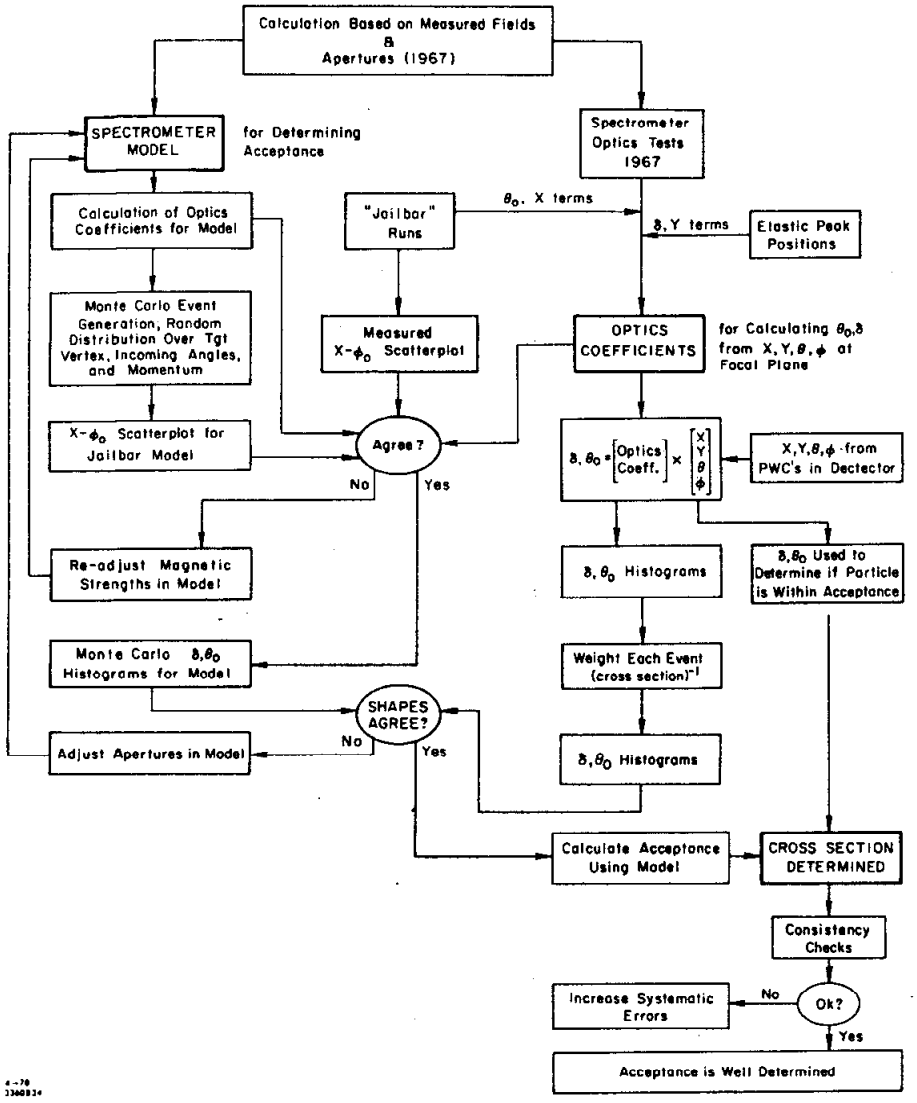

Fig. A1-3

A flowchart of the various factors which enter into the determination of the optics coefficients for the spectrometer, and the development of a magnetic model of the spectrometer used in Monte Carlo determination of the acceptance.

OPTICS COEFFICIENTS

The optics coefficients are the elements of the matrix which transform the parameters of a track as measured in the detector (X and Y positions and angles) into the parameters of the particle leaving the target (X position at target, angles θ_0 and ϕ_0 and momentum δ). See Figure II-3 for a sketch showing the various parameters.

For a spectrometer constructed of ideal magnetic elements, these coefficients can be calculated, and the design and construction of the spectrometer was based on such calculations. After construction, the field properties of each magnet were measured and the coefficients were recalculated. The calculations were succeeded by explicit measurement on the spectrometer in optics experiments of 1967 and 1968. Some measurements made during the present experiment have been used to modify these earlier results. These new measurements, "jailbar" runs and studies of the elastic peak position in the δ, θ_0 plane, both rely upon being able to define the angles or momentum of scattered particles entering the detector. The results were used to adjust the optics coefficients until the reconstructed angles or momentum agree with the known input. The final set of optics coefficients (see Table III-1) used in the analysis of the experiment were those given by the 1967 tests except for 8 coefficients whose values were explicitly measured during this experiment. We will next describe the original optics measurements and the new measurements made during this experiment.

Optics Tests (1967)

In 1967, optics measurements were conducted on the 20 GeV spectrometer. A low intensity electron beam was set up and directed into the spectrometer which was positioned along the beam line (0°). The momentum of the beam was set by the Beam Switchyard magnets and, by use of small bending magnets, the incoming (horizontal and vertical) angles and the X offset relative to the spectrometer center line could be controlled. Fluorescent screens located in the detector hut measured the final position and angle of the beam for different values of these parameters.

The optics data consisted of a set of points with 4 incoming parameters θ_0, X_0, δ, and ϕ_0, and 4 final parameters, as measured in the hut, X, Y, θ, and ϕ. Fits of the incoming parameters as functions of the hut parameters resulted in determination of the optics coefficients. Data were taken for various central momenta ranging from 4 to 17.5 GeV and for target X_0 offsets from -3 to +3 centimeters. We refit the entire data set because the kinematic range of the 1967 optics test matched the parameters in our experiment (E´ ranging from 2.5 to 17.5 GeV and an 18 cm long target at angles between 6° and 20.6° corresponding to target projected widths as large as ±3 cm). This provided the initial set of optics coefficients.

Jailbar Tests

After the fall cycle of E89 (1973) and, again, after the winter cycle (1974), a series of "jailbar" runs were taken on the 20 GeV spectrometer as a check of the optics coefficients. These runs were taken with a mask in front of the spectrometer entrance window. The mask consisted of a set of 6 vertical brass bars, 3/16" wide and approximately 5" high with 3/16" gaps between the bars. From the front they looked like jailbars, and their purpose was to define θ_0 for particles entering the spectrometer. A thin target was used to produce a point source of scattered electrons. See Figure A1-4 for a sketch of the set-up during the jailbar runs.

The idea of the jailbar analysis is simple. We produce a θ_0 distribution for the events from a jailbar run and obtain an image of the jailbars themselves, since each jailbar subtends a swath of constant θ_0 for a point target. These swaths should correspond to the θ_0-δ dis tions of the inter-jailbar spaces as determined by optical surveys. If they do not, then the optics coefficients must be adjusted until agreement is attained between surveyed jailbar positions and the clusters of events reconstructed in θ_0. To get an impression of the sensitivity of this technique, see Figure A1-5. The image of the jailbars is apparent in the X-Y scatterplot at the focal plane shown at the top of the figure.

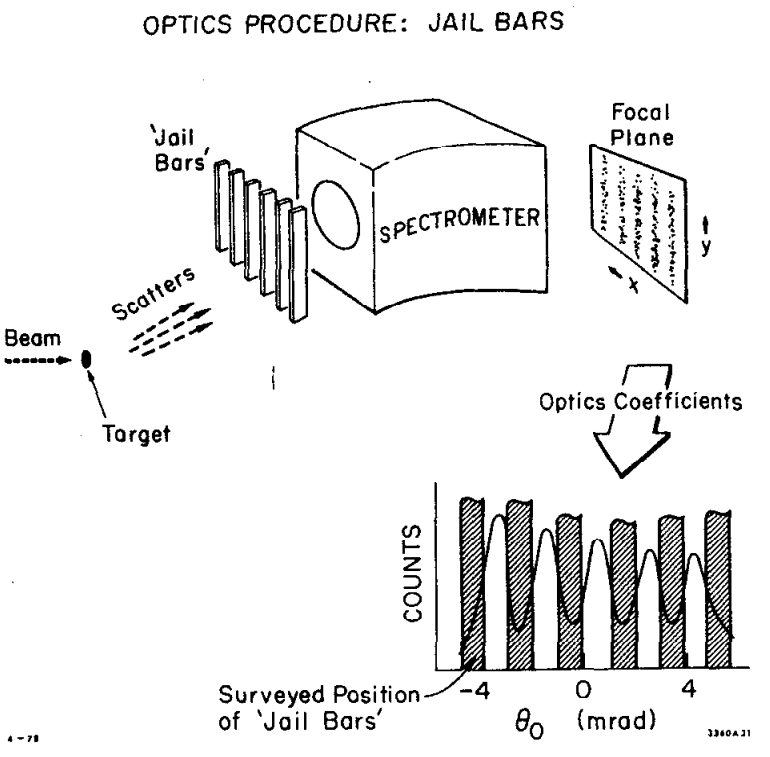

Fig. A1-4

A sketch of the "jailbar" run set-up, indicating the comparison of the reconstructed θ_0 histograms with the surveyed jailbar positions. The optics coefficients are adjusted to give agreement between the two.

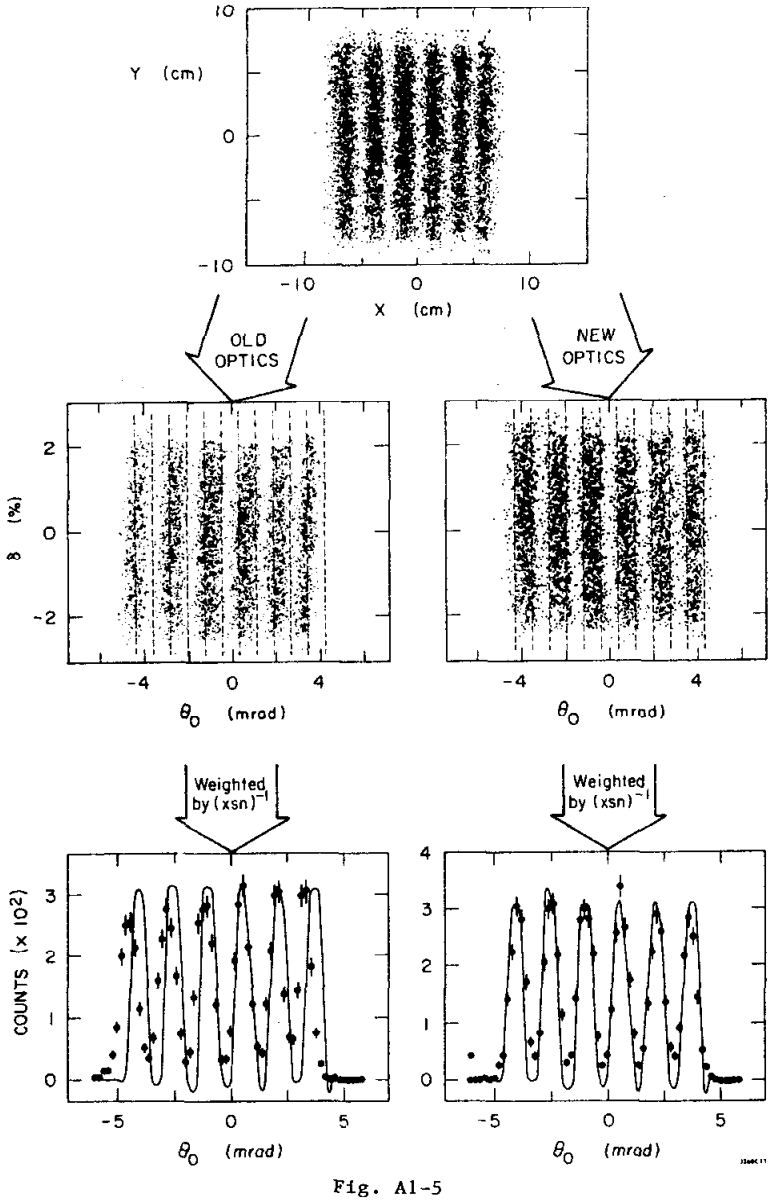

Fig. A1-5

Illustration of the difference between using the original ("old") optics coefficients and those modified during the course of this experiment ("new") when reconstructing Θ_0 distributions from jailbar runs. For comparison, the dashed lines (in the middle figures) and the solid lines (in the lower figures) are set to agree with the survey positions of the jailbars.

The jailbar data calculated using the original coefficients (labeled "old optics") shows an obvious anomaly. The data is shifted from what is expected, and the clusters of events are tilted in the δ, Θ_0 plane. Closer inspection reveals that the clusters were closer together on the left side than on the right and that the total Θ_0 separation from one edge cluster to the opposite side did not match the surveyed positions.

Shifts in the data were remedied by changing the X offset of the wire chamber zero position. The tilt was corrected by modifying the (Θ_0/Y) term, and the uneven spacing of the clusters was cured by modifying the (Θ_0/X^2) coefficient. The (Θ_0/X) term (i.e., the Θ_0 dispersion) was modifed to make the overall spacing of the clusters agree with the surveys. These changes were correlated with one another (e.g., the (Θ_0/X^2) change shifts all the clusters in the same direction, as does the X offset), and to handle these correlations a simple method was used to modify the optics coefficients.

With a given set of optics coefficients, we can analyze a jailbar run and produce a histogram of the number of events versus Θ_0. Each event is weighted by the inverse of the cross section (which varies over the acceptance) so as to weight each jailbar slot equally. The quantity we calculate is the fraction of events which have a reconstructed Θ_0 which fell into the inter-jailbar spaces as determined by the survey. This fraction is about 75%; the 25% background arising from spectrometer and wire chamber resolution, multiple scattering and scattering from the edges of the jailbars. We varied the optics coefficients and observed the change in this fraction. We choose as the most correct set of optics coefficients those producing the maximum fraction of events falling into the inter-jailbar space.

Since the fitted optics coefficients are not independent, a search for the optimum set was conducted in 4-parameter space. The parameters are X-offset, Θ_0/X, Θ_0/X^2, and Θ_0/X^3. There were jailbar runs at 5 different momenta: 4.5, 7, 10, 14, and 17.5 GeV. For each run, we determined the position in the parameter space at which the fraction of events from the inter-jailbar spaces was highest. Graphs

of the fraction of events from the inter-jailbar spaces plotted versus each of the 4 coefficients above were used to search for optimum values of the coefficients. Each graph was strongly peaked, and the value of the coefficients near the peak was insensitive to allowing the other coefficients to vary or holding them fixed at near their final values. The jailbar runs contained up to 30,000 events, so the peak positions could be determined with high accuracy. Using this method, we could determine (θ_0/X) for each run to .0025, the X offset to .25 mm, (θ_0/X^2) to .001, and θ_0/X^3 to ≈.0004. Determining (θ_0/X) to .0025 (about a nominal value of ≈.6) is about a ½% measurement, equivalent to measuring the X separation from one edge cluster to the far side (≈14 cm) to an accuracy of ≈.7 mm, which is quite consistent with the spectrometer and PWC resolution.

As a result of the jailbar measurements, we made the following adjustments in the optics coefficients. The optimal value of (θ_0/X^2) was consistent with .005 ±.001, a change from the old value of -.0025. The optimal values of (θ_0/X^3) was consistent with values between 0 and .0004; the .0004 value was chosen to match the shape of the calculated spectrometer acceptance with observation.

The optimal value for the dispersion (θ_0/X) and the X-offset change as the spectrometer momentum varies. That the dispersion changes with spectrometer energy, E′, is made clear in Figure A1-6. By careful inspection, one can see that the X histogram at 4.5 GeV is about 3% wider than the one at 17.5 GeV. Since the θ_0 distributions are unchanged, this implies a smaller value of (θ_0/X) at low E′. In Figures A1-7 and A1-8, the measured values of (θ_0/X) and of X-offset are plotted versus E′ with the results of a straight line fit shown in each case. Overplotted are values determined using only the inner 4 jailbars, done to ensure that a possible acceptance fall-off at the outer two jailbars was not giving false results. In addition to the above changes, (θ_0/Y) was changed from .03 to 0 to eliminate the tilt in the jailbar clusters in the δ, θ_0 plane evident in Figure A1-5. A summary of the above changes is listed in Table III-1.

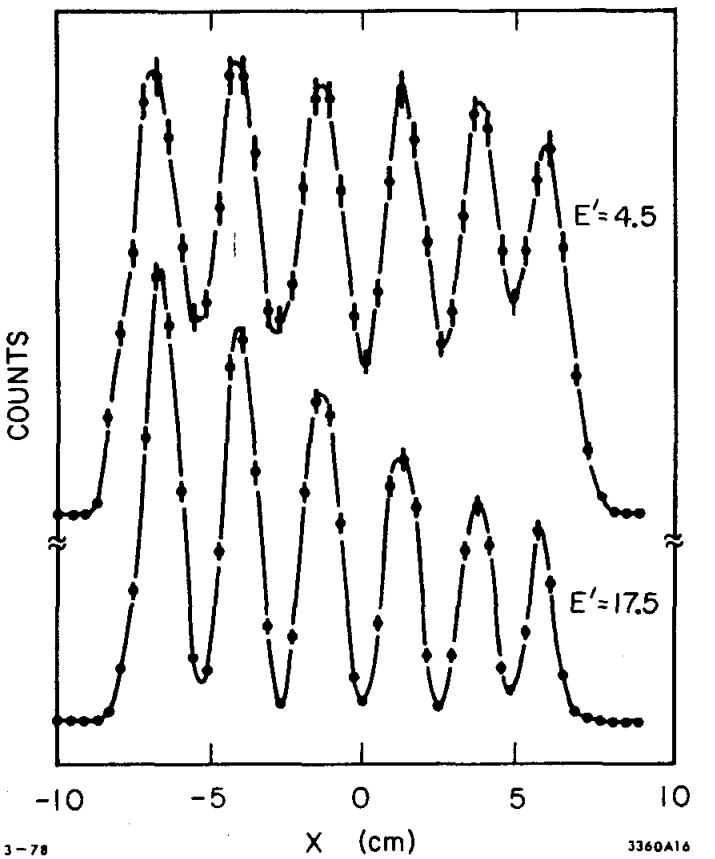

Fig. A1-6

Distributions of the X position (at the spectrometer focal plane in the detector) of events from jailbar runs at E′=4.5 and 17.5 GeV. The lower energy distribution is ≈3% wider. Since the entering θ_0's are the same for the two runs, this difference in width implies that the theta dispersion (θ_0/X) is smaller at low momentum. The line is drawn to guide the eye.

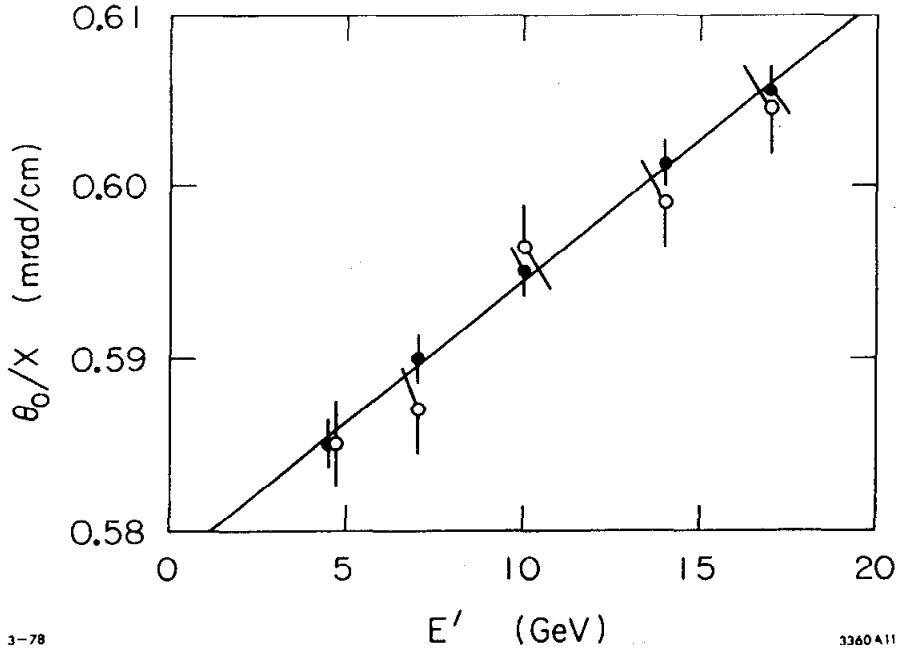

Fig. A1-7

A graph of the theta dispersion as measured by the jailbar runs at several different values of spectrometer momentum, plotted versus the momentum. The line is a fit to the closed circles. The open circles are from a similar measurement using only the inner 4 jailbars to insure that a possible fall-off in acceptance near the outer two jailbars was not invalidating the measurement.

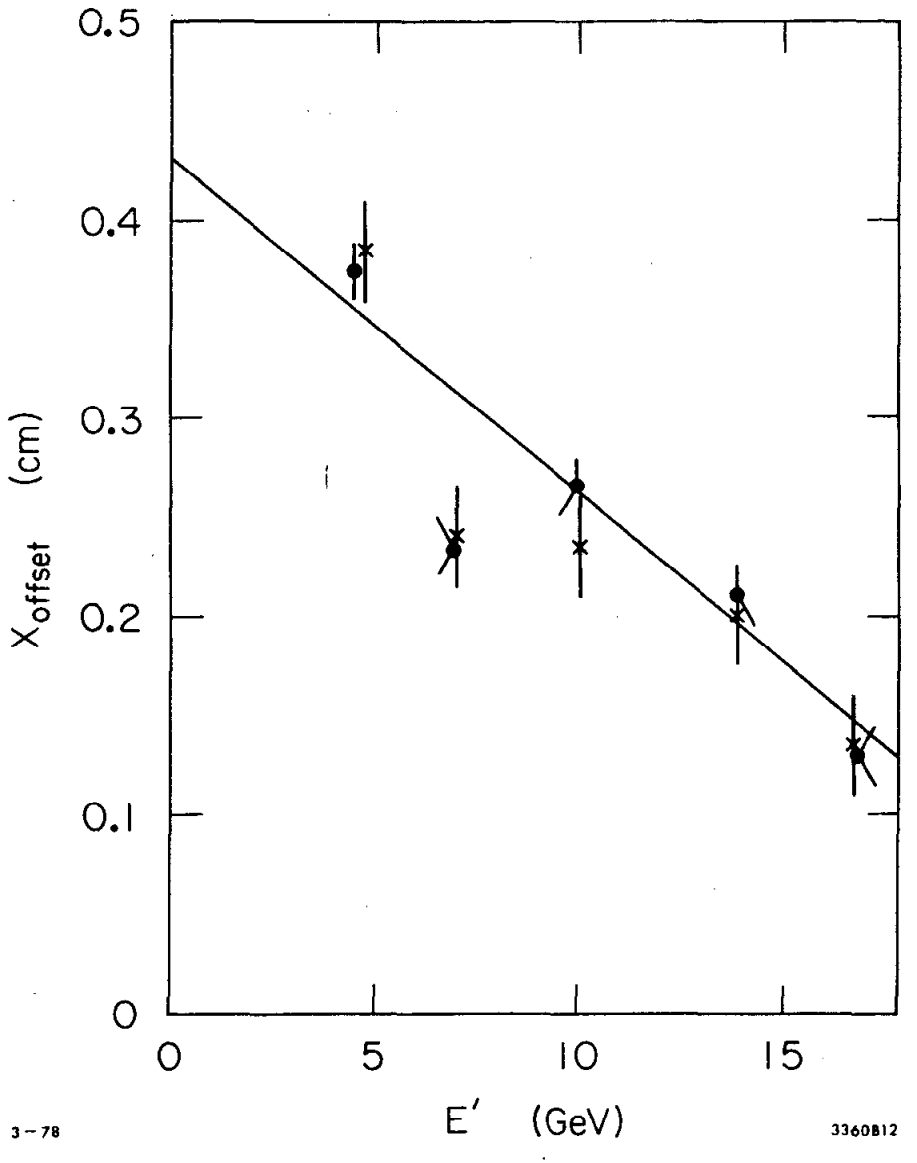

Fig. A1-8

A plot of the X offset of the PWC center relative to the spectrometer central ray (θ_0=0) as measured by the jailbars. A fit to the momentum dependence is shown. The X's are the measurements using only the inner 4 jailbars.

Elastic Peak Positions

In jailbar runs, optics coefficients were adjusted to give agreement between (known) incoming θ_o and reconstructed θ_o. In a similar manner, known elastic peak positions (in the δ, θ_o plane) allowed us to adjust optics coefficients involving the momentum. If elastic scattering events are displayed in a two-dimensional scatterplot of θ_o versus δ, they should group together in a swath across the δ-θ_o plane. This is just the line of constant W=.938 GeV. Figure A1-1 shows a constant W line in the δ, θ_o plane. If this swath deviates from the position calculated for the particular beam energy, scattering angle and spectrometer central momentum, this is evidence for an error in the measurement of one of these quantities or a mistake in the optics coefficients of the transfer matrix.

In particular, if the slope of the swath across the δ-θ_o plane is tilted with respect to the line expected for W=.938, this indicates an error either in the (θ_o/X) or (δ/Y) coefficient. Since the theta dispersion (θ_o/X) is determined by the jailbar analysis, the slope of the elastic peak swath determines the momentum dispersion (δ/Y). Consider Figure A1-9 for an illustration of the method used to measure (δ/Y).

In Figure A1-9, the points are the average values of δ of events within a bin at the corresponding θ_o. The three sets of points correspond to three elastic peak runs (taken sequentially), but with the spectrometer's central momentum stepped by 1% in order to study the position of the peak in different regions of the δ, θ_o plane. The lines drawn show the calculated (expected) variation of δ with θ_o for the elastic peak (i.e., W=.938 GeV) at the given E_o, Θ, and spectrometer central momentum P′ of each of the runs. If the points fall right on the line, this indicates that the momentum, δ, is accurately calculated. To study the deviation between measured and expected δ, we measured and graphed the deviation in the average momentum of a bin, Dev (δ), versus δ. This is shown in Figure A1-10.

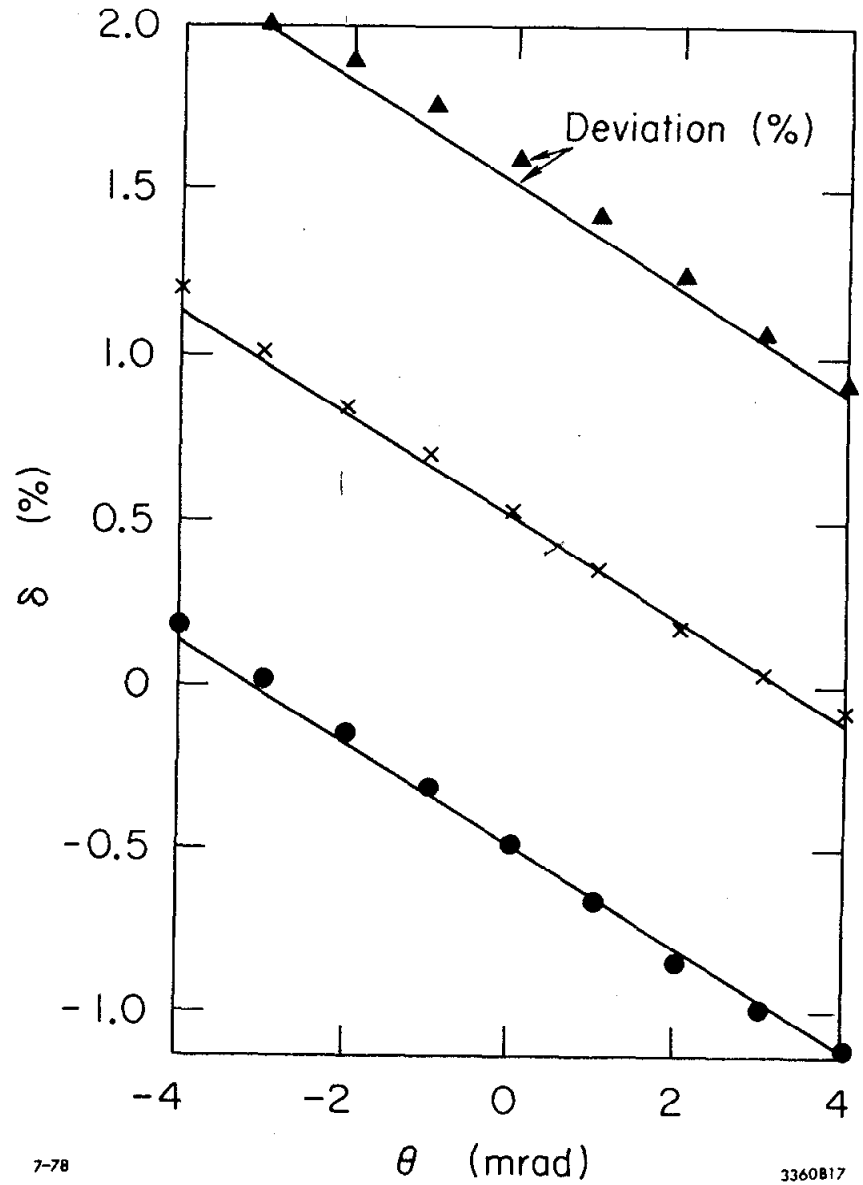

Fig. A1-9

A plot of the average δ for points within given θ_o bins, for three elastic peak runs taken with spectrometer central momentum differing by 1% steps. The calculated δ as a function of θ_o is shown by the line (calculated for measured E_o, Θ, E′). Deviations between measured and calculated δ allows a measurement of the momentum dispersion (δ/Y).

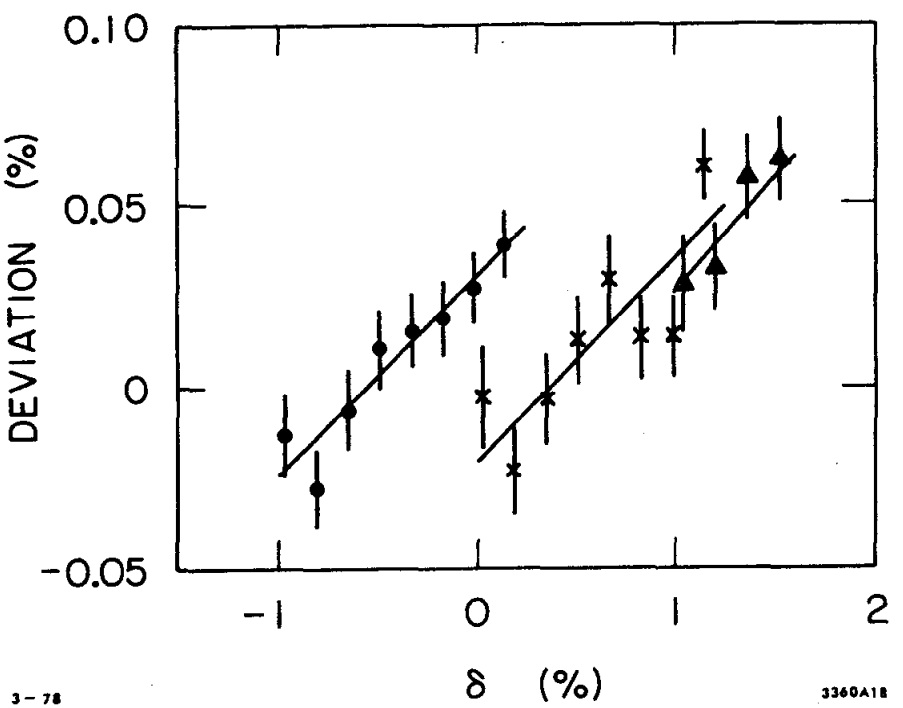

Fig. A1-10

For the three elastic peaks shown in Figure A1-9, the deviation of the average momentum, δ, of a Θ_o bin from the expected value is plotted versus the average δ of the bin. The non-zero slopes here indicate that the (old) value of the momentum dispersion (δ/Y) used to produce Figure A1-9 were correct, for this particular case, by ≈3.5%.

The slopes of the deviation versus δ in Figure A1-10 indicate that the old momentum dispersion (δ/Y) used to calculate the elastic peak position in Figure A1-9 had been incorrect. We fit the deviation to a linear function of δ, (i.e., Dev(%) = a+b * δ), determining the correct value of (δ/Y) to be $(\delta/Y)_{new} = (\delta/Y)_{old} * (1+b)$. This method determined (δ/Y) for an individual run to an accuracy of approximately 1/2%.

Since elastic peaks were measured at various secondary energies and angles, we can obtain values of the momentum dispersion as a function of spectrometer momenta. The results are displayed in Figure A1-11; the values of (δ/Y) are fit by a rise of 9% as momenta goes from 2.5 to 17.5 GeV.

We were able to use the fact that we measure (δ/Y) at three very close values of spectrometer momentum (as shown in Figure A1-9) to provide a measurement of a second order coefficient, (δ/Y^2). (δ/Y^2) was adjusted so that the measured values of (δ/Y) from the three runs were equal. This required changing (δ/Y^2) from its original value of .0041 to a value of .0062.

In addition to the slope of the deviation (in Figure A1-10) versus δ, there is an offset from 0. This offset shows up as a shift of the average W of an elastic peak from its expected value of .938 GeV. We corrected for this offset by changing the Y offset of the PWC's from their old value of .65 cm to .77 cm. These changes, as well as the changes to the Θ_o/X, Θ_o/X^2, Θ_o/X^3 and X offset values are summarized in Table III-1. We discuss these measured changes in the optics coefficients before proceeding to a discussion of the calculation of the spectrometer's acceptance.

Discussion of Changes

An investigation of possible causes of these measured changes in the coefficients was conducted by making modifications in the model of the spectrometer. The changes appeared rather large, and we wished to investigate how they could be simulated in the model in an effort to discover possible explanations for the shifts in coefficients.

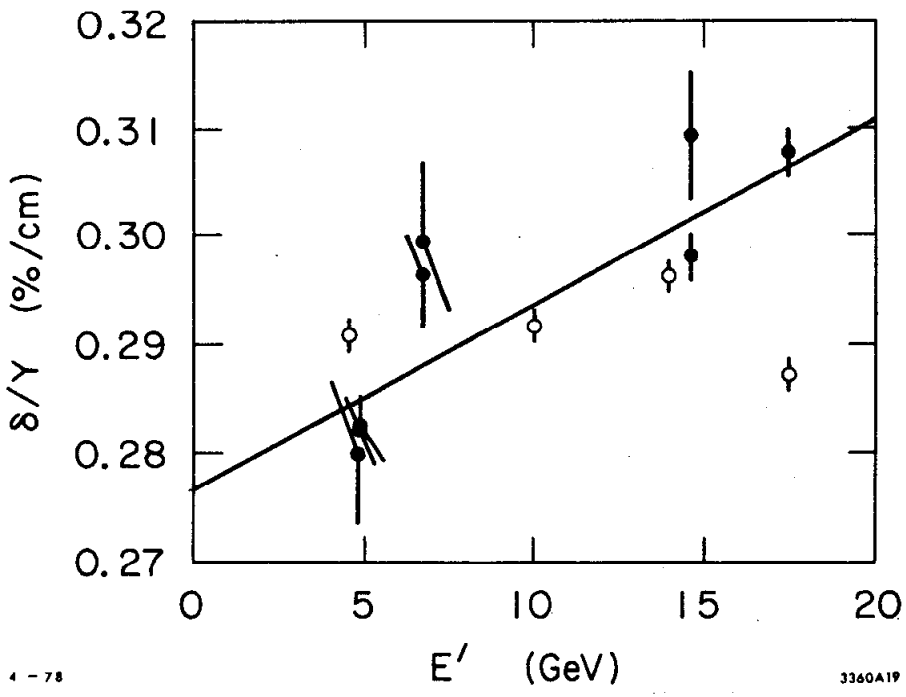

Fig A1-11

Graph of the momentum dispersion as determined from the elastic peak slopes in the δ, θ_0 plane plotted versus spectrometer momentum, E′. The open circles are (δ/Y) as measured in the 1967 optics tests on the 20 GeV spectrometer. The line is a fit of the E′ dependence of (δ/Y) to our measurements (dark circles).

1) (θ_0/X) and (δ/Y) increase by 4% and 9%, respectively, as spectrometer momentum changes from 2.5 to 17.5 GeV. This can be simulated by increasing the magnet field of Q201 and Q204 by 1% and Q202 - Q203 by .6% relative to their nominal values as momentum goes from 2.5 to 17.5 GeV. The quadrupole currents are kept within tolerances of .2%, so this explanation seems unlikely; however, it was the only way found which would cause such a variation.

2) (θ_0/Y) changes from .03 to 0. This coefficient is sensitive to a quadrupole rotated by 45° from the standard alignment of the 4 quadrupoles. B201 has such a rotated quadrupole component (due to the fact that its return coil "yoke" is shifted to one side to allow beam pipe clearance), which was adjusted in the model to give (θ_0/Y)=0. The quadrupole field gradient was adjusted to a value of .085 kGauss/cm*m to give (θ_0/Y)=0 in the model. This compares with its measured strength of .036 kGauss/cm*m. An alternate way to change (θ_0/Y) from .03 to 0 in the model is to rotate Q201 by .15°. We feel that uncertainties of the strength of the quadrupole component of B201 of this size are reasonable (the field gradient is≈ 6% of the field gradient of the first quad, Q201). The change of (θ_0/Y) from .03 to 0 has less than 1% effect on the cross section.

3) (θ_0/X^2) changes from -.0025 to .005. A sextupole rotated by 90° from the standard polarity of the three sextupoles most easily affects this term. The magnet B201 has such a measured sextupole component that extends the length of the magnet due to the notch that runs down its side (once again, to allow beam pipe clearance). By adjusting this component's strength to .006 kGauss/cm^2 (its measured value is .013 kGauss/cm^2), (θ_0/X^2) is changed to .005 as measured by the jailbar runs. The change of (θ_0/X^2) from .0025 to .005 affects the cross section by less than 1%.

4) X-OFFSET and Y-OFFSET. The offset of the axis of the central ray relative to the surveyed center line changes with momentum (by 2 or 3 mm), and it probably arises from quadrupole steering; possibly from an offset quadrupole component in B201. The changes introduced into the cross section due to these effects are ≈1%.

The changes in the optics coefficients listed above were of concern to us. Our investigations of possible causes for these changes point to the multipole components of B201 as candidates for most of these changes. With the exceptions of the momentum dependence of the Θ_0 and P dispersions, the changes found will affect the cross sections by less than 1%. The effect of the E´ dependence of the dispersions is large, however, We feel that we know the dispersions within an overall systematic error of 4% but, unfortunately, are not sure what may have caused this change from the old values.

At the end of the appendix we discuss the systematic errors introduced into the cross section due to possible errors in the optics coefficients. Now we discuss checks of the model of the spectrometer and their effect on the calculation of its acceptance.

MODEL AND DETERMINATION OF ACCEPTANCE

In determining cross sections, we must know the optics coefficients to calculate the δ and Θ_0 for each particle in order to count the number of events within the acceptance. We also must know the size of the acceptance of the spectrometer, and that is what we discuss in this section.

Since measurements of the optics coefficients revealed changes from previous measurements, it was necessary to update calculations of the acceptance as well. With the aid of a model of the spectrometer (magnet positions and currents and apertures) and a "ray-trace" method of "swimming" Monte Carlo events through the model, we redetermined the acceptance of the spectrometer and verified that the model was an accurate simulation of the real spectrometer. Our procedures for accomplishing this are presented here and are shown on the left side of Figure A1-3.

If a sample of particles has angle Θ_0 within ±4 mrads, has angle ϕ_0 within the "ϕ-slit" opening of ±8 mrads, and has momentum within ±2% of the spectrometer central momentum, then most of these

particles will traverse the spectrometer and strike the trigger counters. The product of the range of ϕ_0, the range of Θ_0, and the range of δ of the set of particles which strike the trigger counters (and are within the "software" limits on Θ_0 and δ) is the acceptance. Because the nominal ϕ_0 acceptance as defined by the ϕ_0 slits is further limited by apertures within the spectrometer, we use a Monte Carlo generation of events through the spectrometer model in order to calculate the actual ϕ_0 acceptance as a function of δ and Θ_0. Figure A1-12 demonstrates that apertures cut into the X-Y acceptance defined by the scintillator counter, TR3. This is evident from the decrease of events near the positive X side of the counter area.

In addition to the fits of the 1967 optics data yielding the coefficients, a measurement of the acceptance was made at that time. For a given momentum and a given X offset, a Θ_0-ϕ_0 acceptance plot in the focal plane was made by fixing either Θ_0 or ϕ_0 and varying the other angle until the ray no longer passed through the spectrometer.

A model was developed originally by E.A. Taylor[2], to match the optics and acceptance data of these 1967 tests. We have modified this model to agree with the data taken during the course of E89. The model is composed of individual elements representing dipoles, quadrupoles, sextupoles, or drift spaces with a field strength and an aperture size associated with each element. Each element is divided into many segments along its length, and the particle's positions and angles and momentum upon entering a segment determine its outgoing positions and angles. The transformation matrix for each segment is first order only (i.e., outgoing quantities depend only linearly upon entering parameters). It was found to be sufficient to divide the bending elements into 4 segments, quadrupoles into 20, and sextupoles into 8 segments in order not to lose accuracy (within the resolution) of the final position of an event due to this linear approximation.

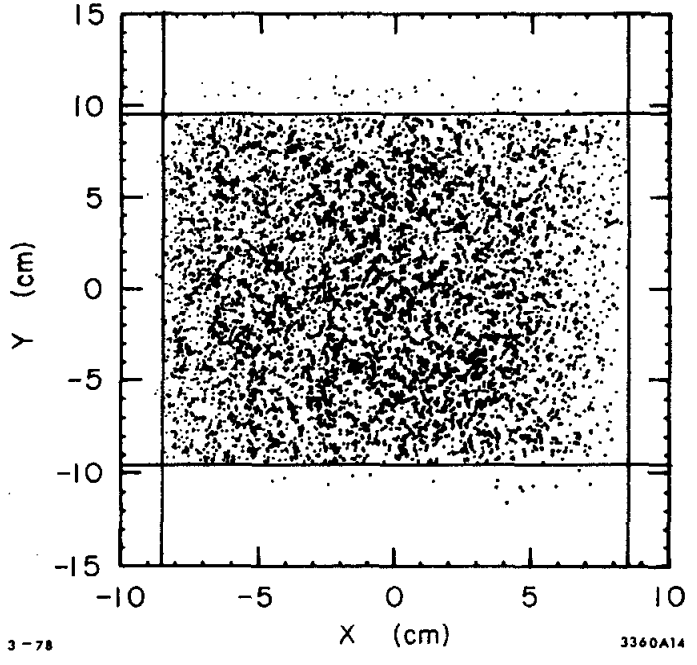

Fig. A1-12

A scatterplot of X versus Y for events at the position of TR3 (trigger scintillator) with the size of TR3 indicated by the lines. Depletion of events near the positive X edge indicate that apertures within the spectrometer are cutting into the acceptance.

A random distribution over target position and incoming angles and momentum is generated by Monte Carlo techniques. These parameters include a target of length 17.78 cm displaced 1 cm upstream of the pivot, ϕ_o slits of ±2, 4, or 8 milliradians, and random X_o and Θ_o within ±3 cm and ±6 milliradians, respectively, to match our experimental conditions. Particle trajectories are traced through each element in turn, and at the end of each segment a test is performed to see if a particle has struck an aperture. For a given δ and Θ_o the fraction of events which traverse the entire spectrometer determines the ϕ_o acceptance at that value of δ and Θ_o.

Consider again the flowchart outlining our study of the optics and acceptance of the spectrometer, Figure A1-3. To make the problem of modifying the model until it agrees with the data manageable, we have separated two aspects of the model: the magnetic field properties and the apertures.

To check the magnetic field properites, we first determined that a calculation of the optics coefficients of the model agreed approximately with the measured optics coefficients. To obtain agreement, we changed various magnetic field strengths as indicated in the previous section. We then compared a scatterplot of X (in the detector) versus ϕ_o (incoming) from the jailbar data with an X-ϕ_o scatterplot obtained from the model (with a simulated jailbar mask). See Figure A1-13. Note that the old model showed significant geometric aberrations that were absent in the data distributions obtained with the measured optics coefficients. This was corrected in the new model by doubling the magnetic strength of the first sextupole. We do not know what caused this effective doubling of the field strength of the sextupole, but perhaps its field was increased by fringe fields from the nearby coil of the bending magnet, B201. Note that this is a different correction than the change to the sextupole component of B201 (which was rotated by 90^o from the standard configuration). The sextupole component of B201 had very little effect on this geometric aberration.

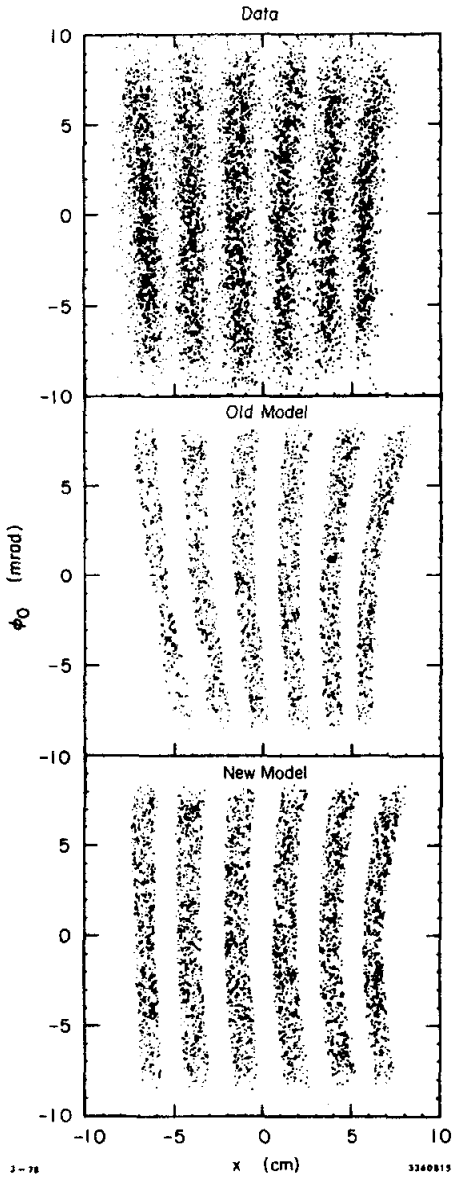

Fig. A1-13

A comparison of X-ϕ_o scatterplots from a jailbar data run, and from 2 Monte Carlo runs with a simulated jailbar mask. The original data showed aberrations not seen in the data; the final model agreed better with the data.

Now we have determined the magnetic field strengths of the model by demanding agreement between the model's optics coefficients and the measured ones and by requiring that the simulated ϕ_o-X scatterplot agrees with the measured scatterplot.

Once we are satisfied that the magnetic field strengths in the model are well determined, we can then adjust apertures in the model to obtain agreement between the measured shapes of Θ_o and δ distributions as reconstructed from the data with those generated by the model.

The shapes of histograms versus momentum and theta are compared for model and data. See Figure A1-14. Note that in both the data and the model, the histograms decrease from Θ_o=0, δ=0. The apertures of the model were adjusted until reasonable agreement was attained between data and model.

Distributions in δ and Θ_o are produced for those (Monte Carlo) events which successfully pass through the spectrometer and strike the trigger counter. In this way, we obtain a (Θ_o-δ) density distribution and fit a function to this to obtain the ϕ_o acceptance $F(\Theta_o,\delta)$. We normalized $F(\Theta_o,\delta)$ at Θ_o,δ=0 to the nominal size of the ϕ_o slits; the idea being that for those particles with near-central values of Θ_o and δ, the only limiting aperture of ϕ_o occurs at the ϕ_o slits (i.e., all ϕ_o values between ±8mrads are accepted). This has been confirmed within the model with explicit rays traced through and had been confirmed for the real spectrometer in the optics tests of 1967.

After the consistency of model and data is confirmed, the fits of the ϕ_o acceptance $F(\Theta_o,\delta)$ are coded for each of the scattering angles ($6^o \rightarrow 20.6^o$) and for each of the ϕ_o slits (2, 4, and 8 mrads), and these are used in production of cross sections. For graphs of the acceptance of the spectrometer versus X_o positon at the target, see Figure A1-15, and for a plot of constant contours of $F(\Theta_o,\delta)$ see Figure A1-16.

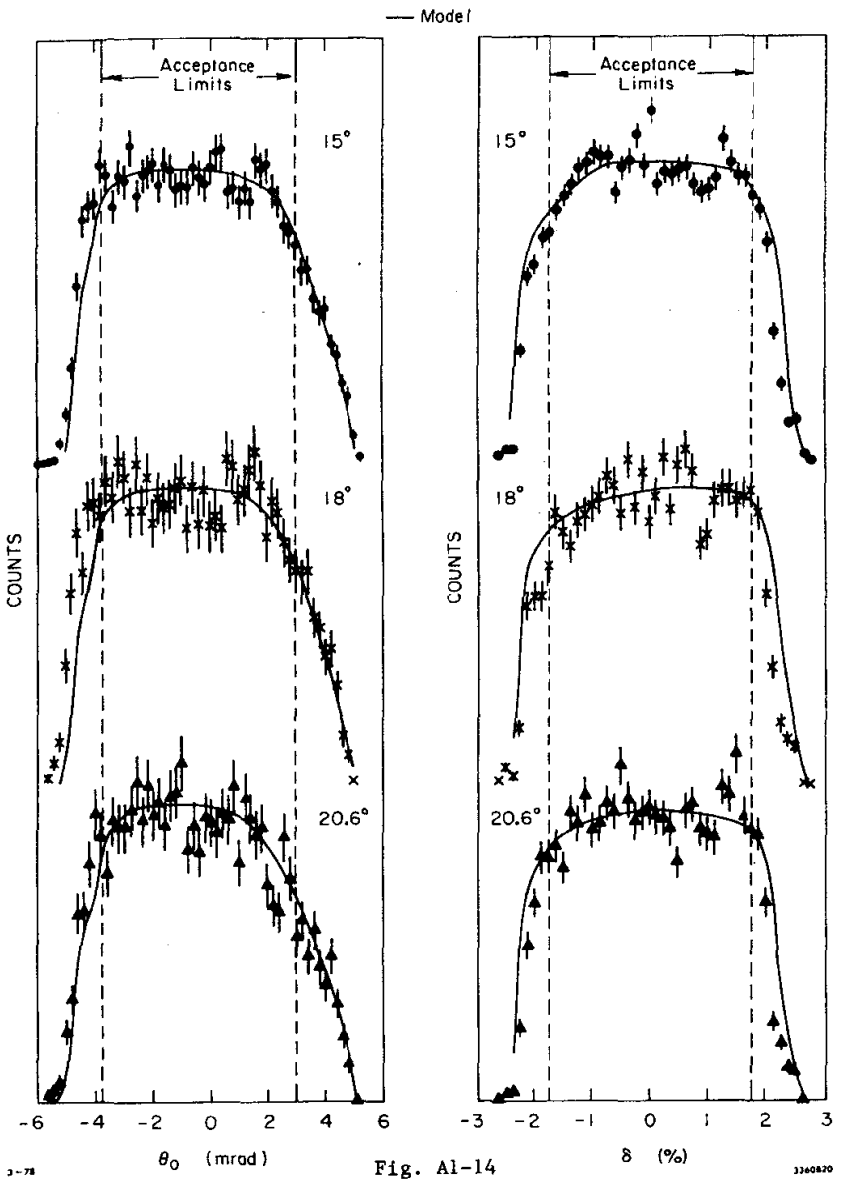

Fig. A1-14

A comparison of histograms in Θ_o and δ from experimental data runs (points) with Θ_o and δ histograms from a Monte Carlo of the spectrometer model (line). The acceptance limits on Θ_o and δ used in the analysis are indicated.

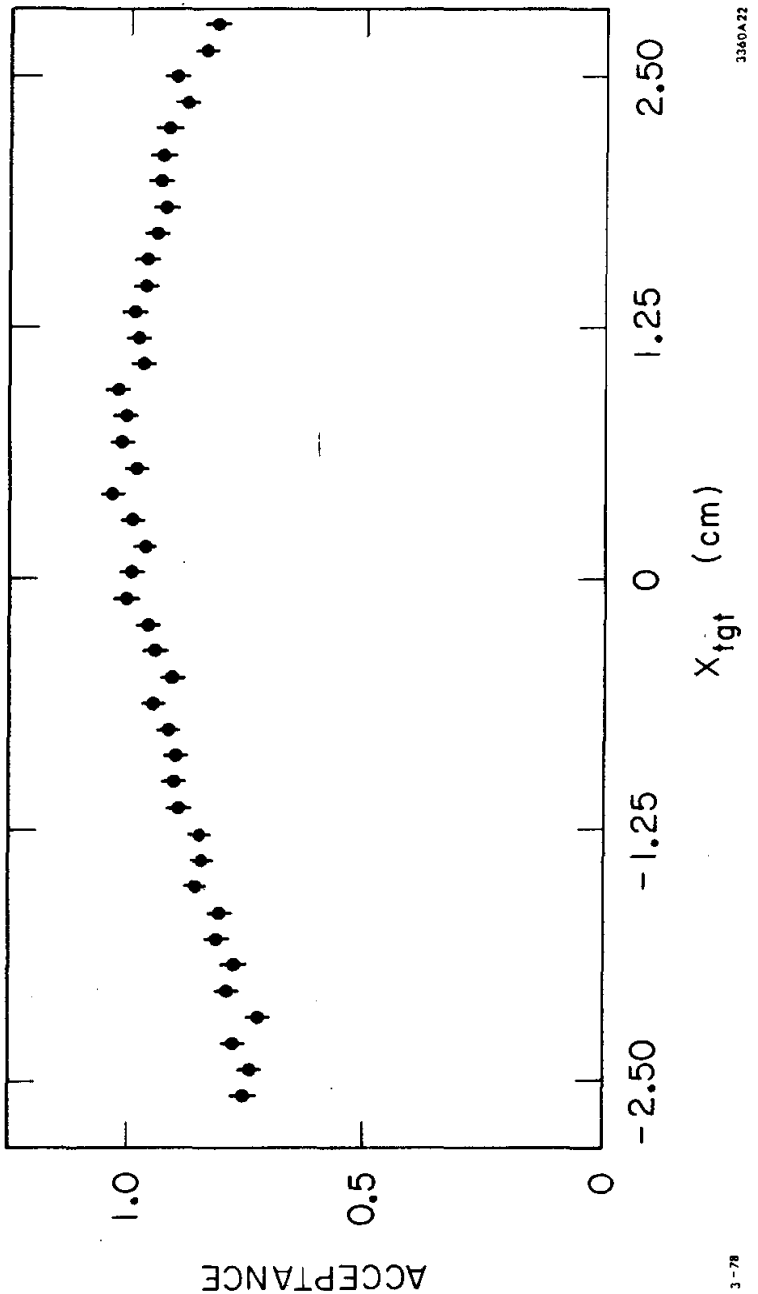

Fig. A1-15

The spectrometer acceptance, normalized to its nominal value, plotted versus the X position of the target vertex (relative to the spectrometer axis). The graph shows the fall-off in acceptance at the ends of the target.

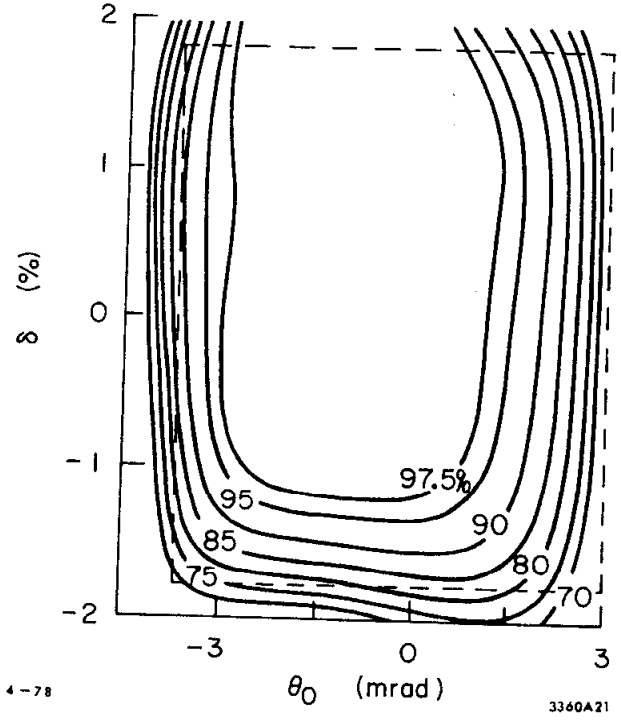

Fig. A1-16

A contour plot of the ϕ_o acceptance (normalized to the nominal value of the ϕ_o slit) plotted versus δ and Θ_o. The value of the ϕ_o acceptance is from a fit of the results of a Monte Carlo simulation using the spectrometer model. This contour plot is for $\Theta=20.6^o$. The dashed line denotes the acceptance limits used in the analysis.

There are two major sources of systematic error in determining the acceptance of the spectrometer. The first is an error in our Monte Carlo calculation of the correction to the nominal accptance, $\Delta\Theta_o \Delta\phi_o \Delta\delta$, and the second arises from errors in our determination of the theta and momentum dispersions.

Our major criterion for judging the correctness of the acceptance calculation is that the shapes of histograms in P and Θ_o from experimental data runs agree with those produced by a Monte Carlo of the model. If we change parameters in the Monte Carlo, such as aperture sizes, until there is a clearly discernible difference between model and data, the acceptance changes by 2% or less. So we assign 2% as the size of a possible systematic error in the acceptance calculation.

The dispersions are proportionality constants relating δ (or Θ_o) to Y (or X). When we set software limits in δ and Θ_o to define the acceptance, the corresponding limits on X and Y are affected by errors in the dispersion. These errors are directly reflected in the cross section because the number of counts falling within the $\Delta\delta$ and $\Delta\Theta_o$ acceptance is proportional to the corresponding product $\Delta X \cdot \Delta Y$. Looking again at a graph of the (δ/Y) dispersions as measured by elastic peak positions (Figure A1-7), it appears that there could be systematic errors as large as 3% to account for the (greater than statistical) spread of the points about the fit. Similar considerations for the Θ_o dispersion give an estimate of 1%. These two dispersions are positively correlated because an error of 1% in the Θ_o dispersion would introduce an error of 1% in the determined value of the P dispersion. Thus, we add the two errors linearly to obtain 4% as an estimate of systematic uncertainty in the cross section due to lack of knowledge of the theta and momentum dispersions.

Surveys of the detector relative to the spectrometer centerline indicated that it varied as much as 3 mm for different spectrometer angles. This could introduce an error as large as 1% due to an offset in the central θ of the spectrometer.

The error on the dispersions is largely uncorrelated with the error in the acceptance calculation because the Monte Carlo model is constrained to agree with the shape of the θ_o and δ data histograms. However, the error due to an offset is correlated with errors in the acceptance because the acceptance calculation depends on the location of the $\theta = 0$, $P = 0$ point. Thus we add these two errors linearly, and add their sum in quadrature with the dispersion error to obtain the overall systematic error associated with the spectrometer of 5%.

CONSISTENCY CHECKS ON OPTICS COEFFICIENTS AND ACCEPTANCE

This section describes various checks on the internal consistency of the optics and acceptance of the spectrometer. First of these is the comparison of cross sections using a restricted subset of the δ- Θ_o plane ($|\delta|<1\%$, $|\theta_o|<2.25$ mrads) with those calculated using the full range of δ and θ_o, ($|\delta| <1.75\%$, $-3.75<\theta_o<3$ mrads). This ratio of "inner" to "outer" cross sections for each angle appears in Figure A1-17. The inner cross section is much less affected than the outer by variations in the calculated acceptance because the apertures of the spectrometer do not cut into the inner acceptance. The errors on the inner cross sections are thus dependent primarily on errors in the optics coefficients. Also, because the range of track variables is smaller, the effect of higher order optics coefficients is lessened. The inner cross section is expected, therefore, to be more nearly correct and the inconsistency of inner and outer cross section is a lower limit on the error of the acceptance calculation and optics coefficients. In addition, a comparison is made of cross sections measured at the same kinematic point but using different ϕ_o slits. If the acceptance is well determined the two values should be equal.

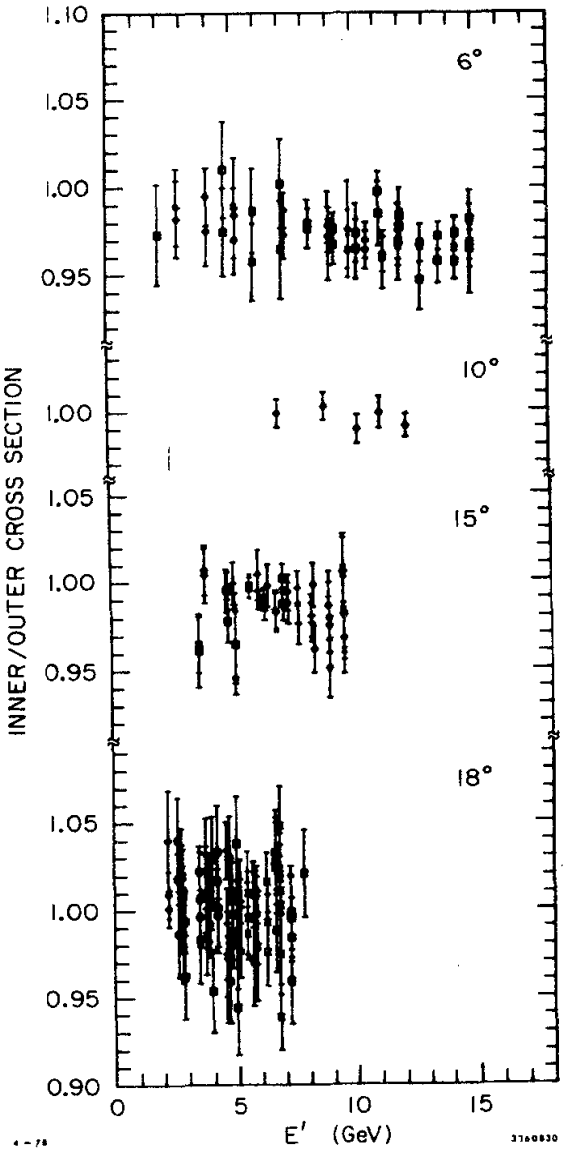

Fig. A1-17

The ratio of cross sections obtained using "inner" apertures to those obtained using the standard "outer", apertures normally used in the analysis.

From the observed consistency of "inner" and "outer" cross sections within about 3% and the consistency of cross sections using different ϕ_o slits within 2%, we conclude that our estimte of the systematic errors was justified and that we know the acceptance of the spectrometer within a possible systematic error of ±5%.

APPENDIX I--REFERENCES

1. The vertical angle, ϕ_o, can be delimited by slits at the spectrometer entrance because all scattered particles have the same vertical position in the target (within the vertical spread of the beam of approximately 2 mm). Because scattered particles can have different X_o positions at the target, slits at the spectrometer entrance will not define a unique range of accepted θ_o.

2. E.A. Taylor, SLAC Technical Note 71-26.